HEINRICH HEINE
UNIVERSITÄT DÜSSELDORF

Generation and investigation of a faithful model for familial Alzheimer's disease with presenilin mutations

Inaugural-Dissertation

zur Erlangung des Doktorgrades
der Mathematisch-Naturwissenschaftlichen Fakultät
der Heinrich-Heine-Universität Düsseldorf

vorgelegt von

Vanessa Kurth
aus Düsseldorf

Düsseldorf, August 2016

aus dem Institut für Neuropathologie

der Heinrich-Heine-Universität Düsseldorf

Gedruckt mit der Genehmigung der

Mathematisch-Naturwissenschaftlichen Fakultät der

Heinrich-Heine-Universität Düsseldorf

Referent: Prof. Dr. Sascha Weggen

Korreferent: Prof. Dr. Vlada B. Urlacher

Tag der mündlichen Prüfung:

Ich versichere an Eides Statt, dass die vorgelegte Dissertation

Generation and investigation of a faithful model for familial Alzheimer's disease with presenilin mutations

von mir selbständig und ohne unzulässige fremde Hilfe unter Beachtung der „Grundsätze zur Sicherung guter wissenschaftlicher Praxis an der Heinrich-Heine-Universität Düsseldorf" erstellt worden ist.

Des Weiteren versichere ich, dass die Dissertation zuvor keiner anderen Universität oder Fakultät vorgelegt wurde und ich bislang keinerlei andere Promotionsversuche getätigt habe.

Düsseldorf, den 22.08.2016

_____ _____

Ort / Datum Vanessa Kurth

Für meinen

Opa Willi!

CONTENTS

Summary

Presenilin-1 (PSEN1) is an important protein in the development of Alzheimer's disease (AD). As the catalytic subunit of the γ-secretase complex, it is involved in the production of pathogenic Aβ peptides. Heterozygous mutations in the PSEN1 gene, which are autosomal-dominantly inherited in familiar AD (FAD), have been shown to influence the Aβ production and to induce an early disease onset. Until now, investigations on the function of PSEN1 mutations have been predominantly performed in overexpression mode systems, which do not reflect the heterozygous and endogenous expression of wt and mutant PSEN1 in FAD patients. Observations from these experiments have led to varying and partially contradicting hypotheses on the general function of PSEN1 mutations.

The objective of this doctoral thesis was to establish a stem cell based, isogenic FAD PSEN1 model system for an investigation of the molecular function of heterozygous PSEN1 mutations, including the suggested hypotheses. The dRMCE technique was used to perform heterozygous knock-ins of PSEN1 mutations into the conditional allele of a commercially available, murine embryonic stem cell line by targeted recombination. Each single cell clone of the 26 generated, embryonic stem cell lines was screened for successful recombination by specific PCR analysis. The average efficiency of the dRMCE technique was 48 %. Heterozygous transcription and translation of wt and mutant PSEN1 was confirmed by mRNA and protein levels. A differentiation of the embryonic FAD PSEN1 stem cell lines into neural stem cells was performed for functional investigations. Here, the stem cell status was confirmed by the expression of stem cell markers and the successful differentiation into neurons, astrocytes and oligodendrocytes. Observations from co-IP experiments and the investigation of Aβ profiles in the FAD PSEN1 stem cell lines demonstrated that PSEN1 mutations do not have a dominant-negative effect.

The isogenic FAD PSEN1 model system, which has been established in this doctoral thesis, should be used for further investigations on the clarification of the general function of FAD PSEN1 mutations, since no other model system with a comparably high number of different FAD PSEN1 mutations is available.

Zusammenfassung

Presenilin-1 (PSEN1) ist ein wichtiger Faktor in der Entstehung von Alzheimer, da es als katalytische Untereinheit des γ-Sekretase Komplexes maßgeblich an der Produktion von pathogenen Aβ Peptiden beteiligt ist. Heterozygote Mutation im PSEN1 Gen, die in der familiären Form von Alzheimer (FAD) autosomal-dominant vererbt werden, haben einen Einfluss auf die Aβ Produktion und führen zu einem frühen Krankheitsbeginn. Bisherige Untersuchungen zur Funktion von PSEN1 Mutationen wurden überwiegend in Überexpressions-Model-Systemen durchgeführt, die der heterozygoten und endogenen Expression von wt und mutiertem PSEN1 in FAD PSEN1 Patienten widersprechen. Aus den Beobachtungen wurden verschiedene und teilweise widersprüchliche Hypothesen über die generelle Funktion von PSEN1 Mutationen erstellt.

Das Ziel dieser Doktorarbeit war die Etablierung eines Stammzell-basierten, isogenen FAD PSEN1 Model Systems, zur Untersuchung der molekularen Funktion von heterozygoten PSEN1 Mutationen, einschließlich der vorgeschlagenen Hypothesen. Unter Anwendung der dRMCE Technik wurden mittels zielgerichteter Rekombination heterozygote PSEN1 Mutationen in das konditionelle PSEN1 Allel einer kommerziell erhältlichen, embryonalen Stammzell-Linie aus der Maus eingefügt. Die erfolgreiche Integration der PSEN1 Mutationen wurde in einzelnen Zellklonen für jede der 26 generierten, embryonalen PSEN1 Stammzell-Linien mit einem speziell entwickelten, PCR-basierten Verfahren validiert. Die gemittelte Effizienz der dRMCE Technik betrug 48 %. Eine heterozygote Transkription und Translation des wt und mutierten PSEN1 Allels wurde auf mRNA- und Protein-Ebene bestätigt. Die embryonalen FAD PSEN1 Stammzell-Linien wurden für die funktionellen Untersuchungen der Mutation in neurale Stammzellen differenziert und deren Stammzellstatus über die Expression von spezifischen Stammzell-Markern und der erfolgreichen Differenzierung in Neurone, Astrozyten und Oligodendrozyten bestätigt. Ergebnisse aus co-IP Experimenten und aus Untersuchungen der Aβ Profile in den FAD PSEN1 Stammzell-Linien haben gezeigt, dass PSEN1 Mutationen keine trans dominant-negativen Effekte haben.

Das im Rahmen dieser Doktorarbeit etablierte, isogene FAD PSEN1 Model System sollte für zukünftige Untersuchungen zur Aufklärung der allgemeinen Funktion von FAD PSEN1 Mutationen eingesetzt werden, da bisher kein vergleichbares Model System mit einer ähnlich hohen Anzahl an FAD PSEN1 Mutation zur Verfügung steht.

Abbreviations

Aβ	amyloid-β
AD	Alzheimer's disease
ADAM	a disintegrin and metalloprotease
AICD	APP intracellular domain
Aph-1	anterior pharynx-defective-1
APP	β-amyloid precursor protein
APS	ammonium persulfate
BACE	β-site APP cleaving enzyme
BCA	bicinchonic acid
BSA	bovine serum albumin
CAA	cerebral amyloid angiopathy
CHAPSO	3-[(3-cholamidopropyl)dimethylammonio]-2-hydroxy-1-propanesulfonate
CSF	cerebrospinal fluid
CTF	C-terminal fragment
DAPT	N-[N-(3,5-Difluorophenacetyl-L-alanyl)]-S-phenylglycine t-butyl ester
DMSO	Dimethylsulfoxide
DTT	dithiothreitol
E. coli	*Escherichia coli*
EDTA	ethylenediaminetetraacetic acid
e.g.	for example
EGF	Epidermal Growth Factor
ER	endoplasmic reticulum
ES cell	embryonic stem cell
FAD	Famillial AD
FCS	fetal calve serum
FDG	fluorodeoxyglucose
FGF	Fibroblast growth factor
FL	full length
g	gramm
h	hour

HEPES	4-(2-hydroxyethyl)-1-piperazineethanesulfonic acid
i.e.	that is
IP	immunoprecipitation
kDa	kilo Dalton
KPI	kunitz-type protease inhibitor domain
L	liter
LIF	Leukemia inhibitory factor
M	molar
m	mili
MEF	mouse embryonic fibroblast
MES	2-(*N*-morpholino)ethanesulfonic acid
min	minute
MRI	magnetic resonance imaging
n	nano
NEP	neuroepithelial precursor
Nct	Nicastrin
nm	nano meter
NSC	neural stem cell
NTF	N-terminal fragment
P	pico
PAGE	polyacrylamide gelelectrophoresis
PBS	phosphate-buffered saline
PCR	Polymerase chain reaction
Pen-2	presenilin enhancer-2
PET	positron emission tomography
PI	protease inhibitor
PiB	Pittsburg Compound B
PS	Presenilin
PSEN	Presenilin
PVDF	polyvinylidene fluoride
RT	room temperature
s	second

SAD	Sporadic AD
SDS	sodium dodecyl sulfate
SPP	signal peptide peptidase
TAE	tris acetic acid
TBS	Tris-buffered saline
TBST	Tris-buffered saline tween
TEMED	N,N,N',N' tetramethylethylenediamine
TFPP	type 4 prepilin peptidase
TMD	transmembrane domain

Amino acids

A	Ala	Alanine
C	Cys	Cysteine
D	Asp	Aspartic acid
E	Glu	Glutamic acid
F	Phe	Phenylalanine
G	Gly	Glycine
I	Ile	Isoleucine
K	Lys	Lysine
L	Leu	Leucine
M	Met	Methionine
N	Asn	Asparagine
P	Pro	Proline
Q	Gln	Glutamine
R	Arg	Arginine
S	Ser	Serine
T	Thr	Threonine
V	Val	Valine
W	Trp	Tryptophan
Y	Tyr	Tyrosine

1. Introduction

1.1 Alzheimer's disease

Alzheimer's disease (AD) is an irreversible neurodegenerative disorder of the central nervous system, which was first described in 1906 by the German psychiatrist Alois Alzheimer (Alzheimer 1907). Macroscopically, its hallmarks are severe cerebral atrophy, frequently starting in the medial temporal lobe, which includes the hippocampus and progressing towards the cortex where a reduction of the white matter and thinning of the cerebral gyri is observed (Fox *et al.* 1996, Rossor *et al.* 1996, Gregory *et al.* 2006, Bateman *et al.* 2011, Braak & Del Tredici 2011) [Figure 1].

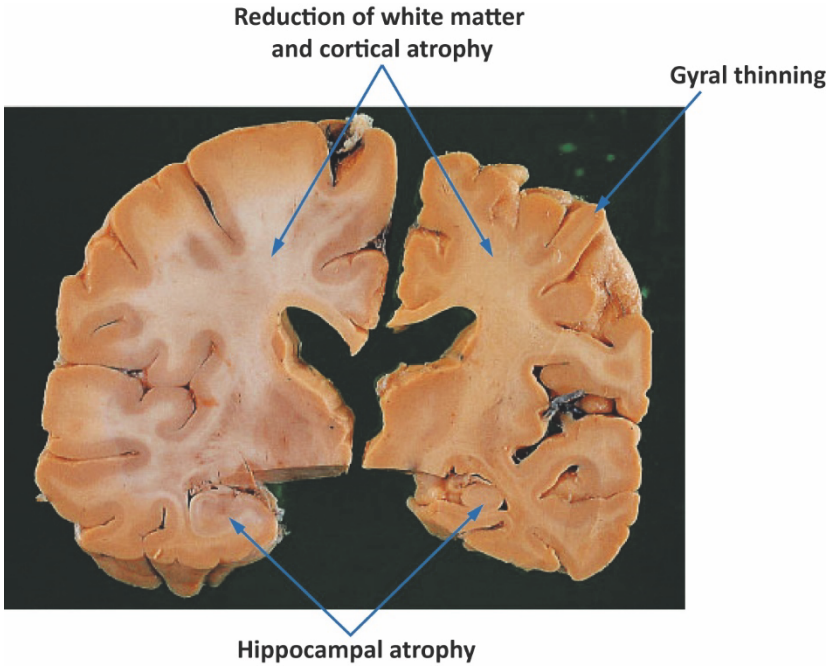

Figure 1: Comparison of brain slices from a normal brain at age 70 (left slice) and an AD brain (right slice). The AD brain shows atrophy in the cortex and hippocampus with a reduction of white matter and gyral thinning (modified after (Ellison *et al.* 2004)).

Clinical symptoms arise as a consequence of the progressive degeneration of neurons in affected brain regions. Memory decline as a result of hippocampal atrophy is an early feature in AD (Fox et al. 1996, Rossor et al. 1996, Fox *et al.* 1998, 2015 Alzheimer's disease

facts and figures). Further symptoms appear in the later stages of the disease. Amongst these symptoms are spatial and time confusion, altered behaviour including apathy and depression and motor symptoms, such as difficulties in walking, speaking and swallowing (2015 Alzheimer's disease facts and figures). AD onset occurs either sporadic in patients predominantly after 65 years of age or between the third and six life decade in response to inherited mutations in AD relevant genes. Based on the age of onset and the degree of genetic determination, AD cases are generally divided into two groups (Bateman et al. 2011, Tanzi 2012, Herrup 2015):

1. Late-onset sporadic AD (SAD) with varying degree of genetic influence
2. Early-onset familial AD (FAD) with autosomal-dominant inheritance pattern

Until now, no therapies to prevent the onset of AD, to stop disease progression or to restore lost brain tissue and neural integrity are available. According to the World Alzheimer Report 2015, 46 million people worldwide suffer from dementia, with a proportion of 50 – 80 % for AD (Abbott 2011, World Alzheimer Report 2015). Approximately 5.3 million U.S. Americans had AD in 2015. Including patients with other forms of dementia, the total payments for their health care, long-term care and hospice services were estimated to be US$ 226 billion, (2015 Alzheimer's disease facts and figures). Since age is still the predominant risk factor for the development of AD, the incidence and prevalence of AD will continuously rise with an increasing live expectancy of society (Tanzi 2012, Herrup *et al.* 2013, 2015 Alzheimer's disease facts and figures). In 2050, the number of people with AD has been estimated to be above 13 million (Hebert *et al.* 2013).
Consequently, the identification of the underlying pathomechanisms and the subsequent development of effective therapies for AD is of urgent medical and also economic interest.

1.2 The amyloid cascade hypothesis of Alzheimer's disease pathology

The *post mortem* examination of brain tissue from AD patients has revealed the presence of extra- and intracellular protein deposits (Alzheimer 1907, Schellenberg & Montine 2012). Based on their protein composition, two different types of protein aggregates were identified: amyloid plaques and neurofibrillary tangles [Figure 2 A, B].

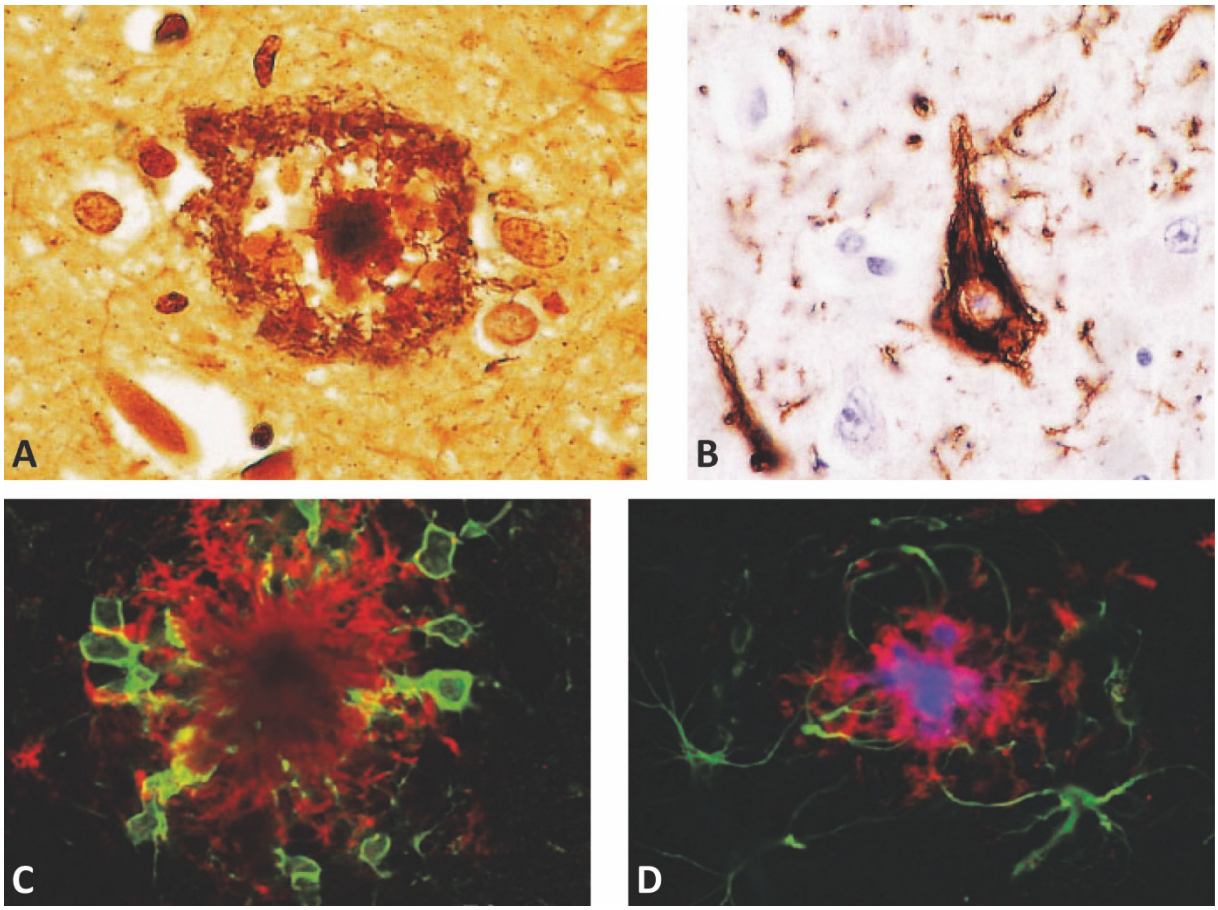

Figure 2: Protein aggregates in the brain of AD patients. (**A**) Silver stained extracellular amyloid plaque. (**B**) Immunostained intracellular neurofibrillary tangle (figures A and B were adopted from (Ellison et al. 2004)). (**C**) Immunostained microglia (green) around an Aβ plaque (red). (**D**) Immunostained astrocytes (green) around an Aβ plaque (red) (figures C and D were adopted from (Heneka *et al.* 2015)).

The extracellular amyloid plaques are composed of aggregated amyloid beta (Aβ) peptides, a proteolytic cleavage product of the amyloid precursor protein (APP). Intracellular neurofibrillary tangles are composed of hyperphosphorylated Tau, a cyto-plasmic protein, which stabilizes microtubules by binding to tubulin during its polymerization (Weingarten *et al.* 1975, Grundke-Iqbal *et al.* 1986, Selkoe 2001, Iqbal *et al.* 2009).

In 1992, the amyloid cascade hypothesis was postulated. It suggests that aberrant aggregation of secreted Aβ peptides in the brain is causative for the initiation of a cascade of pathogenic events which ultimately lead to AD (Hardy & Higgins 1992, Hardy & Selkoe 2002, Haass & Selkoe 2007, Karran *et al.* 2011, Reitz 2012, Selkoe & Hardy 2016) [Figure 3]. Those "aggregate stress" events include inflammation, changes in the ionic homeostasis, the production of toxic oxygen species and Tau hyper-phosphorylation by altered kinase/ phosphatase activity.

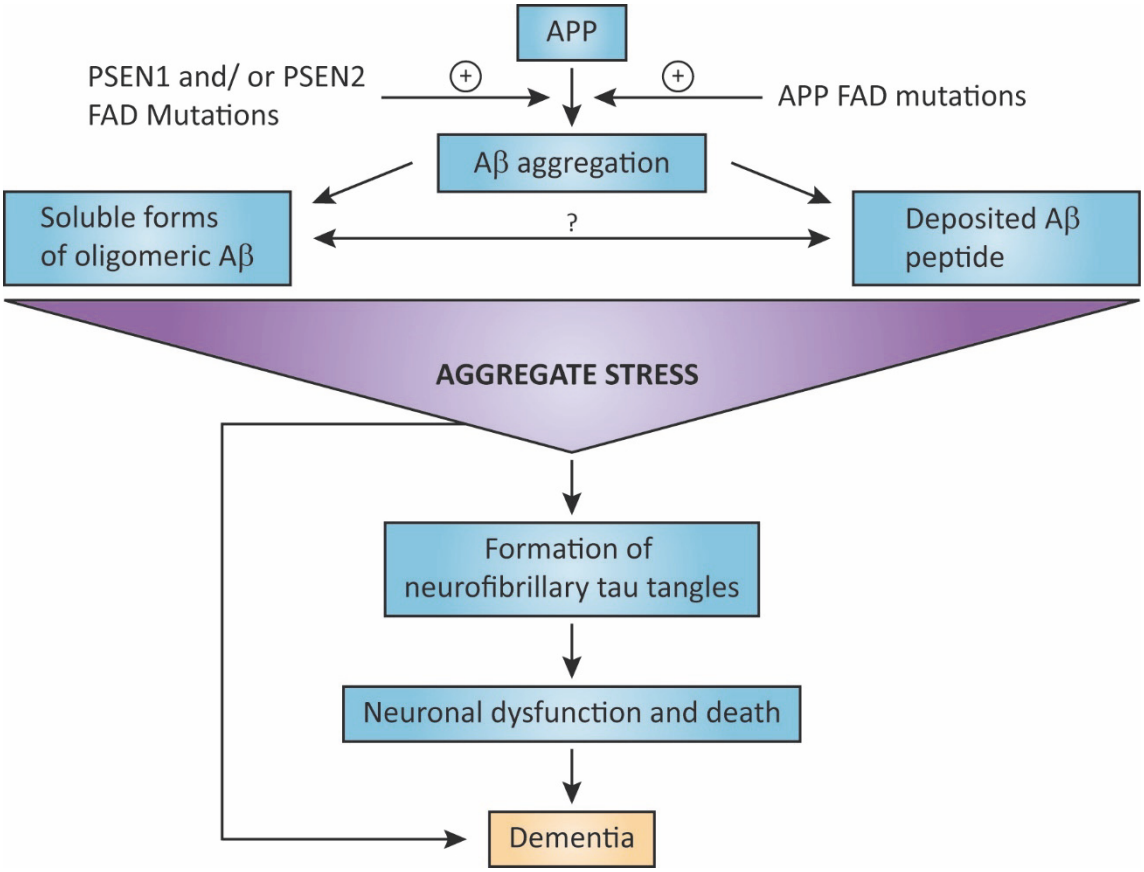

Figure 3: The amyloid cascade hypothesis. APP is cleaved into Aβ peptides, which aggregate and either deposit in the brain or form soluble Aβ oligomers. Aberrant Aβ secretion induces aggregate stress, including inflammation, production of toxic oxygen species, changes in the ionic homeostasis and altered kinase/phosphatase activity. The subsequent formation of neurofibrillary Tau tangles causes neuronal dysfunction and death. Mutations in the PSEN1, PSEN2 and APP gene, as observed in FAD, enhance the generation of aberrant Aβ aggregates (modified after (Karran et al. 2011, Reitz 2012)).

The amyloid cascade hypothesis has been supported by the identification of genetic disorders, risk factors and by functional studies, which emphasize the central importance of Aβ in the etiology of AD.

AD associated mutations were found in the APP gene (chromosome 21), the PSEN1 gene (chromosome 14) and the PSEN2 gene (chromosome 1), which are directly involved in the generation of Aβ peptides. Pathogenic mutations in the APP, PSEN1 and PSEN2 genes are causative for an early disease onset in FAD patients (Goate *et al.* 1991, Sherrington *et al.* 1995, Levy-Lahad *et al.* 1995, Karran et al. 2011, Tanzi 2012). Furthermore, a protective mutation in the APP gene (A673T) has been associated with reduced Aβ production and an absence of amyloid pathology (Peacock *et al.* 1993, Jonsson *et al.* 2012, Benilova *et al.* 2014, Maloney *et al.* 2014). Last, trisomy of chromosome 21 in Down syndrome patients causes neuropathological changes as observed in AD, which has been attributed to enhanced Aβ production as a result of the additional APP gene (Wisniewski *et al.* 1985, Leverenz & Raskind 1998, Schellenberg & Montine 2012). Importantly, Tau mutations cause Fronto-temporal dementia, not AD (Goedert & Jakes 2005).

Further evidence for the amyloid cascade hypothesis was provided by the discovery of Aβ related risk factor genes in AD. The most prominent candidate is apolipoprotein E (ApoE), which has been shown to bind to Aβ and to affect many pathogenic mechanisms in AD, such as Aβ aggregation and Aβ clearance (Strittmatter *et al.* 1993, Naslund *et al.* 1995, Jiang *et al.* 2008, Kim *et al.* 2009, Schellenberg & Montine 2012, Heneka et al. 2015). The three human ApoE isoforms, ApoE2, ApoE3 and ApoE4 have been associated with an reduced risk (ε2 allele), a neutral risk (ε3 allele) and an increased risk (ε4 allele) for the development of AD (Corder *et al.* 1994, Farrer *et al.* 1997, Kim et al. 2009, Schellenberg & Montine 2012). Inheritance of the ε4 allele increases the AD risk 2-3 fold in heterozygous carrier and approximately 12 fold in homozygous carrier (Roses 1996, Kim et al. 2009, Schellenberg & Montine 2012).

In accordance with the amyloid cascade hypothesis, functional studies have supported direct and downstream effects of Aβ on the neuropathological events in AD. Aβ peptides have been shown to disrupt synaptic plasticity in transgenic mice, which could be successfully prevented by Aβ targeted compound and antibody treatment (Hsia *et al.* 1999, Chapman *et al.* 1999, Walsh *et al.* 2002, Klyubin *et al.* 2005, Shankar *et al.* 2008, Palop & Mucke 2010, Benilova *et al.* 2012, Muller-Schiffmann *et al.* 2016). Microglia and astrocytes, which contribute to the maintenance of synapse function in the brain, release proinflammatory cytokines upon binding of Aβ in human and transgenic mice (Araque *et al.* 1999, El Khoury *et al.* 2003, Heneka *et al.* 2005, Stewart *et al.* 2010, Verkhratsky *et al.* 2010, Ji *et al.* 2013,

Heneka et al. 2015) [Figure 2 C,D]. Cytokine concentrations have been correlated with Aβ levels in a transgenic AD mouse model (Patel *et al.* 2005). Furthermore, Aβ induced activation of microglia and astrocytes was shown to trigger the production of neurotoxic reactive oxygen species, including nitric oxide (NO), superoxide (O_2^-), peroxynitrite (NO_3^-) and hydrogen peroxide (H_2O_2), in primary cell culture studies, transgenic mice and *post mortem* brains of AD patients (Meda *et al.* 1995, Vodovotz *et al.* 1996, Bal-Price *et al.* 2002, Jekabsone *et al.* 2006, Heneka et al. 2005, Heneka et al. 2015). A downstream effect of Aβ on Tau hyperphosphorylation and subsequent neurofibrillary tangle formation was observed by cerebral injection of Aβ in mice, in APP and Tau double transgenic mice and by Aβ treatment of cultured neurons (Gotz *et al.* 2001, Lewis *et al.* 2001, Rapoport *et al.* 2002). Tau hyperphosphorylation is associated with reduced tubulin binding and subsequent destabilisation of microtubules, which is believed to suppress sufficient intracellular and axonal transport of nutrients and to disrupt the structural integrity of neurons (Iqbal *et al.* 1986, Alonso *et al.* 1994, Li *et al.* 2007, Iqbal et al. 2009, Herrup et al. 2013). Aβ deposition was also observed to precede tangle formation in a transgenic mouse model (Oddo *et al.* 2003). Complementary, Aβ directed immunotherapy or a genetically induced reduction in Aβ levels simultaneously lead to a clearance of phosphorylated Tau (Oddo *et al.* 2004, Chabrier *et al.* 2012, Muratore *et al.* 2014). Furthermore, Aβ induced behavioural deficits in APP transgenic mice were prevented by a Tau knockout (KO), clearly indicating a downstream effect of Aβ (Roberson *et al.* 2007). The amyloid cascade hypothesis has been challenged with special regard to its linearity and emphasis on Aβ as the molecular culprit of AD. Amyloid deposition has also been observed in about 20 % - 40 % of cognitive healthy elderly persons aged 60 – 90 years, which has been interpreted as a challenge to the amyloid cascade hypothesis (Aizenstein *et al.* 2008, Price *et al.* 2009, Villemagne *et al.* 2013, Herrup 2015). However, significantly higher Aβ burdens were observed in cognitive declined patients compared to cognitive healthy controls (Villemagne et al. 2013). Furthermore, longitudinal studies have demonstrated a correlation of high Aβ deposits in cognitive healthy elderly persons with a significantly faster rate of cognitive decline in comparison to low Aβ levels (Stomrud *et al.* 2010, Villemagne *et al.* 2011, Lim *et al.* 2013, Villemagne et al. 2013).
Taken together, the observations from genetic studies and pathologic events in AD favour a major contribution of the Aβ peptide and strongly support the amyloid cascade hypothesis.

1.3 APP processing and generation of Aβ peptides

The generation of Aβ peptides is a central event in the pathology of AD. Aβ peptides are proteolytic cleavage products of APP, a ubiquitously expressed type I transmembrane protein. The APP gene is located on chromosome 21 and consists of 19 exons (Kang *et al.* 1987, De Strooper & Annaert 2000). Following translation, APP undergoes posttranslational modifications, including N- and O-glycosylation, sulfation and phosphorylation in the endoplasmic reticulum (ER), Golgi compartments and at the cell surface (Weidemann *et al.* 1989, Hung & Selkoe 1994, Suzuki *et al.* 1994b, Walter *et al.* 1997, De Strooper & Annaert 2000). By alternative splicing of exons 7, 8 and 15, APP isoforms are generated, which do (APP-751, APP-770) or do not (APP-695) contain a Kunitz-type protease inhibitor domain (KPI) (Kitaguchi *et al.* 1988, Ponte *et al.* 1988, Mattson 1997, De Strooper & Annaert 2000) [Figure 4].

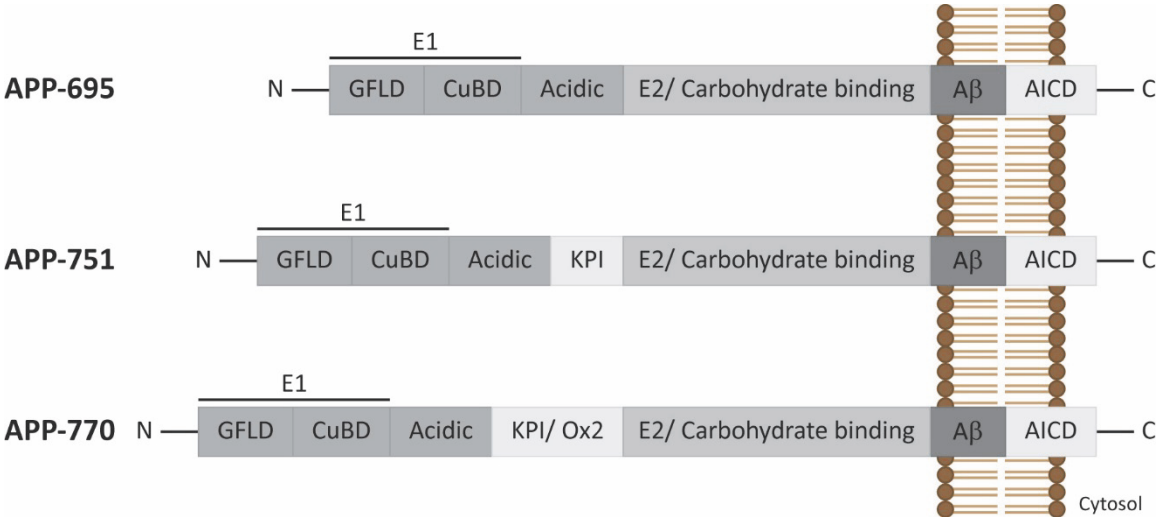

Figure 4: APP isoforms, generated by alternative splicing. GFLD: N-terminal growth factor like domain; CuBD: copper-binding domain; Acidic: domain with a high content of acidic amino acids; KPI: Kunitz-type protease inhibitor domain; Ox2: Ox2 antigen-like domain; E2: Conserved region of the central APP domain; AICD: APP intracellular domain (modified after (Jefferson *et al.* 2011)).

APP-695 is the predominant isoform in the brain, whereas APP-751 and APP-770 are mostly expressed in non-neural tissues (e.g. muscle, kidney and heart). Within the brain, cell-type specific APP isoform expression was found. APP-695 is almost exclusively expressed in neurons, whereas APP-751 and APP-770 are mainly expressed in glial cells, including

astrocytes, microglia and oligodendrocytes (Konig *et al.* 1992, Forloni *et al.* 1992, Mattson 1997). Several physiological functions have been postulated for APP (Turner *et al.* 2003, Wolfe & Guenette 2007, Zheng & Koo 2011, Nhan *et al.* 2015). For example, because of the structural resemblance of the N-terminal APP growth factor like domain (GFLD) to ligand recognition sites in growth factors and type I membrane receptors, APP was proposed to be a growth factor or cell surface receptor (Kang et al. 1987, Reinhard *et al.* 2005, Coburger *et al.* 2014, Deyts *et al.* 2016). This was supported by the observation that APP stimulates neurite outgrowth and proliferation as well as by the identification of several ligand-like binding partners, including Aβ (Ohsawa *et al.* 1997, Ohsawa *et al.* 1999, Lorenzo *et al.* 2000, Lu *et al.* 2003, Reinhard et al. 2005, Zheng & Koo 2011). APP was also identified as a cell adhesion molecule connecting the pre- and the postsynapse by the formation of APP *trans*-dimers via interaction of their E1 domains. This has been demonstrated in mice by an APP KO either at the pre- or the postsynape and *in vitro* by the deletion of the E1 domain (Soba *et al.* 2005, Wang *et al.* 2009, Stahl *et al.* 2014, Klevanski *et al.* 2014). APP KO mice are viable, but show deficits in grip strength and locomotion as well as impaired learning and memory (Dawson *et al.* 1999, Muller *et al.* 1994, Zheng *et al.* 1995, Tremml *et al.* 2002, Senechal *et al.* 2008).

APP is processed in two consecutive cleavage events by different proteases: 1. shedding and release of the large APP ectodomain into the extracellular space and 2. intramembrane cleavage of the remaining membrane-bound C-terminal fragment, resulting in the release of the APP intracellular domain (AICD) into the cytosol and the secretion of the small Aβ peptides into the extracellular space (Lichtenthaler *et al.* 2011) [Figure 5].

The first cleavage event either leads into the non-amyloidogenic or the amyloidogenic pathway, the latter being responsible for the generation of the pathogenic Aβ peptides.

Two competing proteases, ADAM10 (a disintegrin and metalloprotease domain-containing protein 10) and BACE1 (β-site APP cleaving enzyme, also known as β-secretase) are involved in the shedding of the APP ectodomain (Kuhn *et al.* 2010, Jorissen *et al.* 2010, Lichtenthaler et al. 2011). So called α-cleavage of APP by ADAM10 results in the formation of the soluble APPsα ectodomain, as well as the membrane bound C83 fragment (C-terminal 83 amino acids of APP). Alternatively, β-cleavage of APP by BACE1 leads to the formation of the slightly shorter, soluble APPsβ ectodomain and the membrane bound C99 fragment (C-terminal 99 amino acids of APP).

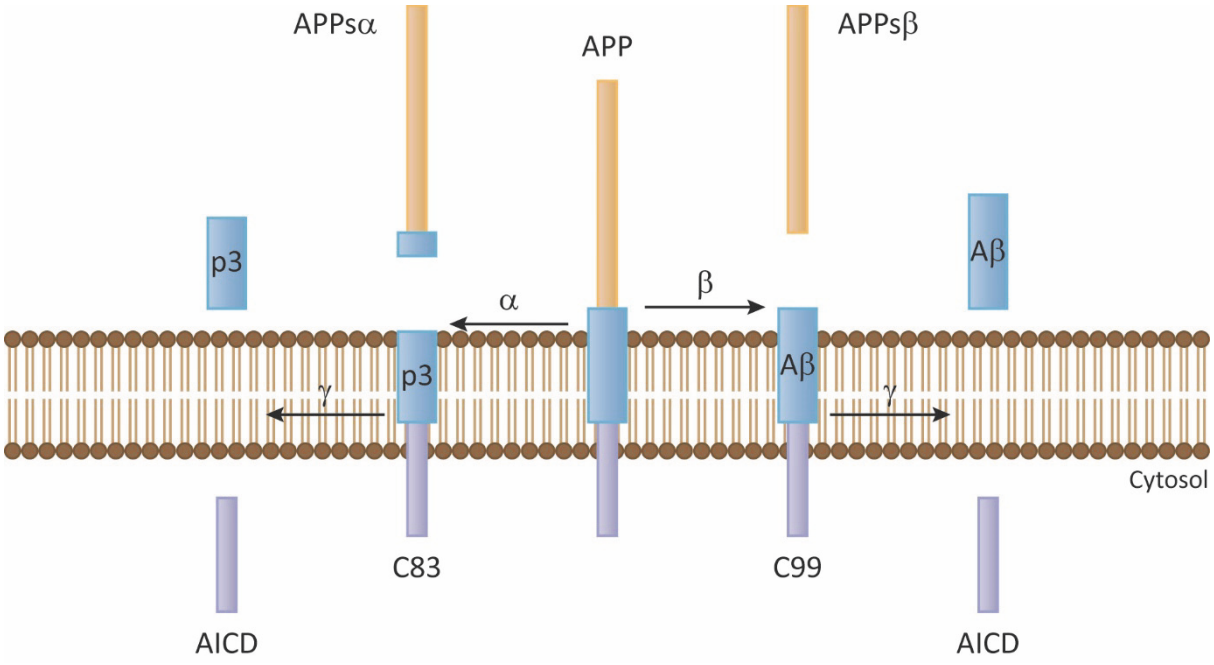

Figure 5: APP processing. APP α-cleavage by ADAM10 releases the APPsα ectodomain and generates a membrane bound C83 fragment (83 amino acids of the APP C-terminus) which is subsequently cleaved into a p3 and the AICD fragment by the γ-secretase complex. APP β-cleavage by BACE1 generates APPsβ and a C99 fragment, which is cleaved by the γ-secretase complex into the AICD fragment and the Aβ peptides. APP processing by α-cleavage prevents the formation of the toxic Aβ species and is thus referred to as the non-amyloidogenic pathway whereas β-cleavage is referred to as amyloidogenic pathway (modified after (Lichtenthaler et al. 2011)).

Subsequently, the membrane bound APP C83 and C99 fragments are both cleaved by the intramembrane protease γ-secretase.

Cleavage of the APP C83 and C99 fragments by γ-secretase leads to the release of the AICD into the cytosol and to the secretion of a small peptide, which is the non-pathogenic p3 peptide in case of the APP C83 fragment or the pathogenic Aβ peptide in case of the APP C99 fragment, into the extracellular space (Dulin *et al.* 2008, Lichtenthaler et al. 2011). Initially, γ-secretase acts as an endopeptidase and cleaves close to the cytoplasmic border of the APP substrate [Figure 6]. This cleavage event, which has been termed ε-cleavage, occurs at two different sites and leads to the generation of Aβ48 and Aβ49 peptides (Gu *et al.* 2001, Weidemann *et al.* 2002). Consistent with the detection of these two long Aβ peptides, two corresponding AICD fragments were identified by mass spectrometry (Gu et al. 2001, Sato *et al.* 2003). Shorter Aβ peptides are then generated by a carboxypeptidase activity of γ-secretase, which cleaves the Aβ48 and Aβ49 peptides sequentially at their C-termini,

approximately after every third amino acid. In the major product line, Aβ49 is cleaved into Aβ46, Aβ43, Aβ40 and Aβ37. In the minor product line, Aβ48 is cleaved into Aβ45, Aβ42 and Aβ38 (Funamoto *et al.* 2004, Qi-Takahara *et al.* 2005, Zhao *et al.* 2005, Haass & Selkoe 2007, Takami *et al.* 2009, Lichtenthaler et al. 2011, Chavez-Gutierrez et al. 2012) [Figure 6].

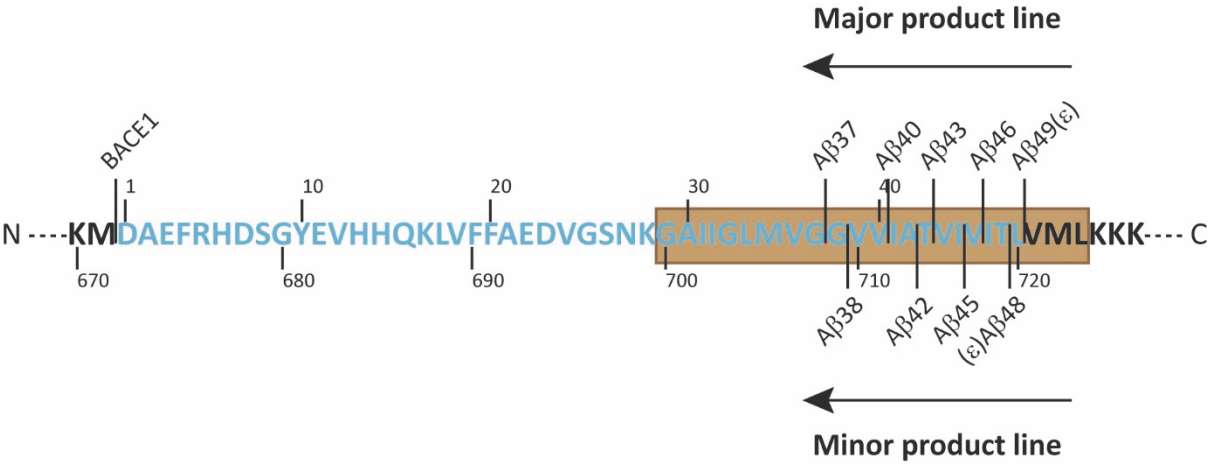

Figure 6: Sequential Aβ processing by γ-secretase. Following APP cleavage by BACE1, the remaining membrane-bound C99 fragment is cleaved by γ-secretase, first at the ε-cleavage site and continuing with consecutive cleavages approximately after every third amino acids. Starting with the initially produced Aβ49 and Aβ48 peptides, shorter Aβ peptides are produced in the major and the minor product lines. Blue: Amino acid sequence of the Aβ peptide. Brown: APP transmembrane domain (modified after (Lichtenthaler et al. 2011, Weggen & Beher 2012)).

Among the varying secreted Aβ peptides, Aβ42 is considered to be the most pathogenic species, since neuropathological studies of *post mortem* brains have demonstrated that Aβ42 peptides deposit first during AD and that they form the highly insoluble core of Aβ plaques (Iwatsubo *et al.* 1994, Gravina *et al.* 1995, Mann *et al.* 1996). A stronger tendency for aggregation in comparison to shorter Aβ peptides was also demonstrated *in vitro* (Jarrett *et al.* 1993, Jarrett & Lansbury 1993). Studies of transgenic mice that exclusively expressed either Aβ42 or Aβ40 also supported the importance of Aβ42 for the amyloid pathology, since only Aβ42 mice, but not Aβ40 mice, developed insoluble amyloid plaques (McGowan *et al.* 2005). Importantly, while for a long time it was thought that the absolute production of either total Aβ or Aβ42 is most important for the development of the amyloid pathology and AD, it has now been recognised that qualitative changes in Aβ production are at least as important as quantitative changes. An increase in the Aβ42/Aβ40 ratio appears to be the

most critical parameter for Aβ aggregation. This increase might be achieved either by an enhanced Aβ42 production or a decreased Aβ40 production (De Strooper 2007, Wolfe 2007, Chavez-Gutierrez et al. 2012).

1.4 The γ-secretase complex

The intramembrane protease γ-secretase is an aspartyl-type protease complex, consisting of four subunits presenilin (PSEN), nicastrin (Nct), Aph-1 (anterior pharynx-defective-1) and Pen-2 (presenilin enhancer-2) in an equal stoichiometry (Edbauer *et al.* 2003, Fraering *et al.* 2004, De Strooper 2003, Sato *et al.* 2007) [Figure 7].

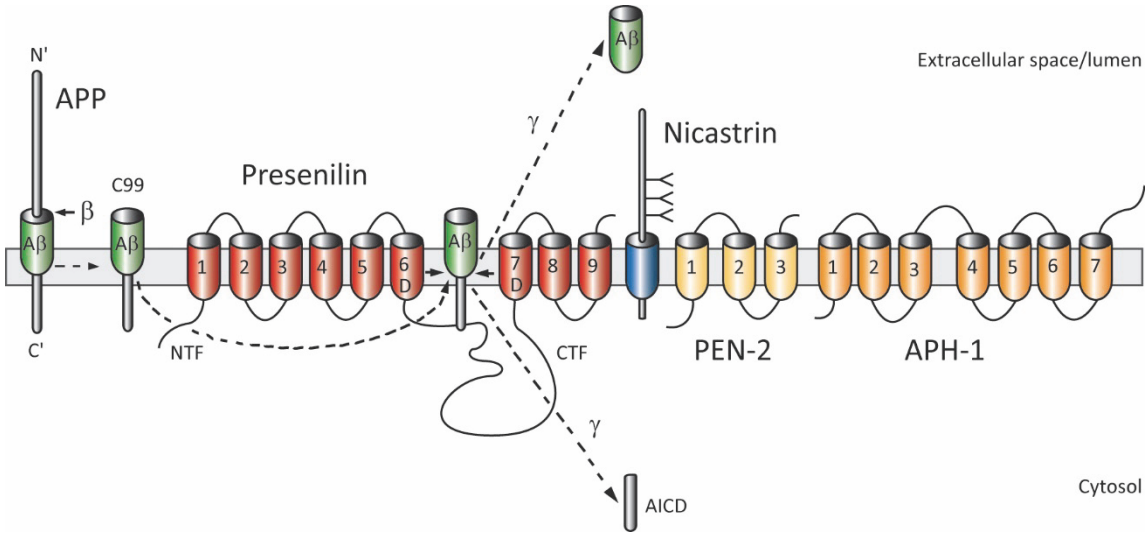

Figure 7: The γ-secretase complex consists of four subunits: PSEN1 (presenilin), Nct (nicastrin), Pen-2 (presenilin enhancer-2) and Aph-1 (anterios pharynx-defective-1). PSEN is the catalytic subunit and contains two aspartates, located in TMDs 6 and 7. Upon assembly of the γ-secretase complex, endoproteolytic cleavage of PSEN occurs within the cytoplasmic loop between TMDs 6 and 7, resulting in a PSEN N-terminal fragment (NTF) and a C-terminal fragment (CTF), which remain non-covalently attached (modified after (Haass & Selkoe 2007)).

PSEN is a ~ 50 kDa protein that contains 9 transmembrane domains (TMDs). The two PSEN homologues PSEN1 and PSEN2 share ~ 63 % overall amino-acid identity with up to 95 % homology within the TMDs (Rogaev *et al.* 1995, Haass 1997). Reduced Aβ generation in PSEN1 KO and completely abolished Aβ generation in PSEN1/PSEN2 double-KO cells have

revealed that PSEN is the catalytic subunit of the γ-secretase complex (De Strooper *et al.* 1998, Herreman *et al.* 2000, Zhang *et al.* 2000). Nct is a ~ 130 kDa type I transmembrane protein with a large glycosylated extracellular domain, which might play a role in γ-secretase substrate recognition (Shah *et al.* 2005, Xie *et al.* 2014, Sun *et al.* 2015). Aph-1 is a 25 kDa protein with 7 TMDs that stabilizes the γ-secretase complex (Xie et al. 2014). Three distinct Aph-1 isoforms have been identified: Aph-1a, Aph-1aL and Aph-1b (Francis *et al.* 2002). Despite their rather low amino-acid homology of ~ 44 %, they share an overall similar structure (De Strooper & Annaert 2010). Finally, Pen-2 is a ~ 12 kDa protein that contains 3 TMDs and is required for maturation of presenilin and γ-secretase activity (Sun et al. 2015).

The γ-secretase complex assembles in the ER and Golgi apparatus. According to current models, immature Nct and Aph-1 form a precursor complex in the ER (Takasugi *et al.* 2003, LaVoie *et al.* 2003, Shirotani *et al.* 2004, Steiner *et al.* 2008). Maturation of Nct is initiated by subsequent binding of PSEN (Edbauer *et al.* 2002, Leem *et al.* 2002, Takasugi et al. 2003).

Finally, upon binding of Pen-2, PSEN is endoproteolytically cleaved between TMDs 6 and 7 within its large cytosolic loop domain, resulting in the generation of an N-terminal fragment (NTF) and a C-terminal fragment (CTF) and subsequent catalytic activation of the γ-secretase complex (Thinakaran *et al.* 1996, Ratovitski *et al.* 1997, Hu & Fortini 2003, Takasugi et al. 2003, Haass 2004, Prokop *et al.* 2004, Brunkan *et al.* 2005). Following assembly, the mature γ-secretase complex is released from the ER/Golgi and predominantly localizes at the plasma membrane and in endo-somal/lysosomal compartments (Kaether *et al.* 2006, Steiner et al. 2008, Sannerud *et al.* 2016).

The γ-secretase was revealed to be an aspartyl protease when it was demonstrated that mutagenesis of the two conserved aspartyl residues in PSEN1 TMDs 6 (D257) and 7 (D385) and the corresponding conserved aspartyl residue on PSEN2 TMD 7 (D366) abolished the proteolytic activity of the complex (Wolfe *et al.* 1999, Steiner *et al.* 1999). Furthermore, the active site of the catalytic D385 residue in PSEN1 TMD 7 is embedded in a GxGD signature motif, which does not correspond to the classical D(T/S)G(T/S) signature motif of aspartyl proteases, but is highly conserved among the aspartyl proteases of the signal peptide peptidase (SPP) and type 4 prepilin peptidase (TFPP) family (Steiner *et al.* 2000, Haass & Steiner 2002, Perez-Revuelta *et al.* 2010).

1.5 Regulated intramembrane proteolysis

Enzymatic cleavage of peptide bonds by an aspartyl protease is a chemical reaction that requires the presence of water (Suguna *et al.* 1987) [Figure 8].

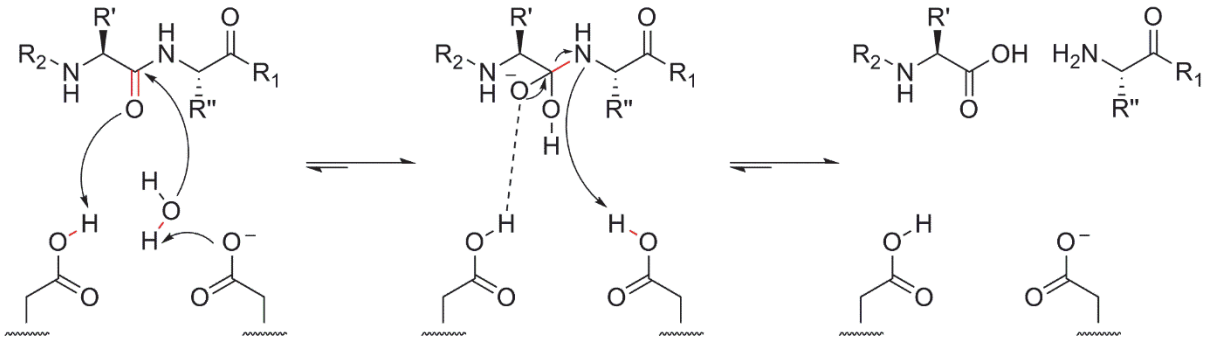

Figure 8: Cleavage mechanism of a peptide bond by an aspartyl protease. The water molecule between the two aspartate residues is activated by the abstraction of hydrogen and performs a nucleophilic attack on the carbonyl carbon of the peptide bond. An oxyanion tetrahedral intermediate is formed and enables the protonation of the scissile amide nitrogen. Subsequent rearrangement leads to the cleavage of the peptide bond. Chemical bonds that are changed during the proteolysis are highlighted in red (modified after (Suguna et al. 1987)).

Consequently, the catalytic domains of proteases are usually located within an aqueous compartment. However, PSEN1 the catalytic subunit of the γ-secretase complex is embedded in the hydrophobic membrane. Thus the question is how intramembrane proteolysis is facilitated.

Cysteine-scanning mutagenesis experiments have revealed that the catalytic aspartates D257 and D385 are exposed to water within a hydrophilic pore, which is formed inside the membrane with contributions from the PSEN1 TMDs 6 and 7 (Tolia *et al.* 2006, Sato *et al.* 2006). The existence of a water-accessible cavity was confirmed by cross-linking experiments and electron microscopy (Sato et al. 2006, Sato *et al.* 2008, Tolia *et al.* 2008, Renzi *et al.* 2011). Recently, an atomic structure of the human γ-secretase complex at 3.4 Å resolution was determined by single-particle cryo-electron microscopy. The 20 TMDs of the γ-secretase complex (PSEN1: 9 TMDs, Nct: 1 TMD, Aph-1: 7 TMDs and Pen-2: 3 TMDs) were shown to assemble in a horseshoe-shaped structure (Lu *et al.* 2014, Bai *et al.* 2015) [Figure 9].

At the thick end of the horseshoe, TMDs 1, 5 and 7 of Aph-1 interacted with the TMD of Nct. The TMDs 2 and 4 of Aph-1 associated with TMDs 8 and 9 of PSEN1 at the centre of the

structure. At the thin end, TMD 4 of PSEN1 interacted with the 3 TMDs of Pen-2. The large Nct ectodomain interacted with both ends of the horseshoe (Bai et al. 2015).

The catalytic aspartate residues D257 and D385 in PSEN1 TMDs 6 and 7 and the P433, A434 and L435 residues of the PAL signature motive, located in TMD 9, faced a cavity at the centre of the horseshoe-structure (Lu et al. 2014, Bai et al. 2015). The PAL motive is assumed to play a role in γ-secretase substrate recognition (Wang *et al.* 2004, Wang *et al.* 2006a, Sato et al. 2008). The distance between D257 and D385 measured approximately 10.6 Å, which is considerably wider than in other active aspartyl proteases.

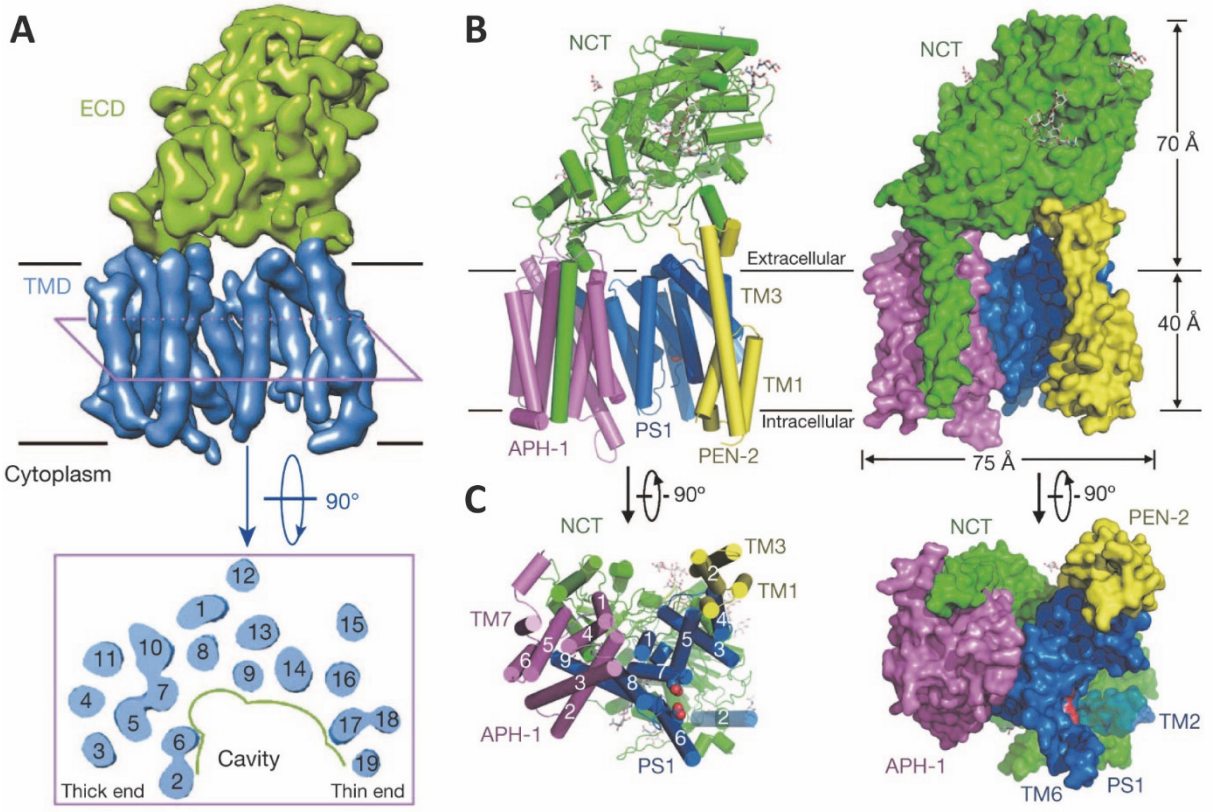

Figure 9: Structure of the human γ-secretase complex as determined by cryo-electron microscopy. (**A**) Lower resolution structure of 4.5 Å. The TMDs of the γ-secretase complex are highlighted in blue, the Nct ectodomain (ECD) is highlighted in green. The 20 TMDs of the γ-secretase complex are assembled around a water-filled cavity within the membrane in a horseshoe-shaped structure (figure was adopted from (Lu et al. 2014)). (**B**) Higher resolution structure at 3.4 Å. Visualisation of the γ-secretase structure in cartoon (left) and surface view (right). N-glycans, attached to the surface of the Nct ECD, are displayed in stick. (**C**) Perpendicular view of the γ-secretase structure from the intracellular side of the lipid membrane. The flexible TMD 2 of PSEN1 (here named PS1) is displayed as semi-transparent. The catalytic aspartate residues D257 and D385 in the PSEN1 TMDs 6 and 7 are highlighted in red (figures B and C were adopted from (Bai et al. 2015)).

It was therefore proposed that substrate binding triggers a closer alignment of the aspartates by a conformational change of the protease, thereby facilitating catalysis (Bai et al. 2015) [Figure 10 A].

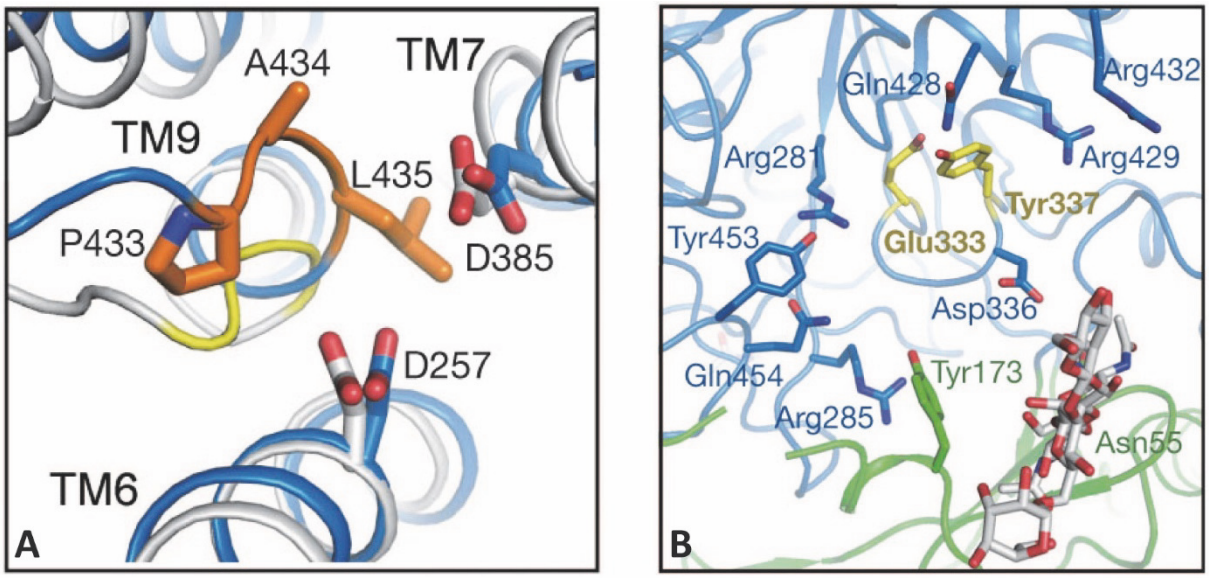

Figure 10: (**A**) The catalytic PSEN1 aspartate residues D257 and D385 are located in close proximity to the residues of the PAL signature motif (P433, A435, L435) in TMD 9, which is assumed to play a role in substrate recognition. (**B**) Nicastrin residues E333 and Y337, which might be responsible for γ-secretase substrate recruitment, are surrounded by several charged and polar residues in a hydrophilic pocket, which is the putative substrate binding site (figures were adopted from (Bai et al. 2015)).

The cryo-electron microscopy structure also revealed that the Nct ectodomain is located immediately above the central cavity and itself harboured a hydrophilic pocket. The Nct residues E333 and Y337, which are assumed to be responsible for γ-secretase substrate recruitment, were buried in this hydrophilic pocket, suggesting that this might be the substrate-binding site (Shah et al. 2005, Dries *et al.* 2009, Lu et al. 2014, Bai et al. 2015) [Figure 10 B].

1.6 Putative PSEN functions beyond its protease activity

PSEN might be involved in several cellular processes besides its role as the catalytic subunit of the γ-secretase complex. These include protein trafficking, autophagy and ER Ca^{2+} regulation (Parks & Curtis 2007, De Strooper & Annaert 2010, Sepulveda-Falla *et al.* 2014, Duggan & McCarthy 2016). Trafficking of several proteins, including N-cadherin (neuronal cadherin; also known as CDH2), the intercellular adhesion molecule 5 (ICAM5; also known as telencephalin), epidermal growth factor receptor (EGFR) and β1 integrin appeared to be disrupted in PSEN1 deficient cells (Uemura *et al.* 2003, Esselens *et al.* 2004, Parks & Curtis 2007, Repetto *et al.* 2007, Zou *et al.* 2008, De Strooper & Annaert 2010). Aberrant protein trafficking and subsequent protein accumulation in diverse cellular compartments was independent of γ-secretase activity. This was proven by the utilisation of either γ-secretase inhibitors or catalytically-dead PSEN1 mutants, which did not induce trafficking defects and protein accumulation as observed in PSEN1 deficient cells.

A potentially related γ-secretase independent function of PSEN1 is its involvement in autophagy, the major lysosomal pathway for the degradation of cytosolic protein aggregates and organelles, which are too large to be degraded by the proteasome (Rubinsztein 2006, Mizushima 2007, Klionsky 2007, Lee *et al.* 2010, Neely *et al.* 2011). During autophagy, a cytoplasmic region is enveloped with a double-membrane to form autophagosomes, which subsequently fuse with late endosomes or lysosomes. These contain the vacuolar $[H^+]$ ATPase (v-ATPase) proton pump, which acidifies the newly created autolysosome, which is crucial for the activation of resident proteases like cathepsins (Yamamoto *et al.* 1998, Lee et al. 2010). Full length (FL) PSEN1 was suggested to bind to and modulate the N-glycosylation of the v-ATPase V0a1 subunit in the ER and to affect its delivery to the lysosomes. Delayed proteolytic clearance of autophagic substrates and their accumulation in autophagic vacuoles was observed in PSEN1 deficient cells and has been attributed to an inadequate autolysosome acidification as a result of failed V0a1 maturation (Lee et al. 2010, Wolfe *et al.* 2013). However, while endo-lysosomal dysfunction in PSEN1 deficient cells has also been observed by other laboratories, this specific molecular mechanism could not be reproduced in two other studies (Zhang *et al.* 2012, Coen *et al.* 2012).

PSEN might also be involved in the Ca^{2+} homeostasis (Green & LaFerla 2008, Mattson 2010, De Strooper & Annaert 2010). While results in PSEN1 deficient cells have been contradictory,

many studies have observed that the release of Ca^{2+} from the ER to the cytosol is exaggerated in cells expressing PSEN1 mutants associated with FAD. As a potential molecular mechanism it has been proposed that PSEN1 itself forms constitutive ER Ca^{2+} leak channels (Tu *et al.* 2006, Zhang *et al.* 2010). It was further shown that PSEN1 might physically interact with and modulate the function of two ER membrane embedded receptors that release Ca^{2+} into the cytosol: the inositol-3-phosphate activated IP_3 receptor (IP_3R) and the Ca^{2+} activated ryanodine receptor (RyR) (Chan *et al.* 2000, Hayrapetyan *et al.* 2008, Green & LaFerla 2008).

1.7 Gene mutations in familiar Alzheimer's disease

FAD is characterised by an autosomal-dominant inheritance pattern, leading to an early disease onset approximately between 30-60 years of age (Bateman et al. 2011). Mutations occur in the genes encoding APP (chromosome 21), PSEN1 (chromosome 14) and PSEN2 (chromosome 1). Carriers of these pathogenic mutations have a 95 % lifetime risk to develop AD (Loy *et al.* 2014). FAD represents less than 1 % of all AD cases. However, the clinical and pathological features are highly similar to the more common sporadic form of the disease (Bateman et al. 2011, LaFerla & Green 2012)[Table 1].

This includes established biomarkers of the disease, such as a reduction in Aβ42 levels and an increase in total Tau and phospho-Tau levels in the cerebrospinal fluid (CSF) of FAD and sporadic AD (SAD) patients (Strozyk *et al.* 2003, Mayeux *et al.* 2003, Fagan *et al.* 2007, Tapiola *et al.* 2009, Grimmer *et al.* 2009, Bateman et al. 2011, Bateman *et al.* 2012, Fagan *et al.* 2014). Nevertheless, subtle variations in the occurrence of neuropathological features have been found in the comparison of FAD and SAD patients. For instance, although amyloid deposits in the walls of cerebral vessels, as observed in cerebral amyloid angiopathy (CAA), are a common feature in both FAD and SAD, they occur more frequently in FAD patients with PSEN1 mutations or with APP mutations within the Aβ sequence (Mann *et al.* 2001, Grabowski *et al.* 2001, Kumar-Singh *et al.* 2002, Basun *et al.* 2008, Bateman et al. 2011, Schellenberg & Montine 2012). Furthermore, cotton wool plaques, which have a ball-like shape and are devoid of a dense amyloid core, were predominantly found in FAD patients with PSEN1 mutations (Steiner *et al.* 2001, Takao *et al.* 2002, Tabira *et al.* 2002, Bateman et al. 2011, Schellenberg & Montine 2012).

Table 1: Comparison of familial Alzheimer's disease (FAD) with sporadic Alzheimer's disease (SAD)
CAA: cerebral amyloid angiopathy; CSF: cerebrospinal fluid; FDG: fluorodeoxyglucose; MRI: magnetic resonance imaging; PET: positron emission tomography; PiB: Pittsburg Compound B (table adopted from (Bateman et al. 2011)).

Measure	FAD findings	SAD findings
Clinical presentation	Episodic (recent) memory and judgment impairment in most; seizures and myoclonus not rare	Episodic (recent) memory and judgment impairment in most; seizures rare in early disease, more common in late disease
Atypical presentation	Yes – behavioural presentations; spastic paraparesis	Yes – behavioural and language presentations; posterior cortical atrophy
Age of onset	< 60 years for most, can be as early as mid-20s; > 60 years rarely reported	> 60 years for most < 50 years rarely reported
Duration of illness	Average 6 to 9 years	Average 7 to 10 years
Atrophy – volumetric MRI	Hippocampal atrophy, temporo-parietal cortical loss	Hippocampal atrophy, temporo-parietal cortical loss
Hypermetabolism – FDG-PET	Temporo-pariental hypometabolism	Temporo-pariental hypometabolism
Amyloid imaging – PiB-PET	Precuneus/ posterior cingulate and prefrontal; consistent striatal binding	Precuneus/ posterior cingulate and prefrontal; less consistent striatal binding
Pathology	Plaques and tangles in all; CAA in most; Cotton wool plaques in some	Plaques and tangles in all; CAA in most
CSF Aβ42	Decreased	Decreased
CSF Tau, p-Tau181	Increased	Increased
Blood Aβ42/Aβ40 ratio	Increased	Variable

More than 300 mutations have been found so far in over 500 families, with the highest proportion in the PSEN1 gene (73 %), according to the enlisted mutations in the Alzforum Mutations Database, which is constantly updated (Loy et al. 2014, Alzforum Mutations Database). The majority of these mutations are point mutations. However, a few deletions and insertions have been found in the PSEN1 gene [Figure 11].

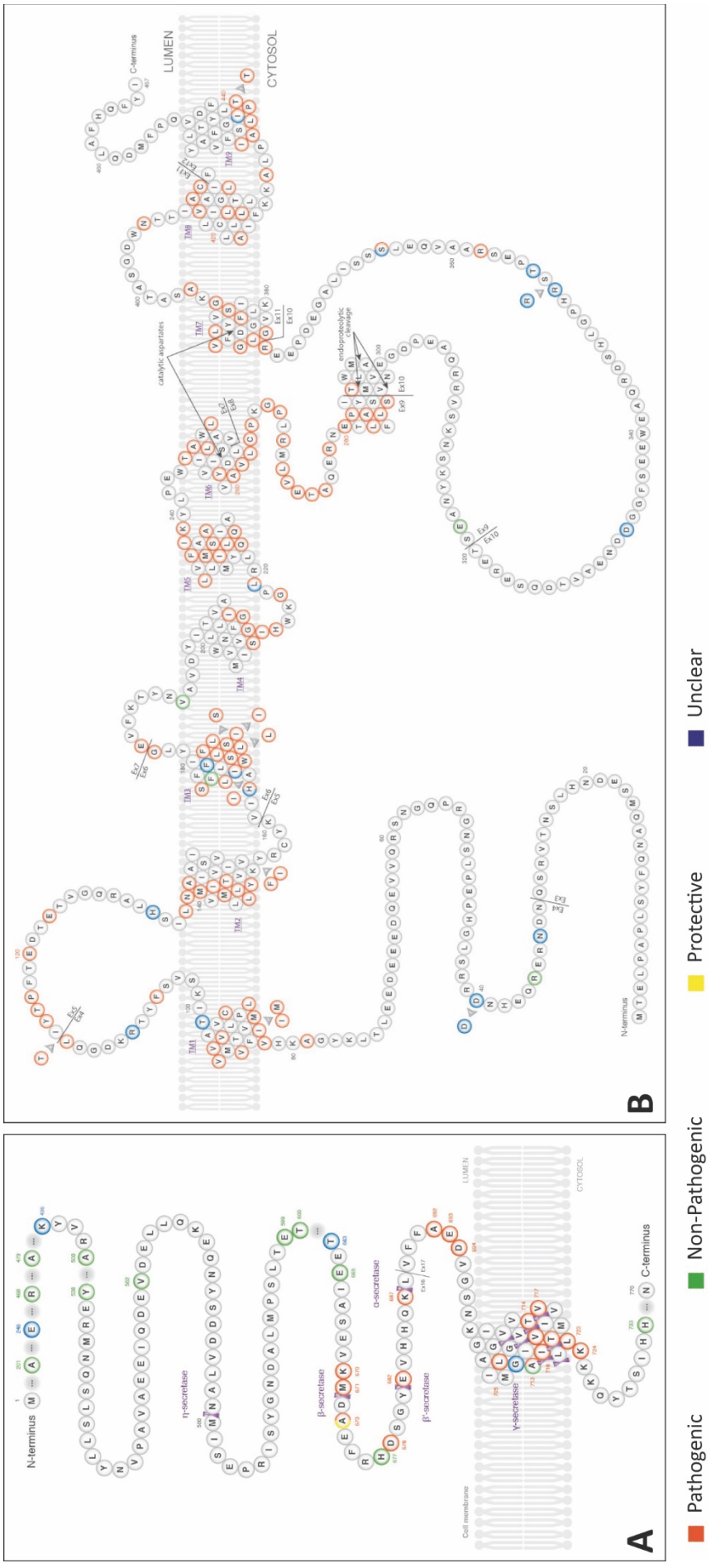

Figure 11: Amino acid sequence of the APP (**A**) and PSEN1 (**B**) proteins, including sites of mutations, insertions and deletions (figures were adopted from (Alzforum Mutations Database)).

The first FAD mutation in the APP gene, the so called “London mutation” (V717I) was discovered in an English family in 1991 (Goate et al. 1991). Soon after, further mutations at the same and other sites were discovered and it became apparent that FAD APP mutations cluster around specific regions in the Aβ sequence within the APP sequence. For instance, mutations at position V717, including the “London mutation” (V717I) and the “Indiana mutation” (V717F), as well as neighbouring mutations are located at the C-terminal end of the Aβ sequence where γ-secretase cleavage occurs. These mutations have been identified to increase the Aβ42/Aβ40 ratio (Murrell *et al.* 1991, Suzuki *et al.* 1994a, Tamaoka *et al.* 1994, Scheuner *et al.* 1996, Bergman *et al.* 2003, Hecimovic *et al.* 2004, Weggen & Beher 2012, Schellenberg & Montine 2012, Muratore et al. 2014).

Another hotspot for APP FAD mutations was found around the BACE1 cleavage site, including the “Swedish mutation” (KM670/671NL) and mutations at position A673. The “Swedish mutation” converts the APP sequence into a better substrate for BACE1 and thereby enhances Aβ levels by six- to eightfold in transfected cells and up to threefold in human fibroblasts from FAD patients (Mullan *et al.* 1992, Citron *et al.* 1992, Cai *et al.* 1993) (Citron *et al.* 1994, Weggen & Beher 2012, Schellenberg & Montine 2012). The A673V mutation is the only FAD mutations that has been reported to be recessive and that is associated with an increase in Aβ production, amyloid plaque pathology and cognitive decline only in homozygous carriers (Di Fede *et al.* 2009, Giaccone *et al.* 2010, Benilova et al. 2014, Maloney et al. 2014). Importantly, another mutation at the same position (A673T) was found to be protective against AD. This mutation caused a 40 % reduction of Aβ peptides *in vitro* as a result of reduced APP cleavage by BACE1, which might lead to a delayed Aβ aggregation in the brain and explain the absence of cognitive decline in the carriers (Peacock et al. 1993, Jonsson et al. 2012, Benilova et al. 2014, Maloney et al. 2014).

In contrast to APP, mutations in PSEN1 are scattered through the entire protein sequence with no apparent clustering in certain regions [Figure 11 B]. To clarify the pathogenic effects of PSEN1 mutations on the development of AD, a variety of *in vivo* and *in vitro* model systems have been generated and applied for a thorough investigation.

1.8 PSEN1 model systems

FAD mutations in the PSEN1 gene are heterozygous in patients. Only one of the two PSEN1 alleles harbours the mutation, whereas the second allele is wildtype (wt), leading to approximately equal expression of mutant and wt PSEN1 in the presence of two wt PSEN2 alleles (Weggen & Beher 2012). Consequently, γ-secretase complexes should contain to approximately 50 % wt and 50 % mutant PSEN1 [Figure 12].

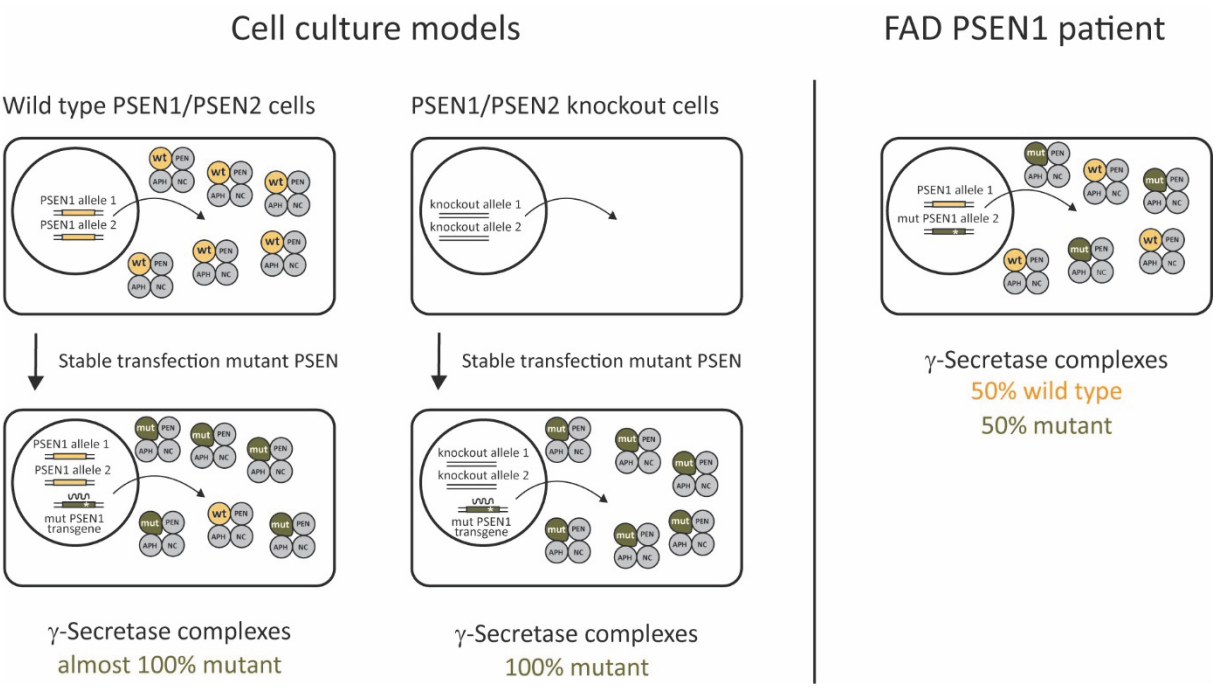

Figure 12: Cell culture models for the investigation of FAD PSEN1 mutations. The majority of cell culture models have been generated by stable overexpression of PSEN1 mutants in either established cell lines with endogenous PSEN1 and PSEN2 expression (left) or in PSEN1/PSEN2 double-KO cell lines (middle). The γ-secretase complexes in these cell lines contain close to or 100 % mutant PSEN1, either because of the displacement of wt PSEN from the endogenous γ-secretase complexes or because of the complete absence of PSEN in the double-KO cell lines. In contrast, FAD PSEN1 patients express only endogenous levels of PSEN1 and they harbour one wt and one mutant PSEN1 allele in the presence of two wt PSEN2 alleles, which should result in an equal ratio of γ-secretase complexes with wt and mutant PSEN1 (figure adopted from (Weggen & Beher 2012)).

It is important to note that an increased PSEN1 expression, in comparison to age-matched, healthy control patients, has never been observed in FAD patients (Hendriks *et al.* 1997).

Furthermore it has to be considered that an overexpression of PSEN1 does not increase the overall γ-secretase activity, since the maximum number of formed protease complexes is limited by the protein levels of the other three subunits Nct, Aph-1 and Pen-2 (De Strooper 2003, Edbauer et al. 2003, Fraering et al. 2004, Sato et al. 2007). Instead, ectopic overexpression of FAD PSEN1 mutations leads to a replacement of wt PSEN1 from the γ-secretase complexes, shifting the 50/50 ratio of wt and mutant γ-secretase complexes towards 100 % mutant γ-secretase complexes, which is in striking disagreement with the allelic representation in FAD PSEN1 patients (Thinakaran *et al.* 1997, Weggen & Beher 2012). Losing the wt γ-secretase complexes in the cell culture and mouse models that overexpress the FAD PSEN1 mutation might have a substantial influence on substrate processing, including Aβ generation, and also γ-secretase independent PSEN1 functions that needs to be considered.

Different *in vitro* and *in vivo* model systems have been generated to investigate the molecular mechanisms of FAD PSEN1 mutations on the development of AD.

Since sporadic and familiar AD share similar pathological features, it is hypothesized that the molecular mechanisms, uncovered by the utilization of FAD mutations, may be translated to the etiology of SAD (LaFerla & Green 2012).

The different model systems will be presented in the following:

(1) Overexpression of PSEN1 mutations in cells with endogenous PSEN1 and PSEN2 expression:

The most common model system for FAD PSEN1 mutations has been to stably or transiently overexpress PSEN1 mutations in cell lines with endogenous PSEN1 and PSEN2 expression [Figure 12]. Human embryonic kidney 293 (HEK293) cells, Chinese hamster ovary (CHO) cells, mouse neuroblastoma 2a (N2a) cells and green monkey kidney (COS-1) cells have been frequently used for that purpose (Borchelt *et al.* 1996, Murayama et al. 1999, Saura *et al.* 2000, Steiner et al. 2000, Moehlmann et al. 2002, Berezovska *et al.* 2005, Czirr *et al.* 2007, Page et al. 2008, Okochi *et al.* 2013, Li et al. 2016). Recently, a human neural progenitor cell line and a human stem cell line, which are capable to differentiate into mature neurons and glial cells, have also been employed (Koch et al. 2012, Choi *et al.* 2014, Kim *et al.* 2015).

The introduction and subsequent overexpression of mutant PSEN1 in this cell culture model consequently leads to a replacement of PSEN1 wt from the γ-secretase complex. Accordingly, despite its several benefits, including high availability of the mentioned permanent cell lines, low costs as well as an easy generation and maintenance, this cell culture model does not represent the heterozygous and endogenous equal expression of wt and mutant PSEN1 alleles in FAD patients. Consequently, molecular mechanisms of PSEN1 mutations, which have been uncovered with this cell culture model, might not be relevant to FAD patients and need to be interpreted with caution (Thinakaran et al. 1997, Weggen & Beher 2012).

(2) Overexpression of PSEN1 mutations in PSEN1 / PSEN2 KO cells:

In another, very common model system FAD PSEN1 mutations are stably overexpressed in either PSEN1 and PSEN2 single or double KO mouse embryonic fibroblast (MEF) cell lines (Song *et al.* 1999, Herreman et al. 2000, Shimojo et al. 2007, Bentahir et al. 2006, Heilig et al. 2013, Kretner et al. 2016). In PSEN1 / PSEN2 double-KO MEF cells, endogenous PSEN expression has been completely abolished. Consequently, an overexpression of mutant PSEN1 will result in 100 % γ-secretase complexes, which contain the introduced mutant PSEN1.
This cell culture model shares the advantages of the previously described overexpression model system regarding availability of the KO MEF cells, low costs and easy generation and maintenance. However, the presence of 100 % mutant γ-secretase complex is again in contrast to the 50 / 50 distribution of wt and mutant PSEN1 in FAD patients [Figure 12].

(3) Cell-free assays for the investigation of PSEN1 mutations:

Cell-free *in vitro* assays have been developed to specifically study the enzymatic properties of PSEN1 wt or PSEN1 mutants within the γ-secretase complex in an more simplified, isolated system that excludes factors, which have to be considered in a cellular environment, such as subcellular localisation and substrate availability, which is especially important for the validation of target specific compounds that alter the enzymatic activity of the γ-secretase complex (Weggen *et al.* 2003, Takahashi *et al.* 2003, Ebke *et al.* 2011). Kinetics of

wt and mutant γ-secretase complexes have also been studied *in vitro* (Sato et al. 2003, Kakuda *et al.* 2006, Shimojo et al. 2008, Fluhrer *et al.* 2008, Chavez-Gutierrez et al. 2012, Szaruga et al. 2015).

Although in itself cell-free, PSEN1 *in vitro* assays require the purification of γ-secretase complexes from their location in eukaryotic cellular membranes. Consequently, the PSEN1 composition of the purified γ-secretase complexes is dependent on the available PSEN1 proteins within the respective cell line or tissue samples. For example, if membranes from cell lines with PSEN1 overexpression are used for the γ-secretase purification, the ratio of wt and mutant PSEN1 will again not reflect the γ-secretase composition in FAD patients.

(4) Transgenic animals:

PSEN1 cell culture models are suitable for the investigation of γ-secretase activity, but they reach their limit for more complex investigations that require animal models, such as the development of amyloid pathology. A variety of specific mouse models have been developed to address these questions, since no single mouse model recapitulates all aspects of human AD (Philipson *et al.* 2010, Van Dam & De Deyn 2011, LaFerla & Green 2012, Webster *et al.* 2014).

The majority of transgenic animals for the investigation of FAD PSEN1 mutations have been generated by injection of a vector construct, encoding for the respective mutation, into fertilized murine eggs, leading to a promoter-driven overexpression of the PSEN1 mutation (Thinakaran et al. 1996, Duff *et al.* 1996, Borchelt et al. 1996, Citron *et al.* 1997). To investigate the contribution of FAD PSEN1 mutations to Aβ generation and plaque formation, transgenic mice overexpressing the respective FAD mutation, are usually crossbred with transgenic mice that overexpress human mutant APP, predominantly containing the APP Swedish mutation (KM670/671NL) that converts the APP sequence into a better substrate for BACE1 and thereby enhances Aβ levels by six- to eightfold (Mullan et al. 1992, Citron et al. 1992, Cai et al. 1993, Citron et al. 1994, Vassar *et al.* 1999, Lin *et al.* 2000, Philipson et al. 2010, Weggen & Beher 2012, LaFerla & Green 2012). The overexpression of PSEN1 mutants in transgenic mice again contradicts the γ-secretase composition in FAD patients and is therefore as problematic as the previously described cell culture model systems with PSEN1 overexpression.

However, a few knock-in animals with homozygous or heterozygous expression of FAD PSEN1 mutations have also been generated by genome engineering of murine embryonic stem (ES) cells via homologous recombination and subsequent transfer into the uteri of pseudo-pregnant mice (Guo *et al.* 1999, Nakano et al. 1999, Siman *et al.* 2000, Saito et al. 2011, Vidal et al. 2012, Veeraraghavalu *et al.* 2013, Xia et al. 2015).
Heterozygous knock-in mice are a good model for the investigation of FAD PSEN1 mutations, because of their equal and endogenous expression of wt and mutant PSEN1, which coincides with the allele representation in FAD patients. However, the generation of knock-in mice by homologous recombination, the subsequent breeding and maintenance is more time-consuming and expensive in comparison to cell culture models, which might explain the limited number of generated knock-in mice with FAD PSEN1 mutations.

(5) Patient-derived fibroblasts and iPS cells:

As an alternative to overexpression models, isolated fibroblasts from FAD PSEN1 patients have been used as cell culture model, either directly or after reprogramming into induced pluripotent stem (iPS) cells (Scheuner et al. 1996, Takahashi *et al.* 2007, Lee et al. 2010, Dolmetsch & Geschwind 2011, Yagi *et al.* 2011, Sproul *et al.* 2014, Mohamet *et al.* 2014, Choi *et al.* 2015, Mungenast *et al.* 2015). Fibroblasts and reprogrammed iPS cells from FAD PSEN1 patients are suitable cell culture models for the investigation of PSEN1 mutations, because of their endogenous and heterozygous PSEN1 expression. However, the insufficient availability of FAD patient samples in general, as well as the low accessibility of different FAD PSEN1 mutations and the lack of genetically matched control cells for samples from different patients are a major drawback (Bock *et al.* 2011, Weggen & Beher 2012, Soldner & Jaenisch 2012, Rouhani *et al.* 2014, Mungenast et al. 2015). Furthermore, reprogramming of isolated fibroblasts into iPS cells is highly expensive and laborious.

(6) Genome-engineered cells:

A novel approach for the generation of cell lines with genome-integrated FAD PSEN1 mutations are genomic engineering techniques that exploit cellular DNA repair mechanisms. These techniques include zinc-finger-nucleases, transcription activator-like effector nucleases (TALENs) and the Cas nuclease of the CRISPR/Cas system (clustered regularly interspaced short palindromic repeats) (Urnov *et al.* 2010, Miller *et al.* 2011, Ran *et al.* 2013). The common feature of these nucleases is the induction of a site specific, genomic DNA double-strand break to trigger cellular repair mechanisms, which either leads to a deletion, an insertion or a replacement of the targeted sequence by homologous recombination with a provided donor template that includes the desired mutation (Sander & Joung 2014). A major challenge of the zinc-finger and TALEN system is the DNA-binding specificity of the nucleases, making an extensive screening process of the engineered cell clones, to ensure the absence of undesired, genomic off-target effects, inevitable (Maeder *et al.* 2008, Juillerat *et al.* 2014). The specificity was dramatically improved in the CRISPR/Cas system by replacement of the previous protein-DNA interaction for a DNA targeting, short guiding RNA, which leads the nuclease to the target sequence (Sander & Joung 2014, Hsu *et al.* 2014, Mungenast et al. 2015). Although the efficiency of the CRISPR/Cas system is continuously improved, the introduction of site specific mutations remains so far challenging (Sander & Joung 2014, Mungenast et al. 2015, Paquet *et al.* 2016).
The TALEN system and the CRISPR/Cas system have recently been used for the heterozygous introduction of PSEN1 mutations into human iPS cells (Woodruff *et al.* 2013, Paquet et al. 2016).

1.9 The influence of PSEN1 mutations on Aβ production

The influence of mutations in the PSEN1 gene on the processing of APP and other γ-secretase substrates has been thoroughly studied in patient-derived samples, in cell culture models, in *in vitro* models and in *in vivo* mouse models, since 1995, when the first FAD PSEN1 mutations were discovered (Sherrington et al. 1995). According to the findings in the performed studies, three different hypotheses on the effect of FAD PSEN1 mutations have been postulated: (1) a gain-of-function mechanism, (2) a loss-of-function mechanism and (3) a dominant-negative effect.

Initially, an increase in the production of the Aβ42 peptide and in the Aβ42/Aβ40 ratio has been observed in the plasma and isolated fibroblasts of FAD PSEN1 patients (Scheuner et al. 1996). These observations could be reproduced in cell culture models with PSEN1 overexpression, in transgenic PSEN1 mouse models, in PSEN1 knock-in mice and in the CSF of FAD PSEN1 patients (Duff et al. 1996, Borchelt et al. 1996, Citron et al. 1997, Murayama et al. 1999, Nakano et al. 1999, Vidal et al. 2012, Potter *et al.* 2013). It was thus proposed that PSEN1 mutations selectively increase the Aβ42 production via a toxic gain-of-function mechanism.

The gain-of-function hypothesis was challenged by the observation that some FAD PSEN1 mutations reduced Aβ40 production in comparison to PSEN1 wt (Siman et al. 2000, Qi et al. 2003, Bentahir et al. 2006, Kumar-Singh et al. 2006, Shen & Kelleher 2007, Shimojo et al. 2007). Therefore, the previously observed increase in the Aβ42/Aβ40 ratio was attributed to a reduction in Aβ40 levels, rather than to an increase in Aβ42 production and a partial loss-of-function mechanism was postulated for PSEN1 mutations. Additionally, an impaired generation of AICD and NICD (NOTCH intracellular domain) by γ-secretase mediated cleavage of the substrates APP and NOTCH, which has been observed in cell lines with overexpression of PSEN1 mutations, provided further evidence for the postulated loss-of-function mechanism of FAD PSEN1 mutations (Song et al. 1999, Moehlmann et al. 2002, Chen *et al.* 2002, Walker et al. 2005).

More recent data suggested that FAD PSEN1 mutations do not cause a general loss of γ-secretase activity, but rather induce a quantitative shift in the Aβ production (De Strooper 2007, Wolfe 2007, Kuperstein *et al.* 2010, Quintero-Monzon et al. 2011, Chavez-Gutierrez et

al. 2012, Fernandez et al. 2014, Li et al. 2016). Low Aβ40 and Aβ38 levels and high Aβ42 and Aβ43 levels were observed in γ-secretase *in vitro* assays for several FAD PSEN1 mutations in comparison to wt PSEN1, indicating an impairment of the fourth γ-secretase cleavage event, converting Aβ43 into Aβ40 (major product line) and Aβ42 into Aβ38 (minor product line) (Chavez-Gutierrez et al. 2012, Szaruga et al. 2015). The accumulation of longer Aβ peptides (> Aβ42) was attributed to a reduced carboxypeptidase-like γ-secretase activity. Since biophysical and biochemical studies have shown that FAD PSEN1 mutations alter the conformation of the active site of the γ-secretase complex, it has been hypothesised that these changes might promote a premature release of Aβ43 and Aβ42 from the γ-secretase complex, thereby interrupting further sequential cleavage into Aβ40 and Aβ38 (Berezovska et al. 2005, Chavez-Gutierrez et al. 2012, Tominaga *et al.* 2016).

Last, a complete loss-of-function mechanism with a potentially dominant-negative effect of FAD PSEN1 mutations has been postulated (Heilig et al. 2010, Heilig et al. 2013, Xia et al. 2015). Almost completely abolished Aβ40, Aβ42, AICD and NICD production was observed in PSEN1/PSEN2 double-KO cell lines with induced overexpression of the FAD PSEN1 C410Y and L435F mutations and in the corresponding homozygous PSEN1 C410Y and PSEN1 L435F knock-in mice. The phenotype of both homozygous knock-in mice was similar to PSEN1/PSEN2 double-KO mice, with perinatal lethality and skeletal abnormalities, indicating a complete loss-of-function of the PSEN1 C410Y and the PSEN1 L435F mutation (Shen *et al.* 1997, Xia et al. 2015). Importantly, it should be noted that heterozygous knock-in mice, which are the actual model for heterozygous PSEN1 mutations in FAD patients, were healthy and that lethality is no general characteristic of homozygous FAD PSEN1 expression, since homozygous knock-in mice for the FAD PSEN1 mutations M164V, L166P, I213T and P264L were viable (Nakano et al. 1999, Siman et al. 2000, Vidal et al. 2012, Veeraraghavalu et al. 2013, Xia et al. 2015). Equal expression of PSEN1 wt and either PSEN1 C410Y or PSEN1 L435F in PSEN1/PSEN2 double-KO cells, which had been transfected with equal quantities of wt and mutant PSEN1, could rescue the production of Aβ40, Aβ42, AICD and NICD (Heilig et al. 2013). However, their levels remained lower in comparison to double-KO cells, which only overexpressed PSEN1 wt. It was thus postulated that heterozygous FAD PSEN1 mutations exert a trans dominant-negative effect on PSEN1 wt, reducing its catalytic activity, by physical interaction of wt and mutant PSEN1 and the putative formation of a PSEN1 dimer, which has been demonstrated in some studies by co-immunoprecipitation (Schroeter et al.

2003, Heilig et al. 2013). However, other studies have provided evidence against the formation of PSEN1 dimers or oligomers (Deng *et al.* 2006, Sato et al. 2007).

In summary, the mechanism of FAD PSEN1 mutations and their effects on Aβ generation remain highly controversial and contradictory findings have been reported for many individual mutations. A re-investigation of a large number of FAD PSEN1 mutations in an isogenic model system is absolutely necessary to examine the proposed mechanisms of PSEN1 mutations and to exclude any artefacts that might have been previously generated by the application of insufficient overexpression model systems, which do not reflect the endogenous and heterozygous expression of PSEN1 mutations in FAD patients, but nevertheless have been predominantly used in the performed studies.
Accordingly, the generation of an isogenic model system by the applications of a genomic engineering technique was the objective of this doctoral thesis.

2. Objective

Objective of this doctoral thesis was to establish an isogenic cell culture model for the investigation of FAD PSEN1 mutations. Murine ES cells, containing a reporter-tagged insertion between Exon 4 and 6 in one of the two PSEN1 alleles, were purchased from the International Mouse Phenotype Consortium (IMPC). By the application of an innovative gene-targeting strategy termed dual recombinase mediated cassette exchange (dRMCE), the reporter-tagged inserted cassette was exchanged via recombination for a murine PSEN1 exon 5-12 cDNA including partial sequence of the PSEN1 intron 4 (PSEN1 exon 4'-12) to restore expression of the conditional PSEN1 allele. The exchange was facilitated by iCre and Flpo recombinases, targeting the loxP and FRT flanked sites of the inserted cassette on the conditional PSEN1 allele, as well as on the PSEN1 cDNA. Mutations and protein-tags were easily introduced into the PSEN1 exon 4'-12 cDNA by PCR to yield a set of different replacement constructs for the recombination.
Heterozygous PSEN1 ES cell lines with endogenous expression of both PSEN1 alleles were thus created from one parental ES cell line, assuring an identical genomic background of the differentially modified PSEN1 ES cell lines.

The thesis included the following key subjects:

1. Generation of heterozygous PSEN1 ES cell lines by dRMCE:
    - Cloning and sequencing of the pDREV-1 PSEN1 exon 4'-12 constructs for dRMCE.
    - Generation of a PCR-based system for the validation of positive ES clones.
    - Validation of equal PSEN1 translation and transcription in both alleles.
2. Differentiation of ES cells into neural stem cells (NSCs).
3. Characterization of PSEN1 function within the generated heterozygous and endogenous stem cell model:
    - Investigation of putative trans dominant-negative effects of FAD PSEN1 mutations.
    - Analysis of FAD PSEN1 mutations induced changes on APP processing in comparison to PSEN1 wt.

3. Material

3.1 Cell lines

C57/Bl6/N JM8A3.01 PSEN1 parental	Male, murine ES cells, heterozygous for the Psen1 tm2a (EUCOMM) Wtsi allele. Clone ID: EPD0794_4_A06 MGI Allele ID: 1202717	(http://www.mousephenotype.org/)
C57/Bl6/N JM8A3.01 PSEN1 wt	Male, murine ES cells, endogenously expressing two PSEN1 wt alleles.	
C57/Bl6/N JM8A3.01 PSEN1 wt 3xFlag	Male, murine ES cells, endogenously expressing one PSEN1 wt allele and one PSEN1 wt 3xFlag allele.	
C57/Bl6/N JM8A3.01 PSEN1 P117L	Male, murine ES cells, endogenously expressing one PSEN1 wt allele and one PSEN1 P117L allele.	
C57/Bl6/N JM8A3.01 PSEN1 P117L + D385N	Male, murine ES cells, endogenously expressing one PSEN1 wt allele and one PSEN1 P117L + D385N allele.	
C57/Bl6/N JM8A3.01 PSEN1 N135I	Male, murine ES cells, endogenously expressing one PSEN1 wt allele and one PSEN1 N135I allele.	
C57/Bl6/N JM8A3.01 PSEN1 N135S	Male, murine ES cells, endogenously expressing one PSEN1 wt allele and one PSEN1 N135S allele.	
C57/Bl6/N JM8A3.01 PSEN1 L166P	Male, murine ES cells, endogenously expressing one PSEN1 wt allele and one PSEN1 L166P allele.	
C57/Bl6/N JM8A3.01 PSEN1 L166P 3xFlag	Male, murine ES cells, endogenously expressing one PSEN1 wt allele and one PSEN1 L166P 3xFlag allele.	
C57/Bl6/N JM8A3.01 PSEN1 L166P + D385N	Male, murine ES cells, endogenously expressing one PSEN1 wt allele and one PSEN1 L166P + D385N allele.	
C57/Bl6/N JM8A3.01 PSEN1 L166P + D385N 3xFlag	Male, murine ES cells, endogenously expressing one PSEN1 wt allele and one PSEN1 L166P + D385N 3xFlag allele.	
C57/Bl6/N JM8A3.01 PSEN1 L166P + D385N + M292D 3xFlag	Male, murine ES cells, endogenously expressing one PSEN1 wt allele and one PSEN1 L166P + D385N + M292D 3xFlag allele.	
C57/Bl6/N JM8A3.01 PSEN1 L173W	Male, murine ES cells, endogenously expressing one PSEN1 wt allele and one PSEN1 L173W allele.	

C57/Bl6/N JM8A3.01 PSEN1 L173W + D385N	Male, murine ES cells, endogenously expressing one PSEN1 wt allele and one PSEN1 L173W + D385N allele.	
C57/Bl6/N JM8A3.01 PSEN1 I213T	Male, murine ES cells, endogenously expressing one PSEN1 wt allele and one PSEN1 I213T allele.	
C57/Bl6/N JM8A3.01 PSEN1 M233V	Male, murine ES cells, endogenously expressing one PSEN1 wt allele and one PSEN1 M233V allele.	
C57/Bl6/N JM8A3.01 PSEN1 M233V + D385N	Male, murine ES cells, endogenously expressing one PSEN1 wt allele and one PSEN1 M233V + D385N allele.	
C57/Bl6/N JM8A3.01 PSEN1 M233V + D385N 3xFlag	Male, murine ES cells, endogenously expressing one PSEN1 wt allele and one PSEN1 M233V + D385N 3xFlag allele.	
C57/Bl6/N JM8A3.01 PSEN1 M233V + D385N + M292D 3xFlag	Male, murine ES cells, endogenously expressing one PSEN1 wt allele and one PSEN1 M233V + D385N + M292D 3xFlag allele.	
C57/Bl6/N JM8A3.01 PSEN1 R278I	Male, murine ES cells, endogenously expressing one PSEN1 wt allele and one PSEN1 R278I allele.	
C57/Bl6/N JM8A3.01 PSEN1 E280A	Male, murine ES cells, endogenously expressing one PSEN1 wt allele and one PSEN1 E280A allele.	
C57/Bl6/N JM8A3.01 PSEN1 M292D + D385N	Male, murine ES cells, endogenously expressing one PSEN1 wt allele and one PSEN1 M292D + D385N allele.	
C57/Bl6/N JM8A3.01 PSEN1 ΔHL	Male, murine ES cells, endogenously expressing one PSEN1 wt allele and one PSEN1 ΔHL (Loop deletion G330-L369) allele.	
C57/Bl6/N JM8A3.01 PSEN1 G384A	Male, murine ES cells, endogenously expressing one PSEN1 wt allele and one PSEN1 G384A allele.	
C57/Bl6/N JM8A3.01 PSEN1 D385N	Male, murine ES cells, endogenously expressing one PSEN1 wt allele and one PSEN1 D385N allele.	
C57/Bl6/N JM8A3.01 PSEN1 C410Y	Male, murine ES cells, endogenously expressing one PSEN1 wt allele and one PSEN1 C410Y allele.	
C57/Bl6/N JM8A3.01 PSEN1 L435F	Male, murine ES cells, endogenously expressing one PSEN1 wt allele and one PSEN1 L435F allele.	

NSC PSEN1 wt	Male, murine neural stem cells, differentiated from C57/Bl6/N JM8A3.N1 PSEN1 wt.	
NSC PSEN1 P117L	Male, murine neural stem cells, differentiated from C57/Bl6/N JM8A3.N1 PSEN1 P117L.	
NSC PSEN1 P117L + D385N	Male, murine neural stem cells, differentiated from C57/Bl6/N JM8A3.N1 PSEN1 P117L + D385N.	
NSC PSEN1 N135S	Male, murine neural stem cells, differentiated from C57/Bl6/N JM8A3.N1 PSEN1 N135S.	
NSC PSEN1 L166P	Male, murine neural stem cells, differentiated from C57/Bl6/N JM8A3.N1 PSEN1 L166P.	
NSC PSEN1 L166P + D385N	Male, murine neural stem cells, differentiated from C57/Bl6/N JM8A3.N1 PSEN1 L166P + D385N.	
NSC PSEN1 L166P + D385N 3xFlag	Male, murine neural stem cells, differentiated from C57/Bl6/N JM8A3.N1 PSEN1 L166P + D385N 3xFlag.	
NSC PSEN1 L173W	Male, murine neural stem cells, differentiated from C57/Bl6/N JM8A3.N1 PSEN1 L173W.	
NSC PSEN1 L173W + D385N	Male, murine neural stem cells, differentiated from C57/Bl6/N JM8A3.N1 PSEN1 L173W + D385N.	
NSC PSEN1 I213T	Male, murine neural stem cells, differentiated from C57/Bl6/N JM8A3.N1 PSEN1 I213T.	
NSC PSEN1 M233V	Male, murine neural stem cells, differentiated from C57/Bl6/N JM8A3.N1 PSEN1 M233V.	
NSC PSEN1 M233V + D385N	Male, murine neural stem cells, differentiated from C57/Bl6/N JM8A3.N1 PSEN1 M233V + D385N.	
NSC PSEN1 R278I	Male, murine neural stem cells, differentiated from C57/Bl6/N JM8A3.N1 PSEN1 R278I.	
NSC PSEN1 E280A	Male, murine neural stem cells, differentiated from C57/Bl6/N JM8A3.N1 PSEN1 E280A.	
NSC PSEN1 G384A	Male, murine neural stem cells, differentiated from C57/Bl6/N JM8A3.N1 PSEN1 G384A.	
NSC PSEN1 C410Y	Male, murine neural stem cells, differentiated from C57/Bl6/N JM8A3.N1 PSEN1 C410Y.	
NSC PSEN1 L435F	Male, murine neural stem cells, differentiated from C57/Bl6/N JM8A3.N1 PSEN1 L435F.	
NSC PSEN1 D385N	Male, murine neural stem cells, differentiated from C57/Bl6/N JM8A3.N1 PSEN1 D385N.	

3.2 Bacterial Strains

Strain	Genotype	
Library Efficiency *E. coli* DH5α	F⁻ Φ80*lac*ZΔM15 Δ(*lac*ZYA-*arg*F) U169 *rec*A1 *end*A1 *hsd*R17(r_k^-, m_k^+) *pho*A *sup*E44 *thi*-1 *gyr*A96 *rel*A1 λ^-	Thermo Fisher Scientific
MAX Efficiency *E. coli* DH10B	F- *mcr*A Δ(*mrr-hsd*RMS-*mcr*BC) ϕ80*lac*ZΔM15 Δ*lac*X74 *rec*A1 *end*A1 *ara*D139 Δ (*ara*, *leu*)7697 *gal*U *gal*K λ- *rps*L *nup*G /pMON14272 / pMON7124	Thermo Fisher Scientific

3.3 Virus Strains

Strain	Genotype	
APP-695 adenovirus	Ad5/CMV-APP: Human type five, E1a-deleted, replication-deficient recombinant adenovirus carrying an expression cassette for human APP-695	(Yuan *et al.* 1999)

3.4 Antibodies

3.4.1 Primary Antibodies

Name	Antigen	Species	Type	
Actin	Actin C-terminus	rabbit	Polyclonal	Sigma-Aldrich, Muenchen
Anti-βIII-tubulin	βIII-tubulin C-terminus (AA 441-448)	mouse	Monoclonal	Sigma-Aldrich, Muenchen
BACE	Human BACE residues surrounding His490	rabbit	Monoclonal	Cell-Signaling Technology
CT-15	Human Aβ C-terminus (AA 1-15)	rabbit	Polyclonal	(Hahn *et al.* 2011, Hieke *et al.* 2011)
Flag	Flag Tag	mouse	Monoclonal	Sigma-Aldrich, Muenchen
GFAP	GFAP	rabbit	Monoclonal	Sigma-Aldrich, Muenchen
Mouse anti-V5 Tag	V5 Tag	mouse	Monoclonal	Invitrogen, Karlsruhe
Nestin/ rat-401	Nestin	mouse	Monoclonal	DSHB, USA

Nicastrin	Human Nicastrin C-terminus (AA 693-709)	rabbit	Polyclonal	Sigma-Aldrich, Muenchen
O4 (IgM)	Oligodendrocyte Marker O4	mouse	Monoclonal	R&D Systems, USA
Pen-2	Human Pen-2 residues surrounding Lys11	rabbit	Polyclonal	Cell-Signaling Technology
PSEN1 CTF	Human PSEN1 C-terminus	rabbit	Polyclonal	Cell-Signaling Technology
PSEN1 NTF	Human PSEN1 N-terminus (AA 1-70)	rabbit	Polyclonal	Santa Cruz Biotechnology
Sox2	Sox2	rat	Monoclonal	eBioscience, USA

3.4.2 Secondary Antibodies

Antigen	**Conjugate**	**Species**	
Goat IgG	IRDye 800CW (A_{Em} = 795 nm)	donkey	LI-COR Biotechnology, USA
Mouse IgG	Alexa Fluor® 488 (A_{Em} = 519 nm)	goat	ThermoFisher Scientific
Mouse IgG	Alexa Fluor® 546 (A_{Em} = 573 nm)	goat	ThermoFisher Scientific
Mouse IgG	IRDye 800CW (A_{Em} = 795 nm)	goat	LI-COR Biotechnology, USA
Mouse IgM	Alexa Fluor® 488 (A_{Em} = 519 nm)	goat	ThermoFisher Scientific
Rabbit IgG	Alexa Fluor® 488 (A_{Em} = 519 nm)	goat	ThermoFisher Scientific
Rabbit IgG	IRDye 800CW (A_{Em} = 795 nm)	goat	LI-COR Biotechnology, USA
Rat IgG	Cy3 (A_{Em} = 570 nm)	goat	Millipore, USA

3.5 Plasmids

Name	
pDIRE	Addgene, (Osterwalder *et al.* 2010)
pDREV-1	Addgene, (Osterwalder et al. 2010)
pDREV-1 PSEN1 exon 4‘-12 wt	
pDREV-1 PSEN1 exon 4‘-12 wt 3xFlag	
pDREV-1 PSEN1 exon 4‘-12 P117L	
pDREV-1 PSEN1 exon 4‘-12 P117L + D385N	
pDREV-1 PSEN1 exon 4‘-12 N135I	
pDREV-1 PSEN1 exon 4‘-12 N135S	
pDREV-1 PSEN1 exon 4‘-12 L166P	
pDREV-1 PSEN1 exon 4‘-12 L166P 3xFlag	
pDREV-1 PSEN1 exon 4‘-12 L166P + D385N	
pDREV-1 PSEN1 exon 4‘-12 L166P + D385N 3xFlag	

pDREV-1 PSEN1 exon 4‘-12 L166P + M292D + D385N	
pDREV-1 PSEN1 exon 4‘-12 L166P + M292D + D385N 3xFlag	
pDREV-1 PSEN1 exon 4‘-12 L173W	
pDREV-1 PSEN1 exon 4‘-12 L173W + D385N	
pDREV-1 PSEN1 exon 4‘-12 I213T	
pDREV-1 PSEN1 exon 4‘-12 M233V	
pDREV-1 PSEN1 exon 4‘-12 M233V + D385N	
pDREV-1 PSEN1 exon 4‘-12 M233V + D385N 3xFlag	
pDREV-1 PSEN1 exon 4‘-12 M233V + M292D + D385N	
pDREV-1 PSEN1 exon 4‘-12 M233V + M292D + D385N 3xFlag	
pDREV-1 PSEN1 exon 4‘-12 R278I	
pDREV-1 PSEN1 exon 4‘-12 E280A	
pDREV-1 PSEN1 exon 4‘-12 M292D + D385N	
pDREV-1 PSEN1 exon 4‘-12 ΔHL	
pDREV-1 PSEN1 exon 4‘-12 G384A	
pDREV-1 PSEN1 exon 4‘-12 D385N	
pDREV-1 PSEN1 exon 4‘-12 D385N 3xFlag	
pDREV-1 PSEN1 exon 4‘-12 C410Y	
pDREV-1 PSEN1 exon 4‘-12 L435F	
pUC57 PSEN1 exon 4‘-12	GenScript, USA

3.6 Primer

Name	Locus	Sequence
pDREV-1 BstBI f	pDREV-1 plasmid	AGG AAC TTC GAA CCT TTC TT
pDREV-1 PacI r	pDREV-1 plasmid	TGA TCA TTA ATT AAT CCC AG
PSEN1_P117L_For	PSEN1 Exon 5	CCT CTG TAG AAT CTA CAC CCT GTT CAC AGA AGA CAC TGA GAC
PSEN1_P117L_Rev	PSEN1 Exon 5	GTC TCA GTG TCT TCT GTG AAC AGG GTG TAG ATT CTA CAG AGG
PSEN1_N135I_For	PSEN1 Exon 5	GCC CTG CAC TCG ATC CTG ATC GCG GCC ATC A
PSEN1_N135I_Rev	PSEN1 Exon 5	TGA TGG CCG CGA TCA GGA TCG AGT GCA GGG C
PSEN1_N135S_For	PSEN1 Exon 5	GCC CTG CAC TCG ATC CTG AGC GCG GCC ATC A
PSEN1_N135S_Rev	PSEN1 Exon 5	TGA TGG CCG CGC TCA GGA TCG AGT GCA GGG C
PSEN1_L166P_For	PSEN1 Exon 6	GGT CAT CCA CGC CTG GCC TAT TAT TTC ATC TCT GTT
PSEN1_L166P_Rev	PSEN1 Exon 6	AAC AGA GAT GAA ATA ATA GGC CAG GCG TGG ATG ACC
PSEN1_P166L_For	PSEN1 Exon 6	GGT CAT CCA CGC CTG GCT TAT TAT TTC ATC TCT GTT
PSEN1_P166L_Rev	PSEN1 Exon 6	AAC AGA GAT GAA ATA ATA AGC CAG GCG TGG ATG ACC
PSEN1_L173W_For	PSEN1 Exon 6	TGG CTT ATT ATT TCA TCT CTG TTG TGG CTG TTC TTT TTT TCG TTC AT
PSEN1_L173W_Rev	PSEN1 Exon 6	ATG AAC GAA AAA AAG AAC AGC CAC AAC AGA GAT GAA ATA ATA AGC CA

PSEN1_I213T_For	PSEN1 Exon 7	TGG TCG GGA TGA TTG CCA CCC ACT GGA AAG G
PSEN1_I213T_Rev	PSEN1 Exon 7	CCT TTC CAG TGG GTG GCA ATC ATC CCG ACC A
PSEN1_M233V_For	PSEN1 Exon 7	TTA TGA TCA GTG CCC TCG TGG CCC TGG TAT TTA TC
PSEN1_M233V_Rev	PSEN1 Exon 7	GAT AAA TAC CAG GGC CAC GAG GGC ACT GAT CAT AA
PSEN1_R278I_For	PSEN1 Exon 8	TGG TTG AAA CAG CTC AGG AAA TCA ATG AGA CTC TCT TTC CAG C
PSEN1_R278I_Rev	PSEN1 Exon 8	GCT GGA AAG AGA GTC TCA TTG ATT TCC TGA GCT GTT TCA ACC A
PSEN1_E280A_For	PSEN1 Exon 8	AAA CAG CTC AGG AAA GAA ATG CCA CTC TCT TTC CAG CTC TTA TC
PSEN1_E280A_Rev	PSEN1 Exon 8	GAT AAG AGC TGG AAA GAG AGT GGC ATT TCT TTC CTG AGC TGT TT
PSEN1_S290C_For	PSEN1 Exon 8/9	CTC TTT CCA GCT CTT ATC TAT TCC TGC ACA ATG GTG TGG TTG
PSEN1_S290C_Rev	PSEN1 Exon 8/9	CAA CCA CAC CAT TGT GCA GGA ATA GAT AAG AGC TGG AAA GAG
PSEN1_D292M_For	PSEN1 Exon 9	AGC TCT TAT CTA TTC CTC AAC AAT GGT GTG GTT GGT GAA TAT GGC TG
PSEN1_D292M_Rev	PSEN1 Exon 9	CAG CCA TAT TCA CCA ACC ACA CCA TTG TTG AGG AAT AGA TAA GAG CT
PSEN1_M292D_For	PSEN1 Exon 9	AGC TCT TAT CTA TTC CTC AAC AGA CGT GTG GTT GGT GAA TAT GGC TG
PSEN1_M292D_Rev	PSEN1 Exon 9	CAG CCA TAT TCA CCA ACC ACA CGT CTG TTG AGG AAT AGA TAA GAG CT
PS1 dHL for2	PSEN1 Exon 10 ΔHL	AGT GGT TCT ACG AGT GAA GAC CCG GAG GA
PS1 dHL rev2	PSEN1 Exon 10 ΔHL	TTC ACT CGT AGA ACC ACT GTC CTG TGT CT
PSEN1_G384A_For	PSEN1 Exon 11	AGA GGA GTA AAA CTT GGA CTG GCC GAT TTC ATT TTC TAC AGT GTT C
PSEN1_G384A_Rev	PSEN1 Exon 11	GAA CAC TGT AGA AAA TGA AAT CGG CCA GTC CAA GTT TTA CTC CTC T
PSEN1_D385N_For	PSEN1 Exon 11	GGA GTA AAA CTT GGA CTG GGA AAT TTC ATT TTC TAC AGT GTT C
PSEN1_D385N_Rev	PSEN1 Exon 11	GAA CAC TGT AGA AAA TGA AAT TTC CCA GTC CAA GTT TTA CTC C
PSEN1_N385D_For	PSEN1 Exon 11	GGA GTA AAA CTT GGA CTG GGA GAT TTC ATT TTC TAC AGT GTT C
PSEN1_N385D_Rev	PSEN1 Exon 11	GAA CAC TGT AGA AAA TGA AAT CTC CCA GTC CAA GTT TTA CTC C
PSEN1_C410Y_For	PSEN1 Exon 11	GGA ACA CAA CCA TAG CCT ACT TTG TAG CCA TAC TGA T
PSEN1_C410Y_Rev	PSEN1 Exon 11	ATC AGT ATG GCT ACA AAG TAG GCT ATG GTT GTG TTC C
PSEN1_L435F_For	PSEN1 Exon 12	AAG CGT TGC CAG CCT TCC CCA TCT CCA TC
PSEN1_L435F_Rev	PSEN1 Exon 12	GAT GGA GAT GGG GAA GGC TGG CAA CGC TT
PS1_3xFlag_For	PSEN1 Exon 10	GAC TAC AAA GAC CAT GAC GGT GAT TAT AAA GAT CAT GAC ATC GAT TAC AAG GAT GAC GAT GAC AAG CGC TCC ACT CCC GAG TCA AG

PS1_3xFlag_Rev	PSEN1 Exon 10	CTT GTC ATC GTC ATC CTT GTA ATC GAT GTC ATG ATC TTT ATA ATC ACC GTC ATG GTC TTT GTA GTC ATG AGG CCC CAG GTG ACT GT
PS1 Ex4_seq_for	PSEN1 Exon 4	AAT GAC AGC CAA GAA CGG CA
PS1 Ex5_seq_for	PSEN1 Exon 5	AAT CTA CAC CCC ATT CAC AG
PS1 Ex5_seq_rev	PSEN1 Exon 5	CTT GTA GCA CCT GTA TTT AT
PS1 Ex7 for	PSEN1 Exon 7	GGA AGT ATT TAA GAC CTA CA
PS1_ex12_seq_r	PSEN1 Exon 12	AGT AAT GTA AGG CAC AGG CC
F1	EUCOMM cassette before recombination	AGC AGA GCG GGT AAA CTG GC
F2-b	EUCOMM cassette before recombination	TGG AGA AAA CCT TGG GTG AG
F9	EUCOMM cassette before recombination	CCA ACC TGC CAT CAC GAG ATT
F11-b2	EUCOMM cassette after recombination; Puromycin CDS	GCA ACC TCC CCT TCT ACG AG
R2-b1	EUCOMM cassette before recombination	GCC GCT TGT CCT CTT TGT TA
R9-b	EUCOMM cassette before recombination	TGT TTT CCA TGT ATG TCT TCT GG
I1	pDIRE plasmide; iCre CDS	GAC TAC CTC CTG TAC CTG CAA GCC AG
I2	pDIRE plasmide; iCre CDS	CTG CCA ATG TGG ATC AGC ATT CTC
P1	pDIRE plasmide; iCre CDS	CAG CCT GAG CTT CGA CAT CGT GAA C
P2	pDIRE plasmide; iCre CDS	CTC AGG AAC TCG TCC AGG TAC ACC
RT-PCR_rev	EUCOMM cassette after recombination; PSEN1 Exon 11	TGG TTG TGT TCC AGT CTC CA

3.7 Reagents

3.7.1 Chemicals

30 % Acrylamide 37.5:1, Bis-acrylamide	National Diagnostics, USA
Agar	Roth, Karlsruhe
Agarose	Bio-Budget, Krefeld
Ammoniumpersulfate (APS)	Sigma-Aldrich, Muenchen

Aqua-Poly/Mount	Polysciences, Inc., USA
Bicine	Calbiochem, Darmstadt
Bis-Tris	Calbiochem, Darmstadt
Bromphenolblue	Roth, Karlsruhe
Bovine Serum Albumin (BSA)	Sigma-Aldrich, Muenchen
CHAPSO	Roth, Karlsruhe
Desoxynucleotide-tri-phosphate (dNTP)	New England Biolabs, USA
Dimethylsulfoxide (DMSO)	Sigma-Aldrich, Muenchen
Dithiothreitol (DTT)	Sigma-Aldrich, Muenchen
Dry-milk (fat free)	OXOID, GB
Ethanol	Roth, Karlsruhe
Ethylenediaminetetraacetic acid (EDTA)	Roth, Karlsruhe
Fluor Save Reagent	Calbiochem, Darmstadt
Glacial Acetic Acid	Merck, Darmstadt
Glycine	Roth, Karlsruhe
Hoechst 33258 solution	Sigma-Aldrich, Muenchen
Hydrochloric acid (HCl)	Sigma-Aldrich, Muenchen
4-(2-hydroxyethyl)-1-piperazineethanesulfonic acid (HEPES)	Sigma-Aldrich, Muenchen
Igepal (NP40)	Sigma-Aldrich, Muenchen
Imidazole	Sigma-Aldrich, Muenchen
Isopropanol	Roth, Karlsruhe
Magnesium chloride ($MgCl_2$)	Roth, Karlsruhe
2-(*N*-morpholino)ethanesulfonic acid (MES)	Roth, Karlsruhe
Methanol	Roth, Karlsruhe
Midori Green Advance DNA Stain	NIPPON Genetics EUROPE, Düren
Paraformaldehyde (PFA)	Sigma-Aldrich, Muenchen
Phosphatidylcholine (PC)	Sigma-Aldrich, Muenchen
Potassium phosphate dibasicanhydrous (K_2HPO_4)	Sigma-Aldrich, Muenchen
Potassium phosphate monobasic (KH_2PO_4)	Sigma-Aldrich, Muenchen
Protease inhibitor cocktail tablets, EDTA-free	Roche, Mannheim
Protein A/G PLUS-Agarose Immunoprecipitation Reagent	Santa Cruz Biotechnology

Random Hexamers (pd(N_6))	Thermo Fisher Scientific
Sodium azide (NaN_3)	Merck, Darmstadt
Sodium chloride (NaCl)	Roth, Karlsruhe
Sodium dodecyl sulfate (SDS)	BioRad, Munich
Sodium hydroxide (NaOH)	Merck, Darmstadt
Sucrose	Sigma-Aldrich, Muenchen
TEMED (N,N,N',N' tetramethylethylenediamine)	BioRad, Munich
TRIS	Roth, Karlsruhe
TRIS-HCl	Roth, Karlsruhe
Triton-X 100 (Surfact-Amps 20)	Pierce, Bonn
Tryptone	Roth, Karlsruhe
Tween-20	Roth, Karlsruhe
Yeast Extract	Roth, Karlsruhe

3.7.2 Cell culture reagents

Accutase® solution	Sigma-Aldrich, Muenchen
B-27 Supplement	Thermo Fisher Scientific
β-Mercaptoethanol	Thermo Fisher Scientific
BSA Fraction V (7.5 %)	Thermo Fisher Scientific
Chicken Serum	Thermo Fisher Scientific
D-Glucose	Sigma-Aldrich, Muenchen
DMEM/F-12, HEPES	Thermo Fisher Scientific
DMEM, high glucose, GlutaMAX, pyruvate	Thermo Fisher Scientific
DMSO	Roth, Karlsruhe
DPBS, no calcium, no magnesium (PBS -/-)	Thermo Fisher Scientific
DPBS, calcium, magnesium (PBS +/+)	Thermo Fisher Scientific
EDTA	Sigma-Aldrich, Muenchen
Fetal Bovine Serum (FBS)	Millipore, USA
Fetal Bovine Serum (FBS)	Thermo Fisher Scientific
Gelatin solution (2 %)	Sigma-Aldrich, Muenchen

Goat Serum	Sigma-Aldrich, Muenchen
Ham‘s F-12, GlutaMAX	Thermo Fisher Scientific
Heparin	Sigma-Aldrich, Muenchen
Knockout DMEM	Thermo Fisher Scientific
Laminin	Sigma-Aldrich, Muenchen
L-Glutamine	Thermo Fisher Scientific
Matrigel™ Basement Membrane Matrix Growth Factor Reduced	BD Biosciences, USA
Murine LIF	Millipore, USA
N-2 Supplement	Thermo Fisher Scientific
Phosphoramidon	Enzo Life Sciences, Belgium
Poly-D-lysine hydrobromide	Sigma-Aldrich, Muenchen
Recombinant Murine EGF	PeproTech, USA
Recombinant Murine FGF	PeproTech, USA
Trypsin (2.5 %), no phenol red	Thermo Fisher Scientific

3.7.3 Antibiotics

Ampicillin	Sigma-Aldrich, Muenchen
Nourseothricin (NTC)	Jena Bioscience, Jena
Penicillin-Streptomycin	Thermo Fisher Scientific
Puromycin	Merck, Darmstadt

3.7.4 APP substrate and Aβ peptides

APP C100 V5–His_6	C-terminal 100 amino acids of APP, cloned into the multiple cloning site of pET-DEST42 and expressed in *E. coli* BL21 star	pET-DEST42: Thermo Fisher Scientific

Aβ 40, 42 peptide	AnaSpec, USA

3.7.5 γ-secretase inhibitors

DAPT	Merck, Darmstadt
LY-411575	Eli Lilly, USA

3.7.6 Size standards

PageRuler™ Plus Prestained Protein ladder (10 - 250 kDa)	Thermo Scientific
Quick-Load® 2-log DNA Ladder (0.1 - 10 kb)	New England Biolabs, USA

3.7.7 Enzymes

3.7.7.1 General Enzymes

Name	**Buffer**	
Antarctic Phosphatase	Antarctic Phosphatase Reaction Buffer (10 x)	New England Biolabs, USA
HotStar Taq DNA Polymerase	PCR Buffer (10 x)	Qiagen, Hilden
Phusion High-Fidelity DNA Polymerase	Phusion GC Reaction Buffer (5 x)	Thermo Fisher Scientific
SuperScript II Reverse Transcriptase	FS Buffer (5 x) DTT (0.1 M)	Thermo Fisher Scientific
T4 DNA Ligase	T4 DNA Ligase Buffer (10 x)	New England Biolabs, USA

3.7.7.2 Restriction endonucleases

Name	**Buffer**	
BstBI	NEBuffer 4 (10 x) + BSA	New England Biolabs, USA
DpnI	Phusion GC Reaction Buffer (5x)	New England Biolabs, USA
NcoI	NEBuffer 3 (10 x) + BSA	New England Biolabs, USA
NheI	NEBuffer 2 (10 x) + BSA	New England Biolabs, USA
PacI	NEBuffer 4 (10 x) + BSA	New England Biolabs, USA

3.7.8 Kits

BCA Protein Assay Kit	Pierce, Bonn
Genopure Plasmid Maxi Kit	Roche, Mannheim
High Pure RNA Isolation Kit	Roche, Mannheim
Plasmid DNA Mini Kit I	OMEGA, USA
PureLink Genomic DNA Mini Kit	Thermo Fisher Scientific
QIAquick Gel Extraction Kit	Qiagen, Hilden

3.8 Laboratory hardware and appliances

Centrifuges	Eppendorf, Hamburg
	Hettich, Tuttingen
	Beckman, Krefeld
Coplin Staining Jar	Thermo Scientific
Cryo Freezing Container	Nunc, Wiesbaden
Electronic Transferpette (1 µL – 300 µL)	BRAND, Wertheim
Electrophoresis power supply	Consort, Belgium
Freezer (- 20°C)	Liebherr, Bulle
Freezer (- 80°C)	Thermo Scientific
Flat bed shaker	Heidolph, Kehlheim
Gene Pulser Xcell™ Eukaryotic System	Bio-Rad, USA
Glassware	Schott, Mainz
Heating block	Grant, Berlin
Incubator (tissue culture)	Binder, Tuttlingen
Incubator (bacteria)	New Brunswick Scientific, USA
LI-COR ODYSSEY CLx	LI-COR Biotechnology, USA
Light-optical microscope	Wilovert, Wetzlar
Magnetic stirrer	Heidolph, Kehlheim

Microwave	Media Markt
NanoDrop ND-1000 Spectrophotometer	peqlab
Novex Mini-Cell Electrophoresis chamber	Invitrogen, Karlsruhe
PARADIGM Microtiterplate reader	Beckman, Krefeld
pH meter 525	WTW, Weilheim
Pipettes 0.2 µL – 10 µL	Eppendorf, Hamburg
Pipettes 1 µL – 1000 µL	Gilson, USA
Pipettor AccuJet	VWR, Darmstadt
Scale (Max = 110 g)	Sartorius, Goetingen
Scale (Max = 2000 g)	KERN, Balingen
T3 Thermocycler	Biometra, Goettingen
Tank Blotter	CBS Scientific, USA
Vi-CELL XR cell counter	Beckman, Krefeld
Vortexer	IKA, Staufen
Waterbath	Julabo, Seelbach

3.9 Consumables

8-chamber-slides	LMS Consult, Brigachtal
10 cm Petri dishes (bacteria)	Starstedt, Nuembrecht
10 cm Petri dishes (cell culture)	Nunc, Wiesbaden
6-well plates	Nunc, Wiesbaden
12-well plates	Nunc, Wiesbaden
24-well plates	Nunc, Wiesbaden
48-well plates	Nunc, Wiesbaden
96-well plates	Nunc, Wiesbaden
15 mL tubes	Sarstedt, Nuembrecht
50 mL tubes	Sarstedt, Nuembrecht
Cassettes (1.0 mm)	Thermo Fisher Scientific
Cell scraper	TPP, Switzerland
Coverslips (12 mm diameter)	VWR, Darmstadt

Cryotubes	Thermo Fisher Scientific
Disposable gloves	Ansell, Muenchen
Gene Pulser® Electroporation Cuvettes (0.4 cm gap)	Bio-Rad, USA
Immobilion-FL Transfer Membrane (PVDF)	Millipore, USA
Microscope Cover Glasses	VWR, Darmstadt
Needles (0.70, 0.40 and 0.30 mm diameter)	Becton Dickinson, USA
Pasteur pipettes	Roth, Karlsruhe
Pipettes (5 mL – 25 mL)	Sigma-Aldrich, Muenchen
Pipet tips (10/20 µL, 20 µL, 200 µL, 1000 µL)	Starlab, Ahrensburg
Reaction tubes (0.5 mL, 1.5 mL, 2mL)	Eppendorf, Hamburg
Sterile Syringe Filter (0.2 µm)	VWR, Darmstadt
Syringes (5 mL, 10 mL, 20 mL)	BRAUN, Melsung
T25 flask	Nunc, Wiesbaden
Whatman paper	Whatman, Dassel

3.10 Software

Adobe Illustrator CS3

Adobe Photoshop CS3

CLC DNA Workbench 6

EndNote X5

Image Studio Software 2.1

Microsoft Office Professional Plus 2010

Prism GraphPad 5.0

4. Methods

4.1. Molecular Biology

4.1.1 Generation of the replacement construct for dRMCE

The PSEN1 exon 4'-12 sequence for the generation of murine PSEN1 ES cell lines by dRMCE was designed as follows:

- 5'-BstBI restriction sequence
- Parts of PSEN1 intron 4 sequence: Position 26174 – 26618 (445 bp) of NCBI PSEN1 Mouse Genomic RefSeq NC_000078.6
- PSEN1 exon 5-12: NCBI PSEN1 Mouse mRNA NM_008943
- 3'-PacI restriction sequence

The PSEN1 exon 4'-12 sequence was synthesised by GenScript and send as a pUC57 plasmid (pUC57 PSEN1 exon 4'-12).
Using the BstBI and PacI restriction sites, the PSEN1 exon 4'-12 sequence was cloned into the multiple cloning site of the pDREV-1 vector (see chapter 4.1.1.3). The pDREV-1 PSEN1 exon 4'-12 replacement construct includes following features:

- 5'-FRT site
- PSEN1 exon 4'-12
- SV40 polyadenylation site
- puromycin resistance (flanked by rox recombination sites)
- 3'-loxP site

4.1.1.1 Polymerase chain reaction (PCR)

Polymerase chain reaction (PCR) is a technique to amplify DNA sequences. A double stranded DNA sequence is initially denatured at a high temperature (> 95°C). The two single DNA strands hybridize with two complementary, short DNA primers at lower temperature. A DNA polymerase binds to the new formed double stranded DNA at the hybridization site and stepwise elongates it in the presence of desoxynucleotide-tri-phosphate (dNTP) molecules along the single stranded template DNA. Denaturation, hybridization and elongation usually occur at different temperatures, dependent on the primer sequence and DNA polymerase temperature optimum. The DNA polymerase also defines the time needed for the elongation per nucleobase. The denaturation/hybridization/elongation cycle is repeated multiple times, after an initial denaturation phase, to increase the concentration of the PCR product. A prolonged elongation phase is set at the end of the PCR.

4.1.1.2 Restriction-enzyme digest

Restriction endonucleases are enzymes that cut double stranded DNA within a specific recognition sequence either generating blunt or sticky ends. The recognition sequences of restriction enzymes are palindromes of four, six or eight base pairs in length. Blunt ends are generated from a cut at the same position on the forward and reverse DNA strand. Sticky ends have single stranded base overlaps.
In cloning experiments, sticky ends are usually preferred towards blunt ends, since they only anneal with the complementary sticky end of a DNA fragment that has been cut with the same restriction enzyme. To avoid re-ligation of cleavage sites, a combination of two different restriction enzymes for the generation of different sticky ends is usually applied.

The PSEN1 exon 4'-12 sequence on the pUC57 PSEN1 exon 4'-12 plasmid was cut out of the pUC57 plasmid and cloned into the pDREV-1 plasmid using the BstBI and PacI restriction endonucleases.

Digest (50 µL):

1 µg DNA

1x NEBuffer (10 x)

100 µg/mL BSA

10 U restriction enzyme

ddH_2O

The digest is incubated for 3 h at the working temperature for the respective restriction enzyme (usually 37°C). For a double digestion, both restriction enzymes are added in a compatible buffer.

4.1.1.3 Ligation

Ligation is a method to integrate a DNA sequence into a plasmid. Both, the DNA sequence and the plasmid, need to have complementary, usually sticky ends, created by the application of identical restriction enzymes. The multiple cloning site (MCS) of plasmids contains a variety of different restriction sites to facilitate ligation. Restriction sites on the 3'- and 5'-end of the DNA sequence are introduced via the primers for the PCR amplification.
The T4 DNA Ligase catalyses the formation of a phosphodiester-bond between the 5'-phosphate and the 3'-hydroxyl termini in duplex DNA.

A molar ratio of 1:3 for the plasmid and the insert was chosen for the sticky end ligation.
Following digestion of the plasmid by restriction enzymes, a dephosphorylation of the sticky ends was induced to prevent re-ligation. The Antarctic Phosphatase and its reaction buffer were added after completion of the digest.

Dephosphorylation (23.33 µL): 1 h, 37°C

20 µL digest sample

1x Antarctic Phosphatase Reaction Buffer (10 x)

5 U Antarctic Phosphatase (5000 U/mL)

Ligation sample (10 µL):

50 ng plasmid

x ng insert

1x T4 DNA Ligase Buffer (10 x)

400 U T4 DNA Ligase (400 U/µL)

ddH_2O

Ligation program:

100 x { 37°C 1 min; 22°C 1 min; 16°C 1 min }

65°C 10 min

4°C pause

Name	Plasmid	Insert			Restriction enzyme
		Donor plasmid	Primer pair	Restriction product	
pDREV-1 PSEN1 exon 4'-12	pDREV-1	pUC57 PSEN1 exon 4'-12	/	PSEN1 exon 4'-12	BstBI PacI

The ligation program was run in a thermocycler. As a control for re-ligation of the plasmid, a control sample without insert DNA was simultaneously ligated.

4.1.1.4 Transformation in bacteria

Plasmids are amplified in bacteria by transformation.

Materials:

LB-medium:	1 % Tryptone (w/v) 0.5 % Yeast extract (w/v) 1 % NaCl (w/v) ➢ Autoclave and store at 4°C.
LB-agar + 20 µg/mL NTC:	1 % Tryptone (w/v) 0.5 % Yeast extract (w/v) 1 % NaCl (w/v) 1.5 % Agar (w/v)

Add 20 µg/mL NTC (100 mg/mL) after cooling of the autoclaved LB-agar to RT. Pour 15 mL LB-agar + NTC per 10 cm Petri dishes (bacteria). Incubate plates over night at RT for hardening of the LB-agar and store at 4°C.

1. Defrost a 1.5ml Eppendorf tube containing 100 µL competent Library Efficiency *E. coli* DH5α on ice.
2. Either add the purified mutagenesis PCR product (25 µL) or ligation sample (10 µL) to 50 µL cell volume.
3. Mix solution by gently pipetting.
4. Incubate bacteria on ice for 30 min.
5. Incubate at 42°C for 2 min in heating block.
6. Incubate on ice for 2 min.
7. Add LB-medium to a final volume of 500 µL and mix by inverting tube.
8. Incubate at 37°C for 2 h on a shaker (approx. 200 rpm).
9. Centrifugation: 1000 x g, 5 min, RT
10. Resuspend the cell pellet in 50 µL medium.

11. Plate 50 µL cell suspension onto LB-plates containing NTC (20 µg/mL).
12. Incubate plates at 37°C over night.
13. Transfer plates to 4°C when colonies have good size.

4.1.1.5 Mutagenesis PCR

For the generation of murine ES cell lines, pDREV-1 PSEN1 exon 4'-12 replacement constructs with different FAD PSEN1 mutations were prepared by mutagenesis PCR. Forward and reverse primer pairs carrying the desired FAD PSEN1 mutation were designed to introduce the respective mutation by PCR using a template DNA.

PCR sample (50 µL):

50 ng template DNA
1x Phusion GC Reaction Buffer(5 x)
125 ng primer 1
125 ng primer 2
3 % DMSO (100 %)
200 µM dNTP mix (10 mM)
1 U Phusion High-Fidelity DNA Polymerase (2 U/ µL)
ddH_2O

PCR program:

	98°C	30 s
18 x	98°C	8 s
	72°C	30 s
	72°C	3:30 min
	72°C	8 min
	4°C	pause

Name of generated construct	Template DNA	Primer pair
pDREV-1 PSEN1 exon 4‘-12 wt 3xFlag	pDREV-1 PSEN1 exon 4‘-12 D385N 3xFlag	PSEN1_N385D_For PSEN1_N385D_Rev
pDREV-1 PSEN1 exon 4‘-12 P117L	pDREV-1 PSEN1 exon 4‘-12	PSEN1_P117L_For PSEN1_P117L_Rev
pDREV-1 PSEN1 exon 4‘-12 P117L + D385N	pDREV-1 PSEN1 exon 4‘-12 P117L + D385N	PSEN1_D385N_For PSEN1_D385N_Rev
pDREV-1 PSEN1 exon 4‘-12 N135I	pDREV-1 PSEN1 exon 4‘-12	PSEN1_N135I_For PSEN1_N135I_Rev
pDREV-1 PSEN1 exon 4‘-12 N135S	pDREV-1 PSEN1 exon 4‘-12	PSEN1_N135S_For PSEN1_N135S_Rev
pDREV-1 PSEN1 exon 4‘-12 L166P	pDREV-1 PSEN1 exon 4‘-12	PSEN1_L166P_For PSEN1_L166P_Rev
pDREV-1 PSEN1 exon 4‘-12 L166P 3xFlag	pDREV-1 PSEN1 exon 4‘-12 L166P + D385N 3xFlag	PSEN1_N385D_For PSEN1_N385D_Rev
pDREV-1 PSEN1 exon 4‘-12 L166P + D385N	pDREV-1 PSEN1 exon 4‘-12 L166P	PSEN1_D385N_For PSEN1_D385N_Rev
pDREV-1 PSEN1 exon 4‘-12 L166P + D385N 3xFlag	pDREV-1 PSEN1 exon 4‘-12 L166P + M292D + D385N 3xFlag	PSEN1_D292M_For PSEN1_D292M_Rev
pDREV-1 PSEN1 exon 4‘-12 L166P + M292D + D385N	pDREV-1 PSEN1 exon 4‘-12 L166P + D385N	PSEN1_M292D_For PSEN1_M292D_Rev
pDREV-1 PSEN1 exon 4‘-12 L173W	pDREV-1 PSEN1 exon 4‘-12	PSEN1_L173W_For PSEN1_L173W_Rev
pDREV-1 PSEN1 exon 4‘-12 L173W + D385N	pDREV-1 PSEN1 exon 4‘-12 L173W	PSEN1_D385N_For PSEN1_D385N_Rev
pDREV-1 PSEN1 exon 4‘-12 I213T	pDREV-1 PSEN1 exon 4‘-12	PSEN1_I213T_For PSEN1_I213T_Rev
pDREV-1 PSEN1 exon 4‘-12 M233V	pDREV-1 PSEN1 exon 4‘-12	PSEN1_M233V_For PSEN1_M233V_Rev
pDREV-1 PSEN1 exon 4‘-12 M233V + D385N	pDREV-1 PSEN1 exon 4‘-12 M233V	PSEN1_D385N_For PSEN1_D385N_Rev
pDREV-1 PSEN1 exon 4‘-12 M233V + D385N 3xFlag	pDREV-1 PSEN1 exon 4‘-12 M233V + M292D + D385N 3xFlag	PSEN1_D292M_For PSEN1_D292M_Rev
pDREV-1 PSEN1 exon 4‘-12 M233V + M292D + D385N	pDREV-1 PSEN1 exon 4‘-12 M233V + D385N	PSEN1_M292D_For PSEN1_M292D_Rev
pDREV-1 PSEN1 exon 4‘-12 R278I	pDREV-1 PSEN1 exon 4‘-12	PSEN1_R278I_For PSEN1_R278I_Rev
pDREV-1 PSEN1 exon 4‘-12 E280A	pDREV-1 PSEN1 exon 4‘-12	PSEN1_E280A_For PSEN1_E280A_Rev
pDREV-1 PSEN1 exon 4‘-12 M292D + D385N	pDREV-1 PSEN1 exon 4‘-12 D385N	PSEN1_M292D_For PSEN1_M292D_Rev
pDREV-1 PSEN1 exon 4‘-12 G384A	pDREV-1 PSEN1 exon 4‘-12	PSEN1_G384A_For PSEN1_G384A_Rev
pDREV-1 PSEN1 exon 4‘-12 D385N	pDREV-1 PSEN1 exon 4‘-12	PSEN1_D385N_For PSEN1_D385N_Rev
pDREV-1 PSEN1 exon 4‘-12 D385N 3xFlag	pDREV-1 PSEN1 exon 4‘-12 L166P + D385N 3xFlag	PSEN1_P166L_For PSEN1_P166L_Rev
pDREV-1 PSEN1 exon 4‘-12 C410Y	pDREV-1 PSEN1 exon 4‘-12	PSEN1_C410Y_For PSEN1_C410Y_Rev

pDREV-1 PSEN1 exon 4'-12 L435F	pDREV-1 PSEN1 exon 4'-12	PSEN1_L435F_For PSEN1_L435F_Rev

The respective primer pairs for the mutagenesis PCR were designed using the QuikChange® Primer Design Program from Agilent.

Mutagenesis PCR:

1. Set up the PCR sample as described above using the respective template DNA and primer pair.
2. Run the mutagenesis PCR program in a thermocycler.
3. After the PCR program is completed, add 1 µL DpnI restriction endonuclease to the 50 µL PCR sample, mix and incubate for 3 h at 37°C.
    - The DpnI restriction endonuclease destroys the template DNA by cutting it into multiple small fragments. The PCR product remains intact, since DpnI only cleaves methylated DNA. This modification is introduced during amplification of the template DNA in *E. coli*.
4. Purify the PCR product by using the PCR purification protocol for the QIAquick Gel Extraction Kit.
    - Elute with 30 µL ddH_2O.
5. Transform 25 µL of the PCR product into 50 µL Library Efficiency *E. coli* DH5α.

4.1.1.6 Fusion PCR

The fusion PCR is used to induce changes in the DNA sequence of a plasmid that exceeds the capacity of a mutagenesis PCR. Those are, for example, the introduction of a protein tag or fluorophore or the excision of parts of the DNA sequence.

The fusion PCR consists of three PCR reactions. In the first and second PCR, two PCR fragments are independently generated from a template DNA. In the third and final PCR, those two PCR fragments are used in equal stoichiometry as templates. In this case, the

forward primer of the first and third PCR contains a 5'-BstBI restriction site. The reverse primer of the second and the third PCR contains a 3'-PacI restriction site.

PCR sample (50 µL): First and second PCR

200 ng template DNA

1x Phusion GC Reaction Buffer(5 x)

125 ng primer 1

125 ng primer 2

200 µM dNTP mix (10 mM)

1 U Phusion High-Fidelity DNA Polymerase (2 U/ µL)

ddH_2O

PCR sample (50 µL): Third PCR

50 ng template DNA 1 (fragment from 1. PCR)

x ng template DNA 2 (fragment from 2. PCR)

1x Phusion GC Reaction Buffer(5 x)

125 ng primer 1

125 ng primer 2

200 µM dNTP mix (10 mM)

1 U Phusion High-Fidelity DNA Polymerase (2 U/ µL)

ddH_2O

PCR program: First and second PCR

	98°C	30 s
20 x	98°C	8 s
	55°C	30 s
	72°C	40 s
	72°C	8 min
	4°C	pause

PCR program: 3. PCR

	98°C	30 s
18 x	98°C	8 s
	55°C	30 s
	72°C	1:30 min
	72°C	8 min
	4°C	pause

Name	Template DNA	Primer pair		
		1. PCR	2. PCR	3. PCR
pDREV-1 PSEN1 exon 4'-12 L166P + M292D + D385N 3xFlag	pDREV-1 PSEN1 exon 4'-12 L166P + M292D + D385N	pDREV-1 BstBI f PS1_3xFlag_Rev	PS1_3xFlag_For pDREV-1 PacI r	pDREV-1 BstBI f pDREV-1 PacI r
pDREV-1 PSEN1 exon 4'-12 M233V + M292D + D385N 3xFlag	pDREV-1 PSEN1 exon 4'-12 M233V + M292D + D385N	pDREV-1 BstBI f PS1_3xFlag_Rev	PS1_3xFlag_For pDREV-1 PacI r	pDREV-1 BstBI f pDREV-1 PacI r
pDREV-1 PSEN1 exon 4'-12 ΔHL	pDREV-1 PSEN1 exon 4'-12	pDREV-1 BstBI f PS1 dHL rev2	PS1 dHL for2 pDREV-1 PacI r	pDREV-1 BstBI f pDREV-1 PacI r

Fusion PCR:

1. Pipet the samples for the first and second PCR using the respective template DNA and primer pairs.
2. Run the PCR program for the first and second PCR in a thermocycler.
3. After the PCR program is completed, purify the PCR fragments 1 and 2 according to the PCR purification protocol for the QIAquick Gel Extraction Kit.
    - Elute with 30 µL ddH_2O.
4. Measure the DNA concentration with the NanoDrop.
5. Run a 1 % agarose gel for the PCR fragment 1 and 2.
6. Carefully cut out the respective PCR fragment 1 and 2 from the agarose gel under UV light.
    - ➢ Quickly, since UV light destroys DNA!
7. Extract and purify the DNA from the gel slices using the QIAquick Gel Extraction Kit.
8. Measure the DNA concentration of the purified PCR fragments 1 and 2 with the NanoDrop.

9. Calculate equal stoichiometry for the two PCR fragments by choosing 50 ng for one of the two fragments.
    - For example: Fragment 1: 1238 bp: 1.26 x 50 ng = 63 ng
      Fragment 2: 1559 bp: 50 ng
        - Stoichiometry: 1:1.26
10. Pipet the samples for the third PCR using the respective template DNA and primer pair.
11. Run the program for the third PCR in a thermocycler.
12. After the PCR program is completed, purify the PCR fragments 3 according to the PCR purification protocol for the QIAquick Gel Extraction Kit.
13. Measure the DNA concentration with the NanoDrop.
14. Run a 1 % agarose gel for the PCR fragment 3.
15. Carefully cut out the PCR fragment 3 from the agarose gel under UV light.
16. Extract and purify the DNA from the gel slice using the QIAquick Gel Extraction Kit.
17. Measure the DNA concentration with the NanoDrop.
18. Double digest PCR fragment 3 with the BstBI and PacI restriction enzymes.
19. Ligate the digested PCR fragment 3 into the pDREV-1 plasmid.
20. Transform the ligation sample into 50 µL Library Efficiency *E. coli* DH5α.

4.1.2 Agarose gelelectrophoresis

Agarose gelelectrophoresis is a method to analyse and separate DNA by size in an electric field on an agarose-gel matrix.

Materials:

10x TAE buffer:	0.80 M TRIS
	20 mM EDTA
	1 % glacial acetic acid (v/v)

1 % agarose gel:	1 % agarose (w/v)
	1 x TAE buffer
2 % agarose gel:	2 % agarose (w/v)
	1 x TAE buffer

A 2 % agarose gel is more suitable for the separation of small DNA fragments between 100 bp and 1000 bp in size.

1. Prepare either a 1 % or 2 % agarose gel solution by dissolving the appropriate amount of agarose in 1 x TAE buffer using a microwave.
2. Swirl the hot agarose solution and let it cool down for approximately 5 min.
3. Add Midori Green to the 1 % or 2 % agarose gel and further swirl the solution.
    - Use 3 µL Midori Green solution for 25 mL agarose solution.
4. Pour the agarose solution into a cassette and place a comb into the gel.
    - Small gel (25 mL): 5 wells
    - Big gel (50 mL): 12 wells
5. Let the agarose gel harden for 25 min.
6. Remove the comb and place the agarose gel into a running chamber, containing 1 x TAE buffer.
7. Load samples and size standard onto the agarose gel.
8. Run the agarose gel at 100 V for approximately 30 min.
9. Place the agarose gel on an UV table and take pictures or cut out bands for gelextraction of the DNA.

4.1.3 Validation of ES cell clones

ES cell clones are validated by PCR analysis of genomic DNA. A set of 5 primer pairs is used to generate characteristic PCR products of the 3'- and 5'- end of the genomic DNA of (i) the original parental locus, (ii) the deleted locus and (iii) the replaced locus. Based on the existence of a PCR product and its respective size, the examined ES clone can be defined as

parental cell line, deleted locus cell line (failed recombination; negative clone) or replaced locus (successful recombination; positive clone).

Positive ES clones are further screened for unwanted integration of the pDIRE vector by iCre and Flpo specific primer pairs.

Materials:

PCR Master Mix (1x): 2.5 µL PCR Buffer (10 x): 1x
0.5 µL dNTP mix (10 mM): 200 µM
0.13 µL HotStar Taq DNA Polymerase (5 U/µL): 0.625 U

PCR sample (25 µL):

20 ng template DNA
10 pmol primer pair
(5 % DMSO for F1 / R9-b primer pair)
1 x PCR Master Mix
ddH_2O

PCR program:

95°C 15 min
40 x { 95°C 30 s; 54°C 30 s; 72°C 90 s }
72°C 5 min
4°C pause

Primer pairs	End specificity	PCR Product		
		Original locus	Deleted locus	Replaced locus
F2-b R2-b1	5‘-end	1448 bp	1448 bp	no PCR product
F1 R9-b	3‘-end	3585 bp	853 bp	no PCR product
F9 R9-b	3‘-end	1460 bp	no PCR product	no PCR product
F2-b PS1 Ex5_seq_rev	5‘-end	994 bp (wt allele)	994 bp (wt allele)	1109 bp 994 bp (wt allele)
F11-b2 R9-b	3‘-end	no PCR product	no PCR product	851 bp

Run the PCR and analyse the PCR products by agarose gel electrophoresis. As a control for primer contamination, simultaneously run a water control without DNA, including all primer pairs. For further analysis of positive ES clones, run a PCR with the iCre specific primer pair I1/I2 and the Flpo specific primer pair P1/P2. Reduce the number of cycles in the PCR program to 30.

4.1.4 cDNA synthesis

For analysing transcription levels, RNA is isolated from ES cells and converted into complementary DNA (cDNA). Using dNTPs and random hexamers (pd(N_6)) the SuperScript DNA Polymerase synthesizes a complementary DNA strand from single-stranded RNA.

RNA isolation:

1. Centrifuge 1 x 10^6 ES cells: 1000 rpm, 5 min, RT
2. Isolate RNA from pelleted ES cells using the High Pure RNA Isolation Kit.
    - Elute in 70 µL ddH_2O.
3. Measure the RNA concentration with the NanoDrop.
4. Either store the RNA at -80°C or continue with the cDNA synthesis.

cDNA Synthesis:

1. Dilute 1.5 µg RNA in 11 µL ddH_2O.
2. Add 1 µL dNTP mix (10 mM) and 1 µL pd(N_6) (25 µM).
3. Incubate for 5 min at 65 °C.
4. Cool the sample on ice.
5. Add 4 µL FS Buffer (5 x) and 2 µL DTT (0.1 M).
6. Incubate for 2 min at RT.
7. Add 1 µL SuperScript II Reverse Transcriptase (200 U/µL).
8. Run the cDNA synthesis program in a thermocycler.
9. Store the cDNA at -80°C.

cDNA synthesis program:

25°C	10 min
40°C	50 min
70°C	15 min
4°C	pause

4.1.5 Comparison of transcription levels between wt and mutant PSEN1 alleles

To ensure equal transcription levels between the wt and mutant PSEN1 alleles after successful dRMCE (see chapter 4.2.4), cDNA of the ES PSEN1 ΔHL cell line was investigated by PCR analysis with two primer pairs, which generate characteristic and size distinct PCR products for the PSEN1 wt allele and the PSEN1 ΔHL allele.

Materials:

PCR Master Mix (1x):	2.5 µL PCR Buffer (10 x): 1x
	0.5 µL dNTP mix (10 mM): 200 µM
	0.13 µL HotStar Taq DNA Polymerase (5 U/µL): 0.625 U
1. Primer pair:	PS1 Ex5_seq_for
	RT-PCR_rev
2. Primer pair:	PS1 Ex4_seq_for
	RT-PCR_rev

PCR sample (25 µL):

5 µL 1:5 diluted cDNA (see chapter 4.1.4)

10 pmol primer pair

5 % DMSO

1 x PCR Master Mix

ddH_2O

PCR program:

	95°C	15 min
40 x	95°C	30 s
	54°C	30 s
	72°C	90 s
	72°C	5 min
	4°C	pause

Primer pairs	**PCR Products**	
	PSEN1 wt allele	**PSEN1 ΔHL allele**
PS1 Ex5_seq_for RT-PCR_rev	884 bp	764 bp
PS1_Ex4_seq_for RT-PCR_rev	1135 bp	1015 bp

Run the PCR and analyse the PCR products by agarose gel electrophoresis. As a control for primer contamination, simultaneously run a water control without DNA, including all primer pairs.

4.2 Cell culture

Mammalian cell culture experiments were performed under sterile conditions in an S1 lab, using a cell culture laminar flow hood. The consumable materials, including cell culture dishes, pipet tips and plastic tubes, were either purchased sterile or autoclaved before use. All cell culture media were stored at 4°C and pre-warmed before use in a 37°C waterbath. The cells were incubated in an humidified incubator at 37°C and 5 % CO_2.

4.2.1 Embryonic stem cell culture

Cell culture media and reagents:

Knockout DMEM complete:
- Knockout DMEM
- 1 % FBS (100 % stock)
- 2 x L-Glutamine (100 x stock)
- 103 µM β-Mercaptoethanol (50 mM stock)
- 1 x Pen/Strep (100 x stock)
- 1x10^3 U/mL LIF (1x10^7 U/mL stock)

The Knockout DMEM complete medium is prepared in 50 mL aliquots to avoid repeated cycles of warming in the 37°C water bath. LIF is added right before use!

Trypsin 2x + G:
- PBS -/-
- 1.0 mM EDTA
- 5.6 mM D-Glucose
- ➢ Filter sterilize (0.22 µm)
- 1 % Chicken Serum (100 % stock)
- 0.1 % Trypsin (2.5 % stock)
- ➢ Aliquot into 20 mL fractions and store at - 20°C.

0.1 % Gelatin solution:	PBS -/- 0.1 % gelatin solution (2 % stock) ➢ Gelatin solution needs to be warmed to 37°C prior to mix.

4.2.1.1 Thawing of ES cells

1. Coat one well of a 6-well cell culture plate with 1 mL 0.1 % gelatin solution and incubate for 1 h at 37°C in the incubator.
2. Prepare 5 mL Knockout DMEM complete + $1x10^3$ U/mL LIF.
3. Thaw a vial from the -80°C freezer or liquid nitrogen tank in the 37 °C water bath.
4. Dilute 1 mL cell suspension in 5 mL pre-warmed Knockout DMEM.
5. Centrifuge: 1000 rpm, 5 min, RT
6. Remove 0.1 % gelatine solution from the 6-well.
7. Remove the medium supernatant and carefully suspend the cell pellet in pre-warmed 5 mL Knockout DMEM complete + $1x10^3$ U/mL LIF.
8. Transfer 5 mL cell suspension to the coated 6-well.

4.2.1.2 Passaging of ES cells

1. Prepare coated dishes.
    a. 6-well: 1 mL 0.1 % gelatine solution
    b. 10 cm dish: 5 mL 0.1 % gelatine solution
2. Remove the medium and carefully wash the cells on the plate with PBS -/-.
3. Add Trypsin to the cells.
    a. 6-well: 1 mL Trypsin 2x + G
    b. 10 cm dish: 1.5 mL Trypsin 2x + G

4. Incubation: 37°C, 7 min.
5. Carefully disperse cells by pipetting up and down.
6. Add Knockout DMEM to the trypsinized cells and further disperse the cells until you obtain single cells (check under the microscope!)
    a. 6-well: 4 mL Knockout DMEM
    b. 10 cm dish: 8.5 mL Knockout DMEM
7. Centrifuge: 1000 rpm, 5 min, RT
8. Remove 0.1 % gelatine solution from the dishes.
9. Remove the medium supernatant and carefully resuspend the cell pellet in pre-warmed Knockout DMEM complete + $1x10^3$ U/mL LIF.
    a. 6-well: 3 mL Knockout DMEM complete + $1x10^3$ U/mL LIF
    b. 10 cm dish: 10 mL Knockout DMEM complete + $1x10^3$ U/mL LIF
10. Transfer the cell suspension to the coated dishes.

The medium has to be changed daily to maintain pluripotency of the ES cells!

4.2.1.3 Cryopreservation of ES cells

ES cell lines were frozen at - 80°C and in liquid nitrogen for long-term storage.

1. Trypsinize cells on one 10 cm dish and add 8.5 mL Knockout DMEM.
2. Count cell numbers using the Vi-CELL XR cell counter.
3. Centrifuge respective cell suspension volume: 1000 rpm, 5 min, RT
    - $3x10^6$ cells per cryotube
4. Resuspend the cell pellet in filter sterilized Knockout DMEM complete + $1x10^3$ U/mL LIF + 10 % DMSO.
    - 1 mL freezing medium per $3x10^6$ cells per cryotube
5. Place cryotubes into the freezing container and store at - 80°C over night.
6. For long-term storage, transfer cryotubes into the liquid nitrogen tank.

4.2.2 Neural stem cell culture

Cell culture media and reagents:

NSC Medium:	DMEM/F-12, HEPES
	1x L-Glutamine (100x stock)
	1x Pen/Strep (100x stock)
	0.5x B-27 (50x stock)
	0.5x N-2 (100x stock)
	5 µg/mL Heparin (10 mg/mL stock in H_2O)
	10 ng/mL EGF (20 µg/mL stock)
	10 ng/mL FGF (20 µg/mL stock)

The NSC Medium is prepared in 50 mL aliquots to avoid repeated cycles of warming in the 37°C water bath. EGF and FGF are added right before use!

Laminin solution:	PBS -/-
	4 µg/mL Laminin (1 mg/mL stock)

Murine EGF and FGF (20 µg/mL):

Filter sterilize ddH_2O and BSA Fraction V (7.5 %) before use!

1. Pipette 1 mL ddH_2O into the EGF or FGF tube (100 µg each).
2. Incubate 5 min on ice.
3. Pipette 1 mL 0.15% BSA solution into a 15 mL Falcon tube.
4. Add 1 mL EGF or FGF solution to the 15 mL Falcon tube.
5. Wash the EGF or FGF tube 3x with 1 mL 0.15% BSA and pipette into the 15 mL Falcon tube.
6. 5 mL EGF or FGF-solution: 100 x 50 µL aliquots (20 µg/mL); store at -80°C

4.2.2.1 Thawing of NSCs

1. Coat one well of a 6-well cell culture plate with 1 mL Laminin solution and incubate for 1 h at 37°C in the incubator.
2. Prepare 5 mL NSC Medium + 10 ng/mL EGF + 10 ng/mL FGF.
3. Thaw a vial from the liquid nitrogen tank in the 37°C water bath.
4. Dilute 1 mL cell suspension in 5 mL pre-warmed DMEM/F-12.
5. Centrifuge: 1000 rpm, 5 min, RT
6. Remove Laminin solution from the 6-well.
7. Remove the medium supernatant and carefully resuspend the cell pellet in pre-warmed 5 mL NSC Medium + 10 ng/mL EGF + 10 ng/mL FGF.
8. Transfer 5 mL cell suspension to the coated 6-well.

4.2.2.2 Passaging of NSCs

1. Prepare coated dishes.
    a. 6-well: 1 mL Laminin solution
    b. 10 cm dish: 4 mL Laminin solution
2. Remove the medium.
3. Add Accutase to the cells.
    a. 6-well: 1 mL Accutase
    b. 10 cm dish: 1.5 mL Accutase
4. Incubation: 37°C, 3 min.
5. Carefully disperse cells.
6. Add DMEM/ F-12 to the detached cells and further disperse by carefully pipetting up and down until you obtain single cells (check under the microscope!)
    a. 6-well: 4 mL DMEM/ F-12
    b. 10 cm dish: 8.5 mL DMEM/ F-12
7. Centrifuge: 1000 rpm, 5 min, RT

8. Remove Laminin solution from the dishes.
9. Remove the medium supernatant and carefully resuspend the cell pellet in pre-warmed NSC Medium + 10 ng/mL EGF + 10 ng/mL FGF.
    a. 6-well: 3 mL NSC Medium + 10 ng/mL EGF + 10 ng/mL FGF
    b. 10 cm dish: 10 mL NSC Medium + 10 ng/mL EGF + 10 ng/mL FGF
10. Transfer cell suspension to the coated dishes.

The medium has to be changed every two days to maintain NSC proliferation and prevent differentiation!

4.2.2.3 Cryopreservation of NSCs

NSC lines were stored in liquid nitrogen.

1. Detach cells of one 10 cm dish and add 8.5 mL DMEM/ F-12.
2. Count cell numbers using the Vi-CELL XR cell counter.
3. Centrifuge respective cell suspension volume: 1000 rpm, 5 min, RT
    a. $3x10^6$ cells per cryotube
4. Resuspend the cell pellet in filter sterilized NSC Medium + 10 ng/mL EGF + 10 ng/mL FGF + 10 % DMSO.
    a. 1 mL freezing medium per $3x10^6$ cells per cryotube
5. Place cryotubes into the freezing container and store at - 80°C over night.
6. Transfer cryotubes into the liquid nitrogen tank.

4.2.3 Killing curve

The C57/Bl6/N JM8A3.01 PSEN1 parental cell line, which does not harbour a puromycin resistance, was incubated in the presence of increasing puromycin concentrations to determine the ideal concentration for selection, by which approximately 80 % of the seeded cell are either dead or dying.

Materials:

Knockout DMEM complete:	Knockout DMEM
	1 % FBS (100 % stock)
	2 x L-Glutamine (100 x stock)
	103 µM β-Mercaptoethanol (50 mM stock)
	1 x Pen/Strep (100 x stock)
	$1x10^3$ U/mL LIF ($1x10^7$ U/mL stock)

The Knockout DMEM complete medium is prepared in 50 mL aliquots to avoid repeated cycles of warming in the 37°C water bath. LIF is added right before use!

Puromycin (1 mg/mL):	0 µg/mL
	0.2 µg/mL
	0.5 µg/mL
	0.75 µg/mL
	1.0 µg/mL
	1.5 µg/mL
	2.5 µg/mL

Dilute the respective puromycin concentration in Knockout DMEM complete + $1x10^3$ U/mL LIF.

1. Seed 200000 cells per well in 6-well cell culture plates.
2. Change the medium on the next day and include the respective puromycin concentration.
3. Exchange the medium including the respective puromycin concentration daily for approximately one week.
    - Check the cells under the microscope and not the puromycin concentration, by which 80 % of the cells are dead.

The determined, optimal concentration of puromycin was used to generate new ES cell lines. Cells without recombination events did not receive the puromycin resistance, which is located on the replacement sequence and are thus eliminated.

4.2.4 Generation of ES cell lines by dRMCE

Murine ES cell lines, endogenously expressing both PSEN1 alleles were generated from the C57/Bl6/N JM8A3.01 PSEN1 parental cell line by dual recombinase mediated cassette exchange (dRMCE) (Osterwalder et al. 2010).
C57/Bl6/N JM8A3.01 PSEN1 parental cells contain an FRT and loxP flanked cassette between Exon 4 and 6 on one of the two PSEN1 alleles. dRMCE enables an exchange of the inserted cassette on the conditional PSEN1 allele by combined application of the iCre and Flpo recombinase, targeting the loxP and FRT sites. A murine PSEN1 exon 5-12 cDNA including a partial sequence of the PSEN1 intron 4 (PSEN1 exon 4'-12) was chosen to restore expression of the conditional PSEN1 allele.

The recombination process involves two steps [Figure 13]:

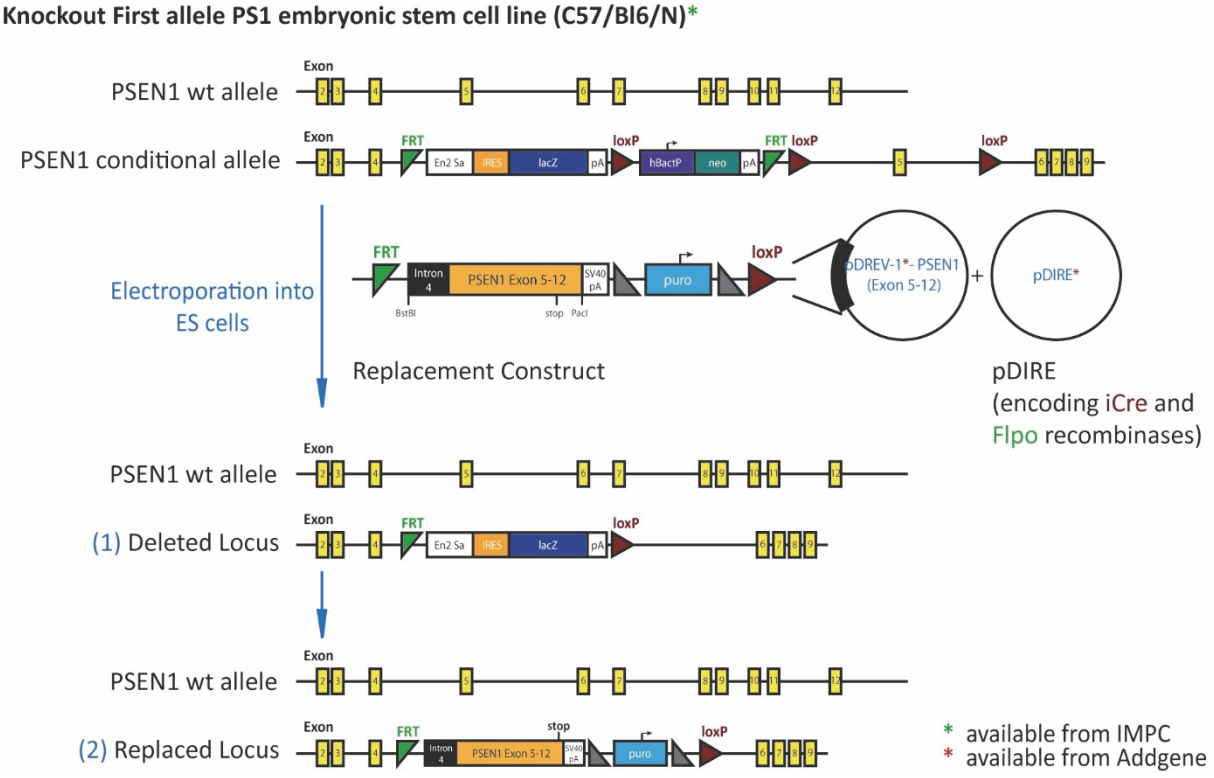

Figure 13: Dual recombinase mediated cassette exchange (dRMCE). The ES cell line, consisting of one PSEN1 wt allele and one PSEN1 conditional allele, is electroporated with the pDREV-1 PSEN1 exon 4'-12 replacement construct and the pDIRE vector. (1) Expression of the iCre recombinase induces a deletion of the DNA sequence between the three loxP sites on the conditional allele and the generation of the deleted locus. (2) The remaining cassette on the deleted locus is now exchanged for the PSEN1 sequence between the FRT and loxP sites on the replacement construct, thereby restoring PSEN1 expression of the conditional allele (replaced locus).

(1) The pDREV-1 PSEN1 exon 4'-12 replacement construct and the pDIRE vector, expressing the iCre and Flpo recombinases, were simultaneously electroporated into the C57/Bl6/N JM8A3.01 PSEN1 parental cells to induce the recombination mediated cassette exchange for the PSEN1 exon 4'-12 sequence. Expression of iCre and Flpo are controlled by two different promoters, the EF1A promoter for iCre and the PGK promoter for Flpo (Osterwalder et al. 2010). Since EF1A is a stronger promoter than PGK (Qin *et al.* 2010), enhanced expression of the iCre recombinase results in excision of the sequence between the three loxP sites on the conditional PSEN1 allele, leading to the generation of the "Deleted locus".

(2) The remaining FRT and loxP flanked cassette on the deleted locus PSEN1 allele subsequently recombines with the FRT and loxP flanked PSEN1 exon 4'-12 sequence on the replacement construct, restoring PSEN1 expression on the replaced locus allele.

Since the PSEN1 wt allele remains unaffected by dRMCE, ES cell lines with heterozygous and endogenous expression of FAD PSEN1 mutations were generated by different PSEN1 exon 4'-12 replacement constructs carrying either FAD PSEN1 mutations and/or protein tags.

Materials:

Cell line:	$1.5x10^7$ C57/Bl6/N JM8A3.01 PSEN1 parental cells
Plasmids:	50 µg pDIRE plasmid
	50 µg pDREV-1 PSEN1 exon 4'-12 plasmid
	(± PSEN1 mutations)

The C57/Bl6/N JM8A3.01 PSEN1 parental cells and subsequent clones are cultured according to chapter 4.1.1.

dRMCE (day 1):

1. C57/Bl6/N JM8A3.01 PSEN1 parental cells are trypsinized and counted using the Vi-CELL XR cell counter.
2. Centrifuge respective cell suspension volume: 1000 rpm, 10 min, RT
    - $1.5x10^7$ cells per electroporation
3. Resuspend the cell pellet in PBS -/-.
    - 800 µL per $1.5x10^7$ cells per electroporation
4. Mix 50 µg pDIRE plasmid + 50 µg respective pDREV-1 PSEN1 exon 4'-12 plasmid in a 2 mL tube with the 800 µL cell solution.
    - Avoid formation of air bubbles!
5. Transfer the cell solution into the electroporation cuvettes (0.4 cm gap).
    - Destroy every air bubble with a small needle (0.30 mm diameter)!
6. Place the cuvette into the Gene Pulser Xcell and electroporate the cells: 0.24 kV, 475 µF, 1 pulse (~ 8 ms)
7. Incubate the cuvette for 20 min on ice.
8. Add the electroporated cell suspension to 10 mL Knockout DMEM complete.

9. Pipet 2 mL of the cell suspension from step 8 into 10 mL Knockout DMEM complete + 10^3 U/mL LIF (calculated for 12 mL!) and transfer to a 10 cm dish. Incubate at 37°C.

Change medium daily!

As a control for the subsequent puromycine selection, electroporate C57/Bl6/N JM8A3.01 PSEN1 parental cells only with the pDIRE plasmid to prevent puromycine resistance by recombination with the pDREV-1 PSEN1 exon4'-12 sequence.

dRMCE (day 3):

Two days after the electroporation procedure, add 0.75 µg/mL puromycin to the Knockout DMEM complete + 10^3 U/mL LIF to kill cells that did not undergo recombination.

The ideal puromycin concentration was determined by a killing curve (see chapter 4.2.3).

dRMCE (day 10 – 12):

Approximately 10 - 12 days after the electroporation, roundish, 3-dimensional and dense single cell clones become visible on the 10 cm dish and should have reached a good size to be picked from the plate for further subculturing. From each electroporation, 6 clones were picked for further validation.

- Prepare a 96-well plate on ice with 40 µL Trypsin 2x + G according to the number of clones picked.
- Prepare a 48-well plate (previously coated for 1 h with 300 µL 0.1 % gelatin solution) with 300 µL Knockout DMEM complete + 10^3 U/mL LIF and store at 37°C.
- Prepare a 200 µL Pipette, set to 20 µL volume.

1. Carefully pick the clones under the microscope with the pipette.
    - Avoid complete destruction of the clone's integrity, to prevent contamination of the remaining clones on your plate with fragments of the picked clone!
2. Transfer the picked clone into one of the trypsin wells on ice.
    - If some fragments from the picked colony are still floating on the plate, remove them with a fresh pipette tip.

3. Incubate the 96-well plate for 7 min at 37°C when you have completed picking of the desired clones.
4. Disperse trypsinized clones by careful pipetting up and sown until you obtain single cells (check under the microscope!). Transfer clones to the 48-well plate.
5. Wash the wells of the 96-well plat that was used for trypsinisation with 175 µL Knockout DMEM complete + 10^3 U/mL LIF and pipette into the respective well of the 48-well plate.
6. Incubate the clones in the 48-well plate at 37°C and change the medium daily.

dRMCE (day 12 – 15):

ES clones in the 48-well plate usually start growing confluent 2-3 days after picking from the 10 cm dish, depending on the respective clone's size. Apart from checking under the microscope, this is easily observed by a change of media colour from pink to orange/yellow. The ES clones have now reached a sufficiently high cell number to extract genomic DNA for validation.

1. Wash ES clones with 75 µL Trypsin 2x + G.
2. Add 75 µL Trypsin 2x + G and incubate for 7 min at 37°C.
3. Carefully disperse trypsinized cells by pipetting.
4. Add 500 µL Knockout DMEM complete + 10^3 U/mL LIF and further disperse cells.
5. Transfer 200 µL of the cell solution into a well of a 24-well plate (previously coated with 500 µL 0.1 % gelatin solution) including 1 mL Knockout DMEM complete + 10^3 U/mL LIF.
    - The remaining cell solution volume (~ 300 µL) is used for the extraction of genomic DNA using the PureLink Genomic DNA Mini Kit.
6. Incubate the clones, transferred to the 24-well plate, at 37°C and change the medium daily.

The ES clones are further passaged via a 6-well plate towards a 10 cm cell culture dish (24-well → 6-well → 10 cm dish), until the cell number is high enough for cryopreservation ($3x10^6$ cells/ cryotube).

In the meantime, the extracted genomic DNA is used for ES clone validation. Negative clones (those that failed recombination or are heterogeneous) are discarded.

4.2.5 Differentiation of ES cells into NSCs

The differentiation protocol was modified according to (Ying & Smith 2003, Conti *et al.* 2005, Nichols & Ying 2006, Pollard *et al.* 2006a).

Materials:

Cell line:	Respective C57/Bl6/N JM8A3.01 PSEN1 cell line (either PSEN1 wt or cell line carrying the desired PSEN1 mutation and or protein-tag)
Knockout DMEM complete:	Knockout DMEM 1 % FBS (100 % stock) 2x L-Glutamine (100x stock) 103 µM β-Mercaptoethanol (50 mM stock) 1x Pen/Strep (100x stock) $1x10^3$ U/mL LIF ($1x10^7$ U/mL stock)

The Knockout DMEM complete medium is prepared in 50 mL aliquots to avoid repeated cycles of warming in the 37°C water bath. LIF is added right before use!

DMEM/F-12 complete:	DMEM/F-12, HEPES 1x Pen/Strep (100x stock) 0.5x B-27 (50x stock) 0.5x N-2 (100x stock) 100 µM β-Mercaptoethanol (50 mM stock)

NSC Medium:	DMEM/F-12, HEPES
	1x L-Glutamine (100x stock)
	1x Pen/Strep (100x stock)
	0.5x B-27 (50x stock)
	0.5x N-2 (100x stock)
	5 µg/mL Heparin (10 mg/mL stock in H_2O)
	10 ng/mL EGF (20 µg/mL stock)
	10 ng/mL FGF (20 µg/mL stock)

The NSC Medium is prepared in 50 mL aliquots to avoid repeated cycles of warming in the 37°C water bath. EGF and FGF are added right before use!

Matrigel solution:	DMEM/F-12, HEPES
	42 µg/mL Matrigel (9.4 mg/mL stock)
	➢ Prepare Matrigel solution with cold DMEM/F-12, HEPES!

Laminin solution:	PBS -/-
	4 µg/mL Laminin (1 mg/mL stock)

Differentiation (day 0):

1. Coat one well of a 6-well plate per differentiation with 1 mL Matrigel solution and incubate at RT for 1 h.
2. Trypsinize and count ES cells according to chapter 4.1.1.2.
3. Wash the Matrigel coated well with Knockout DMEM complete.
4. Seed $1.25x10^5$ ES cells in Knockout DMEM complete + 10^3 U/mL LIF and incubate the cells at 37°C.

Differentiation (day 1):

1. Wash the cells twice with PBS +/+.
2. Add DMEM/F-12 complete.
3. Incubate the cells at 37°C and change the medium daily.

Differentiation (day 6-11):

Depending on the genomic background of the respective ES cell line (PSEN1 wt vs. FAD PSEN1 mutation), differentiation into morphologically distinct neuroepithelial precursors (NEPs) is complete 6 to 11 days after seeding of the ES cells.

1. Use 1 mL PBS -/- to wash the NEPs.
2. Carefully disperse the NEPs and transfer them into a 15 mL falcon tube.
3. Wash the well again with 1 mL PBS -/- and add to the falcon tube.
4. Centrifugation: 1000 rpm, 5 min, RT
5. Remove the PBS -/- and add 200 µL Accutase to the cell pellet.
6. Incubate the tube for 3 min at 37°C and carefully disperse the cells.
7. Centrifugation: 1000 rpm, 5 min, RT
8. Remove the Accutase and dissolve the pellet in 5 mL NSC Medium + 10 ng/mL EGF + 10 ng/mL FGF.
9. Transfer the cell suspension into an uncoated T25 flask and incubate at 37°C.

Add 1 mL fresh NSC Medium, including 10 ng/mL EGF and FGF, sufficient for the total volume of NSC medium (here 5 mL + 1 mL), to the cell suspension every 2 days, until a sufficient number of floating neurospheres has formed (approximately 1-20 neurospheres; varies between FAD PSEN1 cells lines).

Differentiation (day 12-16):

Approximately 5 days after the transfer of the NEPs to an uncoated T25 flask, a sufficient amount of floating neurospheres (~ 1-20) has formed.

1. Pipet the cell culture medium, including the floating neurospheres, into a 15 mL falcon tube.
2. Wash the T25 flask again with 3 mL DMEM/F-12 medium and add to the cell suspension in the tube.
3. Centrifugation: 1000 rpm, 5 min, RT
4. Remove the medium and add 200 µL Accutase to the cell pellet.
5. Incubate the tube for 3 min at 37°C and carefully disperse the cells.
6. Centrifugation: 1000 rpm, 5 min, RT
7. Remove the Accutase and dissolve the pellet in 5 mL NSC Medium + 10 ng/mL EGF + 10 ng/mL FGF.
8. Transfer the cell suspension into the wells of a Laminin coated 6-well cell culture plate and incubate at 37°C.
    - The neurospheres will start to settle onto the Laminin, migrate and form NSCs.
9. Change the NSC Medium + 10 ng/mL EGF + 10 ng/mL FGF daily.

4.2.6 Differentiation into neurons, astrocytes and oligodendrocytes

The intermediate neurospheres of the NSC differentiation protocol (see chapter 4.2.4) were plated onto 8-chamber slides and differentiated into neurons, astrocytes and oligodendrocytes.

Materials:

Differentiation medium:	75 % DMEM, high glucose, GlutaMAX, pyruvate (v/v)
	25 % Ham‘s F-12, GlutaMAX (v/v)
	1 % FBS (100 % stock) (v/v)
	1x Pen/Strep (100x stock)
	1x N-2 (100x stock)

Poly-D-lysine hydrobromide:	PBS -/- 100 µg/mL Poly-D-lysine hydrobromide
Laminin solution:	PBS -/- 4 µg/mL Laminin (1 mg/mL stock)

Coating:

1. Coat the 8-chamber-slide with Poly-D-lysine hydrobromide and incubate for 1 h at 37°C.
2. Remove the Poly-D-lysine hydrobromide solution and wash the well with sterile ddH_2O.
3. Add Laminin solution to the 8-chamber-slide and incubate for 1 h at 37°C.
4. Remove the Laminin solution and wash the wells with sterile ddH_2O.

Differentiation:

1. Pipet the neurospheres into a 6-well containing PBS -/- to remove residual DMEM/F-12 medium.
2. Fill the wells of the 8-chamber-slide with differentiation medium.
3. Choose 4 neurospheres of similar diameter and place one in each corner of the 8-chamber slide by careful pipetting.
    - Prepare one 8-chamber-slide for the simultaneous staining of neurons and astrocytes and one 8-chamber-slide for the staining of oligodendrocytes.
4. After 3 days of incubation, fix cells and stain with antibody markers for neurons, astrocytes and oligodendrocytes.

4.2.7 Immunocytochemistry of NSCs

NSCs, differentiated from ES cells (see chapter 4.2.5), were seeded and fixed on coverslips for antibody staining against the marker proteins Sox2 and Nestin to confirm their neural stem cell status.

Materials:

Antibody buffer: PBS -/-
2 % BSA (w/v)
5 % sucrose (w/v)

➢ Filter sterile!

PBST: PBS -/-
0.1 % Tween (v/v)

Primary antibody		**Secondary antibody**		
Name	**Dilution**	**Name**	**Conjugate**	**Dilution**
Sox2	1:100	Rat IgG	Cy3 (A_{Em} = 570 nm)	1:1000
Nestin/ rat-401	1:100	Mouse IgG	Alexa Fluor® 488 (A_{Em} = 519 nm)	1:1000

Day 1:

1. Seed 80000 NSCs per 24-well on coverslips (12 mm diameter).

Day 2:

1. Remove medium and wash wells with PBS -/-.
2. Fix cells for 13 min with 4 % PFA in PBS -/- at RT.
3. Wash 2x with PBS -/-.
4. Block reactive aldehyde groups and permeabilize for 10 min at RT, shaking.
    - 0.1 M glycine + 0.25 % Triton-X-100 in PBS -/-.
5. Block 60 min at RT, shaking.
    - 30 % goat serum in antibody buffer
6. Incubate primary antibody, diluted in antibody buffer, o/n at 4°C.

7. Wash 3x 10 min with PBST, shaking.
8. Incubate secondary antibody, diluted in antibody buffer, for 45 min to 1 h at RT in the dark, shaking.
9. Wash 3x, shaking:
    - 1x 10 min PBST
    - 1x 10 min 1:1000 Dapi in PBST
    - 1x 10 min PBS -/-
10. Rinse 1x with ddH_2O.
11. Mount coverslips in Fluor Save Reagent mounting medium.
12. Take pictures, using a fluorescence microscope.
13. Store coverslips at 4°C in the dark.

4.2.8 Immunocytochemistry of neurons, astrocytes and oligodendrocytes

Differentiated neurospheres (see chapter 4.2.6) were fixated inside the 8-chamber slides and stained for the neuron, astrocyte and oligodendrocyte markers -βIII-tubulin, GFAP and O4 to confirm their potential to differentiate into the respective cell types of the central nervous system.

Materials:

PBS-T: PBS -/-
0.1 % Triton-X 100

Primary antibody		**Secondary antibody**		
Name	**Dilution**	**Name**	**Conjugate**	**Dilution**
Anti-βIII-tubulin	1:100	Mouse IgG	Alexa Fluor® 546 (A_{Em} = 573 nm)	1:200
GFAP	1:200	Rabbit IgG	Alexa Fluor® 488 (A_{Em} = 519 nm)	1:200
O4 (IgM)	1:200	Mouse IgM	Alexa Fluor® 488 (A_{Em} = 519 nm)	1:200

1. Fix cells for 30 min with 4 % PFA in PBS -/- at 37°C.
2. Wash 1x with PBS -/-.

3. Remove the detachable chambers on the 8-chamber-slides.
4. Incubate primary antibody (diluted in buffer) for 1 h at 37°C.
    - Anti-βIII-tubulin and GFAP: PBS-T + 10 % goat serum
    - O4: PBS -/- + 10 % goat serum
5. Wash 3x for 5 min with PBS -/-.
6. Incubate secondary antibody, including 1 % Hoechst 33258 solution, for 30 min at RT in the dark.
7. Wash 3x for 5 min with PBS -/-.
8. Rinse 1x with ddH_2O.
9. Mount coverslips in Aqua-Poly/Mount mounting medium.
10. Take pictures, using a fluorescence microscope.
11. Store coverslips at 4°C in the dark.

4.2.9 Infection of NSCs with adenovirus particles

NSCs were infected with an APP695 adenovirus to facilitate detection of newly generated Aβ peptides.

Materials:

NSC Medium:	DMEM/F-12, HEPES
	1x L-Glutamine (100x stock)
	1x Pen/Strep (100x stock)
	0.5x B-27 (50x stock)
	0.5x N-2 (100x stock)
	5 µg/mL Heparin (10 mg/mL stock in H_2O)
	10 ng/mL EGF (20 µg/mL stock)
	10 ng/mL FGF (20 µg/mL stock)

The NSC Medium is prepared in 50 mL aliquots to avoid repeated cycles of warming in the 37°C water bath. EGF and FGF are added right before use!

Phosphoramidon (10 mM):	10 µM
LY-411575 (15 mM):	0.5 µM
APP-695 adenovirus ($2.3x10^{11}$ virus particles/mL):	100 virus particles/cell

Day 1:

1. Seed $1.5x10^6$ cells/well in three wells of a 6-wells cell culture plate per NSC line.
    - Seed in the evening!

Day 2:

1. Prepare 2 mL NSC medium, including 10 ng/mL EFG, 10 ng/mL FGF and 100 APP-695 adenovirus particles/cell.
    - 100 APP-695 adenovirus particles / cell: 0.65 µL particles / well

2. Incubate the NSCs with the NSC Medium including the APP-695 adenovirus for 3 h at 37°C.
3. Wash the wells once with DMEM/F-12, HEPES.
4. Add fresh NSC Medium (2 mL), including 10 ng/mL EFG and 10 ng/mL FGF.
    - To inhibit the generation of Aβ peptides, add 0.5 µM LY-411575 to the NSC Medium.

Day 3:

1. Change the NSC Medium after 24 h. Add 10 µM phosphoramidon to 1 mL NSC Medium, including 20 ng/mL EFG and 20 ng/mL FGF.
    - For the Aβ inhibition control, again add 0.5 µM LY-411575 to the NSC Medium.

Day 4:

1. After 24 h, aliquot the NSC Medium, containing the generated Aβ peptides and store them at -20°C.
2. Scrape the cells off the 6-well plate and pool them for each NSC line.
3. Prepare cell lysates.

The detection of Aβ40 and Aβ42 peptides in the NSC Medium aliquots was carried out by our collaboration partner at the company Asceneuron in Lausanne using the Meso Scale Discovery electrochemiluminescence (ECL) immunoassay (Bucur & Schlenoff 2006, Ousson *et al.* 2013). Avidin-coated MULTI-ARRAY 96-well plates were coated with a biotinylated monoclonal anti-$A\beta_{17\text{-}24}$ (4G8) capture antibody. Ruthenium (Ru^{2+})-labelled G2-10 and A387 monoclonal antibodies were used for the detection of the Aβ40 and Aβ42 peptides, respectively. Aβ40 and Aβ42 standard peptides were simultaneously measured:

Aβ40 [ng/mL]: 12, 6, 3, 1.5, 0.75, 0.375, 0.1875, 0.093

Aβ42 [ng/mL]: 2, 1, 0.5, 0.25, 0.125, 0.0625, 0.03125, 0.0156

4.3 Protein Biochemistry

4.3.1 Cell lysate preparation

For the analysis of intracellular proteins, cells were lysed in NP40 buffer.

Materials:

NP 40 buffer:	50 mM TRIS-HCl, pH 7.8 150 mM NaCl 1 % NP40 (v/v) ➢ Store at 4°C.
25x Protease Inhibitor (PI):	Dissolve one Protease inhibitor cocktail tablet (EDTA-free) in 2 mL ddH_2O. Aliquot and store at -20°C.

1. Remove medium.
2. Wash cells 1x with PBS -/-.
3. Add 1.5 mL PBS -/- per 10 cm dish and scrape cells off the plate.
4. Transfer the scraped cells into a 15 mL Falcon tube.
5. Wash the 10 cm dish with 4.5 mL PBS -/- and add to the cell solution into the falcon tube.
6. Centrifugation: 4000 rpm, 3 min, RT
7. Remove the PBS -/-.
8. Resuspend the cell pellet in NP40 buffer + 1x PI.
9. Incubate the resuspended cells on ice for 20 min.
    - Vortex every 5 min.
10. Centrifugation: 13000 x g, 15 min, 4°C
11. Transfer the supernatant into a fresh tube and store at -20°C.

4.3.2 Membrane preparation

Membrane preparations of ES cells were used to perform co-immunoprecipitation experiments and γ-secretase *in vitro* assays. Cellular membranes can be obtained by disrupting the cells and subsequent differential centrifugation steps. Neglecting soluble cell components, membrane proteins, such as the γ-secretase complex, are carefully solubilized from extracted cell membranes by addition of detergents. Since soluble proteins are lost during the process, membrane preparations have a much higher purity in comparison to cell lysates with regard to membrane proteins.

Materials:

Homogenization buffer:	50 mM HEPES, pH 7.0 250 mM sucrose 5 mM EDTA, pH 8.0 ➢ Store at 4°C.
25x Protease Inhibitor (PI):	Dissolve one Protease inhibitor cocktail tablet (EDTA-free) in 2 mL ddH_2O. Aliquot and store at -20°C.
CHAPSO stock:	10 % in ddH_2O

Day 1:

1. Prepare 10x 10 cm dishes with confluent ES cells for the membrane preparation.
2. Remove the medium.
3. Wash the 10 cm plates with 10 mL PBS -/- each and discard the PBS -/-.
4. Add 1.5 mL PBS -/- per 10 cm dish and scrape cells off the plate.
5. Transfer the cell solution into a 15 mL Falcon tube.
6. Wash the 10 cm dish with 4.5 mL PBS -/- and add to the cell solution in the falcon tube.
7. Centrifugation: 4000 rpm, 3 min, RT.

8. Remove the PBS -/-.
9. Dissolve the cell pellet in 10 mL Homogenization buffer + 1x PI.
10. Disrupt the cells using the Nitrogen Cavitation Bomb: ~ 120 bar (= 1750 psi)
    - Collect the disrupted cells in an ice cold 50 mL Falcon tube.
11. Centrifugation: 4000 rpm, 10 min, 4°C.
    - Keep the supernatant!
12. Centrifugation: 3000 x g, 10 min, 4°C
    - Keep the supernatant!
13. Centrifugation: 170000 x g, 1 h, 4°C
14. Remove the supernatant.
15. Suspend the membrane pellet in 2 mL ice cold 0.1 M sodium bicarbonate, pH 11.3 and aliquot into 1 mL samples tube.
16. Centrifugation: 170000 x g, 1 h, 4°C
17. Remove the supernatant from the two tubes.
18. Store the membrane pellet (each from $5x10^6$ cells) at -80°C.

Day 2:

1. Dissolve the membrane pellet from one tube in 525 µL Homogenization buffer + 1x PI.
2. Add CHAPSO to a final concentration of 1 %.
    - Add 58 µL 10 % CHAPSO to 525 µL membrane solution
3. Incubate for 90 min on a rotary wheel at 4°C.
4. Centrifugation: 170000 x g, 1 h, 4°C
5. Store the solubilized membrane at –80°C.

4.3.3 Bicinchonic acid (BCA) protein assay

Protein concentrations from cell lysates or membrane preparations were simultaneously measured against a BSA standard using the BCA Protein Assay Kit.

1. Prepare a 1 mg/mL BSA stock solution in the respective sample buffer:
    a. Cell lysates: NP40 buffer (see chapter 4.3.1)
    b. Membrane preparation: Homogenization buffer (see chapter 4.3.2)
2. Dilute the BSA stock solution for the BCA assay as follows:

Final BSA concentration [µg/mL]	Volume of BSA stock solution [µL]	Volume of sample buffer [µL]
0	0	100
100	10	90
200	20	80
300	30	70
400	40	60
500	50	50
600	60	40

3. Prepare the protein sample in triplicates with a final volume of 25 µL each.
    a. 2.5 µL cell lysate + 22.5 µL NP40 buffer
    b. 5 µL membrane solution + 20 µL Homogenization buffer
4. Load the BSA standard in duplicates and the respective protein sample in triplicates onto a 96-well plate.
5. Mix BCA Reagent A and B in a 50:1 ratio.
6. Add 200 µL of the mixed BCA reagent solution to the BSA standard and the protein samples.
7. Incubate the 96-well plate for 30 min at 60°C.
8. After incubation, measure the samples in the PARADIGM Microtiterplate reader at 540 nm wavelength and calculate the sample concentration.

4.3.4 SDS-Polyacrylamide gelelectrophoresis (SDS-PAGE)

SDS-PAGE is a method for the separation of proteins within a sample. Upon application of a SDS containing sample buffer, proteins are overall negatively charged and separated according to their electrophoretic mobility within an applied electric field. A polyacrylamide gel for the protein separation is obtained from cross-linking of acrylamide with bis-acrylamide. Polymerization is induced by addition of a radical initiator APS. The gel pore size is variable and depends on the ratio of acrylamide to bis-acrylamide.

Materials:

Bis-tris gel buffer:	1.6 M Bis-tris pH 6.4
APS stock:	10 % in ddH_2O
20x MES buffer:	1 M MES 1 M TRIS 69.3 mM SDS 20.5 mM EDTA
4x SDS sample buffer:	1.44 M Bis-tris 0.64 M Bicine 4 % SDS (v/v) 100 mM DTT 0.05 % Bromphenoleblue (w/v) 25 % Glycerol (w/v)

1. Prepare the resolving and stacking solution for a 12 % bis-tris gel as follows without APS and TEMED:

	12 % Resolving solution		4 % Stacking solution	
	1 gel	**2 gels**	**1 gel**	**2 gels**
30 % Acrylamide/Bis-acrylamide (37.5:1)	2.64 mL	5.28 mL	350 µL	700 µL
1.6 M Bis-tris pH 6.4	1.65 mL	3.30 mL	500 µL	1000 µL
ddH_2O	2.26 mL	4.52 mL	1.14 mL	2.28 mL
10 % APS	33 µL	66 µL	20 µL	40 µL
TEMED	11 µL	22 µL	5 µL	10 µL

2. Add APS and TEMED to the 12 % resolving solution to initiate polymerization.
3. Quickly fill the resolving gel solution into a Novex gel cassette and overlay with isopropanol.
4. After complete polymerization (approximately 25 min at RT), remove the isopropanol and wash the resolving gel with ddH_2O.
5. Add APS and TEMED to the stacking solution.
6. Fill the stacking gel solution on top of the resolving gel and add a 12 slots comb.
7. Remove the comb after complete polymerization (approximately 20 min at RT) and wash the 12 slots thoroughly with ddH_2O.
8. Place the gel cassette into the electrophoresis chamber.
9. Fill the electrophoresis chamber with 1x MES-buffer.
10. Dilute protein samples in 4x SDS sample buffer to a total volume of 15 µL.
11. Load the gel with the 15 µL protein samples and 2 µL of the Prestained Protein ladder (10 - 250 kDa).
12. Run the SDS-PAGE at 150 V for approximately 1 h.

4.3.5 Western Blot

Following SDS-PAGE, the separated proteins are transferred from the gel onto a PVDF membrane by Western blotting for subsequent immunostaining of the proteins.

Materials:

Transfer buffer:	25 mM TRIS
	192 mM Glycine
	20 % ethanol (v/v)

1. Prepare one transfer cassette per Western blot including 2 whatman paper and 3 flat sponges.
2. Place the transfer cassette in the tank blotter and fill it with transfer buffer.
3. Activate the PVDF membrane with methanol.
4. Build the blotting stack as follows

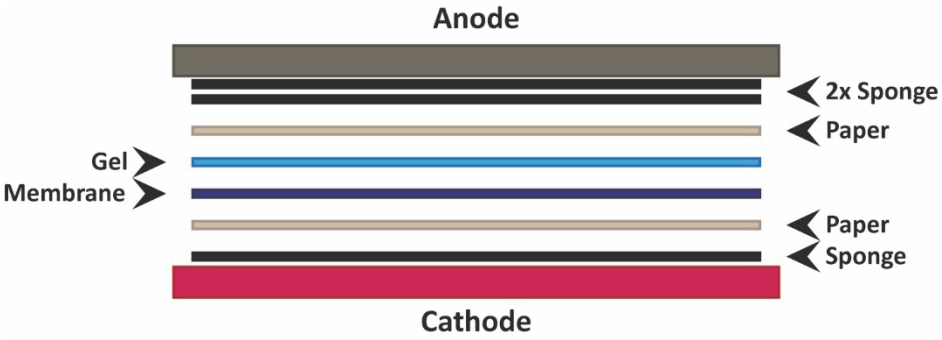

5. Blot the gel for 2 h at 200 mA.

4.3.6 Immunostaining of PVDF membranes

Materials:

10x TBS, pH 7.4:	0.25 M TRIS
	1.37 M NaCl
	27 mM KCl
1x TBST	1x TBS
	0.01 % Tween-20 (v/v)
5 % skim milk solution:	5 % non-fat dry milk (w/v)
	TBST

Primary antibody			Secondary antibody			
Name	**Dilution**	**Buffer**	**Name**	**Conjugate**	**Dilution**	**Buffer**
Actin	1:10000	TBST + 0.02 % NaN_3	Rabbit IgG	IRDye 800CW (A_{Em} = 795 nm)	1:15000	5 % milk solution + 0.02 % NaN_3
CT-15	1:3500	TBST + 0.02 % NaN_3				
Nicastrin	1:1000	5 % milk solution + 0.02 % NaN_3				
Pen-2	1:1000	TBST + 0.02 % NaN_3				
PSEN1 CTF	1:1000	TBST + 0.02 % NaN_3				
PSEN1 NTF	1:200	TBST + 0.02 % NaN_3				
Flag	1:1000	5 % milk solution + 0.02 % NaN_3	Mouse IgG	IRDye 800CW (A_{Em} = 795 nm)	1:10000	5 % milk solution + 0.02 % NaN_3
Mouse anti-V5 Tag	1:500	TBST + 0.02 % NaN_3				

Day 1:

1. After Western blotting, quickly wash the membrane with 1x TBS shaking.
2. Block the membrane with 5 % milk solution for 1 h at RT shaking.
3. Wash the membrane 3x with 1x TBST for 15 min shaking.
4. Prepare the primary antibody in the respective dilution and buffer.
5. Incubate the membrane with the primary antibody over night at 4°C shaking.

Day 2:

1. Remove the primary antibody.
    - Save the primary antibody solution for repeated use!
2. Wash the membrane 3x with 1x TBST for 15 min shaking.
3. Prepare the secondary antibody in the respective dilution and buffer.
4. Incubate the membrane with the secondary antibody for 1 h at RT shaking.
5. Wash the membrane 2x with 1x TBST for 15 min and 1x with 1x TBS buffer for 15 min shaking.
6. Read the fluorescence signal of the antibody-labelled proteins on the membrane using the LI-COR ODYSSEY CLx.

Quantitative protein detection by the LI-COR system occurs in the near-infrared spectral region (700 – 900 nm), using secondary antibodies conjugated to infrared dyes. The fluorescence signal was calculated with the Image Studio Software 2.1 following scanning with the LI-COR ODYSSEY CLx.

4.3.7 Immunoprecipitation (IP)

Immunoprecipitation is a technique which exploits the specific antigen-antibody interaction. In the first step, a protein of interest binds to an antibody, which is coupled to a solid matrix. To enable protein-protein interactions, the matrix-bound protein of interest is subsequently incubated with a protein solution, usually whole cell lysates. Proteins that do not interact with the matrix-bound protein of interest are lost during the subsequent washing steps. However, interaction partners may be co-immunoprecipitated and identified in the subsequent SDS-PAGE / Western Blot / Immunostaining (see chapters 4.3.4 – 4.3.6) analysis of the elution fraction from the matrix.

Materials:

Homogenization buffer:	50 mM HEPES, pH 7.0 250 mM sucrose 5 mM EDTA, pH 8.0 ➢ Store at 4°C.
25x Protease Inhibitor (PI):	Dissolve one Protease inhibitor cocktail tablet (EDTA-free) in 2 mL ddH_2O. Aliquot and store at -20°C.
CHAPSO stock:	10 % in ddH_2O (w/v)
4x SDS sample buffer:	1.44 M Bis-tris 0.64 M Bicine 4 % SDS (v/v) 100 mM DTT 0.05 % Bromphenoleblue (w/v) 25 % Glycerol (w/v)

Day 1:

1. Pipet 20 µL Protein A/G PLUS-Agarose beads per IP in a 1.5 mL tube.
2. Centrifugation: 1000 x g, 5 min, 4°C
3. Remove the supernatant and resolve the beads in 200 µL homogenization buffer.
4. Centrifugation: 1000 x g, 5 min, 4°C
5. Remove the supernatant.
6. Incubate 160 µg membrane solution (see chapter 4.3.2) in the presence and absence of an antibody with the Protein A/G PLUS-Agarose beads.
    - Unspecific protein binding to the beads is evaluated in the absence of an antibody.
        a. Flag antibody: 4 µg
        b. PSEN1 NTF antibody: 4 µg

7. Incubate the IP samples over night on a rotary wheel at 4°C.
    - ➢ As a control for protein degradation, also incubate the membrane solution without beads over night on the rotary wheel at 4°C.

Day 2:

1. Centrifugation: 1000 x g, 5 min, 4°C
2. Carefully remove the supernatant without disturbing the beads pellet
3. Wash the pellet 2x with 200 µL homogenization buffer + 0.25 % CHAPSO + 1x PI on a rotary wheel for 5 min at 4°C.
    - Take a 100 µL aliquot of the supernatant from the first washing step!
4. Heat the beads for 5 min at 65°C in 80 µL 1x SDS sample buffer in homogenization buffer.
5. Centrifugation: 16430 x g, 10 min, RT
6. Store the supernatant at -20°C.

Analyse the protein composition of the supernatant by SDS-PAGE / Western Blot / Immunostaining.

4.3.8 γ-secretase *in vitro* assay

The catalytic activity of the γ-secretase complex within the membrane solution (see chapter 4.3.2) was analysed using an *in vitro* assay. A substrate was incubated with the immunoprecipitated, antibody bound membrane. The cleavage product was subsequently detected in the eluate from the beads by SDS-PAGE / Western Blot / Immunostaining.

Materials:

Homogenization buffer: 50 mM HEPES, pH 7.0
250 mM sucrose
5 mM EDTA, pH 8.0

- ➢ Store at 4°C.

25x Protease Inhibitor (PI):	Dissolve one protease inhibitor cocktail tablet (EDTA-free) in 2 mL ddH_2O. Aliquot and store at -20°C.
CHAPSO stock:	10 % in ddH_2O (w/v)
DAPT stock:	10 mM in DMSO
APP C100 V5–His_6:	118.03 µM in: 20 mM TRIS-HCl, pH 7.8 150 mM NaCl 200 mM Imidazol
4x SDS sample buffer:	1.44 M Bis-tris 0.64 M Bicine 4 % SDS (v/v) 100 mM DTT 0.05 % Bromphenoleblue (w/v) 25 % Glycerol (w/v)

Day 1:

1. Pipet 20 µL Protein A/G PLUS-Agarose beads per IP in a 1.5 mL tube.
2. Centrifugation: 1000 x g, 5 min, 4°C
3. Remove the supernatant and resolve the beads in 200 µL homogenization buffer.
4. Centrifugation: 1000 x g, 5 min, 4°C
5. Remove the supernatant.
6. Incubate 40 µg membrane solution (see chapter 4.3.2) in 100 µL homogenization buffer + 1 % CHAPSO + 1x PI with the Protein A/G PLUS-Agarose beads in the presence of the following antibodies:
    a. Flag antibody (1 mg/mL): 1 µg: 1 µL
    b. PSEN1 NTF antibody (200 µg/mL): 1 µg: 5 µL
    c. Nicastrin antibody: 1 µL
    d. Nicastrin antibody: 1 µL
7. Incubate the IP samples over night on a rotary wheel at 4°C.

Day 2:

1. Centrifugation: 1000 x g, 5 min, 4°C
2. Carefully remove the supernatant without disturbing the beads pellet
3. Wash the pellet 2x with 100 µL homogenization buffer + 0.25 % CHAPSO + 1x PI on a rotary wheel for 5 min at 4°C.
4. Centrifugation: 1000 x g, 5 min, 4°C
5. Add 3 µM APP C100 V5–His_6 (and 1 µM DAPT) in 30 µL homogenization buffer + 0.25 % CHAPSO + 0.1 % phosphatidylcholine + 1x PI to the samples:
    a. Membrane + Flag antibody: 3 µM APP C100 V5–His_6
    b. Membrane + PSEN1 NTF antibody: 3 µM APP C100 V5–His_6
    c. Membrane + Nicastrin antibody: 3 µM APP C100 V5–His_6
    d. Membrane + Nicastrin antibody: 3 µM APP C100 V5–His_6 + 1 µM DAPT
6. Incubate the samples for 20 h at 37°C.

Day 3:

1. Add 10 µL 4x SDS sample buffer and heat the samples for 5 min at 65°C.
2. Centrifugation: 16430 x g, 10 min, RT
3. Store the supernatant at -20°C.

Analyse the protein composition of the supernatant by SDS-PAGE / Western Blot / Immunostaining.

5. Results

5.1 Identification of positive ES cell clones

Murine ES cell lines, endogenously expressing heterozygous PSEN1 FAD mutations were generated from the C57/Bl6/N JM8A3.01 PSEN1 parental cell line by dual recombinase mediated cassette exchange (dRMCE) (see chapter 4.2.4) (Osterwalder et al. 2010).
16 PSEN1 mutations have been chosen to reinvestigate the contribution to the Aβ40 and Aβ42 production and the putative trans dominant-negative effect on the PSEN1 wt allele (Heilig et al. 2013, Xia et al. 2015, Szaruga et al. 2015, Kretner et al. 2016) [Table 2].

Table 2: PSEN1 mutations for the reinvestigation of Aβ40 and Aβ42 production and the putative trans dominant-negative effect on PSEN1 wt.

FAD PSEN1 mutations for the investigation of Aβ40 and Aβ42 production	**PSEN1 mutations for the investigation of the putative trans dominant-negative effect**
PSEN1 wt	PSEN1 wt
PSEN1 P117L	PSEN1 L166P
PSEN1 L166P	PSEN1 L166P + D385N
PSEN1 L173W	PSEN1 L166P + D385N 3xFlag
PSEN1 I213T	PSEN1 M233V
PSEN1 M233V	PSEN1 M233V + D385N
PSEN1 R278I	PSEN1 M233V + D385N 3xFlag
PSEN1 E280A	PSEN1 D385N
PSEN1 G384A	
PSEN1 C410Y	
PSEN1 L435F	

The C57/Bl6/N JM8A3.01 PSEN1 parental cell line contains a synthetic cassette on one of the two PSEN1 alleles, which is located between PSEN1 exon 4 and 6 and flanked by one FRT and one loxP recombinase recognition site.
The genomic engineering technique dRMCE facilitates the targeted replacement of the synthetic cassette by simultaneous electroporation of the C57/Bl6/N JM8A3.01 PSEN1 parental cell line with the pDREV-1 replacement construct and the pDIRE vector, encoding for the Flpo and iCre recombinases [Figure 13]. The replacement sequence on the pDREV-1

vector consists of parts of the intron sequence 4, the exon 5-12 cDNA, including a stop codon as well as a puromycin resistance and is also flanked by one FRT and one loxP site.

Electroporation of equal quantities of the pDREV-1 and pDIRE vector with the C57/Bl6/N JM8A3.01 PSEN1 parental cell line first generates the deleted locus by a deletion of the sequence between the three loxP sites. The remaining sequence of the deleted locus, which is flanked by one FRT and one loxP site, is in a second step exchanged for the replacement sequence on the pDREV-1 vector, generating the replaced locus and restoring PSEN1 expression of the conditional allele.

A timeline for the engineering of PSEN1 ES cell lines by dRMCE is shown in Figure 14.

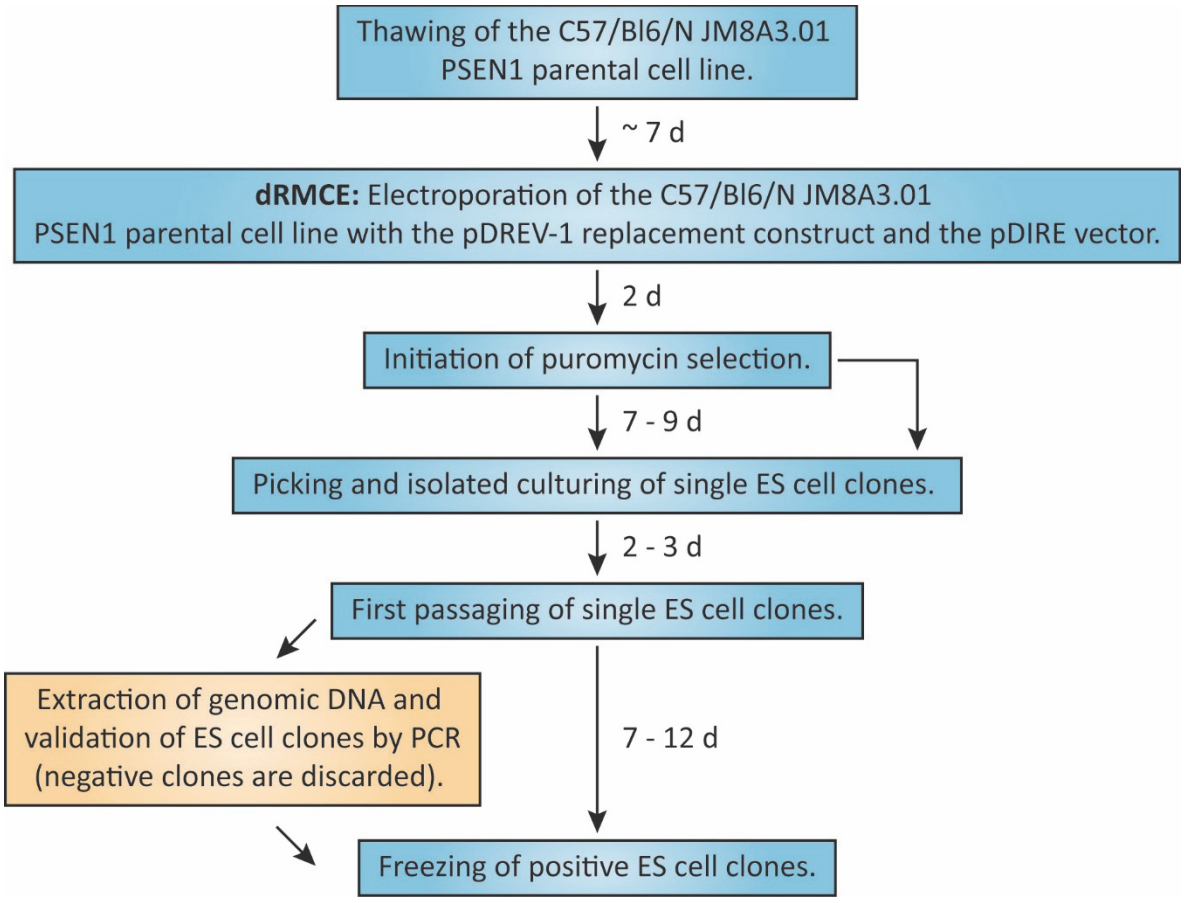

Figure 14: Timeline of ES cell engineering by dual recombinase mediated cassette exchange (dRMCE). Density of the C57/Bl6/N JM8A3.01 PSEN1 parental cell line was sufficiently confluent for electroporation approximately 7 days after thawing. A puromycin selection was induced two days after electroporation with the pDREV-1 replacement construct, which contains the PSEN1 exon 4'-12 replacement sequence, including the respective PSEN1 mutation and the pDIRE vector, encoding for the Flpo and iCre recombinases. Puromycin selection was continued until single ES cell clones had reached a sufficient size for picking and isolated culturing. Genomic DNA was extracted during the first passaging of the ES cell clones and used for the simultaneous PCR-based validation of the ES cell clones during culturing. Negative ES cell clones, which had failed successful replacement of the synthetic cassette in the conditional allele by the PSEN1 replacement sequence on the pDREV-1 vector, were discarded. Positive ES cell clones were cryopreserved at -80°C.

Approximately 12 to 14 days after electroporation, single ES clones with typical round, 3-dimensional ES cell morphology and a dense core [Figure 15 A] were picked from the plate and cultured separately.

A

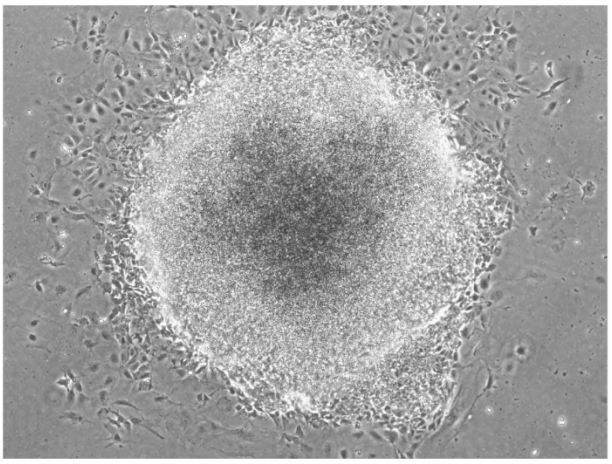

B

Primer	bp	Locus	Primer	bp	Locus
F2-b / R2-b1	1448	original	F2-b / PS1 Ex5_seq_rev	/	original
	1448	deleted		/	deleted
	/	replaced		1109	replaced
F1 / R9-b	3585	original		994	wt allel
	853	deleted	F11-b2 / R9-b	/	original
	/	replaced		/	deleted
F9 / R9-b	1460	original		851	replaced
	/	deleted			
	/	replaced			

C

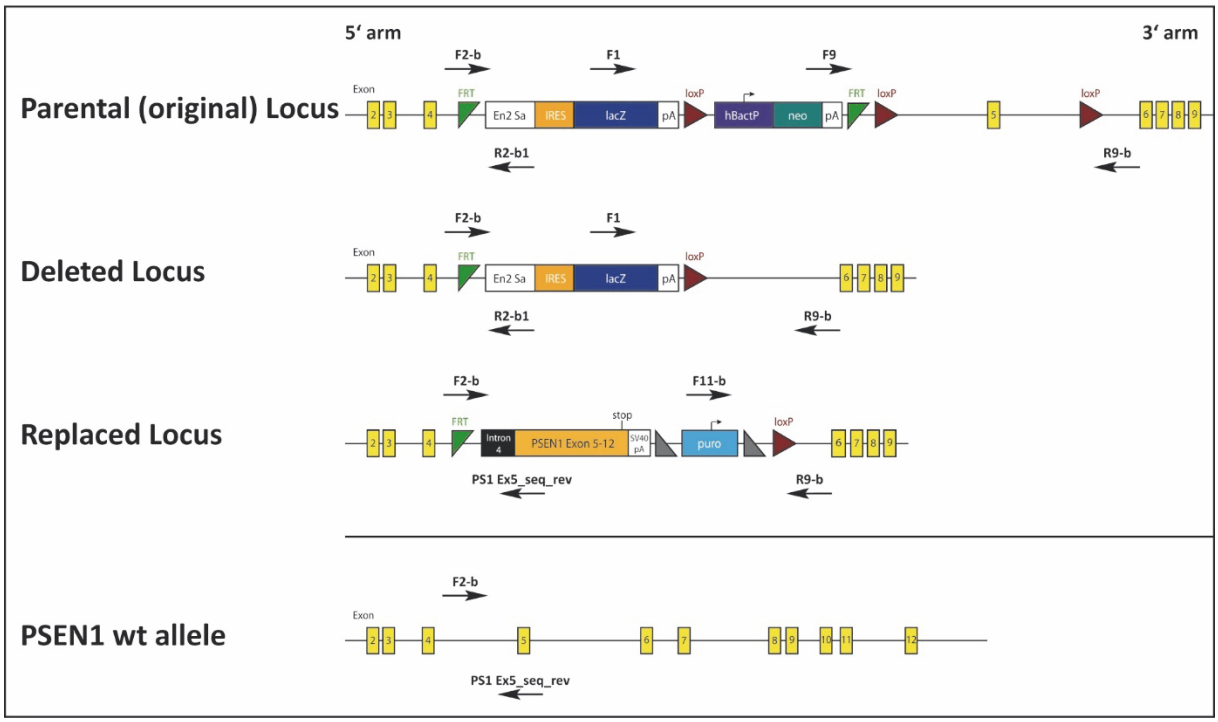

Figure 15: (**A**) A typically round ES cell clone 11 days after electroporation. The ES cell clone has a dense core of pluripotent stem cells and is surrounded by differentiated cells. (**B**) Primer pairs for the PCR-based validation of ES cell clones. Each primer pair produces a PCR product of a distinct size, which is either specific for the original parental, the deleted or the replaced locus. (**C**) Respective positions of the validation primers on the original parental locus, the deleted locus, the replaced locus and the dRMCE unchanged PSEN1 wt allele. Yellow boxes represent the PSEN1 exons 2 – 9.

The genomic background of the picked clones was validated by PCR analysis, using extracted genomic DNA as template DNA and a set of 5 different primer pairs, which spanned the recombination sites on the 5' and 3' arms of the original parental, the deleted and the replaced locus.

The primer pairs were designed to be specific for one of the three described loci. However, the F2-b / R2-b1 and F 1 / R9-b primer pairs recognised both, the original and the deleted locus. Furthermore, the F2-b / PS1 Ex5_seq_rev primer pair also recognised a band for the PSEN1 wt allele, which is present in the parental ES cell line and in every engineered ES cell line, since it remains unchanged during dRMCE.

By the presence or absence of PCR products for the applied primer pairs on an agarose gel, the original, the deleted and the replaced loci were discriminated. The ES cell clones were thereby categorised into positive, negative or heterozygous clones. A positive clone only showed PCR bands for the primer pairs that recognised the replaced locus. A negative clone only showed bands for the deleted locus and a heterozygous clone accordingly displayed bands for both loci. In response to the thorough dilution of the cell suspension after electroporation, ES cell clones usually grow from a single ES cell. A heterozygous clone might therefore originate from two ES cells, one harbouring the deleted and one harbouring the replaced locus, which grew in close proximity and eventually formed one clone.

The 5 primer pairs, their recognition of the original, the deleted and the replaced locus, including the corresponding PCR product sizes are listed in Figure 15 B. The respective positions of the primers on the three loci and the PSEN1 wt allele are shown in Figure 15 C.

In the initial PCR analysis, the primer pair F2-b / PS1 Ex5_seq_rev was applied to differentiate positive from negative clones. A double band was visible for positive clones; the lower band (994 bp) corresponds to the PSEN1 wt allele and the upper band (1109 bp) to the successfully replaced PSEN1 allele. Negative clones, that had failed successful recombination, accordingly only show the lower band of the PSEN1 wt allele [Figure 16].

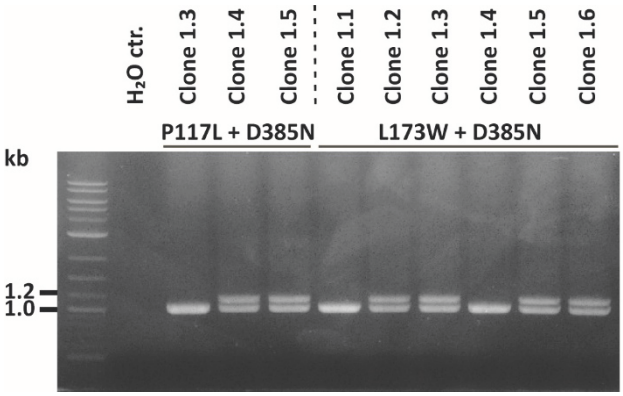

Primer	bp	Locus	Negative clone	Positive clone
F2-b / PS1 Ex5_seq_rev	1109	replaced	-	+
	994	wt allele	+	+

Figure 16: Initial PCR-based validation of ES cell clones, exemplified by two ES cell lines following dRMCE mediated introduction of the PSEN1 P117 + D385N and the PSEN1 L173W + D385N double mutations. Positive clones showed a double band for the replaced locus (1109 bp) and the unchanged PSEN1 wt allele (994 bp). Negative clones only showed a single band for the PSEN1 wt allele.

In the above exemplified validation, PSEN1 P117 + D385N clone 1.3 and PSEN1 L173W + D385N clone 1.1 and clone 1.4 are negative.

The positive ES cell clones were further validated, including the other 4 primer pairs, to evaluate successful 5'- recombination and to exclude heterozygous ES clones.

Figure 17 shows the distinct pattern of PCR bands that was observed for a positive clone, a negative clone and a heterozygous clone.

In Figure 17 A, PCR products were exclusively generated for the primer pairs that recognise the replaced locus and the PSEN wt allele. Correspondingly, this ES cell clone is positive. In contrast, the ES cell clone in Figure 17 B only showed PCR products for the deleted locus and the PSEN1 wt allele and is therefore negative. The ES clone in Figure 17 C showed PCR bands for both the replaced and the deleted locus and is consequently heterozygous.

In a final PCR analysis, all positive ES cell clones were investigated for the undesired genomic integration of the iCre and Flpo recombinases, which might occur in the process of dRMCE (Osterwalder et al. 2010). A PCR, in the presence of the pDIRE vector as positive control, was performed, using primer pairs, which recognise the iCre and Flpo CDS respectively (data not shown). A genomic integration of neither the iCre nor the Flpo recombinase has been observed in any of the generated PSEN1 ES cell lines (data not shown).

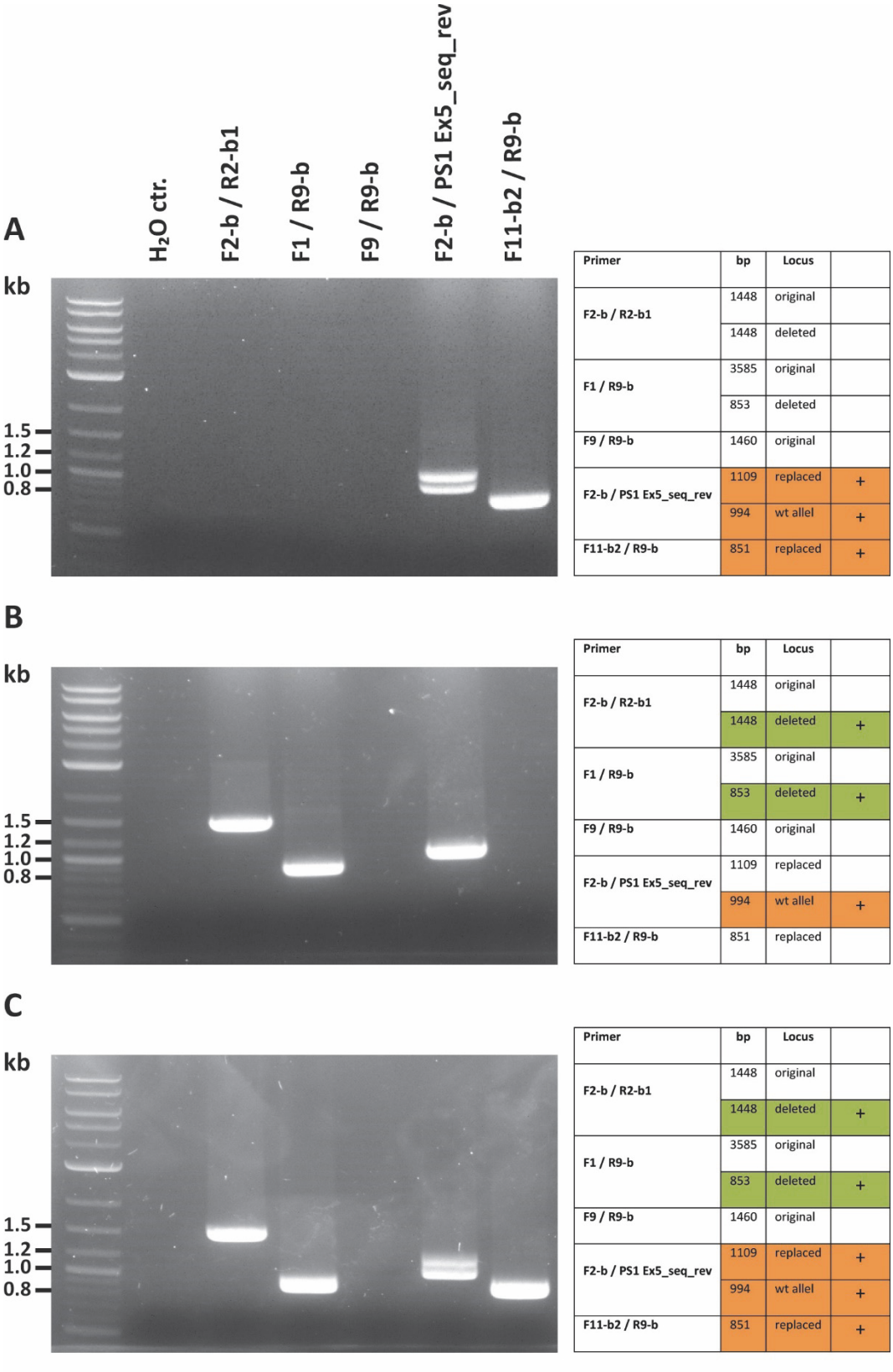

Primer	bp	Locus	
F2-b / R2-b1	1448	original	
	1448	deleted	
F1 / R9-b	3585	original	
	853	deleted	
F9 / R9-b	1460	original	
F2-b / PS1 Ex5_seq_rev	1109	replaced	+
	994	wt allel	+
F11-b2 / R9-b	851	replaced	+

Primer	bp	Locus	
F2-b / R2-b1	1448	original	
	1448	deleted	+
F1 / R9-b	3585	original	
	853	deleted	+
F9 / R9-b	1460	original	
F2-b / PS1 Ex5_seq_rev	1109	replaced	
	994	wt allel	+
F11-b2 / R9-b	851	replaced	

Primer	bp	Locus	
F2-b / R2-b1	1448	original	
	1448	deleted	+
F1 / R9-b	3585	original	
	853	deleted	+
F9 / R9-b	1460	original	
F2-b / PS1 Ex5_seq_rev	1109	replaced	+
	994	wt allel	+
F11-b2 / R9-b	851	replaced	+

Figure 17: Validation of ES cell clones by PCR analysis, using 5 primer pairs. (**A**) A positive ES clone, exclusively showing PCR bands for the replaced locus and the PSEN1 wt allele. (**B**) A negative ES clone, exclusively showing PCR bands for the deleted locus and the PSEN1 wt allele. (**C**) A heterozygous ES clone, showing PCR bands for the replaced locus, the deleted locus and the PSEN1 wt allele.

The efficiency of the dRMCE technique was evaluated by the number of positive and negative clones per engineered PSEN1 ES cell line. The respective values for each cell line are shown in Table 3.

Table 3: Efficiency of the dRMCE technique. For each PSEN1 ES cell line, the total number of investigated cell clones and the respective proportion of positive and negative clones in number and percentage are shown.

PSEN1 ES cell line	**Number of clones**	**Positive clones**		**Negative clones**	
		Number	**[%]**	**Number**	**[%]**
PSEN1 wt	14	8	43	6	57
PSEN1 wt 3xFlag	6	3	50	3	50
PSEN1 P117L	6	2	33	4	67
PSEN1 P117L + D385N	6	3	50	3	50
PSEN1 N135I	6	1	17	5	83
PSEN1 N135S	6	3	50	3	50
PSEN1 L166P	6	3	50	3	50
PSEN1 L166P 3xFlag	6	2	33	4	67
PSEN1 L166P + D385N	6	2	33	4	67
PSEN1 L166P + D385N 3xFlag	6	3	50	3	50
PSEN1 L166P + D385N + M292D 3xFlag	6	3	50	3	50
PSEN1 L173W	6	3	50	3	50
PSEN1 L173W + D385N	6	4	67	2	33
PSEN1 I213T	6	3	50	3	50
PSEN1 M233V	6	3	50	3	50
PSEN1 M233V + D385N	6	2	33	4	67
PSEN1 M233V + D385N 3xFlag	6	4	67	2	33
PSEN1 M233V + D385N + M292D 3xFlag	6	2	33	4	67
PSEN1 R278I	6	2	33	4	67
PSEN1 E280A	6	4	67	2	33
PSEN1 M292D + D385N	6	2	33	4	67
PSEN1 ΔHL	14	8	57	6	43
PSEN1 G384A	6	3	50	3	50
PSEN1 D385N	6	3	50	3	50
PSEN1 C410Y	6	3	50	3	50
PSEN1 L435F	6	3	50	3	50
∑	**172**	**82**	**48**	**90**	**52**

In summary, 48 % of all investigated ES cell clones were positive.

Following electroporation of the C57/Bl6/N JM8A3.01 PSEN1 parental cell with the first two replacement constructs, 14 ES clones were picked for the PSEN1 wt and PSEN1 ΔHL cell line. However, after their evaluation it was obvious that the number of successfully recombined positive clones after dRMCE was sufficiently high. The number of picked ES cell clones was thus reduced to 6 in the following dRMCE experiments.

5.2 Evaluation of allelic transcription rate in ES cell lines

To confirm equal transcription of the PSEN1 wt allele and the restored PSEN1 allele after successful dRMCE, RNA was isolated from the generated ES PSEN1 wt and ES PSEN1 ΔHL cell lines and reverse transcribed into cDNA (see chapter 4.1.4) for subsequent PCR analysis.
Both ES cell lines consist of one PSEN1 wt allele and one dRMCE engineered, restored PSEN1 allele The PSEN1 wt allele contains intron sequences between the PSEN1 exons, whereas the PSEN1 sequence on the restored PSEN1 allele continues with a cDNA for the exons 5-12 after intron 4 (see chapter 4.2.4).
In case of the ES PSEN1 wt cell line, the conditional PSEN1 allele was replaced for a PSEN1 wt cDNA by dRMCE. The introduced PSEN1 cDNA on the restored PSEN1 allele of the ES PSEN1 ΔHL cell line has a 120 bp deletion in the PSEN1 wt sequence, corresponding to the amino acids G330-L369 in the hydrophilic loop. Consequently, in an RT-PCR analysis, the ES PSEN1 ΔHL cDNA should produce two distinct PCR products, one for the PSEN1 wt allele and one 120 bp smaller product for the PSEN1 ΔHL allele. A PCR was simultaneously run with the ES PSEN1 ΔHL cDNA and isolated ES PSEN1 wt and ES PSEN1 ΔHL genomic DNA as size control.
Genomic DNA, in contrast to cDNA, contains the intron sequences of the PSEN1 wt allele. A PCR product is therefore only generated for the respective restored PSEN1 allele. Figure 18 A shows the expected two PCR products for the ES PSEN1 ΔHL cDNA, in the presence of the ES PSEN1 wt and ES PSEN1 ΔHL genomic DNA size controls, for the primer pair PS1 Ex5_seq_for / RT-PCR_rev, which binds to PSEN1 exons 5 and 11.
The two PCR products, corresponding to the PSEN1 wt allele (884 bp) and the restored PSEN1 ΔHL allele (764 bp) of the ES PSEN1 ΔHL cell line were quantified and showed equal intensity, indicating likewise equal transcription of the two alleles [Figure 18 B].

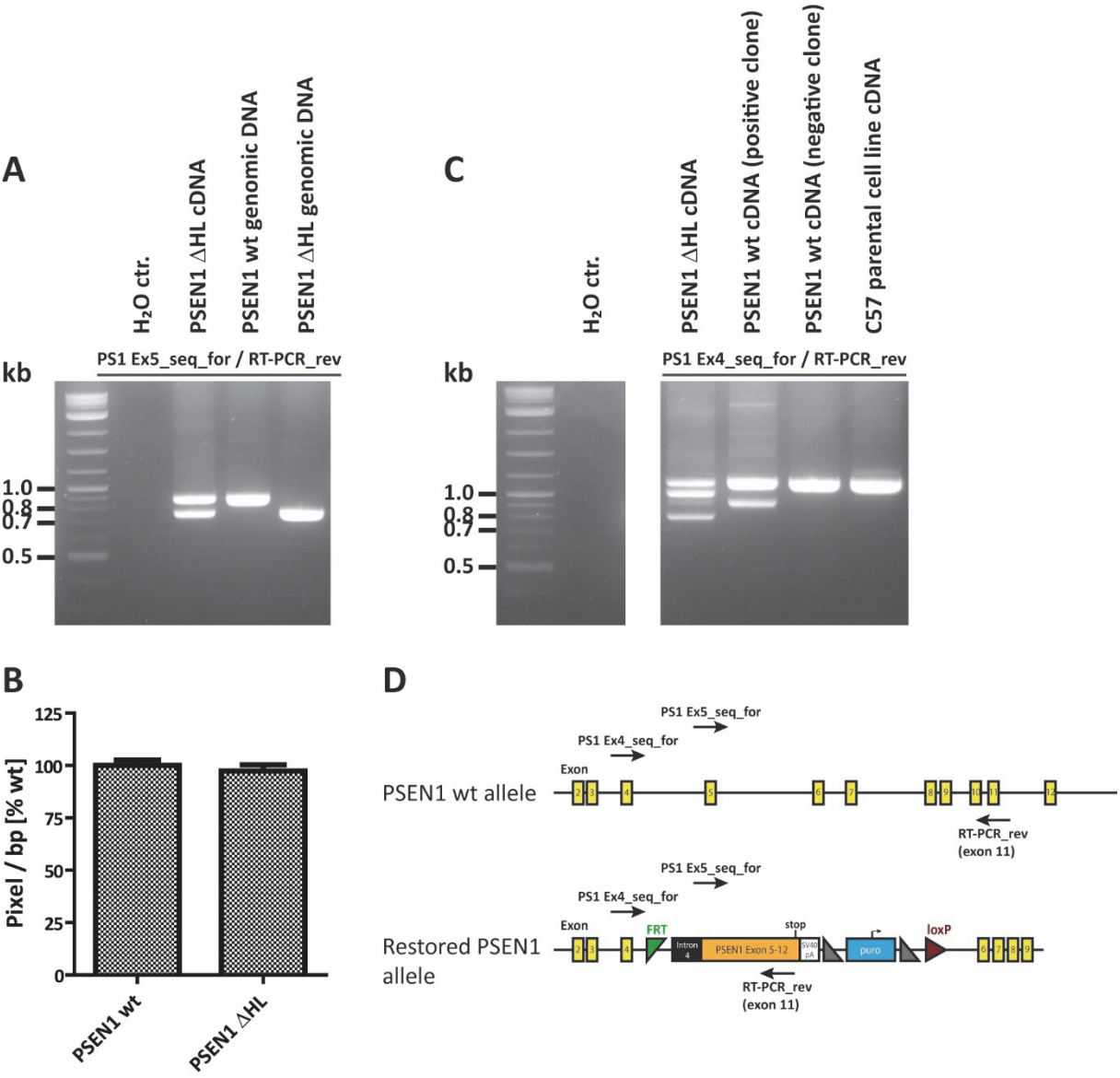

Figure 18: PCR analysis of the allelic transcription rates in dRMCE generated ES cell lines. (**A**) Two PCR products were generated for the ES PSEN1 ΔHL cDNA, using the PS1 Ex5_seq_for / RT-PCR_rev primer pair, which binds to PSEN1 exon 5 and 11. Extracted genomic DNA from ES PSEN1 wt and ES PSEN1 ΔHL cells was used as size controls. The observed PCR bands correspond to the restored PSEN1 allele, since PCR amplification of the PSEN1 wt allele is prevented by the intron based long distance of the primers. In comparison with the ES PSEN1 wt and ES PSEN1 ΔHL genomic DNA it is revealed that the upper band (884 bp) of the ES PSEN1 ΔHL cDNA corresponds to the PSEN1 wt allele and the lower band (764 bp) to the conditional PSEN1 ΔHL allele. (**B**) The generated PCR bands for the PSEN1 wt allele and the PSEN1 ΔHL allele in A were quantified from repeated experiments and reveal equal transcription for both PSEN1 alleles. Values are displayed as mean ± SD (n = 3). (**C**) An additional, smaller PCR band was observed for the PSEN1 ΔHL and PSEN1 wt cDNA when the previous forward primer was replaced by the PS1 Ex4_seq_for primer, which binds to PSEN1 exon 4. This additional PCR product was absent in the cDNA of a negative PSEN1 wt cell line, which had failed recombination and also in the parental ES cell line, indicating a splicing variant of the PSEN1 sequence on the restored PSEN1 allele. (**D**) Respective positions of the applied primers on the PSEN1 wt allele and the restored PSEN1 allele.

The PCR analysis was repeated with cDNA from the ES PSEN1 wt cell line, from a negative ES PSEN1 cell line that had failed successful recombination (deleted locus; see Figure 15 C) and the parental cell line in the presence of the PS1 Ex4_seq_for / RT-PCR_rev primer pair, which binds to PSEN1 exons 4 and 11 [Figure 18 C, D].

Here, an unexpected extra PCR band was observed in the ES PSEN1 ΔHL and in the PSEN1 wt cell line, but not in the negative ES PSEN1 wt or the parental ES cell line, indicating that it was generated from the restored PSEN1 allele, which is generated during successful dRMCE and consequently absent in the negative ES PSEN1 wt and the parental ES cell line.

The extra PCR band of the ES PSEN1 ΔHL cell line was cut out of the gel, purified and sequenced, using the PS1 Ex4_seq_for primer. Thereby it was revealed that the PCR fragment indeed corresponded to the restored PSEN1 ΔHL allele of the ES PSEN1 ΔHL cell line, but contained a deletion of the exon sequences 5 and 6 (210 bp) [Figure 19 A]. Consequently, this additional PCR product could not have been generated with the PS1 Ex5_seq_for / RT-PCR_rev primer pair.

A highly possible explanation for the deletion of exons 5 and 6 is partial alternative splicing of the conditional PSEN1 allele following recombination with the PSEN1 exon 4'-12 sequence on the pDREV-1 replacement construct during dRMCE. This hypothesis is strongly supported by the observation that neither the negative ES PSEN1 wt cell line, which had failed successful recombination, nor the parental ES cell line generated an additional PCR product.

Although the exact reason remains unclear, the partial alternative splicing of the restored PSEN1 allele was certainly induced by the introduced changes in the intron sequence between PSEN1 exon 4 and 5 during dRMCE. The parental ES cell line only contains the first 1764 bp of the 2209 bp intron sequence, followed by an unrelated sequence of 112 bp that contains necessary features for dRMCE, including the FRT recombination site [Figure 19 B].

To increase the likelihood for correct intron splicing, the missing 445 bp of the intron sequence were incorporated between the FRT and exon 5 sequence on the replacement construct, with the intention to complete the intron sequence in the recombination process.

However, because of the 112 bp of unrelated sequence and the inclusion of a BstBI restriction sequence, which was necessary for the cloning of the pDREV-1 replacement construct, the intron sequence of the replaced locus is in total 115 bp longer compared to the wt intron sequence of the PSEN1 wt allele [Figure 19 B]. These additional 115 bp might have induced the partial alternative splicing.

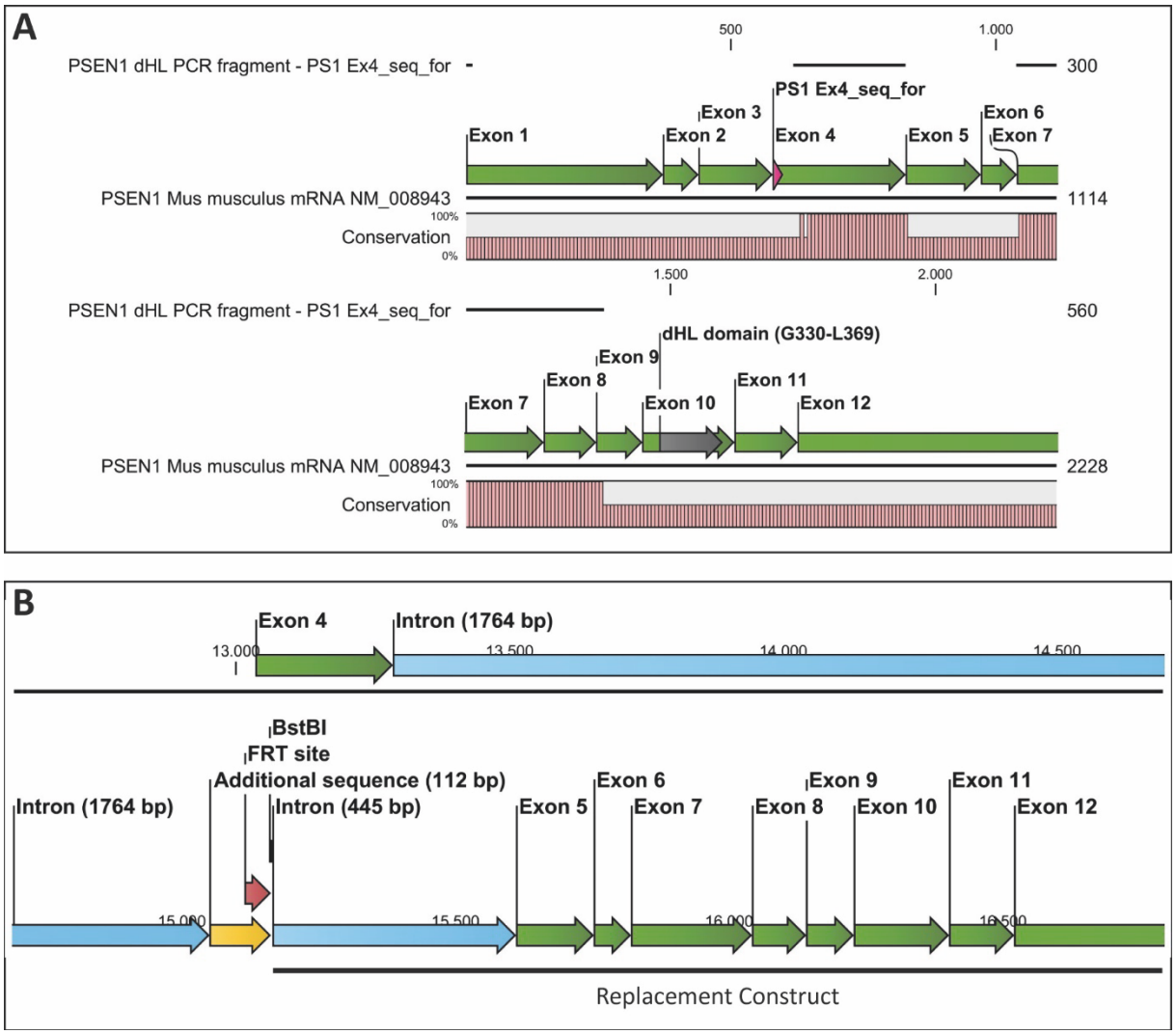

Figure 19: (**A**) The sequence of the additional PCR-fragment, which was generated for the PSEN1 ΔHL cDNA with the PS1 Ex4_seq_for / RT-PCR_rev primer pair (exon 4 / exon11), was aligned with the PSEN1 Mus musculus mRNA reference sequence from NCBI (Accession number: NM_008943). The pink bars represent the presence of the ES PSEN1 ΔHL PCR fragment (upper bars) and the PSEN1 Mus musculus mRNA (lower bars) sequence in the alignment. The sequencing was initiated with the PS1 Ex4_seq_for primer (pink arrow) and displayed good quality until the end of exon 8. Exons 5 and 6 were absent in the sequence of the PCR-fragment (grey gap), indicating that the corresponding mRNA of the restored PSEN1 ΔHL allele was alternatively spliced. (**B**) Illustration of the intron sequence between PSEN1 exons 4 and 5 in the replaced locus after successful recombination by dRMCE. 5'-recombination with the replacement construct occurs at the FRT site (pink arrow). An additional sequence of 115 bp (orange arrow), including the FRT and BstBI site, is placed between the 1764 bp intron sequence of the parental ES cell line and the residual 445 bp intron sequence on the replacement construct.

Although none of the other ES cell lines in table 3 were tested for alternative splicing of the restored PSEN1 allele, it might also occur in all of them.

Nevertheless, analysis of the ES PSEN1 ΔHL and PSEN1 wt cDNA revealed that the mRNA with the deletion of exons 5 and 6 is a minor species and that PCR products were predominantly generated from the mRNA that contains exons 5 and 6 [Figure 18 C]. In case of ES PSEN1 ΔHL cell line it was furthermore demonstrated that the PSEN1 wt allele and the restored PSEN1 ΔHL allele are equally transcribed [Figure 18 B].

However, it was still important to elucidate, whether the alternatively spliced mRNA is translated into a stable protein, which might interfere with functional analysis of the ES cell lines.

5.3 Evaluation of allelic protein expression in ES cell lines

Whole cell lysates were prepared from a positive and a negative ES PSEN1 wt clone after dRMCE. The positive ES PSEN1 wt clone (PSEN1 wt +/+) harbours two functional PSEN1 wt alleles, the PSEN1 wt allele of the parental ES cell line and the restored PSEN1 wt allele by successful recombination with the PSEN1 wt cDNA on the pDREV-1 replacement construct during dRMCE. In contrast, the negative ES PSEN1 wt clone (PSEN1 wt + / -), which had failed successful recombination (deleted locus), only harbours the functional PSEN1 wt allele of the parental ES cell line [Figure 13].

Upon formation of the γ-secretase complex, PSEN1 undergoes endoproteolysis and is cleaved into a C-terminal fragment (CTF) and an N-terminal fragment (NTF) between the TMDs 6 and 7 within its large cytosolic loop (Thinakaran et al. 1996).

For the investigation of equal allelic expression and stability of the PSEN1 protein, PSEN1 CTF and NTF levels were detected and quantified with specific antibodies in ES PSEN1 wt +/+ and ES PSEN1 +/- cell lysates by Western blotting [Figure 20]. The PSEN1 CTF (~ 20 kDa) and NTF (~ 30 kDa) levels in the ES PSEN1 wt + / - cell line were reduced by approximately 50 % in comparison to the respective protein levels in the ES PSEN1 wt +/+ cell line [Figure 20 C].

These results are in perfect accordance with the above described fact that the ES PSEN1 wt +/- cell line only contained one functional PSEN1 wt allele in contrast to the ES PSEN1 wt +/+ cell line, which contained two functional PSEN1 alleles. They further indicate that the

restored PSEN1 wt allele in the ES PSEN1 wt +/+ cell line is functional after dRMCE and expressed equal PSEN1 levels in comparison to the unmodified PSEN1 wt allele.

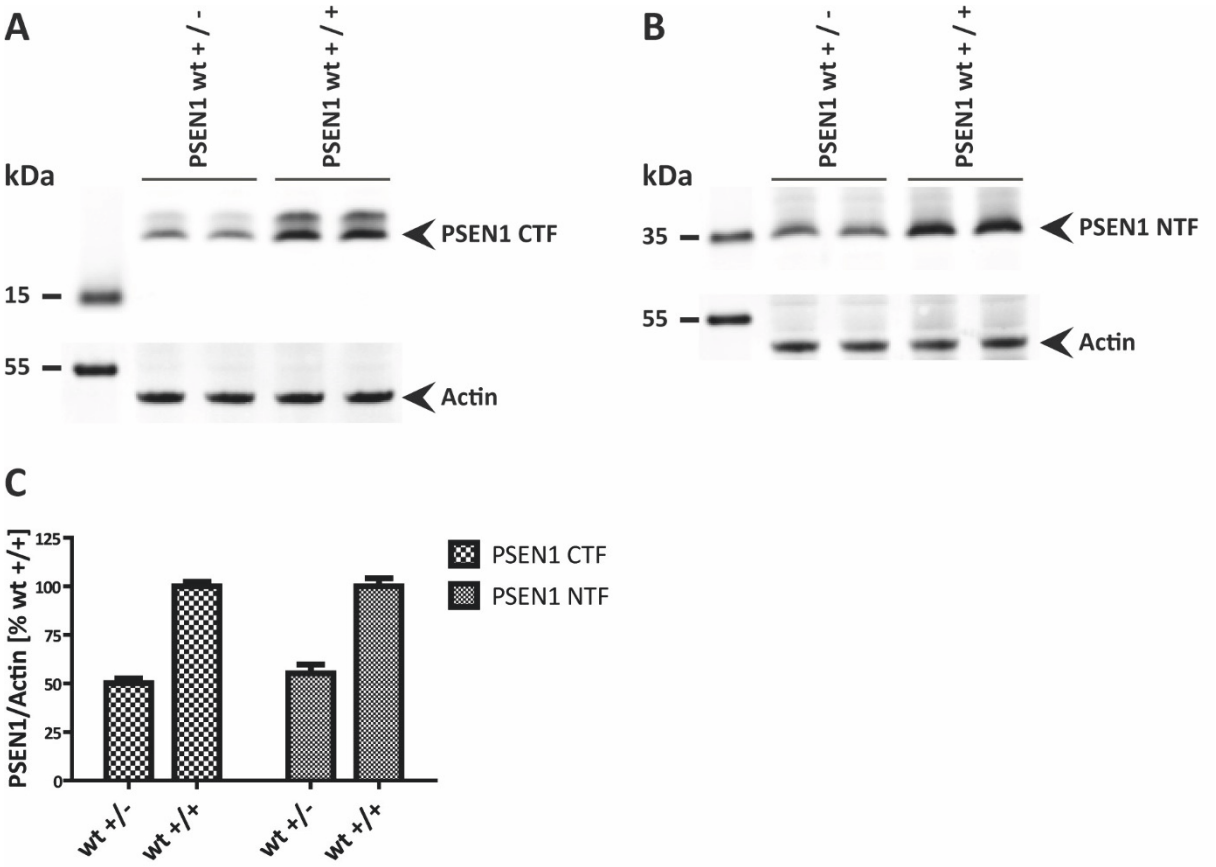

Figure 20: (**A, B**) Protein expression levels of the PSEN1 CTF and NTF in whole cell lysates from the ES PSEN1 wt +/+ and ES PSEN1 wt +/- cell line. PSEN1 fragments were detected by Western blotting with specific, polyclonal antibodies against PSEN1 CTF and NTF. Actin levels are shown as a control for equal protein loading. (**C**) Quantification of the Western blotting results for the PSEN1 CTF and NTF protein bands revealed an approximately 50 % reduction in the ES PSEN1 wt +/- cell line in comparison to the ES PSEN1 wt +/+cell line. The PSEN1 CTF and NTF levels were normalised to actin levels and set to 100 % in the ES PSEN1 wt + /+ for quantification. Values are displayed as mean ± SD from duplicate measurements of four independent experiments (n = 4).

Importantly, no additional NTF has been observed for the ES PSEN1 wt +/+ cell line, even at longer exposures of the Western blots (not shown), which could have been translated from the alternatively spliced mRNA (deletion of PSEN1 exons 5 and 6, Figure 18 C) into an 8 kDa smaller NTF. This indicates that either the alternatively spliced mRNA or the translated protein is unstable and degraded.

In conclusion, the performed experiments with the positive and negative ES PSEN1 wt cell line confirmed equal and functional expression of the PSEN1 wt allele and the restored PSEN1 allele.

5.4 Differentiation of ES cells into neural stem cells (NSCs)

In order to investigate the effect of FAD PSEN1 mutations in a neural cell type, dRMCE engineered PSEN1 ES cell lines were differentiated into neural stem cells (NCS), which can be also further differentiated into neurons, astrocytes and oligodendrocytes.

On day 0 of the differentiation, ES cells were seeded in their regular ES medium, containing the growth factor LIF. Accordingly, on day 1, the cells still showed the typical dense ES cell morphology with no visible borders between single cells and enlarged nuclei [Figure 21 A]. The ES medium was exchanged for differentiation medium on day 1. On day 2, cell morphology started to change. The cells became spiky at their edges and cell death occured [Figure 21 B]. On day 4, cells had differentiated into neuroepithelial precursors (NEPs) and formed rosette structures [Figure 21 C]. Differentiation into NEPs continued untill day 6. In some cases, ES cells were still present on the plate and remained unchanged [Figure 21 D]. NEPs were detached from the plate and cultured without coating. Starting at day 7, the formation of floating neurospheres was observed [Figure 21 E]. The neurospheres were collected and plated on a coated dish and eventually started to attach and migrate. Migrating NSCs were recognised by their characteristic morphology [Figure 21 F].

The time periods for the differentiation into NEPs, the formation of NSCs as well as the overall differentiation efficiency depended on the respective ES cell line and some variations have been observed between the different FAD PSEN1 ES cell lines and the PSEN1 wt cell line. This was not further investigated but a possible explanation could be a differential influence of the FAD PSEN1 mutation on NOTCH processing, since NOTCH is a substrate for the γ-secretase and plays an important role in stem cell self-renewal and differentiation processes (Liu *et al.* 2010).

To confirm successful differentiation into NSCs, the NSC PSEN1 wt and the NSC PSEN1 L166P lines were stained for the NSC markers Sox2 and Nestin by immunocytochemistry (Pollard *et al.* 2006b, Pollard & Conti 2007) [Figure 22]. Sox2 is a transcription factor that is involved in

the maintenance of stem cell self-renewal. Nestin is an intermediate filament protein, which is expressed in progenitor cells of the central nervous system.

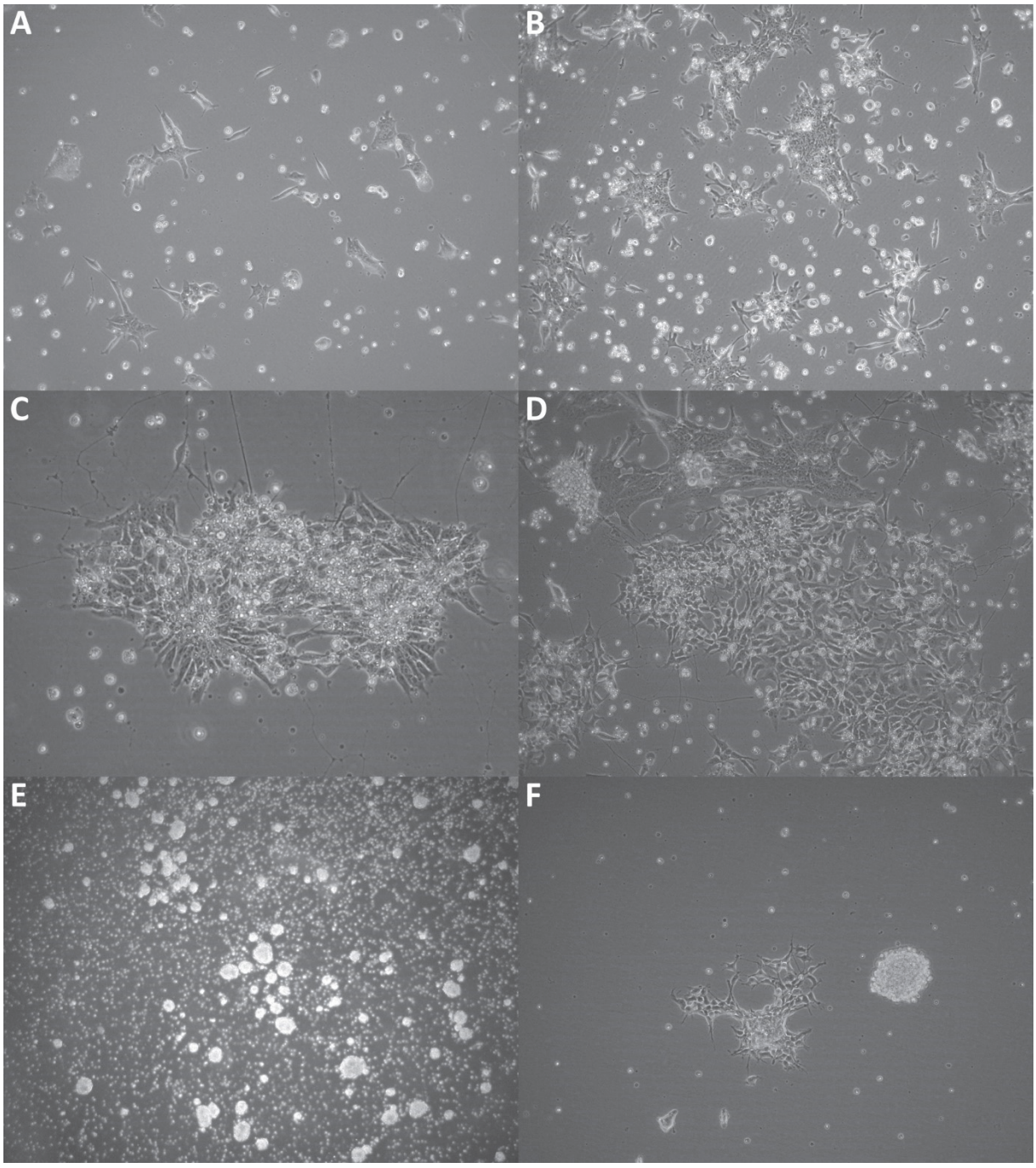

Figure 21: Differentiation of the ES PSEN1 wt cell line into the NSC PSEN1 wt line. (**A**) Day 1. ES cells show typical dense morphology (10 x magnification). (**B**) Day 2. ES cells start to become spiky at their edges (10 x magnification). (**C**) Day 4. Formation of rosette structures by neuroepithelial precursors (NEPs) (20 x magnification). (**D**) Day 5. From top to bottom: an ES cell colony, NEPs forming rosette structures and further differentiated NEPs (10 x magnification) (**E**) Day 7. Floating neurospheres (2.5 x magnification). (**F**) Day 8. A floating neurosphere (right) next to attached and migrating NSCs (10 x magnification).

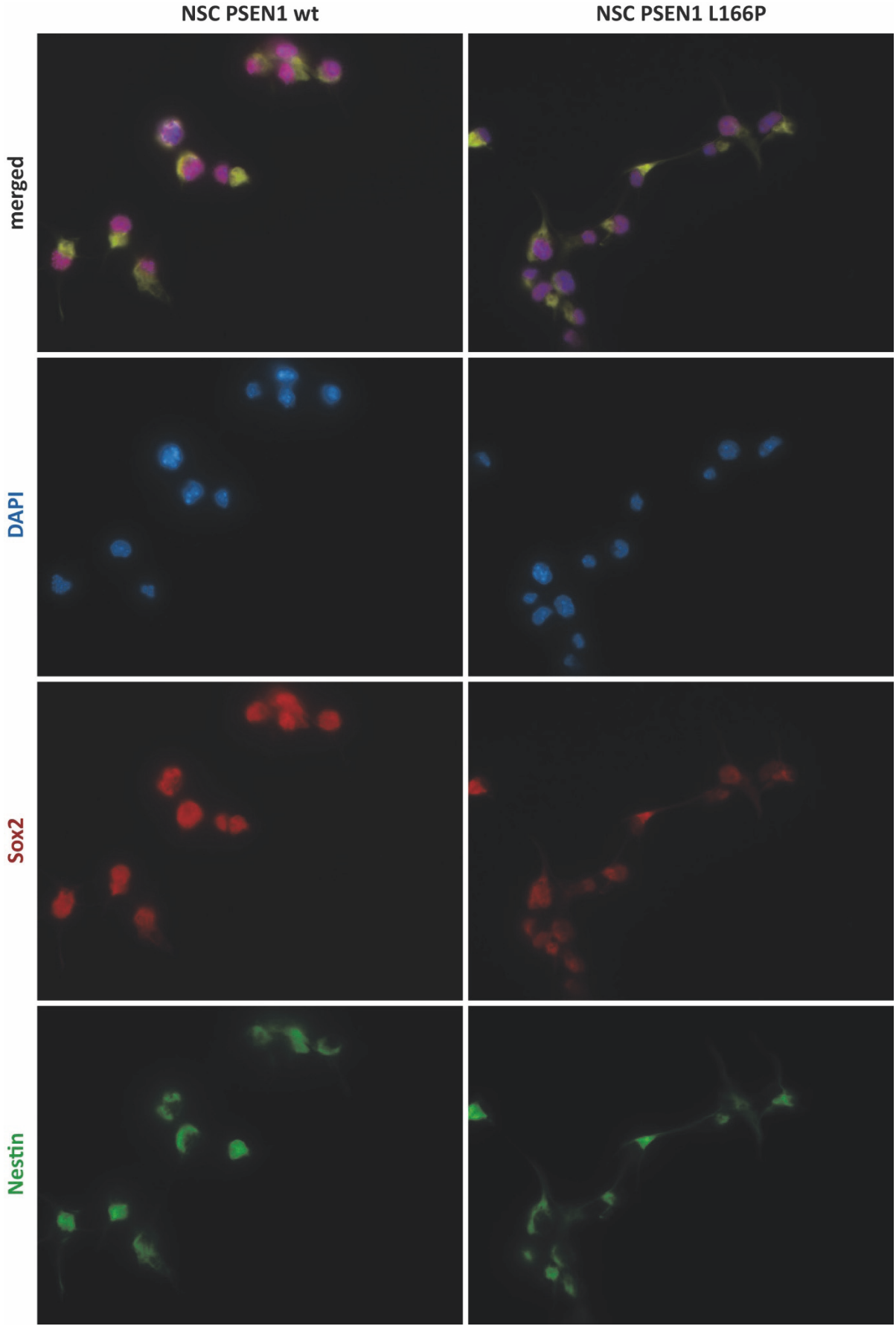

Figure 22: Staining of the NSC PSEN1 wt and the NSC PSEN1 L166P lines for the NSC markers Sox2, Nestin and the nuclear marker DAPI by immunocytochemistry. The top panel is an overlay of all three stainings.

Figure 22 shows that both NSC lines expressed Sox2 and Nestin, thereby confirming successful differentiation of the ES cell lines into NSCs by the applied protocol (see chapter 4.2.5). All other NSC PSEN1 lines were differentiated by the exact same protocol and displayed the same characteristic NSC morphology.

5.5 Differentiation into neurons, astrocytes and oligodendrocytes

Neurospheres, an intermediate cell type during the differentiation of ES PSEN1 cell lines into NSCs, were evaluation for their ability to form three major cell types of the developed brain, which are neurons, astrocytes and oligodendrocytes.

Using the NSC differentiation protocol, eight FAD PSEN1 ES cell lines were in parallel differentiated into neurospheres. Figure 23 shows a representative comparison of the number and the size of the neurospheres that were generated from the different FAD PSEN1 cell lines. The PSEN1 wt cell line and the PSEN1 cell lines L166P, M233V, E280A and D385N produced a higher number of neurospheres in comparison to the P117L, R278I and C410Y cell lines.

This variation in differentiation efficiency has already been mentioned in chapter 5.4.

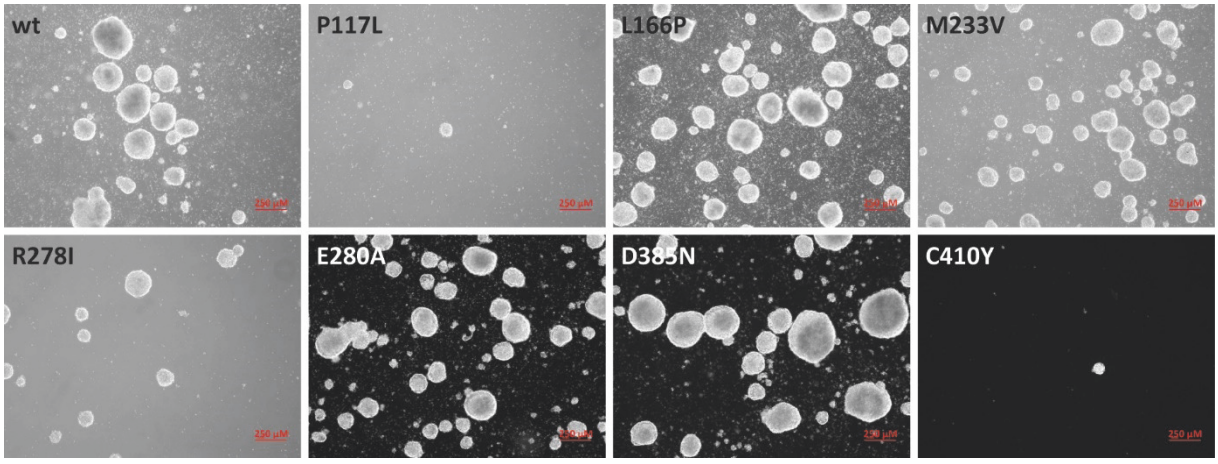

Figure 23: Neurospheres, differentiated from the respective PSEN1 ES cell lines (4 x magnification).

The differentiated neurospheres were stained by immunocytochemistry for the neuron marker β-III tubulin, the astrocyte marker GFAP and the oligodendrocyte marker O4 by immunocytochemistry [Figure 24].

With one exception, neurons, astrocytes and oligodendrocytes were successfully stained for all of the FAD PSEN1 cell lines and showed characteristic cell morphology.

In case of the PSEN1 C410Y cell line, O4 staining was not performed, since only one small neurosphere was formed after the differentiation protocol. β-III tubulin staining revealed successful differentiation of the PSEN1 C410Y cell line into neurons. However, astrocytes were not simultaneously detected by GFAP staining [Figure 24].

In summary, with the exception of the PSEN1 C410Y cell line, a general capacity to differentiate into neurons, astrocytes and oligodendrocytes could be confirmed for all of the investigated FAD PSEN1 ES cell lines. However, whether some PSEN1 mutations, including the PSEN1 C410Y mutation, indeed reduce the capacity to form neurospheres and to generate specific cell types like astrocytes and oligodendrocytes requires validation by repetition and proper quantification of the experiments.

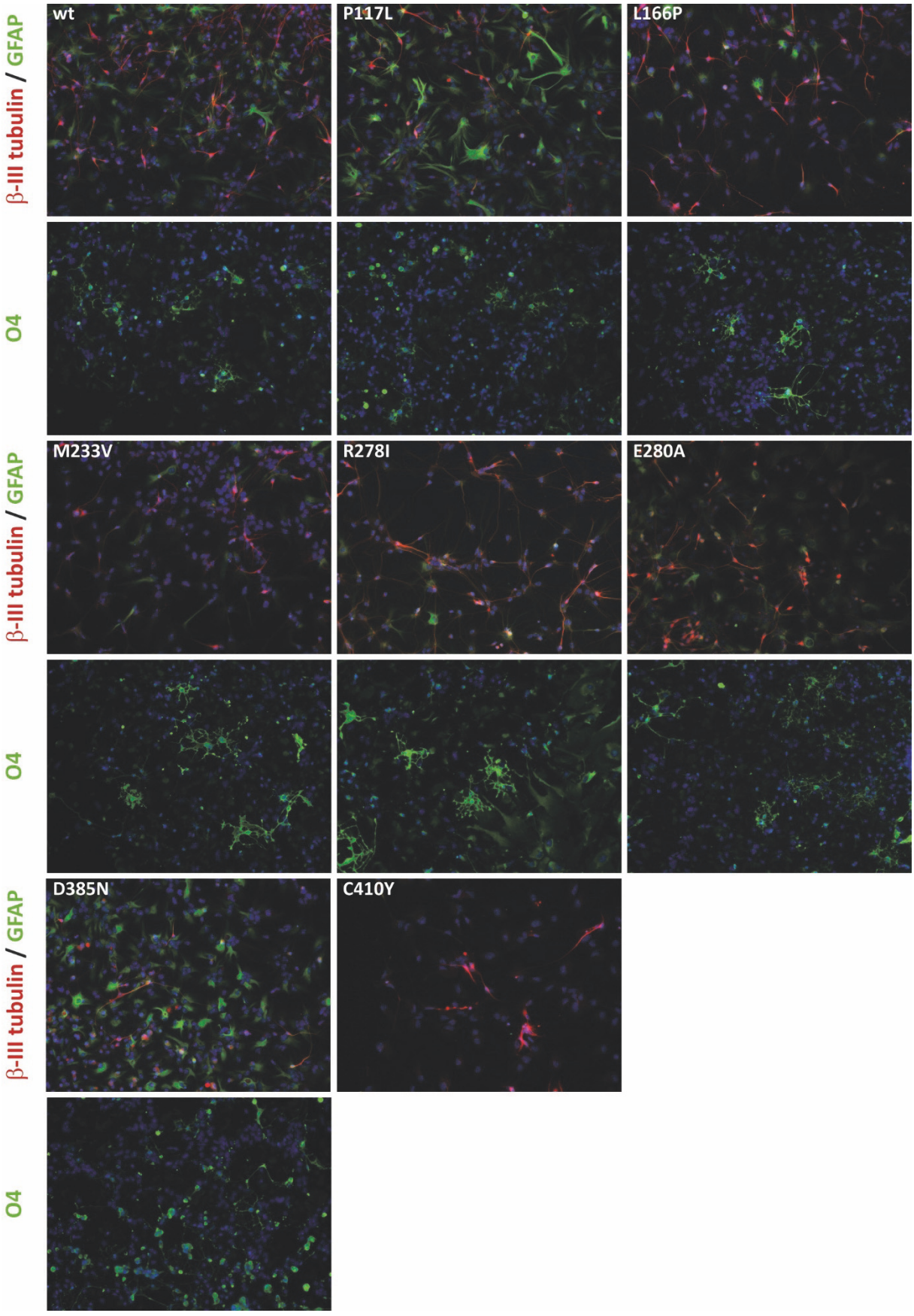

Figure 24: Immunocytochemistry of the differentiated NSC FAD PSEN1 lines. Neurons: β-III tubulin (red), astrocytes: GFAP (green), oligodendrocytes: O4 (green), nuclei: Hoechst 33258 (blue).

5.6 Comparison of Aβ levels in isogenic PSEN1 cell lines

For the comparison of Aβ40 and Aβ42 generation by the different FAD PSEN1 mutations, PSEN1 cell lines were infected with an APP695 adenovirus that induces an overexpression of the human wt APP695. An APP overexpression was necessary to enhance Aβ production, since endogenous mouse Aβ42 levels were not measurable. APP is initially cleaved by BACE1 into a soluble ectodomain and a membrane-bound C99 fragment, which is subsequently cut into Aβ peptides of variable length by the γ-secretase complex.

In an initial experiment, Aβ and BACE1 levels were compared between the ES PSEN1 wt cell line and the derived NSC PSEN1 wt line. In contrast to the NSC PSEN1 wt line, Aβ levels were not detectable in the ES PSEN1 wt cell (data not shown), which is most likely due to the considerably lower BACE1 expression [Figure 25 A]. Consequently, the influence of FAD PSEN1 mutations on the generation of Aβ40 and Aβ42 and on the Aβ42/Aβ40 ratio was analysed in the PSEN1 NSC lines and not in the PSEN1 ES cell lines.

The NSC lines were infected for 3 h with 100 APP695 adenovirus particles per cell. 24 h after the infection, the medium was changed and fresh medium was conditioned for another 24 h. Subsequently, the supernatants were sent to our collaborators at the company Asceneuron in Lausanne for quantitative measurement of Aβ40 and Aβ42 levels with the Meso Scale Discovery electrochemiluminescence (ECL) immunoassay. The absolute Aβ40 and Aβ42 concentrations in the NSC PSEN1 lines were calculated from Aβ40 and Aβ42 standard curves and normalised to the APP FL expression in the corresponding cell lysates to compensate for potential differences in cell numbers and infection rates [Figure 25 C, D]. The Aβ42/Aβ40 ratios were calculated from normalised Aβ40 and Aβ42 concentrations as percentage from wt [Figure 25 B]. Consistent with reported values in the literature, all of the investigated FAD PSEN1 mutations caused an increase in the Aβ42/Aβ40 ratio compared to PSEN1 wt [Figure 25 B] (Nakano et al. 1999, Schroeter et al. 2003, Walker et al. 2005, Bentahir et al. 2006, Kumar-Singh et al. 2006, Shimojo et al. 2007, Kaneko et al. 2007, Shimojo et al. 2008, Heilig et al. 2010, Kretner et al. 2011, Saito et al. 2011, Vidal et al. 2012, Koch et al. 2012, Cacquevel et al. 2012, Fernandez et al. 2014, Xia et al. 2015, Li et al. 2016).

This increase was particularly high for the PSEN1 P117L, PSEN1 L173W, PSEN1 I213T and PSEN1 M233V mutations, ranging from approximately 2.5-7 fold. A moderate increase of 1.2-2 fold was observed for the Aβ42/Aβ40 ratio in the other six mutations.

A reduction in either Aβ40 or Aβ42 has not been observed in comparison to PSEN1 wt for any of the investigated FAD PSEN1 mutations [Figure 25 C, D].

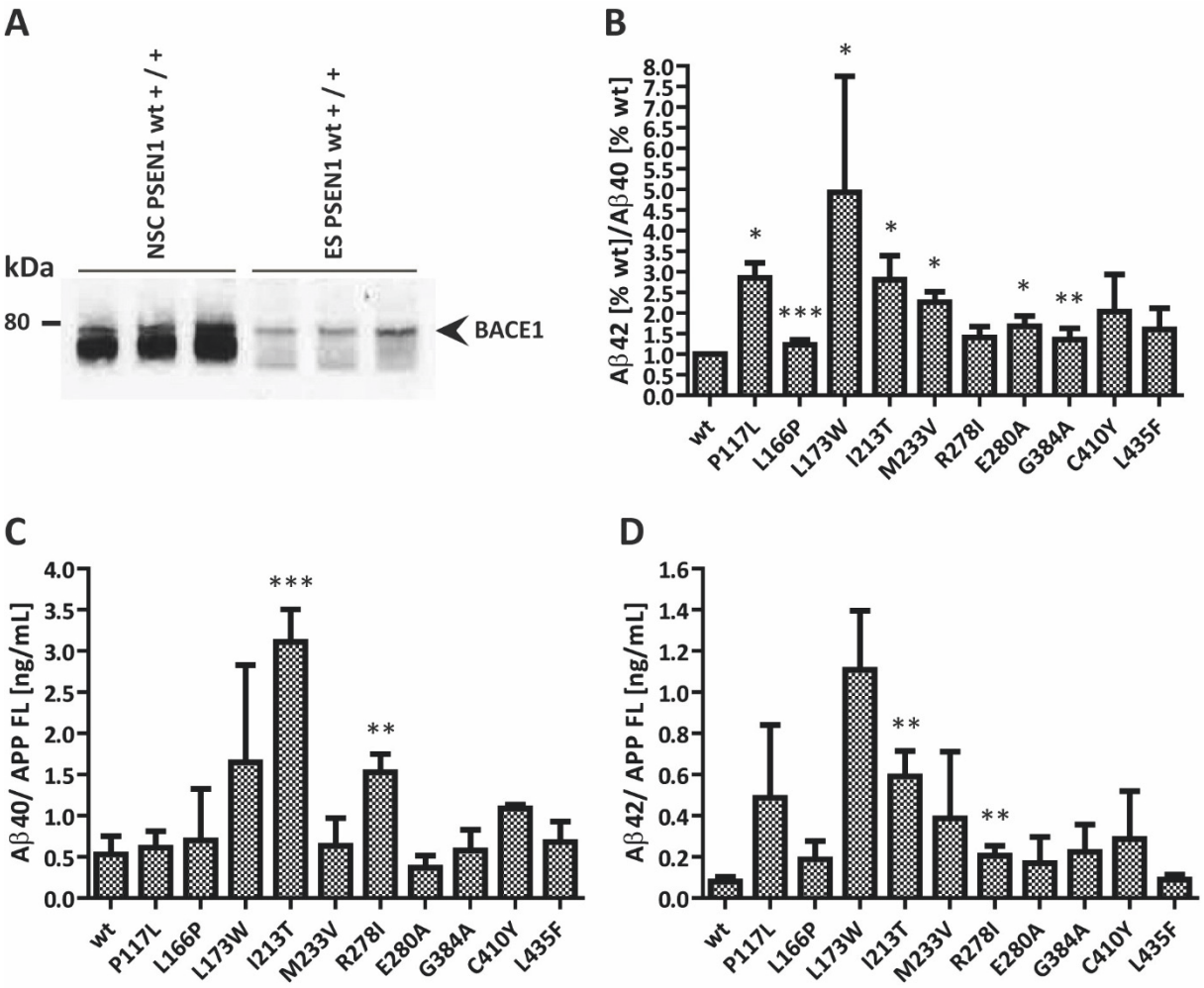

Figure 25: (**A**) BACE1 expression in the NSC PSEN1 wt +/+ line compared to the ES PSEN1 wt +/+ cell line was detected by Western blotting with a monoclonal antibody against BACE. (**B**) Aβ42/Aβ40 ratio of the APP695 adenovirus infected FAD NSC PSEN1 cell lines. The Aβ42/Aβ40 ratios were calculated from normalised Aβ40 and Aβ42 concentrations as percentage from wt. (**C**, **D**) Aβ40 and Aβ42 concentration of the APP695 adenovirus infected FAD NSC PSEN1 cell lines. The concentrations were calculated from raw ECL counts with a standard curve and subsequently normalised to APP FL expression levels. Values are displayed as mean ± SD (wt: n=6; others: n=3). Means were compared to wt by unpaired t tests. *** p<0.001, ** p<0.01, * p<0.05.

The PSEN1 L173W and PSEN1 R278I mutations showed a 3 fold, the PSEN1 C410Y mutation a 4 fold and the PSEN1 I213T mutation a 6 fold increase in Aβ40. The PSEN1 E280A mutation

showed a slight, but not statistically significant decrease in Aβ40. The remaining FAD PSEN1 mutations had approximately the same Aβ40 levels as PSEN1 wt. Regarding the Aβ42 levels, any of the FAD PSEN1 mutations at least showed a slight increase in comparison to PSEN1 wt. The increase in the Aβ42 concentration was 6 fold for PSEN1 P117L, 14 fold for PSEN1 L173W, 7 fold for PSEN1 I213T and 5 fold for PSEN1 M233V.

5.7 FAD PSEN1 mutations are not dominant-negative

One of the major hypotheses on the function of heterozygous FAD PSEN1 mutations revolves around a putative dominant-negative effect. Dominant-negative mutations are defined by two characteristics: 1. An adverse influence of the mutant protein on the function of the wt protein and 2. a physical interaction between mutant and wt protein (Herskowitz 1987, Veitia 2007).

Previous investigations on the dominant-negative hypothesis of FAD PSEN1 mutations have been performed in overexpression model systems and produced contradicting results (Schroeter et al. 2003, Sato et al. 2007, Heilig et al. 2013). It is thus important to re-investigate the putative dominant-negative effect again and by the application of an isogenic model system with heterozygous expression of wt and mutant PSEN1 from two endogenous PSEN1 alleles. Focus of the conducted experiments was to answer the following questions:

1. Is the enzymatic activity of wt PSEN1 altered in the presence of mutant PSEN1?
2. Does a physical and functional interaction between wt and mutant PSEN1 occur?

The first experiment was designed to investigate a functional interaction between PSEN1 wt and PSEN1 D385N in the heterozygous ES PSEN1 D385N cell line. The artificial D385N mutation abolishes the catalytic activity of the PSEN1 protein, including endoproteolysis of FL PSEN1 into an NTF and CTF, since D385 is one of PSEN1's two catalytic aspartate residues (Wolfe et al. 1999). However, in case of a putative interaction between PSEN1 wt and PSEN1 D385N in the ES PSEN1 D385N cell line, PSEN1 wt might compensate for the loss of endoproteolytic activity and cleave PSEN1 D385N in trans.

To investigate the putative trans-cleavage of PSEN1 D385N by PSEN1 wt, PSEN1 FL, CTF and NTF levels were detected and quantified with specific antibodies in ES PSEN1 wt +/+, ES PSEN1 +/- and ES PSEN1 D385N cell lysates by Western blotting [Figure 26].

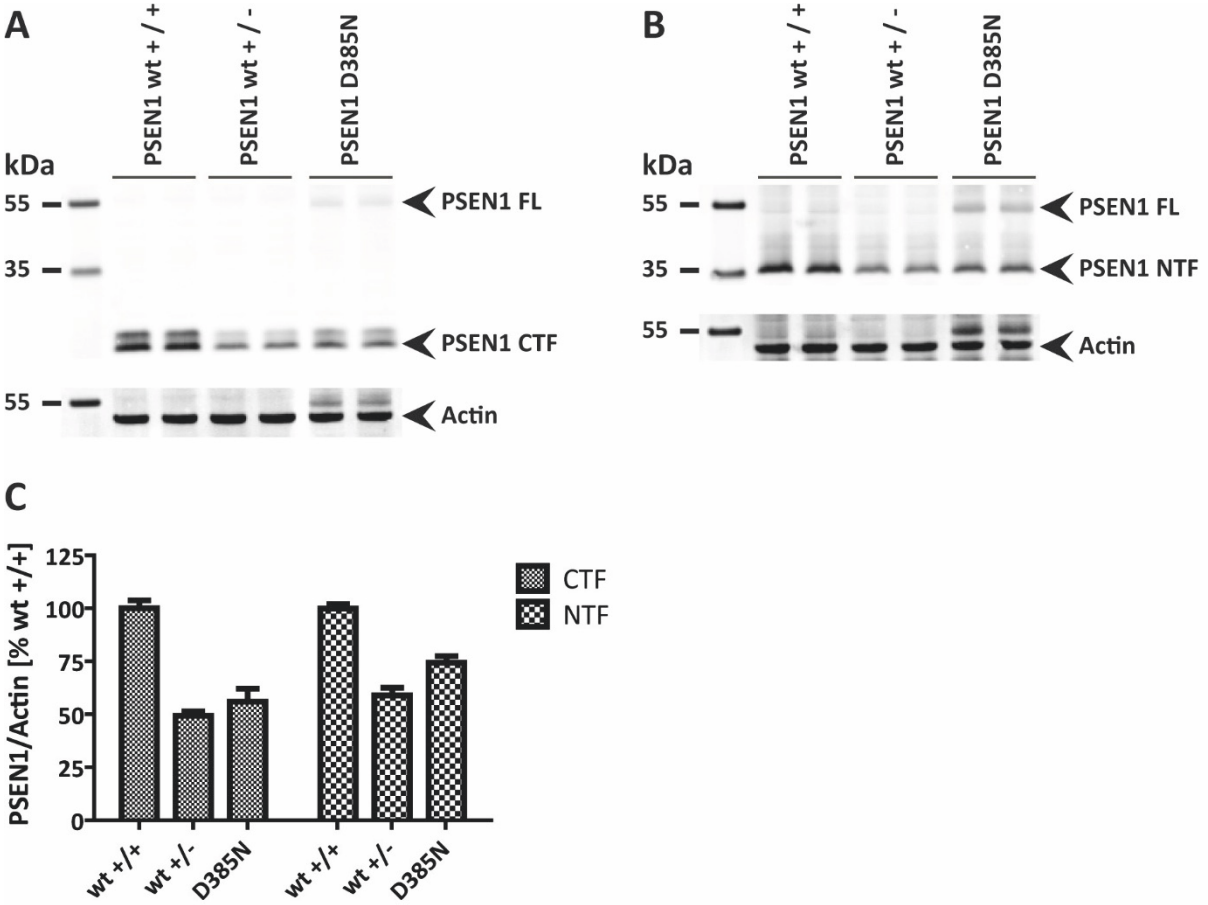

Figure 26: (**A, B**) Protein expression levels of the PSEN1 CTF, NTF and FL protein in whole cell lysates from the ES PSEN1 wt +/+, ES PSEN1 wt +/- and the ES PSEN1 D385N cell line. PSEN1 fragments were detected by Western blotting with specific, polyclonal antibodies against PSEN1 CTF and NTF. Actin levels are shown as a control for equal protein loading. The additional protein bands in the PSEN1 D385N samples after reprobing with the actin antibody are residual PSEN1 FL signals (**C**) Quantification of the Western blotting results for the PSEN1 CTF and NTF protein bands revealed an approximately 50 % and 44 % reduction of the CTF, and a 42 % and 26 % reduction of the NTF in the ES PSEN1 wt +/- and PSEN1 D385N cell line in comparison to the ES PSEN1 wt +/+ cell line. The PSEN1 CTF and NTF levels were normalised to actin levels and set to 100 % in the ES PSEN1 wt +/+ for quantification. Values are displayed as mean ± SD from duplicate measurements of three independent experiments (n = 3).

In comparison to PSEN1 wt +/+, an approximately 50 % reduction in the PSEN1 CTF and NTF levels was again measured in the lysates from the ES PSEN1 wt +/- cell line, which only harbours one functional PSEN1 wt allele (see Figure 20 C) [Figure 26 C].

PSEN1 CTF and NTF levels were also reduced by 44 % and 26 % in lysates from the ES PSEN1 D385N cell line. Furthermore, PSEN1 FL was simultaneously detected, confirming the endoproteolysis deficiency of the PSEN1 D385N protein and the absence of trans-cleavage by functional interaction with the PSEN1 wt protein. However, it remains to be elucidated, why approximately 20 -25 % higher NTF than CTF levels were detected in lysates from the ES PSEN1 D385N cell line, since endoproteolysis of PSEN1 FL generates equal CTF and NTF levels.

The second experiment was designed to investigate the putative alteration in the enzymatic activity of PSEN1 wt by mutant PSEN1 (see chapter 4.2.9).

As an alternative to the 1:1:1:1 stoichiometry of the γ-secretase subunits PSEN1, Nct, Aph-1 and Pen-2, the formation of γ-secretase complexes, which contain PSEN1 dimers (2:1:1:1) or the assembly of multimeric γ-secretase complexes (2:2:2:2) has been suggested (Schroeter et al. 2003) [Figure 27].

In a previous publication, an increased Aβ42/Aβ40 ratio was observed when PSEN1 wt and the catalytically inactive double mutant PSEN1 M146L + D385A were coexpressed (Schroeter et al. 2003). Schroeter et al. attributed this observation to a dominant- negative effect of PSEN1 M146L + D385N and a dimerization of wt and mutant PSEN1, which caused an enhanced activity of wt PSEN1. However, even after several repeats of the experiment, the observed increase in the Aβ42/Aβ40 ratio was variable and not statistically significant.

For an investigation of the suggested functional interaction, the Aβ42/Aβ40 ratio was compared between the NSC PSEN1 wt cell line, the NSC PSEN1 D385N cell line, the two FAD cell lines NSC PSEN1 L166P and NSC PSEN1 M233V and the respective catalytically inactive double mutations NSC PSEN1 L166P + D385N and NSC PSEN1 M233V + D385N after infection with an APP695 adenovirus. The L166P and M233V mutations are both associated with a very early AD onset below 30 years of age and are therefore considered as strong FAD mutations (Houlden *et al.* 2001, Moehlmann et al. 2002).

For a quantitative detection of Aβ42 and Aβ40 levels, the NSC lines were infected with an APP695 adenovirus. 24 h after the infection, fresh medium was conditioned for another 24 h and subsequently send to our collaboration partners at the company Asceneuron in Lausanne for measurement with the Meso Scale Discovery electrochemiluminescence (ECL) immunoassay.

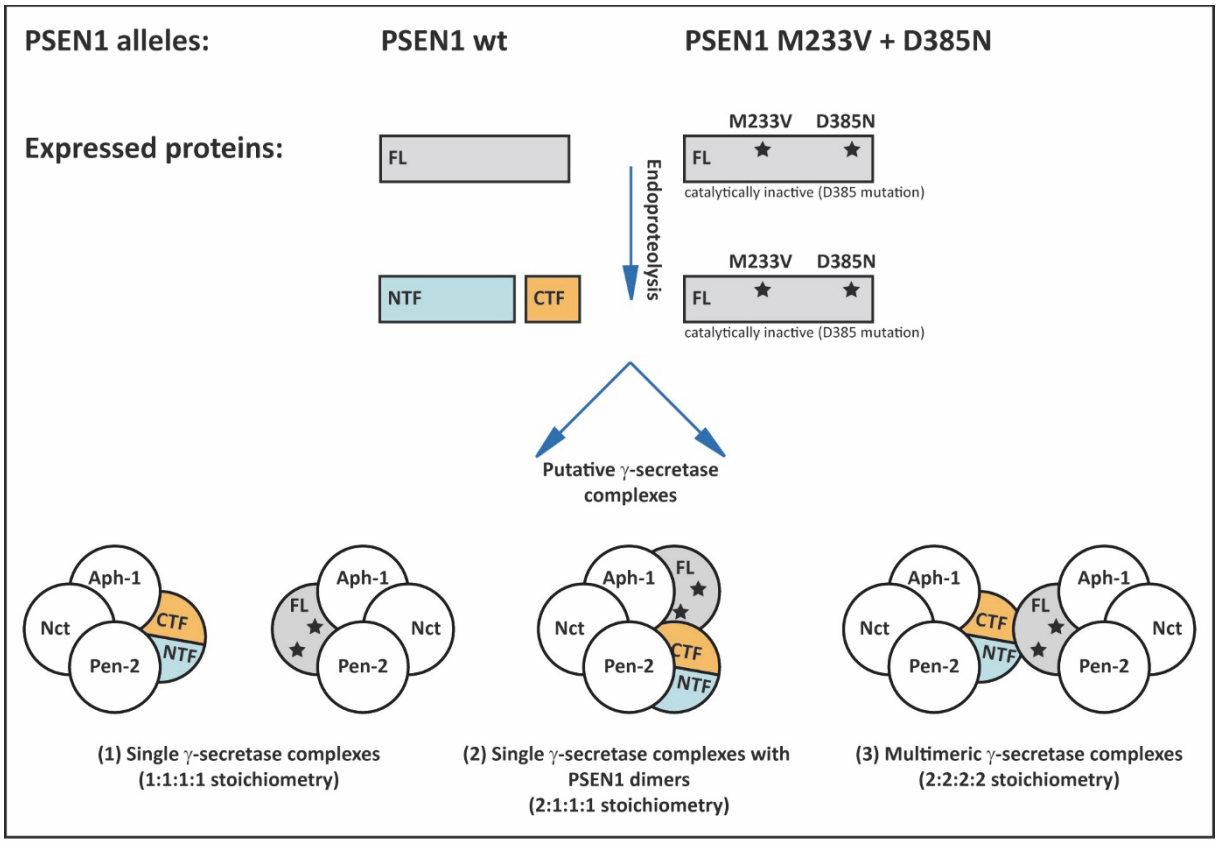

Figure 27: The heterozygous ES PSEN1 M233V + D385N cell line consists of one PSEN1 wt allele and one PSEN1 M233V + D385N allele. Following protein expression, the full length (FL) PSEN1 protein undergoes endoproteolysis into an N-terminal fragment (NTF) and a C-terminal fragment (CTF) after assembly with the γ-secretase subunits Nct, Aph-1 and Pen-2. Mutation of the D385 residue, one of PSEN1's two catalytic aspartates, leads to an endoproteolysis deficiency. Possible formations of γ-secretase complexes include (1) single γ-secretase complexes, with 1:1:1:1 stoichiometry of the subunits PSEN1, Aph-1, Nct and Pen-2, (2) single γ-secretase complexes, containing PSEN1 dimers (2:1:1:1) and (3) multimeric γ-secretase complexes, consisting of two single γ-secretase complexes. Star symbols represent sites of mutations. M233V is an FAD PSEN1 mutation (modified after (Schroeter et al. 2003)).

An expected, equal Aβ42/Aβ40 ratio was observed for PSEN1 wt and PSEN1 D385N [Figure 28]. Unlike absolute Aβ42 and Aβ40 levels, the Aβ42/Aβ40 ratio is not influenced by the number of functional PSEN1 wt alleles and corresponding PSEN1 wt expression levels (NSC PSEN1 wt line: 2x PSEN1 wt allele; NSC PSEN1 D385N line: 1x PSEN1 wt allele, 1x PSEN1 D385N allele). Treatment with the LY-411575 γ-secretase inhibitor at 0.5 µM was sufficient for a complete inhibition of Aβ42 and Aβ40 production.

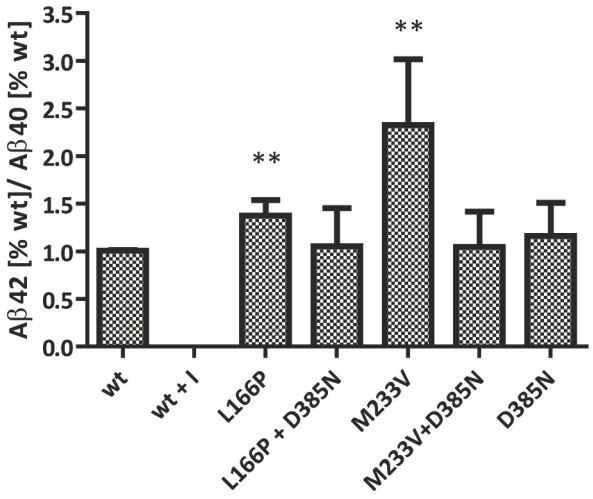

Figure 28: Aβ42/Aβ40 ratio of the APP695 adenovirus infected NSC PSEN1 cell lines, including a 0.5 µM γ-secretase inhibitor control for PSEN1 wt (wt + I). The elevated Aβ42/Aβ40 ratios in the NSC lines with heterozygous expression of the FAD PSEN1 mutations L166P and M233V are reverted to wt levels by the introduction of the catalytically inactive D385N mutation. The Aβ42/Aβ40 ratios were calculated from normalised Aβ40 and Aβ42 concentrations as percentage from wt. Values are displayed as mean ± SD (M233V + D385N: n=3; others: n=5). Means were compared to wt by unpaired t tests. *** p<0.001, ** p<0.01, * p<0.05.

The PSEN1 L166P and M233V cell lines showed statistically significant increases in the Aβ42/Aβ40 ratio of 1.4-2.3 fold compared to PSEN1 wt, as already observed in Figure 25 B. However, with the introduction of the catalytically inactive D385N mutation, the Aβ42/Aβ40 ratio is not enhanced, as observed in the previous publication, but instead reverted to PSEN1 wt levels in the heterozygous PSEN1 L166P + D385N and NSC PSEN1 M233V + D385N cell lines, demonstrating the absence of a functional interaction between wt and mutant PSEN1 or an influence on the enzymatic activity of PSEN1 wt by mutant PSEN1.

The putative physical interaction between PSEN1 proteins was investigated by co-immuno-precipitation (co-IP) in the third experiment (see chapter 4.3.7).

To discriminate wt and mutant PSEN1, two heterozygous ES PSEN1 cell lines with a FAD + D385N double mutation and a flag-tag were generated: ES PSEN1 L166P + D385N 3xFlag and ES PSEN1 M233V + D385N 3xFlag. The 3xFlag-tag was cloned into the hydrophilic loop of PSEN1. Again, the D385N mutation prevents endoproteolysis into an NTF and CTF, as already previously observed in Figure 26 A, B. Consequently, the PSEN1 L166P + D385N 3xFlag and the PSEN1 M233V + D385N 3xFlag proteins remain a FL protein, in contrast to the PSEN1 wt protein, which is simultaneously expressed in both corresponding cell lines.

Membrane fractions were prepared from both ES double mutation 3xFlag cell lines (ES PSEN1 L166P + D385N 3xFlag and ES PSEN1 M233V + D385N 3xFlag) and solubilised in a buffer containing 1 % of the detergent CHAPSO, to preserve the integrity and activity of the γ-secretase complex (Li *et al.* 2000, Kimberly *et al.* 2003b). The solubilised membrane preparations were simultaneously incubated with protein A/G agarose beads alone, as control for putative nonspecific interactions of the solubilised membrane proteins with the agarose beads and in the presence of either anti-Flag antibody or anti-PSEN1 NTF antibody. After washing and elution from the beads, the presence of PSEN1 and the γ-secretase subunits Nct and Pen-2 was detected in the immunoprecipitated material by Western blotting and subsequent immunostaining with five different antibodies: (1) anti-Nicastrin, which recognises the Nct subunit of the γ-secretase complex, (2) anti-Flag, which recognises the flag-tag of the mutant PSEN1 FL proteins, (3) the anti-PSEN1 NTF, which recognises both, the mutant PSEN1 FL proteins and the PSEN1 NTF, (4) anti-PSEN1 CTF, which recognises PSEN1 CTF and (5) anti-Pen-2, which recognises the Pen-2 subunit of the γ-secretase complex.

The anti-Flag antibody in the co-IP experiment is supposed to exclusively bind the mutant PSEN1 FL protein (L166P + D385N 3xFlag or M233V + D385N 3xFlag) to the agarose beads. In case of an interaction between mutant and wt PSEN1 proteins in the heterozygous ES PSEN1 double mutation 3xFlag cell lines, PSEN1 wt NTF and CTF should be co-immunoprecipitated and detected in the eluate fraction. The anti-PSEN1 NTF antibody, which was used in parallel as a control, is expected to bind both, the mutant PSEN1 FL protein and the PSEN1 wt NTF to the agarose beads. PSEN1 wt CTF should be co-Immunoprecipitated by PSEN1 wt NTF.

Figure 29 shows the results of the co-IP experiments with both the anti-Flag and the anti-PSEN1 NTF antibodies. According to expectations, the mutant PSEN1 M233V + D385N 3xFlag FL protein (~ 55 kDa) and the PSEN1 wt NTF (~ 30 kDa) and CTF (~ 20 kDa) were detected in the eluate fraction of the co-IP experiment, which was performed with the anti-PSEN1 NTF antibody [Figure 29, right blot]. Furthermore, the presence of co-immunoprecipitated Nct (~ 130 kDa) and Pen-2 (~ 12 kDa) proteins demonstrated that the integrity of the γ-secretase complex was preserved in the solubilised membrane fractions.

Using the anti-Flag antibody, Nct and Pen-2 again co-immunoprecipitated with the FL mutant PSEN1 L166P + D385N 3xFlag and PSEN1 M233V + D385N 3xFlag protein, demonstrating that the endoproteolysis deficient PSEN1 FL proteins also assembled into γ-

secretase complexes, as previously reported (Nyabi *et al.* 2003) [Figure 29, left and middle blot].

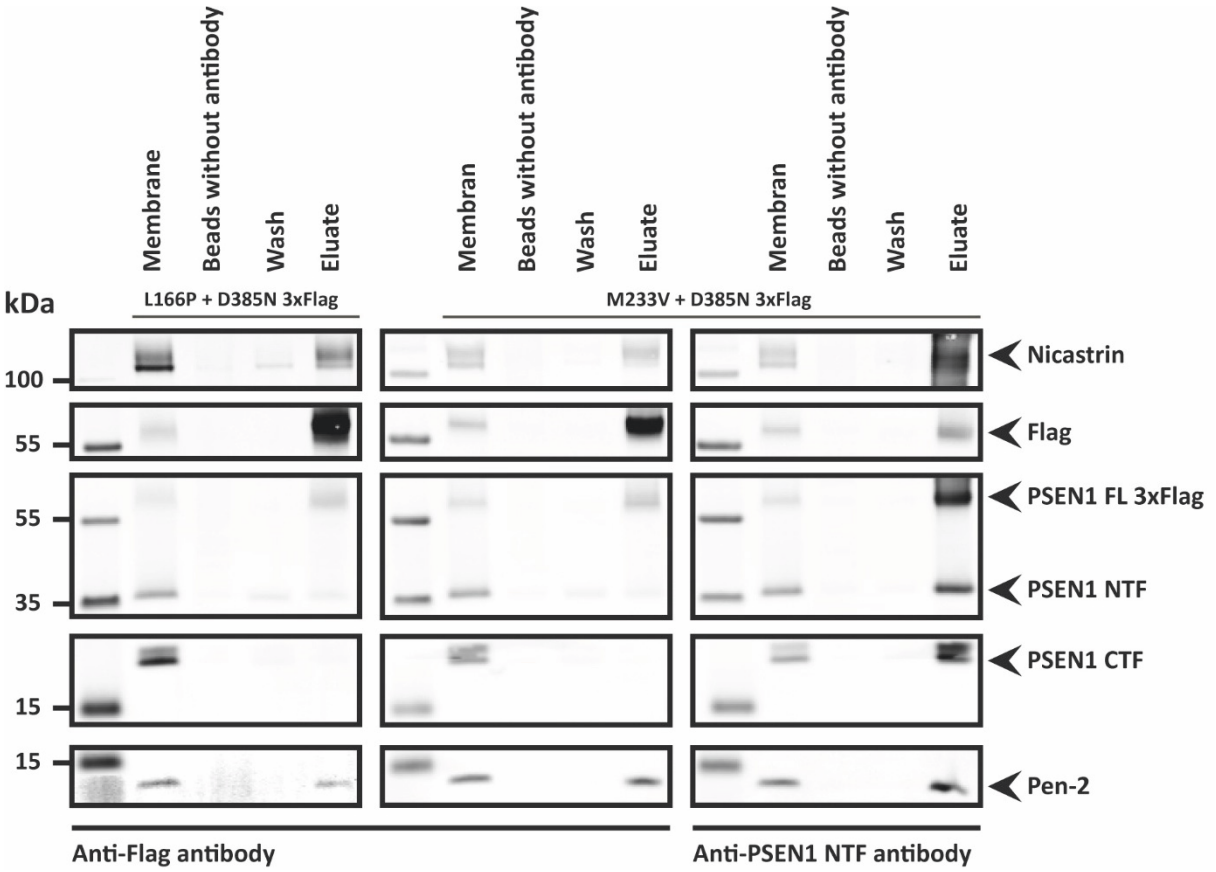

Figure 29: Co-immunoprecipitation (IP) experiments with solubilised membrane fractions of the ES PSEN1 L166P + D385N 3xFlag and the ES PSEN1 M233V + D385N 3xFlag cell line. Membrane preparations were incubated with agarose beads in the presence of either anti-Flag antibody (left and middle blot) or anti-PSEN1 NTF antibody (right blot). The components of the γ-secretase complex were detected in the membrane fraction (input), in the control eluate from the incubation of membrane with beads but without antibody, in the wash fraction and in the eluate fraction, using five different antibodies: anti-Nicastrin, anti-Flag (mutant PSEN1 FL 3xFlag), anti-PSEN1 NTF (mutant PSEN1 FL 3xFlag and PSEN1 NTF), anti-PSEN1 CTF and anti-Pen-2. PSEN1 NTF and CTF, generated by endoproteolysis of the PSEN1 wt protein, were absent in the anti-Flag co-IP eluate fractions, revealing that mutant and wt PSEN1 did not interact. The results of one out of three independently performed co-IP experiments are displayed here.

However, the PSEN1 wt NTF and CTF, which are present in the input membrane fraction, were not co-immunoprecipitated with the PSEN1 mutants. The very faint PSEN1 wt NTF band in the fraction of agarose beads without antibody, the wash fraction and the eluate was attributed to a non-specific binding of the hydrophobic PSEN1 NTF to the agarose beads, which has already been reported previously (Sato et al. 2007).

In summary, the above described results of the co-IP experiment indicate the absence of a physical interaction between mutant and wt PSEN1.

In the final experiment, a γ-secretase *in vitro* assay was performed to prove that the functional activity of the γ-secretase complex is not disrupted by the conditions of the co-IP experiment. CHAPSO-solubilised membrane fractions of the ES PSEN1 L166P + D385N 3xFlag and the ES M233V + D385N 3xFlag cell lines were again incubated with agarose beads in the presence of either anti-Flag antibody, anti-PSEN1 NTF antibody or anti-Nicastrin antibody. After washing of the beads, an APP substrate was added and incubated with the beads for 20 h at 37°C. The assay buffer had a final CHAPSO concentration of 0.25 %, which was previously demonstrated to be optimal for γ-secretase activity (Li et al. 2000, Fraering et al. 2004). The C100 V5-His_6 substrate consists of the C-terminal 99 amino acids of APP with an additional methionine at the N-terminus and a V5-His_6-tag at the C-terminus. This substrate corresponds to the membrane-bound APP C99 fragment, which is generated after shedding of the APP ectodomain by BACE. In the presence of an active γ-secretase complex, the C100 V5-His_6 substrate is cleaved within its transmembrane domain into Aβ and an AICD V5-His_6 fragment, which can be detected by Western blotting. To guarantee the exclusive detection of generated AICD V5-His_6 from the C100 V5-His_6 substrate, an anti-V5 antibody was used, which does not recognise putative residual endogenous AICD within the prepared membrane fractions. Figure 30 shows the results of the γ-secretase *in vitro* activity assay.

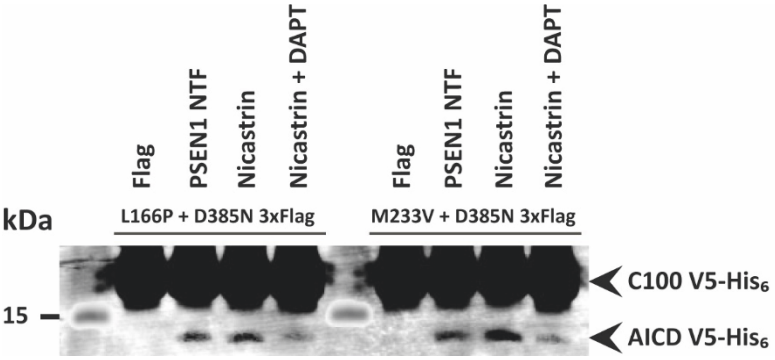

Figure 30: γ-secretase *in vitro* activity assays with membrane preparations of the ES PSEN1 L166P + D385N 3xFlag cell line and the ES PSEN1 M233V + D385N 3xFlag cell line. The CHAPSO-solubilised membranes were immunoprecipitated with either anti-Flag, anti-PSEN1 NTF or anti-Nicastrin antibody. The γ-secretase substrate C100 V5-His_6 was added and generation of the AICD cleavage product was analysed by Western blotting with the anti-V5 antibody. An AICD protein band was observed after immunoprecipitation with the anti-PSEN1 NTF and the anti-Nicastrin antibody. This band was substantially diminished for the addition of the γ-secretase

inhibitor DAPT. In contrast, no AICD was produced when the Immunoprecipitation was performed with the anti-Flag antibody, which only recognises the catalytically inactive double mutant 3xFlag protein. The results of one out of two independently performed co-IP experiments are displayed here.

AICD V5-His_6 was detected, when the solubilised membrane fractions were immunoprecipitated with either anti-Nicastrin antibody or anti-PSEN1 NTF antibody prior to incubation with the C100 V5-His_6 substrate. Furthermore, a substantially reduced AICD V5-His_6 band was observed, when 1 µM of the γ-secretase inhibitor DAPT was added to the substrate solution, demonstrating that the detected cleavage product was generated by the immunoprecipitated γ-secretase complexes. However, no AICD V5-His_6 was detected for the immunoprecipitation with the anti-Flag antibody. The results of the performed γ-secretase activity assay demonstrated that the conditions of the performed co-IP experiments did not disrupt the activity of the γ-secretase complexes. Furthermore it was demonstrated that only the anti-Nicastrin antibody and the anti-PSEN1 NTF antibody, but not the anti-Flag antibody were able to IP active γ-secretase complexes. This was expected, since both the anti-Nicastrin antibody and the anti-PSEN1 NTF antibody are able to bind to any of the suggested γ-secretase complexes: (1) the single γ-secretase complexes, containing one PSEN1 subunit, (2) the single γ-secretase complexes, containing a PSEN1 dimer or (3) the multimeric γ-secretase complexes, formed by the interaction of two single γ-secretase complexes [Figure 27]. In case of the anti-PSEN1 NTF antibody, the capacity to IP γ-secretase complexes that contain wt or mutant PSEN1 was already demonstrated in Figure 29. The previous co-IP experiments have also already demonstrated that γ-secretase complexes, which contain the catalytically inactive double mutant 3xFlag PSEN1 subunit, were exclusively immunoprecipitated by the anti-Flag antibody [Figure 29]. The observed absence of co-immunoprecipitated, catalytically active PSEN1 wt γ-secretase complexes after IP with the anti-Flag antibody was confirmed by the complete absence of the AICD V5-His_6 cleavage product in the corresponding *in vitro* assay samples [Figure 30]. Consequently, the results of the co-IP experiments and the γ-secretase in vitro assay indicate the absence of a physical or functional interaction between PSEN1 proteins.

In summary, neither a physical interaction nor an influence on the enzymatic activity of the wt PSEN1 protein by the mutant PSEN1 protein was observed in the performed experiments for the investigated FAD PSEN1 mutations. A dominant-negative characteristic of FAD PSEN1 mutations could therefore not be confirmed.

6. Discussion

Mutations in the PSEN1 gene have the highest incidence in FAD patients. According to the Alzforum Mutations Database, approximately 73 % of the more than 300 identified FAD mutations in over 500 families worldwide were found in the PSEN1 gene (Loy et al. 2014, Alzforum Mutations Database). Although FAD represents less than 1 % of all AD cases, it has been hypothesized that its disease mechanisms might be translated to the etiology of SAD, since SAD and FAD share similar clinical and neuropathological features (Bateman et al. 2011, LaFerla & Green 2012) [Table 1].

Accordingly, FAD PSEN1 mutations have been thoroughly investigated regarding their contribution to the development of AD. Based on findings in different model systems, contradicting hypotheses have been suggested for the contribution of FAD PSEN1 mutations on the development of AD. In response to qualitative and quantitative changes in the generation of Aβ peptides from APP and in the processing of other γ-secretase substrates, it was proposed that FAD PSEN1 mutations influence the activity of the γ-secretase complex by a gain-of-function mechanism, a partial loss-of-function mechanism or by a trans dominant-negative effect (Scheuner et al. 1996, Duff et al. 1996, Borchelt et al. 1996, Heilig et al. 2013, Xia et al. 2015, Veugelen *et al.* 2016, Xia *et al.* 2016).

The majority of these studies on the function of FAD PSEN1 mutations have been performed in transgenic mice or cell lines with overexpression of PSEN1 mutations. However, it is important to note that FAD PSEN1 mutations are heterozygous in patients and expressed in the presence of one PSEN1 wt allele and two PSEN2 wt alleles, which should result in an approximately equal distribution of 50 % wt and 50 % mutant PSEN1 in cells (Hendriks et al. 1997, Weggen & Beher 2012). This equal distribution of wt and mutant PSEN1 directly affects the composition and the proteolytic activity of γ-secretase complexes within a cellular system, since PSEN1 is the catalytic subunit of the complex. In contrast, the overexpression of FAD PSEN1 mutations in PSEN1 / PSEN2 deficient cell lines leads to the generation of 100 % mutant γ-secretase complexes [Figure 12]. Overexpression of FAD PSEN1 mutations in cell lines with endogenous PSEN1 and PSEN2 expression also leads to the formation of almost 100 % mutant γ-secretase complexes, since the number of γ-secretase complexes is limited by the availability of its other three subunits Nct, Aph-1 and Pen-2 (De Strooper 2003, Edbauer et al. 2003, Fraering et al. 2004, Sato et al. 2007).

Accordingly, overexpression of FAD PSEN1 mutants in cell lines with endogenous PSEN1 expression does not lead to an increased number of γ-secretase complexes. Instead, in response to the excess amount of mutant PSEN1, endogenous wt PSEN1 and PSEN2 proteins are replaced from the γ-secretase complexes and degraded (Weggen & Beher 2012) [Figure 12]. Only a very few number of studies has been performed with patient-derived samples or in model systems with endogenous and heterozygous expression of FAD PSEN1 mutations. These comprise knock-in mouse models, genome-engineered knock-in cell lines and retrieved samples from FAD patients, including isolated fibroblasts, reprogrammed iPS cells from isolated fibroblasts, plasma samples, CSF samples and *post mortem* brain samples (Scheuner et al. 1996, Guo et al. 1999, Nakano et al. 1999, Siman et al. 2000, Flood *et al.* 2002, Wang *et al.* 2006b, Shimojo et al. 2008, Saito et al. 2011, Vidal et al. 2012, Potter et al. 2013, Veeraraghavalu et al. 2013, Woodruff et al. 2013, Sproul et al. 2014, Xia et al. 2015, Szaruga et al. 2015, Paquet et al. 2016). Furthermore, these studies have been confined to a small number of different FAD PSEN1 mutations and they lack confirmation from independent laboratories.

The objective of this thesis was to establish an isogenic murine, embryonic stem (ES) cell model with endogenous and heterozygous expression of a large number of different FAD PSEN1 mutations. An advantage of this model system is the pluripotency of ES cells, which enables a differentiation into neural stem cells (NSCs) and into cell types of the central nervous system, such as neurons, astrocytes and oligodendrocytes.

A parental murine ES cell clone with a synthetic gene cassette insertion between exon 4 and exon 6 in one of the two PSEN1 alleles was purchased from the International Mouse Phenotype Consortium (IMPC) and genome-engineered by the dual recombinase mediated cassette exchange (dRMCE) technique (Osterwalder et al. 2010). The integrity of the conditional PSEN1 allele was restored by recombination mediated replacement of the loxP and FRT flanked synthetic gene cassette with a murine PSEN1 cDNA, consisting of parts of the intron 4 sequence and exons 5-12 (PSEN1 exon 4'-12) [Figure 13].

A set of 26 ES cell lines with heterozygous expression of PSEN1 mutations and protein-tags was generated by the application of different pDREV-1 PSEN1 exon 4'-12 replacement constructs [Table 3]. Estimated by the proportion of successfully recombined (positive) ES cell clones per total number of screened ES clones, an overall efficiency of 48 % was

achieved for the dRMCE technique. In comparison, the TALEN system and the CRISPR/Cas system, which have also been used for the heterozygous knock-in of one PSEN1 mutation, were much less efficient, with a frequency of 1.6 % (192 screened clones) and 2.5-5% (20-40 screened clones) positive recombinants respectively (Woodruff et al. 2013, Paquet et al. 2016).

To confirm the equal transcription and translation of the two PSEN1 alleles (PSEN1 wt allele and dRMCE restored PSEN1 allele) in the engineered ES PSEN1 cell lines, PSEN1 mRNA and protein levels were investigated.

The ES PSEN1 ΔHL cell line was generated to enable a size specific discrimination between transcripts of the PSEN1 wt allele and the restored PSEN1 allele, which contains a 120 bp deletion, corresponding to the amino acids G330-L369 in the hydrophilic loop domain (ΔHL). Indeed, two distinct RT-PCR products, one for the PSEN1 wt allele and one 120 bp smaller product for the PSEN1 ΔHL allele were produced from the synthesised ES PSEN1 ΔHL cDNA. Quantification of the two PCR products confirmed an equal transcription rate of the two PSEN1 alleles. However, an additional PCR product was generated from the ES PSEN1 wt cDNA and the ES PSEN1 ΔHL cDNA when the exon 5 forward primer of the exon 5/exon 11 primer pair was replaced by an exon 4 forward primer. This additional PCR product was not detected in the ES PSEN1 cell line, which had failed successful recombination (negative clone) or in the parental ES cell line, indicating that it was produced from the dRMCE restored PSEN1 allele. Sequencing of the additional PCR product from the PSEN1 ΔHL cDNA revealed a deletion of the exons 5 and 6 (ΔE5/6; 210 bp). This partial alternative splicing of the restored PSEN1 allele after dRMCE most certainly occurred in response to the modification of the intron sequence between exon 4 and 5. The conditional allele in the parental ES cell line contains the first 1764 bp of the 2209 bp intron 4 sequence, followed by an additional, unrelated sequence of 112 bp, including an FRT recombination site. The missing 445 bp of the intron 4 sequence were cloned (BstBI restriction site) between the FRT site and the exon 5 cDNA sequence on the pDREV-1 replacement construct. Consequently, the PSEN1 intron 4 sequence of the restored PSEN1 allele is interrupted by an unrelated sequence of 115 bp (112 bp + 3 bp of the added BstBI restriction site).

Our intention for the completion of the PSEN1 intron 4 sequence in the restored PSEN1 allele was to increase the likelihood for correct intron splicing. Still, partial alternative splicing of the restored PSEN1 allele was observed and has apparently been caused by the

115 bp insertion. However, we did not detect a corresponding truncated PSEN1 protein for the alternatively spliced ΔE5/6 mRNA transcript, when we evaluated the PSEN1 protein expression in the ES PSEN1 cell lines by Western blotting.

Instead, quantification of the PSEN1 NTF and CTF levels revealed that the successfully dRMCE recombined ES PSEN1 cell line (PSEN1 wt +/+) expressed twice the amount of PSEN1 protein in comparison to an ES PSEN1 cell line, which had failed recombination and therefore only harboured one functional PSEN1 wt allele (PSEN1 wt +/-). This result demonstrated that the PSEN1 wt allele and the restored PSEN1 wt allele in the ES PSEN1 wt +/+ cell line expressed equal PSEN1 NTF and CTF levels.

We conclude that the alternatively spliced ΔE5/6 mRNA transcript, which is generated from the restored PSEN1 allele, is not translated into a stable protein and consequently does not interfere with the functional analysis of the ES PSEN1 cell lines.

Since FAD is a disease of the central nervous system, we differentiated the dRMCE engineered ES PSEN1 cell lines into NSCs with the intention to study the molecular effects of the FAD PSEN1 mutations in a neural cell type. Successful differentiation by the applied protocol was demonstrated by the characteristic cell morphology and by the expression of two NSC markers: Sox2, a transcription factor that is involved in the maintenance of stem cell self-renewal and Nestin, an intermediate filament protein that is expressed in progenitor cells of the central nervous system (Pollard et al. 2006b, Pollard & Conti 2007). We could further demonstrate the good quality and multipotency of the ES PSEN1 cell lines by successful differentiation of neurospheres, which are intermediate cell species of the NSC differentiation protocol, from 7 FAD ES PSEN1 cell lines into neurons, astrocytes and oligodendrocytes. While some variations in the capacity to form neurospheres have been observed between all of the 7 investigated FAD ES PSEN1 cell lines, the differentiation of the ES PSEN1 C410Y cell line, first into neurospheres and second into neurons, astrocytes and oligodendrocytes was particularly insufficient. Staining for the neural and astrocyte markers β-III tubulin and GFAP only revealed the presence of neurons. An impairment of self-renewal and a stronger commitment towards the differentiation into neurons has been previously observed for tissue-isolated, murine neural progenitor cells derived neurospheres that had been infected with a PSEN1 C410Y lentivirus. Comparable results were obtained for the PSEN1 ΔE9 mutation and both observations have been associated with an impaired NOTCH

signaling (Veeraraghavalu *et al.* 2010). Consequently, the absence of differentiated astrocytes from PSEN1 C410Y neurospheres in our experiment might have been caused by a combined effect of the low cell number and an enhanced commitment towards the neuronal lineage.

However, in order to draw a final conclusion about the observed variations in the differentiation capacities of the FAD ES PSEN1 cell lines, repetitions of the performed experiments are mandatory. Furthermore, the number and size of the differentiated neurospheres and the proportion of differentiated neurons, astrocytes and oligodendrocytes need to be carefully quantified.

For the investigation of Aβ40 and Aβ42 secretion by the heterozygous FAD PSEN1 cells lines, we chose the NSCs, since they expressed considerably higher amounts of the BACE1 protease in comparison to the ES cell lines [Figure 25 A]. BACE1 cleaves APP into the C99 fragment, which is subsequently further processed by the γ-secretase complex into Aβ peptides of varying length (Lichtenthaler et al. 2011). Consequently, BACE1 expression is important for the generation of Aβ peptides. To enable the detection of Aβ40 and Aβ42 peptides, human APP was overexpressed in the NSC lines by infection with an APP695 adenovirus, since endogenous mouse Aβ42 levels were unfortunately under the detection limit (data not shown). Table 4 illustrates the semi-quantitative Aβ40 levels, the Aβ42 levels and the Aβ42/Aβ40 ratio, which have been previously published for our investigated FAD PSEN1 mutations in different model systems and in comparison to PSEN1 wt. The results of our dRMCE engineered, heterozygous and endogenous FAD PSEN1 stem cell model system are displayed in the last three rows of the table. At first glance, three general conclusions can be drawn from the results in table 4: First, some FAD PSEN1 mutations (L166P, G384A) have been more thoroughly investigated in comparison to others (P117L, L173W). Second, data from comparable heterozygous and endogenous FAD PSEN1 model systems, such as heterozygous knock-in mice, is only available for 4 of the investigated FAD PSEN1 mutations. Third, the Aβ levels in comparison to PSEN1 wt are partially inconsistent within or between the applied model systems for each of the investigated FAD PSEN1 mutations.

Those observed inconsistencies may have different reasons.

Table 4: Semi-quantitative comparison of Aβ40 levels, Aβ42 levels and the Aβ42/Aβ40 ratio between FAD PSEN1 mutations and PSEN1 wt in the applied model systems. ↑: Increased compared to PSEN1 wt. ↓: Decreased compared to PSEN1 wt. →: Unchanged compared to PSEN1 wt.

FAD PSEN1 model systems		FAD PSEN1 mutations									
		P117L	L166P	L173W	I213T	M233V	R278I	E280A	G384A	C410Y	L435F
(1) Overexpression in cells with endogenous PSEN1/PSEN2 expression	Aβ40	↓[14, 16]	↓[14, 16, 21, 28]	↓[16]		↓[14, 16, 28]	↓[8]	↑[12] →[28]	→[4, 17] ↓[10, 14, 28]		↓[27]
	Aβ42	↑[14, 16]	↑[14, 16] →[21, 28]	↑[16]	↑[1]	↑[14, 16, 28]		↑[1, 12, 28]	↑[1, 4, 10, 14, 17, 28]	↑[1]	↓[27]
	Aβ42/Aβ40	↑[16]	↑[16, 21, 28]	↑[16]		↑[16, 28]		↑[12, 28]	↑[10, 28]		
(2) Overexpression in PSEN1/PSEN2 double-KO cells	Aβ40		↓[5, 9, 22, 23]		↓[11]		↓[8, 17, 23]		↓[9, 11, 23]	↓[5, 11, 23]	↓[15, 23, 27]
	Aβ42		↑[3, 5] →[9] ↓[9, 22, 23]		↓[11]		→[17] ↓[23]		↑[9, 11, 23]	→[5] ↓[11, 23]	↓[15, 23, 27]
	Aβ42/Aβ40		↑[5]		↑[11]	↑[7]			↑[11]	↑[5, 11]	↓[15]
(3) Cell-free assays	Aβ40		↓[18, 20, 22]		↓[13, 20]		↓[26]	↓[26]	↓[4, 18, 20]	↓[25]	↓[25]
	Aβ42		→[20] ↓[18, 22]		→[13, 20]		↓[26]	↑[26]	↑[4] →[18] ↓[20]	↓[25]	↓[25]
	Aβ42/Aβ40		↑[24]		↑[13]				↑[24]		
(4) Transgenic mice	Aβ40	→[6]									
	Aβ42	↑[6]									
	Aβ42/Aβ40										
(5) Heterozygous knock-in mice	Aβ40		↓[19]		→[2]		↓[17]				↓[25]
	Aβ42		↑[19]		↑[2]		→[17]				↓[25]
	Aβ42/Aβ40		↑[19]		↑[2]		↑[17]				↑[25]
(6) dRMCE engineered, endogenous and heterozygous cell lines	Aβ40	→	→	↑	↑	→	↑	→	→	↑	→
	Aβ42	↑	↑	↑	↑	↑	↑	↑	↑	↑	↑
	Aβ42/Aβ40	↑	↑	↑	↑	↑	↑	↑	↑	↑	↑

References:

[1] (Murayama *et al.* 1999), **[2]** (Nakano *et al.* 1999), **[3]** (Moehlmann *et al.* 2002), **[4]** (Qi *et al.* 2003), **[5]** (Schroeter *et al.* 2003), **[6]** (Wen *et al.* 2004), **[7]** (Walker *et al.* 2005), **[8]** (Nakaya *et al.* 2005), **[9]** (Bentahir *et al.* 2006), **[10]** (Kumar-Singh *et al.* 2006), **[11]** (Shimojo *et al.* 2007), **[12]** (Kaneko *et al.* 2007), **[13]** (Shimojo *et al.* 2008), **[14]** (Page *et al.* 2008), **[15]** (Heilig *et al.* 2010), **[16]** (Kretner *et al.* 2011), **[17]** (Saito *et al.* 2011), **[18]** (Quintero-Monzon *et al.* 2011), **[19]** (Vidal *et al.* 2012), **[20]** (Chavez-Gutierrez *et al.* 2012), **[21]** (Koch *et al.* 2012), **[22]** (Cacquevel *et al.* 2012), **[23]** (Heilig *et al.* 2013), **[24]** (Fernandez *et al.* 2014), **[25]** (Xia *et al.* 2015), **[26]** (Szaruga *et al.* 2015), **[27]** (Kretner *et al.* 2016), **[28]** (Li *et al.* 2016)

Inconsistencies between independent studies in overexpression model systems might be based on the utilization of either stable or transiently transfected cell lines, which might express variable levels of mutant PSEN1. Furthermore, qualitative and quantitative differences of the Aβ profile between overexpression and endogenous knock-in FAD PSEN1 model systems are very likely, since overexpression of FAD PSEN1 mutations adversely affect the proportion of wt and mutant γ-secretase complexes, as already explained above. Subtle variations in the protocol or the timeline of the experiments could also have an effect on the catalytic activity of the γ-secretase complexes. In case of γ-secretase *in vitro* assays, it is well known that buffer components, the pH value as well as the addition and concentration of lipids and detergents can have a strong effect on γ-secretase activity and lead to a preferential production of certain Aβ species (Kimberly *et al.* 2003a, Fraering et al. 2004, Quintero-Monzon et al. 2011, Okochi et al. 2013). Thus, the cellular source for the purification of the γ-secretase complexes (overexpression, endogenous or heterozygous knock-in FAD PSEN1 cells) and the applied protocols for the purification and performance of the γ-secretase *in vitro* assay might bias the outcome of the experiment.

In the following, a representative comparison between published data from different model systems and our isogenic FAD PSEN1 model system will be given for the FAD PSEN1 mutations L166P, I213T, R278I and L435F, since these mutations, out of all investigated mutations, are the only ones with available data from overexpression cell culture models, from cell-free *in vitro* assays and from heterozygous knock-in mice [Table 4].

The L166P mutation showed a decrease in Aβ40 levels, an increase in Aβ42 levels and an increase in the Aβ42/Aβ40 ratio of approximately 1.2 – 29 fold in the majority of studies in overexpression cell culture models (Moehlmann et al. 2002, Schroeter et al. 2003, Bentahir et al. 2006, Page et al. 2008, Kretner et al. 2011, Koch et al. 2012, Cacquevel et al. 2012, Heilig et al. 2013, Li et al. 2016). Few studies also showed a decrease or unchanged Aβ42 levels (Bentahir et al. 2006, Koch et al. 2012, Cacquevel et al. 2012, Heilig et al. 2013, Li et al. 2016). Cell-free *in vitro* assays for the L166P mutation showed a decrease in Aβ40 levels, decreased or unchanged Aβ42 levels and an increase in the Aβ42/Aβ40 ratio of approximately 3.5 fold (Quintero-Monzon et al. 2011, Chavez-Gutierrez et al. 2012, Cacquevel et al. 2012, Fernandez et al. 2014). A 15-30 % decrease in Aβ40 levels, an increase in Aβ42 levels and an approximately 3-4 fold increase in the Aβ42/Aβ40 ratio were observed in the cortex and hippocampus of heterozygous L166P knock-in mice, which had been

crossbred to APP-transgenic mice at 6-8 month of age (Vidal et al. 2012). At this age, the animal had not developed any amyloid plaques in the brain. Results from our isogenic NSC PSEN1 L166P line revealed unchanged Aβ40 levels, a trend towards an increase in Aβ42 levels and a significant 1.2 fold increase in the Aβ42/Aβ40 ratio.

The I213T mutation showed a decrease in Aβ40 levels, an increase or a decrease in Aβ42 levels and an increase in the Aβ42/Aβ40 ratio of approximately 2 fold in overexpression cell culture models (Murayama et al. 1999, Shimojo et al. 2007). Cell-free *in vitro* assays for the I213T mutation showed a decrease in Aβ40 levels, unchanged Aβ42 levels and an increase in the Aβ42/Aβ40 ratio of approximately 1.3 fold (Shimojo et al. 2008, Chavez-Gutierrez et al. 2012). Endogenous murine Aβ was measured in whole brains of 4-5 months old heterozygous I213T knock-in mice and revealed unchanged Aβ40 levels and an increase in Aβ42 levels. In addition, an approximately 1.2 fold increase in the Aβ42/Aβ40 ratio was observed in primary neuronal cultures, which had been derived from the heterozygous I213T knock-in mice (Nakano et al. 1999). Results from our isogenic NSC PSEN1 I213T line revealed a significant increase in Aβ40 levels, a significant increase in Aβ42 levels and a significant increase in the Aβ42/Aβ40 ratio of approximately 2.8 fold.

The R278I mutation showed a decrease in Aβ40 levels and decreased or unchanged Aβ42 levels in overexpression cell culture models (Nakaya et al. 2005, Saito et al. 2011, Heilig et al. 2013). A cell-free *in vitro* assay that used *post mortem* brain samples from one FAD PSEN1 R278I patient as the source of γ-secretase showed a decrease in Aβ40 levels, unchanged Aβ42 levels and an increase in the Aβ42/Aβ40 ratio (Szaruga et al. 2015). Decreased endogenous Aβ40 levels, unchanged Aβ42 levels and an approximately 1.3 fold increase in the Aβ42/Aβ40 ratio were observed in the insoluble brain fraction of heterozygous R278I knock-in mice at 24 month of age (Saito et al. 2011). Very similar results were obtained with derived MEFs from the heterozygous knock-in mice. Interestingly, in comparison to APP-transgenic mice, heterozygous R278I knock-in mice, which had been crossbred with APP-transgenic mice, did not show any changes in the Aβ40 and Aβ42 levels or the Aβ42/Aβ40 ratio in the insoluble brain fraction at 3 month of age. Results from our isogenic NSC PSEN1 R278I line revealed a significant increase in Aβ40 levels, a significant increase in Aβ42 levels and a significant increase in the Aβ42/Aβ40 ratio of approximately 1.4 fold.

Overexpression of the L435F mutation caused a strong decrease in Aβ40 and Aβ42 levels (Kretner et al. 2016). Furthermore, in two independent studies by the same laboratory, completely abolished γ-secretase activity with no production of Aβ40 or Aβ42 was observed after overexpression of the L435F mutation in PSEN1/PSEN2 deficient MEFs (Heilig et al. 2010, Heilig et al. 2013). A much smaller decrease in endogenous Aβ40 levels (29 %) and Aβ42 levels (17 %) and an approximately 1.3 fold increase in the Aβ42/Aβ40 ratio were observed in the insoluble brain fraction of 3 month old heterozygous L435F knock-in mice (Xia et al. 2015). Similar Aβ40 and Aβ42 reductions were also seen when brain samples from the same mice were used in a γ-secretase in vitro assay. Results from our isogenic NSC PSEN1 L435F line revealed almost unchanged Aβ40 levels and Aβ42 levels and a trend towards an increase in the Aβ42/Aβ40 ratio 1.6 fold.

Overall, a comparison of the different model systems for the FAD PSEN1 mutations L166P, I213T, R278I and L435F revealed that in general substantially higher changes in the Aβ40 levels, the Aβ42 levels and the Aβ42/Aβ40 ratio were observed in overexpression cell culture models compared to heterozygous knock-in mice. In accordance to that, *in vitro* assays with purified γ-secretase complexes from overexpression cell lines also showed substantially higher changes in the Aβ levels and the Aβ42/Aβ40 ratio, compared to *in vitro* assays with purified γ-secretase complexes from either heterozygous knock-in mice or *post mortem* brain samples from FAD patients (Shimojo et al. 2008, Quintero-Monzon et al. 2011, Chavez-Gutierrez et al. 2012, Cacquevel et al. 2012, Xia et al. 2015, Szaruga et al. 2015).

Results from our isogenic FAD PSEN1 model system demonstrated an increase in Aβ42 levels and in the Aβ42/Aβ40 ratio for all of the investigated cell lines [Table 4]. However, a reduction in Aβ40 levels, which was consistently observed in each model system for the L166P, I213T, R278I and L435F mutations, with the exception of heterozygous I213T knock-in mice, could not be confirmed in our isogenic model system [Table 4]. With the putative exception of the E280A mutation, we measured almost unchanged Aβ40 levels in the PSEN1 P117L, L166P, M233V, G384A and L435F cell lines, a trend towards increased Aβ40 levels in the PSEN1 L173W and C410Y cell lines and significantly increased Aβ40 levels in the PSEN1 I213T and R278I cell lines in comparison to PSEN1 wt. However, the large standard deviations, especially in case of the L173W mutation, indicate that further experiments are necessary to definitively determine the absolute Aβ40 concentrations for the investigated

FAD PSEN1 mutations [Figure 25 C]. Furthermore, it is possible that the adenovirus induced overexpression of human APP695 might have influenced the Aβ40 production in our isogenic model system. Therefore, the detection of endogenous, murine Aβ40 levels might be necessary as a validation control.

Our observed 1.4 fold and 1.6 fold increase in the Aβ42/Aβ40 ratio for the R278I and L435F mutations was consistent with the available data from heterozygous R278I and L435F knock-in mice. However, in comparison to heterozygous L166P and I213T knock-in mice, an approximately 3 fold lower Aβ42/Aβ40 ratio (L166P) and an approximately 3 fold higher Aβ42/Aβ40 ratio (I213T) were observed in our model system. The complete loss of γ-secretase activity for the L435F mutation, which was observed in overexpression model systems, could not be confirmed by our experiments (Heilig et al. 2010, Heilig et al. 2013). Our investigated PSEN1 L435F cell line contained one PSEN1 wt and one PSEN1 L435F allele. In case of a complete loss of γ-secretase activity for the approximately 50 % γ-secretase complexes that contain the PSEN1 L435F mutation, approximately 50 % decreased Aβ40 and Aβ42 levels should have been measured in comparison to the PSEN1 wt cell line, which contains two PSEN1 wt alleles. Instead, we observed almost unchanged Aβ40 and Aβ42 levels and a small increase in the Aβ42/Aβ40 ratio. It has to be noted that the described 50 % reduction of Aβ42 and Aβ40 in the heterozygous L435F knock-in mice has only been observed in the performed *in vitro* assay with solubilised brain fractions. The endogenous Aβ levels from brain homogenates of these mice were much less reduced (Xia et al. 2015). All in all, the available data suggest that overexpression and *in vitro* assays exaggerate the effect of the L435F mutation and that the mutant protein retains some or most of its catalytic activity when expressed in the presence of PSEN1 wt. Recently it was suggested that Aβ43 rather than Aβ42 is the predominantly generated pathogenic species by the L435F mutation, comparable to previous observations for the R278I mutation (Saito et al. 2011, Kretner et al. 2016). This observation was supported by the high abundance of Aβ43-containing plaques in brain sections of two FAD PSEN1 L435F patients, indicating a negligible or less important role of Aβ42 for the amyloid pathology in these patients. We have not measured Aβ43 levels in the NSC PSEN1 L435F cell line. However, the fact that Aβ40 and Aβ42 levels appeared to be unchanged in the NSC PSEN1 L435F cell line indicates that such measurements should be performed for this but also for all the other cell lines in future studies.

Finally, the L173W mutation showed a remarkable increase in Aβ42 levels (14 fold) and in the Aβ42/Aβ40 ratio (5 fold). These results could be particularly interesting, since the L173W mutation has not been well studied up to now and since no data are available from patient-derived samples or heterozygous knock-in mice.

The major difference between our results and part of the data in the literature appears to be that in the NSC cell lines the increase in the Aβ42/Aβ40 ratio is mainly driven by an increase of Aβ42 levels. This was consistent with data from some FAD PSEN1 knock-in mouse models (Nakano et al. 1999, Siman et al. 2000, Flood et al. 2002, Vidal et al. 2012). In other knock-in mouse models, the increase in the Aβ42/Aβ40 ratio seemed to result at least in part from a reduction in Aβ40 levels (Wang et al. 2006b, Saito et al. 2011, Vidal et al. 2012, Xia et al. 2015). However, these variations might result from a general limitation in the comparison of Aβ levels in tissue culture supernatants with steady-state Aβ levels in the brain of transgenic mice, which might vary substantially depending on the specific brain areas, the age of the investigated mice, and the extraction protocol used (Saito et al. 2011, Vidal et al. 2012, Xia et al. 2015). Importantly, our results are fully consistent with early data from Scheuner et al. who had found increased Aβ42 but unchanged Aβ40 levels both in plasma and fibroblasts of FAD patients with four different PSEN1 mutations (Scheuner et al. 1996). This was recently confirmed in a study using stable isotope labeling kinetics, which demonstrated in human carriers of different PSEN mutations a 25% increase in the Aβ42 but no change in the Aβ40 production rate in the brain (Potter et al. 2013).

Last, we investigated the putative trans dominant-negative effect of FAD PSEN1 mutations, which is defined by a physical interaction between wt and mutant protein and by an altered enzymatic activity of the wt protein (Herskowitz 1987, Veitia 2007). In case of PSEN1, a physical interaction between wt and mutant PSEN1 might induce a conformational change in the wt protein, which could lead to an altered enzymatic activity.

Previous investigations on a putative physical and functional interaction of wt and mutant PSEN1 were performed in overexpression cell culture models and have produced contradicting results (Schroeter et al. 2003, Sato et al. 2007, Heilig et al. 2013).

Heilig et al. transiently transfected PSEN1/PSEN2 deficient MEFs with expression vectors encoding either wt or mutant PSEN1 (single transfection), or with equal quantities of both expression vectors (co-transfection). The intention of the co-transfection was to achieve an

equal expression of wt and mutant PSEN1, as observed in FAD patients. Aβ42 and Aβ40 levels were measured in cell culture supernatants from both transfection experiments and normalised to PSEN1 wt. In the first, single transfection experiment, Aβ40 and Aβ42 levels were dramatically decreased for most of the investigated FAD PSEN1 mutations (including the L166P and C410Y mutation) and completely abolished for the R278I and the L435F mutation compared to PSEN1 wt. In the second, co-transfection experiments, Aβ40 levels were reduced and Aβ42 levels were increased for most of the investigated FAD PSEN1 mutations compared to PSEN1 wt. Since almost no catalytic activity was observed for most of the FAD PSEN1 mutations in the single transfection experiments, it was concluded that FAD PSEN1 mutations had impaired the ability of PSEN1 wt to produce Aβ40 and that they were able to stimulate the ability of PSEN1 wt to produce Aβ42. Consequently, the changes in the Aβ40 levels, the Aβ42 levels and in the Aβ42/Aβ40, which had been observed in the co-transfection experiments, were not attributed to the catalytic activity of the PSEN1 mutants but to a change in the catalytic activity of PSEN1 wt as a result of a trans dominant-negative effect.

We investigated this putative trans dominant-negative effect of FAD PSEN1 mutations by a comparison of the Aβ42/Aβ40 ratio in 6 heterozygous NSC PSEN1 lines: PSEN1 wt, PSEN1 L166P, PSEN1 L166P + D385N, PSEN1 M233V, PSEN1 M233V + D385N and PSEN1 D385N. The D385 residue is one of the two catalytic PSEN1 aspartates (D257 and D385). A mutation at this site leads to a catalytic inactivation of the γ-secretase complex (Wolfe et al. 1999, Steiner et al. 1999). Consequently, the expressed PSEN1 proteins from the L166P + D385N, the M233V + D385N and the D385N allele in the respective NSC lines are catalytically dead. A comparison of the Aβ42/Aβ40 ratios between the investigated wt and mutant NSC PSEN1 lines revealed a statistically significant increase for the FAD mutations L166P and M233V, which has already been observed in our previous experiments. In contrast, Aβ42/Aβ40 ratios in the NSC PSEN1 L166P + D385N, the NSC PSEN1 M233V + D385N and the NSC PSEN1 D385N lines were unchanged in comparison to the NSC PSEN1 wt line. The absence of an increased Aβ42/Aβ40 ratio in the catalytic inactive, double mutant NSC PSEN1 lines (L166P + D385N and M233V + D385N) compared to the NSC PSEN1 wt line demonstrated (1) that the activity of wt PSEN1 remained unchanged in the presence of catalytic inactive FAD PSEN1 mutations and (2) that the increased Aβ42/Aβ40 ratios in the FAD NSC PSEN1 lines were

induced by the catalytic activity of the respective FAD mutant. These observations strongly argue against a trans dominant-negative effect of FAD PSEN1 mutations.

We adopted our experimental design from an earlier publication (Schroeter et al. 2003). Our data is consistent with their results for an investigation of the PSEN1 M146L + D385A double mutant. A trend towards an increase in the Aβ42/Aβ40 ratio has been observed after co-transfection of PSEN1/PSEN2 deficient MEFs with expression vectors encoding PSEN1 wt and PSEN1 M146L + D385A at equal stoichiometry. However, the observed effect (data not shown in the paper) varied between experiments and was not statistically significant although multiple independent experimental repeats were performed (Schroeter et al. 2003).

The disagreement between our experiments and the published data from Heilig et al. might be based on limitations of their experimental design (Heilig et al. 2013). We used stable cell lines with genome-integrated PSEN1 mutations in one PSEN1 allele in the presence of one PSEN1 wt allele. Both PSEN1 alleles are expressed under the natural, endogenous promoter at equal levels and therefore also share an equal prerequisite to form γ-secretase complexes. Furthermore, the formation of γ-secretase complexes should not be limited by the availability of the other subunits Nct, Aph-1 and Pen-2 in our PSEN1 cell lines, because of the endogenous expression of both PSEN1 alleles. This assumption was supported by the absence of detected FL PSEN1 in our wt and mutant PSEN1 cell lines, with the exception of the endoproteolysis-deficient D385N mutant. Endoproteolysis of FL PSEN1 into an NTF and CTF occurs upon formation of the γ-secretase complex (Thinakaran et al. 1996, Ratovitski et al. 1997, De Strooper *et al.* 2012). Consequently, accumulation of FL PSEN1 indicates the presence of PSEN1 outside of γ-secretase complexes as a result of an excess of PSEN1 in the cell. While Heilig et al. did perform experiments to determine the maximal amount of expression vector DNA to avoid overloading the cells with exogenous PSEN1, some results in their publication such as the accumulation of FL PSEN1 in the double transfection experiments indicated that they might have exceeded this amount. Furthermore, their experimental protocol indicated that in the co-transfection experiments they used a 1:1 mixture of expression vectors encoding PSEN1 wt and the respective PSEN1 mutants. However, for the control condition they added empty vector DNA to the expression vector encoding PSEN1 wt to adjust the total amount of vector DNA. This would have resulted in the expression of only half the amount of PSEN1 protein in the control condition as

compared to the co-transfection condition (Heilig et al. 2013). Taken together, this technical issue might have caused in the cellular γ-secretase complexes the exchange of wt for mutant PSEN1 protein. Since many PSEN1 mutants appear to have reduced catalytic activity this exchange could potentially explain the reduced Aβ40 levels observed in the co-transfection experiments, and which were interpreted by Heilig et al. as evidence for dominant-negative effects of PSEN1 mutations (Page et al. 2008, Kretner et al. 2011, Heilig et al. 2013, Li et al. 2016).

Heilig et al. further supported their hypothesis of a dominant-negative effect of FAD PSEN1 mutations by co-immunoprecipitation (co-IP) experiments, demonstrating a physical interaction between wt and mutant PSEN1 (Heilig et al. 2013). HEK293 cells were transiently co-transfected with equal amounts of expression vectors, encoding either 3xFlag-tagged PSEN1 wt or the 3xHA-tagged PSEN1 435F. For the subsequent co-IP experiments, membrane fractions were prepared and solubilized in a buffer with a final CHAPSO concentration of 4 g/g protein. PSEN1 wt 3xFlag was immunoprecipitated with an anti-Flag antibody and the co-IP of PSEN1 L435F 3xHA was confirmed by Western Blotting with an anti-HA antibody. Reciprocal co-IP experiments were equally successful (Heilig et al. 2013).

We re-evaluated these results with two ES cell lines: PSEN1 L166P + D385N 3xFlag and PSEN1 M233V + D385N 3xFlag. In both of these cell lines, wt and double mutant 3xFlag PSEN1 can be easily discriminated, since the double mutant 3xFlag PSEN1 carries a 3xFlag-tag and remains a FL protein, because of the D385N mutation, unlike wt PSEN1, which is endoproteolytically cleaved into an NTF and CTF. For our co-IP experiments, membrane fractions were isolated from both cell lines and solubilised in a buffer containing 1 % CHAPSO. We did not observe a co-IP of wt NTF or CTF in either cell line after immunoprecipitation with an anti-Flag antibody, demonstrating the absence of a physical interaction between wt and mutant PSEN1. However, co-IP of the γ-secretase subunits Nct and Pen-2 indicated a normal integration of catalytically dead mutant PSEN1 proteins into γ-secretase complexes, as reported previously (Nyabi et al. 2003). These findings were further supported by γ-secretase *in vitro* activity assays. When membrane preparations were immunoprecipitated with the anti-Flag antibody, generation of the AICD V5-His_6 fragment from the recombinant γ-secretase substrate C100 V5-His_6 was not detected. This confirmed that the 3xFlag tagged mutant proteins were catalytically inactive and that no catalytically active PSEN1 wt protein was co-immunoprecipitated in these experiments. In contrast, when

anti-Nct or anti-PSEN1-NTF antibodies were used for the immunoprecipitation, active wt γ-secretase was pulled down and AICD V5-His_6 generation was observed.

Our observations are consistent with results in an earlier publication (Sato et al. 2007). Co-IP experiments with two differentially tagged PSEN1 proteins from stably transfected PSEN1/PSEN2 deficient MEFs demonstrated the absence of a physical interaction between PSEN1 proteins. They concluded that each γ-secretase complex contains only one PSEN1 protein and that all four subunits are present in a stoichiometry of 1:1:1:1. Sato et al. further showed that a CHAPSO concentration of 1 % caused a strong non-specific binding of FL PSEN1, PSEN1 NTF and Nct in their co-IP experiments. This was not observed after membrane solubilisation in 1 % digitonin instead of CHAPSO. Interestingly, when we compared membrane fractions, either solubilised in 1 % CHAPSO or 1 % digitonin, we did not observe any differences in our co-IP experiments (data not shown). Non-specific binding to the agarose beads was observed for very minor amounts of PSEN1 NTF with both detergents, indicating that solubilisation in 1 % CHAPSO might not be problematic for membrane preparations from cell lines with endogenous PSEN1 expression, but that it might cause non-specific binding, if PSEN1 is highly overexpressed. An adverse combination of PSEN1 overexpression and membrane solubilisation in CHAPSO could also provide an explanation for the conflicting results of the protein interaction studies by Heilig et al. (Heilig et al. 2013). According to their method section, membrane aliquots with a protein concentration of 25-50 µg/µL had been solubilised with CHAPSO at a concentration of 4 g/g protein. This should have resulted in a final CHAPSO concentration of 10-20 % in the membrane solutions, which were used undiluted in the subsequent co-IP experiments (Heilig et al. 2013). Consequently, it appears to be fairly possible that the observed interactions between PSEN1 proteins were non-specifically induced by the unsuitable assay conditions.

In summary, using the highly efficient dRMCE genome engineering technique, we succeeded in the development of an innovative and isogenic stem cell culture model system, with endogenous and heterozygous expression of PSEN1 mutations, as observed in FAD PSEN1 patients. This model system consists of 26 ES PSEN1 cell lines with different mutations and protein tags, including 10 cell lines with FAD PSEN1 mutations. An approximately 10 fold higher efficiency was observed for the dRMCE technique, compared to a recently published PSEN1 knock-in study with the CRISPR/Cas system (Paquet et al. 2016). This means that

additional cell lines with other heterozygous PSEN1 mutations or modifications can be easily and quickly generated with substantially less effort and lower costs as compared to other genome engineering methods. 19 out of 26 ES PSEN1 cell lines were successfully differentiated into NSC lines. The stem cell status was confirmed in selected NSC lines by the expression of neural stem cell markers and the differentiation into neurons, astrocytes and oligodendrocytes. Detection of secreted Aβ peptides in cell culture supernatants revealed that Aβ40 levels, Aβ42 levels and the Aβ42/Aβ40 ratios were comparable with available data from other knock-in models in the literature, demonstrating that our murine model system is a suitable alternative to heterozygous knock-in mice and also to FAD PSEN1 patient-derived cell lines, which are only available for a very limited number of PSEN1 mutations and frequently lack genetically matched control cells (Nakano et al. 1999, Shimojo et al. 2008, Bock et al. 2011, Saito et al. 2011, Weggen & Beher 2012, Vidal et al. 2012, Soldner & Jaenisch 2012, Rouhani et al. 2014, Xia et al. 2015, Szaruga et al. 2015, Mungenast et al. 2015). Importantly, in functional studies we were able to demonstrate that FAD PSEN1 mutations do not act in a dominant-negative fashion through the formation of PSEN1 dimers or multimers (Schroeter et al. 2003, Shen & Kelleher 2007, Sato et al. 2007, Heilig et al. 2013).

In the future, our isogenic PSEN1 stem cell model might contribute to the clarification of other controversial hypotheses, such as the proposed effect of FAD PSEN1 mutations on protein trafficking, autophagy, calcium homeostasis, the potency of γ-secretase modulators or the processing of γ-secretase substrates other than APP (Czirr et al. 2007, Parks & Curtis 2007, Lee et al. 2010, Zhang et al. 2010, De Strooper & Annaert 2010, Hahn et al. 2011, Haapasalo & Kovacs 2011, Neely et al. 2011, Crump *et al.* 2013, Sepulveda-Falla et al. 2014, Duggan & McCarthy 2016).

7. References

2015 Alzheimer's disease facts and figures. *Alzheimer's & dementia : the journal of the Alzheimer's Association,* **11,** 332-384.

Abbott, A. (2011) Dementia: a problem for our age. *Nature,* **475,** S2-4.

Aizenstein, H. J., Nebes, R. D., Saxton, J. A. et al. (2008) Frequent amyloid deposition without significant cognitive impairment among the elderly. *Archives of neurology,* **65,** 1509-1517.

Alonso, A. C., Zaidi, T., Grundke-Iqbal, I. and Iqbal, K. (1994) Role of abnormally phosphorylated tau in the breakdown of microtubules in Alzheimer disease. *Proc Natl Acad Sci U S A,* **91,** 5562-5566.

Alzforum Mutations Database. *http://www.alzforum.org/mutations*.

Alzheimer, A. (1907) Über eine eigenartige Erkrankung der Hirnrinde. *Allgemeine Psychiatrie Psychisch-Gerichtliche Med,* **64,** 146-148.

Araque, A., Parpura, V., Sanzgiri, R. P. and Haydon, P. G. (1999) Tripartite synapses: glia, the unacknowledged partner. *Trends in neurosciences,* **22,** 208-215.

Bai, X. C., Yan, C., Yang, G., Lu, P., Ma, D., Sun, L., Zhou, R., Scheres, S. H. and Shi, Y. (2015) An atomic structure of human gamma-secretase. *Nature,* **525,** 212-217.

Bal-Price, A., Matthias, A. and Brown, G. C. (2002) Stimulation of the NADPH oxidase in activated rat microglia removes nitric oxide but induces peroxynitrite production. *J Neurochem,* **80,** 73-80.

Basun, H., Bogdanovic, N., Ingelsson, M. et al. (2008) Clinical and neuropathological features of the arctic APP gene mutation causing early-onset Alzheimer disease. *Archives of neurology,* **65,** 499-505.

Bateman, R. J., Aisen, P. S., De Strooper, B. et al. (2011) Autosomal-dominant Alzheimer's disease: a review and proposal for the prevention of Alzheimer's disease. *Alzheimer's research & therapy,* **3,** 1.

Bateman, R. J., Xiong, C., Benzinger, T. L. et al. (2012) Clinical and biomarker changes in dominantly inherited Alzheimer's disease. *The New England journal of medicine,* **367,** 795-804.

Benilova, I., Gallardo, R., Ungureanu, A. A. et al. (2014) The Alzheimer disease protective mutation A2T modulates kinetic and thermodynamic properties of amyloid-beta (Abeta) aggregation. *J Biol Chem,* **289,** 30977-30989.

Benilova, I., Karran, E. and De Strooper, B. (2012) The toxic Abeta oligomer and Alzheimer's disease: an emperor in need of clothes. *Nature neuroscience,* **15,** 349-357.

Bentahir, M., Nyabi, O., Verhamme, J., Tolia, A., Horre, K., Wiltfang, J., Esselmann, H. and De Strooper, B. (2006) Presenilin clinical mutations can affect gamma-secretase activity by different mechanisms. *J Neurochem,* **96,** 732-742.

Berezovska, O., Lleo, A., Herl, L. D., Frosch, M. P., Stern, E. A., Bacskai, B. J. and Hyman, B. T. (2005) Familial Alzheimer's disease presenilin 1 mutations cause alterations in the conformation of presenilin and interactions with amyloid precursor protein. *J Neurosci,* **25,** 3009-3017.

Bergman, A., Religa, D., Karlstrom, H., Laudon, H., Winblad, B., Lannfelt, L., Lundkvist, J. and Naslund, J. (2003) APP intracellular domain formation and unaltered signaling in the presence of familial Alzheimer's disease mutations. *Experimental cell research,* **287,** 1-9.

Bock, C., Kiskinis, E., Verstappen, G. et al. (2011) Reference Maps of human ES and iPS cell variation enable high-throughput characterization of pluripotent cell lines. *Cell,* **144,** 439-452.

Borchelt, D. R., Thinakaran, G., Eckman, C. B. et al. (1996) Familial Alzheimer's disease-linked presenilin 1 variants elevate Abeta1-42/1-40 ratio in vitro and in vivo. *Neuron,* **17,** 1005-1013.

Braak, H. and Del Tredici, K. (2011) The pathological process underlying Alzheimer's disease in individuals under thirty. *Acta neuropathologica,* **121,** 171-181.

Brunkan, A. L., Martinez, M., Walker, E. S. and Goate, A. M. (2005) Presenilin endoproteolysis is an intramolecular cleavage. *Molecular and cellular neurosciences,* **29,** 65-73.

Bucur, C. B. and Schlenoff, J. B. (2006) Electrogenerated chemiluminescence in polyelectrolyte multilayers: efficiency and mechanism. *Anal Chem,* **78,** 2360-2365.

Cacquevel, M., Aeschbach, L., Houacine, J. and Fraering, P. C. (2012) Alzheimer's Disease-Linked Mutations in Presenilin-1 Result in a Drastic Loss of Activity in Purified gamma-Secretase Complexes. *PloS one,* **7,** e35133.

Cai, X. D., Golde, T. E. and Younkin, S. G. (1993) Release of excess amyloid beta protein from a mutant amyloid beta protein precursor. *Science,* **259,** 514-516.

Chabrier, M. A., Blurton-Jones, M., Agazaryan, A. A., Nerhus, J. L., Martinez-Coria, H. and LaFerla, F. M. (2012) Soluble abeta promotes wild-type tau pathology in vivo. *J Neurosci,* **32,** 17345-17350.

Chan, S. L., Mayne, M., Holden, C. P., Geiger, J. D. and Mattson, M. P. (2000) Presenilin-1 mutations increase levels of ryanodine receptors and calcium release in PC12 cells and cortical neurons. *J Biol Chem,* **275,** 18195-18200.

Chapman, P. F., White, G. L., Jones, M. W. et al. (1999) Impaired synaptic plasticity and learning in aged amyloid precursor protein transgenic mice. *Nature neuroscience,* **2,** 271-276.

Chavez-Gutierrez, L., Bammens, L., Benilova, I. et al. (2012) The mechanism of gamma-Secretase dysfunction in familial Alzheimer disease. *EMBO J,* **31,** 2261-2274.

Chen, F., Gu, Y., Hasegawa, H., Ruan, X., Arawaka, S., Fraser, P., Westaway, D., Mount, H. and St George-Hyslop, P. (2002) Presenilin 1 mutations activate gamma 42-secretase but reciprocally inhibit epsilon-secretase cleavage of amyloid precursor protein (APP) and S3-cleavage of notch. *J Biol Chem,* **277,** 36521-36526.

Choi, S. H., Kim, Y. H., D'Avanzo, C., Aronson, J., Tanzi, R. E. and Kim, D. Y. (2015) Recapitulating amyloid beta and tau pathology in human neural cell culture models: clinical implications. *US neurology,* **11,** 102-105.

Choi, S. H., Kim, Y. H., Hebisch, M. et al. (2014) A three-dimensional human neural cell culture model of Alzheimer's disease. *Nature,* **515,** 274-278.

Citron, M., Oltersdorf, T., Haass, C., McConlogue, L., Hung, A. Y., Seubert, P., Vigo-Pelfrey, C., Lieberburg, I. and Selkoe, D. J. (1992) Mutation of the beta-amyloid precursor protein in familial Alzheimer's disease increases beta-protein production. *Nature,* **360,** 672-674.

Citron, M., Vigo-Pelfrey, C., Teplow, D. B. et al. (1994) Excessive production of amyloid beta-protein by peripheral cells of symptomatic and presymptomatic patients carrying the Swedish familial Alzheimer disease mutation. *Proc Natl Acad Sci U S A,* **91,** 11993-11997.

Citron, M., Westaway, D., Xia, W. et al. (1997) Mutant presenilins of Alzheimer's disease increase production of 42-residue amyloid beta-protein in both transfected cells and transgenic mice. *Nat Med,* **3,** 67-72.

Coburger, I., Hoefgen, S. and Than, M. E. (2014) The structural biology of the amyloid precursor protein APP - a complex puzzle reveals its multi-domain architecture. *Biological chemistry,* **395,** 485-498.

Coen, K., Flannagan, R. S., Baron, S. et al. (2012) Lysosomal calcium homeostasis defects, not proton pump defects, cause endo-lysosomal dysfunction in PSEN-deficient cells. *J Cell Biol,* **198,** 23-35.

Conti, L., Pollard, S. M., Gorba, T. et al. (2005) Niche-independent symmetrical self-renewal of a mammalian tissue stem cell. *PLoS biology,* **3,** e283.

Corder, E. H., Saunders, A. M., Risch, N. J. et al. (1994) Protective effect of apolipoprotein E type 2 allele for late onset Alzheimer disease. *Nature genetics,* **7,** 180-184.

Crump, C. J., Johnson, D. S. and Li, Y. M. (2013) Development and mechanism of gamma-secretase modulators for Alzheimer's disease. *Biochemistry,* **52,** 3197-3216.

Czirr, E., Leuchtenberger, S., Dorner-Ciossek, C., Schneider, A., Jucker, M., Koo, E. H., Pietrzik, C. U., Baumann, K. and Weggen, S. (2007) Insensitivity to Abeta42-lowering nonsteroidal anti-inflammatory drugs and gamma-secretase inhibitors is common among aggressive presenilin-1 mutations. *J Biol Chem,* **282,** 24504-24513.

Dawson, G. R., Seabrook, G. R., Zheng, H. et al. (1999) Age-related cognitive deficits, impaired long-term potentiation and reduction in synaptic marker density in mice lacking the beta-amyloid precursor protein. *Neuroscience,* **90,** 1-13.

De Strooper, B. (2003) Aph-1, Pen-2, and Nicastrin with Presenilin generate an active gamma-Secretase complex. *Neuron,* **38,** 9-12.

De Strooper, B. (2007) Loss-of-function presenilin mutations in Alzheimer disease. Talking Point on the role of presenilin mutations in Alzheimer disease. *EMBO Rep,* **8,** 141-146.

De Strooper, B. and Annaert, W. (2000) Proteolytic processing and cell biological functions of the amyloid precursor protein. *J Cell Sci,* **113 (Pt 11),** 1857-1870.

De Strooper, B. and Annaert, W. (2010) Novel research horizons for presenilins and gamma-secretases in cell biology and disease. *Annu Rev Cell Dev Biol,* **26,** 235-260.

De Strooper, B., Iwatsubo, T. and Wolfe, M. S. (2012) Presenilins and gamma-Secretase: Structure, Function, and Role in Alzheimer Disease. *Cold Spring Harbor perspectives in medicine,* **2,** a006304.

De Strooper, B., Saftig, P., Craessaerts, K., Vanderstichele, H., Guhde, G., Annaert, W., Von Figura, K. and Van Leuven, F. (1998) Deficiency of presenilin-1 inhibits the normal cleavage of amyloid precursor protein. *Nature,* **391,** 387-390.

Deng, Y., Tarassishin, L., Kallhoff, V., Peethumnongsin, E., Wu, L., Li, Y. M. and Zheng, H. (2006) Deletion of presenilin 1 hydrophilic loop sequence leads to impaired gamma-secretase activity and exacerbated amyloid pathology. *J Neurosci,* **26,** 3845-3854.

Deyts, C., Thinakaran, G. and Parent, A. T. (2016) APP Receptor? To Be or Not To Be. *Trends in pharmacological sciences*.

Di Fede, G., Catania, M., Morbin, M. et al. (2009) A recessive mutation in the APP gene with dominant-negative effect on amyloidogenesis. *Science,* **323,** 1473-1477.

Dolmetsch, R. and Geschwind, D. H. (2011) The human brain in a dish: the promise of iPSC-derived neurons. *Cell,* **145,** 831-834.

Dries, D. R., Shah, S., Han, Y. H., Yu, C., Yu, S., Shearman, M. S. and Yu, G. (2009) Glu-333 of nicastrin directly participates in gamma-secretase activity. *J Biol Chem,* **284,** 29714-29724.

Duff, K., Eckman, C., Zehr, C. et al. (1996) Increased amyloid-beta42(43) in brains of mice expressing mutant presenilin 1. *Nature,* **383,** 710-713.

Duggan, S. P. and McCarthy, J. V. (2016) Beyond gamma-secretase activity: The multifunctional nature of presenilins in cell signalling pathways. *Cellular signalling,* **28,** 1-11.

Dulin, F., Leveille, F., Ortega, J. B., Mornon, J. P., Buisson, A., Callebaut, I. and Colloc'h, N. (2008) P3 peptide, a truncated form of A beta devoid of synaptotoxic effect, does not assemble into soluble oligomers. *FEBS Lett,* **582,** 1865-1870.

Ebke, A., Luebbers, T., Fukumori, A., Shirotani, K., Haass, C., Baumann, K. and Steiner, H. (2011) Novel gamma-secretase enzyme modulators directly target presenilin protein. *J Biol Chem,* **286,** 37181-37186.

Edbauer, D., Winkler, E., Haass, C. and Steiner, H. (2002) Presenilin and nicastrin regulate each other and determine amyloid beta-peptide production via complex formation. *Proc Natl Acad Sci U S A,* **99,** 8666-8671.

Edbauer, D., Winkler, E., Regula, J. T., Pesold, B., Steiner, H. and Haass, C. (2003) Reconstitution of gamma-secretase activity. *Nat Cell Biol,* **5,** 486-488.

El Khoury, J. B., Moore, K. J., Means, T. K., Leung, J., Terada, K., Toft, M., Freeman, M. W. and Luster, A. D. (2003) CD36 mediates the innate host response to beta-amyloid. *The Journal of experimental medicine,* **197,** 1657-1666.

Ellison, D., Love, S., Chimelli, L. M., Harding, B., Lowe, J. S. and Vinters, H. V. (2004) Neuropathology: A Reference Text of CNS Pathology. *Elsevier Limited,* **2nd edition**.

Esselens, C., Oorschot, V., Baert, V. et al. (2004) Presenilin 1 mediates the turnover of telencephalin in hippocampal neurons via an autophagic degradative pathway. *J Cell Biol,* **166,** 1041-1054.

Fagan, A. M., Roe, C. M., Xiong, C., Mintun, M. A., Morris, J. C. and Holtzman, D. M. (2007) Cerebrospinal fluid tau/beta-amyloid(42) ratio as a prediction of cognitive decline in nondemented older adults. *Archives of neurology,* **64,** 343-349.

Fagan, A. M., Xiong, C., Jasielec, M. S. et al. (2014) Longitudinal change in CSF biomarkers in autosomal-dominant Alzheimer's disease. *Science translational medicine,* **6,** 226ra230.

Farrer, L. A., Cupples, L. A., Haines, J. L. et al. (1997) Effects of age, sex, and ethnicity on the association between apolipoprotein E genotype and Alzheimer disease. A meta-analysis. APOE and Alzheimer Disease Meta Analysis Consortium. *Jama,* **278,** 1349-1356.

Fernandez, M. A., Klutkowski, J. A., Freret, T. and Wolfe, M. S. (2014) Alzheimer presenilin-1 mutations dramatically reduce trimming of long amyloid beta-peptides (Abeta) by gamma-secretase to increase 42-to-40-residue Abeta. *J Biol Chem,* **289,** 31043-31052.

Flood, D. G., Reaume, A. G., Dorfman, K. S. et al. (2002) FAD mutant PS-1 gene-targeted mice: increased A beta 42 and A beta deposition without APP overproduction. *Neurobiology of aging,* **23,** 335-348.

Fluhrer, R., Fukumori, A., Martin, L. et al. (2008) Intramembrane proteolysis of GXGD-type aspartyl proteases is slowed by a familial Alzheimer disease-like mutation. *J Biol Chem,* **283,** 30121-30128.

Forloni, G., Demicheli, F., Giorgi, S., Bendotti, C. and Angeretti, N. (1992) Expression of amyloid precursor protein mRNAs in endothelial, neuronal and glial cells: modulation by interleukin-1. *Brain research. Molecular brain research,* **16,** 128-134.

Fox, N. C., Warrington, E. K., Freeborough, P. A., Hartikainen, P., Kennedy, A. M., Stevens, J. M. and Rossor, M. N. (1996) Presymptomatic hippocampal atrophy in Alzheimer's disease. A longitudinal MRI study. *Brain : a journal of neurology,* **119 (Pt 6),** 2001-2007.

Fox, N. C., Warrington, E. K., Seiffer, A. L., Agnew, S. K. and Rossor, M. N. (1998) Presymptomatic cognitive deficits in individuals at risk of familial Alzheimer's disease. A longitudinal prospective study. *Brain : a journal of neurology,* **121 (Pt 9),** 1631-1639.

Fraering, P. C., Ye, W., Strub, J. M. et al. (2004) Purification and characterization of the human gamma-secretase complex. *Biochemistry,* **43,** 9774-9789.

Francis, R., McGrath, G., Zhang, J. et al. (2002) aph-1 and pen-2 are required for Notch pathway signaling, gamma-secretase cleavage of betaAPP, and presenilin protein accumulation. *Dev Cell,* **3,** 85-97.

Funamoto, S., Morishima-Kawashima, M., Tanimura, Y., Hirotani, N., Saido, T. C. and Ihara, Y. (2004) Truncated carboxyl-terminal fragments of beta-amyloid precursor protein are processed to amyloid beta-proteins 40 and 42. *Biochemistry,* **43,** 13532-13540.

Giaccone, G., Morbin, M., Moda, F. et al. (2010) Neuropathology of the recessive A673V APP mutation: Alzheimer disease with distinctive features. *Acta neuropathologica,* **120,** 803-812.

Goate, A., Chartier-Harlin, M. C., Mullan, M. et al. (1991) Segregation of a missense mutation in the amyloid precursor protein gene with familial Alzheimer's disease. *Nature,* **349,** 704-706.

Goedert, M. and Jakes, R. (2005) Mutations causing neurodegenerative tauopathies. *Biochimica et biophysica acta,* **1739,** 240-250.

Gotz, J., Chen, F., van Dorpe, J. and Nitsch, R. M. (2001) Formation of neurofibrillary tangles in P301l tau transgenic mice induced by Abeta 42 fibrils. *Science,* **293,** 1491-1495.

Grabowski, T. J., Cho, H. S., Vonsattel, J. P., Rebeck, G. W. and Greenberg, S. M. (2001) Novel amyloid precursor protein mutation in an Iowa family with dementia and severe cerebral amyloid angiopathy. *Ann Neurol,* **49,** 697-705.

Gravina, S. A., Ho, L., Eckman, C. B., Long, K. E., Otvos, L., Jr., Younkin, L. H., Suzuki, N. and Younkin, S. G. (1995) Amyloid beta protein (A beta) in Alzheimer's disease brain. Biochemical and immunocytochemical analysis with antibodies specific for forms ending at A beta 40 or A beta 42(43). *J Biol Chem,* **270,** 7013-7016.

Green, K. N. and LaFerla, F. M. (2008) Linking calcium to Abeta and Alzheimer's disease. *Neuron,* **59,** 190-194.

Gregory, G. C., Macdonald, V., Schofield, P. R., Kril, J. J. and Halliday, G. M. (2006) Differences in regional brain atrophy in genetic forms of Alzheimer's disease. *Neurobiology of aging,* **27,** 387-393.

Grimmer, T., Riemenschneider, M., Forstl, H. et al. (2009) Beta amyloid in Alzheimer's disease: increased deposition in brain is reflected in reduced concentration in cerebrospinal fluid. *Biological psychiatry,* **65,** 927-934.

Grundke-Iqbal, I., Iqbal, K., Tung, Y. C., Quinlan, M., Wisniewski, H. M. and Binder, L. I. (1986) Abnormal phosphorylation of the microtubule-associated protein tau (tau) in Alzheimer cytoskeletal pathology. *Proc Natl Acad Sci U S A,* **83,** 4913-4917.

Gu, Y., Misonou, H., Sato, T., Dohmae, N., Takio, K. and Ihara, Y. (2001) Distinct intramembrane cleavage of the beta-amyloid precursor protein family resembling gamma-secretase-like cleavage of Notch. *J Biol Chem,* **276,** 35235-35238.

Guo, Q., Fu, W., Sopher, B. L., Miller, M. W., Ware, C. B., Martin, G. M. and Mattson, M. P. (1999) Increased vulnerability of hippocampal neurons to excitotoxic necrosis in presenilin-1 mutant knock-in mice. *Nat Med,* **5,** 101-106.

Haapasalo, A. and Kovacs, D. M. (2011) The many substrates of presenilin/gamma-secretase. *Journal of Alzheimer's disease : JAD,* **25,** 3-28.

Haass, C. (1997) Presenilins: genes for life and death. *Neuron,* **18,** 687-690.
Haass, C. (2004) Take five--BACE and the gamma-secretase quartet conduct Alzheimer's amyloid beta-peptide generation. *EMBO J,* **23,** 483-488.
Haass, C. and Selkoe, D. J. (2007) Soluble protein oligomers in neurodegeneration: lessons from the Alzheimer's amyloid beta-peptide. *Nat Rev Mol Cell Biol,* **8,** 101-112.
Haass, C. and Steiner, H. (2002) Alzheimer disease gamma-secretase: a complex story of GxGD-type presenilin proteases. *Trends Cell Biol,* **12,** 556-562.
Hahn, S., Bruning, T., Ness, J. et al. (2011) Presenilin-1 but not amyloid precursor protein mutations present in mouse models of Alzheimer's disease attenuate the response of cultured cells to gamma-secretase modulators regardless of their potency and structure. *J Neurochem,* **116,** 385-395.
Hardy, J. and Selkoe, D. J. (2002) The amyloid hypothesis of Alzheimer's disease: progress and problems on the road to therapeutics. *Science,* **297,** 353-356.
Hardy, J. A. and Higgins, G. A. (1992) Alzheimer's disease: the amyloid cascade hypothesis. *Science,* **256,** 184-185.
Hayrapetyan, V., Rybalchenko, V., Rybalchenko, N. and Koulen, P. (2008) The N-terminus of presenilin-2 increases single channel activity of brain ryanodine receptors through direct protein-protein interaction. *Cell calcium,* **44,** 507-518.
Hebert, L. E., Weuve, J., Scherr, P. A. and Evans, D. A. (2013) Alzheimer disease in the United States (2010-2050) estimated using the 2010 census. *Neurology,* **80,** 1778-1783.
Hecimovic, S., Wang, J., Dolios, G., Martinez, M., Wang, R. and Goate, A. M. (2004) Mutations in APP have independent effects on Abeta and CTFgamma generation. *Neurobiol Dis,* **17,** 205-218.
Heilig, E. A., Gutti, U., Tai, T., Shen, J. and Kelleher, R. J., 3rd (2013) Trans-dominant negative effects of pathogenic PSEN1 mutations on gamma-secretase activity and Abeta production. *J Neurosci,* **33,** 11606-11617.
Heilig, E. A., Xia, W., Shen, J. and Kelleher, R. J., 3rd (2010) A presenilin-1 mutation identified in familial Alzheimer disease with cotton wool plaques causes a nearly complete loss of gamma-secretase activity. *J Biol Chem,* **285,** 22350-22359.
Hendriks, L., Thinakaran, G., Harris, C. L., De Jonghe, C., Martin, J. J., Sisodia, S. S. and Van Broeckhoven, C. (1997) Processing of presenilin 1 in brains of patients with Alzheimer's disease and controls. *Neuroreport,* **8,** 1717-1721.
Heneka, M. T., Carson, M. J., El Khoury, J. et al. (2015) Neuroinflammation in Alzheimer's disease. *Lancet neurology,* **14,** 388-405.
Heneka, M. T., Sastre, M., Dumitrescu-Ozimek, L., Dewachter, I., Walter, J., Klockgether, T. and Van Leuven, F. (2005) Focal glial activation coincides with increased BACE1 activation and precedes amyloid plaque deposition in APP[V717I] transgenic mice. *Journal of neuroinflammation,* **2,** 22.
Herreman, A., Serneels, L., Annaert, W., Collen, D., Schoonjans, L. and De Strooper, B. (2000) Total inactivation of gamma-secretase activity in presenilin-deficient embryonic stem cells. *Nat Cell Biol,* **2,** 461-462.
Herrup, K. (2015) The case for rejecting the amyloid cascade hypothesis. *Nature neuroscience,* **18,** 794-799.
Herrup, K., Carrillo, M. C., Schenk, D. et al. (2013) Beyond amyloid: getting real about nonamyloid targets in Alzheimer's disease. *Alzheimer's & dementia : the journal of the Alzheimer's Association,* **9,** 452-458 e451.
Herskowitz, I. (1987) Functional inactivation of genes by dominant negative mutations. *Nature,* **329,** 219-222.

Hieke, M., Ness, J., Steri, R., Greiner, C., Werz, O., Schubert-Zsilavecz, M., Weggen, S. and Zettl, H. (2011) SAR studies of acidic dual gamma-secretase/PPARgamma modulators. *Bioorg Med Chem,* **19,** 5372-5382.

Houlden, H., Crook, R., Dolan, R. J., McLaughlin, J., Revesz, T. and Hardy, J. (2001) A novel presenilin mutation (M233V) causing very early onset Alzheimer's disease with Lewy bodies. *Neuroscience letters,* **313,** 93-95.

Hsia, A. Y., Masliah, E., McConlogue, L. et al. (1999) Plaque-independent disruption of neural circuits in Alzheimer's disease mouse models. *Proc Natl Acad Sci U S A,* **96,** 3228-3233.

Hsu, P. D., Lander, E. S. and Zhang, F. (2014) Development and applications of CRISPR-Cas9 for genome engineering. *Cell,* **157,** 1262-1278.

Hu, Y. and Fortini, M. E. (2003) Different cofactor activities in gamma-secretase assembly: evidence for a nicastrin-Aph-1 subcomplex. *J Cell Biol,* **161,** 685-690.

Hung, A. Y. and Selkoe, D. J. (1994) Selective ectodomain phosphorylation and regulated cleavage of beta-amyloid precursor protein. *EMBO J,* **13,** 534-542.

Iqbal, K., Grundke-Iqbal, I., Zaidi, T., Merz, P. A., Wen, G. Y., Shaikh, S. S., Wisniewski, H. M., Alafuzoff, I. and Winblad, B. (1986) Defective brain microtubule assembly in Alzheimer's disease. *Lancet,* **2,** 421-426.

Iqbal, K., Liu, F., Gong, C. X., Alonso Adel, C. and Grundke-Iqbal, I. (2009) Mechanisms of tau-induced neurodegeneration. *Acta neuropathologica,* **118,** 53-69.

Iwatsubo, T., Odaka, A., Suzuki, N., Mizusawa, H., Nukina, N. and Ihara, Y. (1994) Visualization of A beta 42(43) and A beta 40 in senile plaques with end-specific A beta monoclonals: evidence that an initially deposited species is A beta 42(43). *Neuron,* **13,** 45-53.

Jarrett, J. T., Berger, E. P. and Lansbury, P. T., Jr. (1993) The carboxy terminus of the beta amyloid protein is critical for the seeding of amyloid formation: implications for the pathogenesis of Alzheimer's disease. *Biochemistry,* **32,** 4693-4697.

Jarrett, J. T. and Lansbury, P. T., Jr. (1993) Seeding "one-dimensional crystallization" of amyloid: a pathogenic mechanism in Alzheimer's disease and scrapie? *Cell,* **73,** 1055-1058.

Jefferson, T., Causevic, M., auf dem Keller, U. et al. (2011) Metalloprotease meprin beta generates nontoxic N-terminal amyloid precursor protein fragments in vivo. *J Biol Chem,* **286,** 27741-27750.

Jekabsone, A., Mander, P. K., Tickler, A., Sharpe, M. and Brown, G. C. (2006) Fibrillar beta-amyloid peptide Abeta1-40 activates microglial proliferation via stimulating TNF-alpha release and H2O2 derived from NADPH oxidase: a cell culture study. *Journal of neuroinflammation,* **3,** 24.

Ji, K., Akgul, G., Wollmuth, L. P. and Tsirka, S. E. (2013) Microglia actively regulate the number of functional synapses. *PloS one,* **8,** e56293.

Jiang, Q., Lee, C. Y., Mandrekar, S. et al. (2008) ApoE promotes the proteolytic degradation of Abeta. *Neuron,* **58,** 681-693.

Jonsson, T., Atwal, J. K., Steinberg, S. et al. (2012) A mutation in APP protects against Alzheimer's disease and age-related cognitive decline. *Nature,* **488,** 96-99.

Jorissen, E., Prox, J., Bernreuther, C. et al. (2010) The disintegrin/metalloproteinase ADAM10 is essential for the establishment of the brain cortex. *J Neurosci,* **30,** 4833-4844.

Juillerat, A., Dubois, G., Valton, J. et al. (2014) Comprehensive analysis of the specificity of transcription activator-like effector nucleases. *Nucleic Acids Res,* **42,** 5390-5402.

Kaether, C., Schmitt, S., Willem, M. and Haass, C. (2006) Amyloid precursor protein and Notch intracellular domains are generated after transport of their precursors to the cell surface. *Traffic,* **7,** 408-415.

Kakuda, N., Funamoto, S., Yagishita, S., Takami, M., Osawa, S., Dohmae, N. and Ihara, Y. (2006) Equimolar production of amyloid beta-protein and amyloid precursor protein intracellular domain from beta-carboxyl-terminal fragment by gamma-secretase. *J Biol Chem,* **281,** 14776-14786.

Kaneko, H., Kakita, A., Kasuga, K. et al. (2007) Enhanced accumulation of phosphorylated alpha-synuclein and elevated beta-amyloid 42/40 ratio caused by expression of the presenilin-1 deltaT440 mutant associated with familial Lewy body disease and variant Alzheimer's disease. *J Neurosci,* **27,** 13092-13097.

Kang, J., Lemaire, H. G., Unterbeck, A., Salbaum, J. M., Masters, C. L., Grzeschik, K. H., Multhaup, G., Beyreuther, K. and Muller-Hill, B. (1987) The precursor of Alzheimer's disease amyloid A4 protein resembles a cell-surface receptor. *Nature,* **325,** 733-736.

Karran, E., Mercken, M. and De Strooper, B. (2011) The amyloid cascade hypothesis for Alzheimer's disease: an appraisal for the development of therapeutics. *Nature reviews. Drug discovery,* **10,** 698-712.

Kim, J., Basak, J. M. and Holtzman, D. M. (2009) The role of apolipoprotein E in Alzheimer's disease. *Neuron,* **63,** 287-303.

Kim, Y. H., Choi, S. H., D'Avanzo, C. et al. (2015) A 3D human neural cell culture system for modeling Alzheimer's disease. *Nature protocols,* **10,** 985-1006.

Kimberly, W. T., Esler, W. P., Ye, W., Ostaszewski, B. L., Gao, J., Diehl, T., Selkoe, D. J. and Wolfe, M. S. (2003a) Notch and the amyloid precursor protein are cleaved by similar gamma-secretase(s). *Biochemistry,* **42,** 137-144.

Kimberly, W. T., LaVoie, M. J., Ostaszewski, B. L., Ye, W., Wolfe, M. S. and Selkoe, D. J. (2003b) Gamma-secretase is a membrane protein complex comprised of presenilin, nicastrin, Aph-1, and Pen-2. *Proc Natl Acad Sci U S A,* **100,** 6382-6387.

Kitaguchi, N., Takahashi, Y., Tokushima, Y., Shiojiri, S. and Ito, H. (1988) Novel precursor of Alzheimer's disease amyloid protein shows protease inhibitory activity. *Nature,* **331,** 530-532.

Klevanski, M., Saar, M., Baumkotter, F., Weyer, S. W., Kins, S. and Muller, U. C. (2014) Differential role of APP and APLPs for neuromuscular synaptic morphology and function. *Molecular and cellular neurosciences,* **61,** 201-210.

Klionsky, D. J. (2007) Autophagy: from phenomenology to molecular understanding in less than a decade. *Nat Rev Mol Cell Biol,* **8,** 931-937.

Klyubin, I., Walsh, D. M., Lemere, C. A. et al. (2005) Amyloid beta protein immunotherapy neutralizes Abeta oligomers that disrupt synaptic plasticity in vivo. *Nat Med,* **11,** 556-561.

Koch, P., Tamboli, I. Y., Mertens, J. et al. (2012) Presenilin-1 L166P mutant human pluripotent stem cell-derived neurons exhibit partial loss of gamma-secretase activity in endogenous amyloid-beta generation. *The American journal of pathology,* **180,** 2404-2416.

Konig, G., Monning, U., Czech, C., Prior, R., Banati, R., Schreiter-Gasser, U., Bauer, J., Masters, C. L. and Beyreuther, K. (1992) Identification and differential expression of a novel alternative splice isoform of the beta A4 amyloid precursor protein (APP) mRNA in leukocytes and brain microglial cells. *J Biol Chem,* **267,** 10804-10809.

Kretner, B., Fukumori, A., Gutsmiedl, A., Page, R. M., Luebbers, T., Galley, G., Baumann, K., Haass, C. and Steiner, H. (2011) Attenuated Abeta42 responses to low potency

gamma-secretase modulators can be overcome for many pathogenic presenilin mutants by second-generation compounds. *J Biol Chem,* **286,** 15240-15251.

Kretner, B., Trambauer, J., Fukumori, A. et al. (2016) Generation and deposition of Abeta43 by the virtually inactive presenilin-1 L435F mutant contradicts the presenilin loss-of-function hypothesis of Alzheimer's disease. *EMBO molecular medicine*.

Kuhn, P. H., Wang, H., Dislich, B., Colombo, A., Zeitschel, U., Ellwart, J. W., Kremmer, E., Rossner, S. and Lichtenthaler, S. F. (2010) ADAM10 is the physiologically relevant, constitutive alpha-secretase of the amyloid precursor protein in primary neurons. *EMBO J,* **29,** 3020-3032.

Kumar-Singh, S., Cras, P., Wang, R. et al. (2002) Dense-core senile plaques in the Flemish variant of Alzheimer's disease are vasocentric. *The American journal of pathology,* **161,** 507-520.

Kumar-Singh, S., Theuns, J., Van Broeck, B. et al. (2006) Mean age-of-onset of familial alzheimer disease caused by presenilin mutations correlates with both increased Abeta42 and decreased Abeta40. *Human mutation,* **27,** 686-695.

Kuperstein, I., Broersen, K., Benilova, I. et al. (2010) Neurotoxicity of Alzheimer's disease Abeta peptides is induced by small changes in the Abeta42 to Abeta40 ratio. *EMBO J,* **29,** 3408-3420.

LaFerla, F. M. and Green, K. N. (2012) Animal models of Alzheimer disease. *Cold Spring Harbor perspectives in medicine,* **2**.

LaVoie, M. J., Fraering, P. C., Ostaszewski, B. L., Ye, W., Kimberly, W. T., Wolfe, M. S. and Selkoe, D. J. (2003) Assembly of the gamma-secretase complex involves early formation of an intermediate subcomplex of Aph-1 and nicastrin. *J Biol Chem,* **278,** 37213-37222.

Lee, J. H., Yu, W. H., Kumar, A. et al. (2010) Lysosomal proteolysis and autophagy require presenilin 1 and are disrupted by Alzheimer-related PS1 mutations. *Cell,* **141,** 1146-1158.

Leem, J. Y., Vijayan, S., Han, P., Cai, D., Machura, M., Lopes, K. O., Veselits, M. L., Xu, H. and Thinakaran, G. (2002) Presenilin 1 is required for maturation and cell surface accumulation of nicastrin. *J Biol Chem,* **277,** 19236-19240.

Leverenz, J. B. and Raskind, M. A. (1998) Early amyloid deposition in the medial temporal lobe of young Down syndrome patients: a regional quantitative analysis. *Experimental neurology,* **150,** 296-304.

Levy-Lahad, E., Wasco, W., Poorkaj, P. et al. (1995) Candidate gene for the chromosome 1 familial Alzheimer's disease locus. *Science,* **269,** 973-977.

Lewis, J., Dickson, D. W., Lin, W. L. et al. (2001) Enhanced neurofibrillary degeneration in transgenic mice expressing mutant tau and APP. *Science,* **293,** 1487-1491.

Li, B., Chohan, M. O., Grundke-Iqbal, I. and Iqbal, K. (2007) Disruption of microtubule network by Alzheimer abnormally hyperphosphorylated tau. *Acta neuropathologica,* **113,** 501-511.

Li, N., Liu, K., Qiu, Y., Ren, Z., Dai, R., Deng, Y. and Qing, H. (2016) Effect of Presenilin Mutations on APP Cleavage; Insights into the Pathogenesis of FAD. *Frontiers in aging neuroscience,* **8,** 51.

Li, Y. M., Lai, M. T., Xu, M. et al. (2000) Presenilin 1 is linked with gamma-secretase activity in the detergent solubilized state. *Proc Natl Acad Sci U S A,* **97,** 6138-6143.

Lichtenthaler, S. F., Haass, C. and Steiner, H. (2011) Regulated intramembrane proteolysis--lessons from amyloid precursor protein processing. *J Neurochem,* **117,** 779-796.

Lim, Y. Y., Pietrzak, R. H., Ellis, K. A. et al. (2013) Rapid decline in episodic memory in healthy older adults with high amyloid-beta. *Journal of Alzheimer's disease : JAD,* **33,** 675-679.

Lin, X., Koelsch, G., Wu, S., Downs, D., Dashti, A. and Tang, J. (2000) Human aspartic protease memapsin 2 cleaves the beta-secretase site of beta-amyloid precursor protein. *Proc Natl Acad Sci U S A,* **97,** 1456-1460.

Liu, J., Sato, C., Cerletti, M. and Wagers, A. (2010) Notch signaling in the regulation of stem cell self-renewal and differentiation. *Current topics in developmental biology,* **92,** 367-409.

Lorenzo, A., Yuan, M., Zhang, Z. et al. (2000) Amyloid beta interacts with the amyloid precursor protein: a potential toxic mechanism in Alzheimer's disease. *Nature neuroscience,* **3,** 460-464.

Loy, C. T., Schofield, P. R., Turner, A. M. and Kwok, J. B. (2014) Genetics of dementia. *Lancet,* **383,** 828-840.

Lu, D. C., Shaked, G. M., Masliah, E., Bredesen, D. E. and Koo, E. H. (2003) Amyloid beta protein toxicity mediated by the formation of amyloid-beta protein precursor complexes. *Ann Neurol,* **54,** 781-789.

Lu, P., Bai, X. C., Ma, D. et al. (2014) Three-dimensional structure of human gamma-secretase. *Nature,* **512,** 166-170.

Maeder, M. L., Thibodeau-Beganny, S., Osiak, A. et al. (2008) Rapid "open-source" engineering of customized zinc-finger nucleases for highly efficient gene modification. *Molecular cell,* **31,** 294-301.

Maloney, J. A., Bainbridge, T., Gustafson, A. et al. (2014) Molecular mechanisms of Alzheimer disease protection by the A673T allele of amyloid precursor protein. *J Biol Chem,* **289,** 30990-31000.

Mann, D. M., Iwatsubo, T., Ihara, Y. et al. (1996) Predominant deposition of amyloid-beta 42(43) in plaques in cases of Alzheimer's disease and hereditary cerebral hemorrhage associated with mutations in the amyloid precursor protein gene. *The American journal of pathology,* **148,** 1257-1266.

Mann, D. M., Pickering-Brown, S. M., Takeuchi, A. and Iwatsubo, T. (2001) Amyloid angiopathy and variability in amyloid beta deposition is determined by mutation position in presenilin-1-linked Alzheimer's disease. *The American journal of pathology,* **158,** 2165-2175.

Mattson, M. P. (1997) Cellular actions of beta-amyloid precursor protein and its soluble and fibrillogenic derivatives. *Physiol Rev,* **77,** 1081-1132.

Mattson, M. P. (2010) ER calcium and Alzheimer's disease: in a state of flux. *Science signaling,* **3,** pe10.

Mayeux, R., Honig, L. S., Tang, M. X., Manly, J., Stern, Y., Schupf, N. and Mehta, P. D. (2003) Plasma A[beta]40 and A[beta]42 and Alzheimer's disease: relation to age, mortality, and risk. *Neurology,* **61,** 1185-1190.

McGowan, E., Pickford, F., Kim, J. et al. (2005) Abeta42 is essential for parenchymal and vascular amyloid deposition in mice. *Neuron,* **47,** 191-199.

Meda, L., Cassatella, M. A., Szendrei, G. I., Otvos, L., Jr., Baron, P., Villalba, M., Ferrari, D. and Rossi, F. (1995) Activation of microglial cells by beta-amyloid protein and interferon-gamma. *Nature,* **374,** 647-650.

Miller, J. C., Tan, S. Y., Qiao, G. J. et al. (2011) A TALE nuclease architecture for efficient genome editing. *Nat Biotechnol,* **29,** 143-U149.

Mizushima, N. (2007) Autophagy: process and function. *Genes & development,* **21,** 2861-2873.

Moehlmann, T., Winkler, E., Xia, X. et al. (2002) Presenilin-1 mutations of leucine 166 equally affect the generation of the Notch and APP intracellular domains independent of their effect on Abeta 42 production. *Proc Natl Acad Sci U S A,* **99,** 8025-8030.

Mohamet, L., Miazga, N. J. and Ward, C. M. (2014) Familial Alzheimer's disease modelling using induced pluripotent stem cell technology. *World journal of stem cells,* **6,** 239-247.

Mullan, M., Crawford, F., Axelman, K., Houlden, H., Lilius, L., Winblad, B. and Lannfelt, L. (1992) A pathogenic mutation for probable Alzheimer's disease in the APP gene at the N-terminus of beta-amyloid. *Nature genetics,* **1,** 345-347.

Muller-Schiffmann, A., Herring, A., Abdel-Hafiz, L. et al. (2016) Amyloid-beta dimers in the absence of plaque pathology impair learning and synaptic plasticity. *Brain : a journal of neurology,* **139,** 509-525.

Muller, U., Cristina, N., Li, Z. W., Wolfer, D. P., Lipp, H. P., Rulicke, T., Brandner, S., Aguzzi, A. and Weissmann, C. (1994) Behavioral and anatomical deficits in mice homozygous for a modified beta-amyloid precursor protein gene. *Cell,* **79,** 755-765.

Mungenast, A. E., Siegert, S. and Tsai, L. H. (2015) Modeling Alzheimer's disease with human induced pluripotent stem (iPS) cells. *Molecular and cellular neurosciences*.

Muratore, C. R., Rice, H. C., Srikanth, P., Callahan, D. G., Shin, T., Benjamin, L. N., Walsh, D. M., Selkoe, D. J. and Young-Pearse, T. L. (2014) The familial Alzheimer's disease APPV717I mutation alters APP processing and Tau expression in iPSC-derived neurons. *Human molecular genetics,* **23,** 3523-3536.

Murayama, O., Tomita, T., Nihonmatsu, N., Murayama, M., Sun, X., Honda, T., Iwatsubo, T. and Takashima, A. (1999) Enhancement of amyloid beta 42 secretion by 28 different presenilin 1 mutations of familial Alzheimer's disease. *Neuroscience letters,* **265,** 61-63.

Murrell, J., Farlow, M., Ghetti, B. and Benson, M. D. (1991) A mutation in the amyloid precursor protein associated with hereditary Alzheimer's disease. *Science,* **254,** 97-99.

Nakano, Y., Kondoh, G., Kudo, T., Imaizumi, K., Kato, M., Miyazaki, J. I., Tohyama, M., Takeda, J. and Takeda, M. (1999) Accumulation of murine amyloidbeta42 in a gene-dosage-dependent manner in PS1 'knock-in' mice. *The European journal of neuroscience,* **11,** 2577-2581.

Nakaya, Y., Yamane, T., Shiraishi, H. et al. (2005) Random mutagenesis of presenilin-1 identifies novel mutants exclusively generating long amyloid beta-peptides. *J Biol Chem,* **280,** 19070-19077.

Naslund, J., Thyberg, J., Tjernberg, L. O. et al. (1995) Characterization of stable complexes involving apolipoprotein E and the amyloid beta peptide in Alzheimer's disease brain. *Neuron,* **15,** 219-228.

Neely, K. M., Green, K. N. and LaFerla, F. M. (2011) Presenilin is necessary for efficient proteolysis through the autophagy-lysosome system in a gamma-secretase-independent manner. *J Neurosci,* **31,** 2781-2791.

Nhan, H. S., Chiang, K. and Koo, E. H. (2015) The multifaceted nature of amyloid precursor protein and its proteolytic fragments: friends and foes. *Acta neuropathologica,* **129,** 1-19.

Nichols, J. and Ying, Q. L. (2006) Derivation and propagation of embryonic stem cells in serum- and feeder-free culture. *Methods Mol Biol,* **329,** 91-98.

Nyabi, O., Bentahir, M., Horre, K. et al. (2003) Presenilins mutated at Asp-257 or Asp-385 restore Pen-2 expression and Nicastrin glycosylation but remain catalytically inactive in the absence of wild type Presenilin. *J Biol Chem,* **278,** 43430-43436.

Oddo, S., Billings, L., Kesslak, J. P., Cribbs, D. H. and LaFerla, F. M. (2004) Abeta immunotherapy leads to clearance of early, but not late, hyperphosphorylated tau aggregates via the proteasome. *Neuron,* **43,** 321-332.

Oddo, S., Caccamo, A., Kitazawa, M., Tseng, B. P. and LaFerla, F. M. (2003) Amyloid deposition precedes tangle formation in a triple transgenic model of Alzheimer's disease. *Neurobiology of aging,* **24,** 1063-1070.

Ohsawa, I., Takamura, C. and Kohsaka, S. (1997) The amino-terminal region of amyloid precursor protein is responsible for neurite outgrowth in rat neocortical explant culture. *Biochem Biophys Res Commun,* **236,** 59-65.

Ohsawa, I., Takamura, C., Morimoto, T., Ishiguro, M. and Kohsaka, S. (1999) Amino-terminal region of secreted form of amyloid precursor protein stimulates proliferation of neural stem cells. *The European journal of neuroscience,* **11,** 1907-1913.

Okochi, M., Tagami, S., Yanagida, K., Takami, M., Kodama, T. S., Mori, K., Nakayama, T., Ihara, Y. and Takeda, M. (2013) gamma-secretase modulators and presenilin 1 mutants act differently on presenilin/gamma-secretase function to cleave Abeta42 and Abeta43. *Cell reports,* **3,** 42-51.

Osterwalder, M., Galli, A., Rosen, B., Skarnes, W. C., Zeller, R. and Lopez-Rios, J. (2010) Dual RMCE for efficient re-engineering of mouse mutant alleles. *Nature methods,* **7,** 893-895.

Ousson, S., Saric, A., Baguet, A., Losberger, C., Genoud, S., Vilbois, F., Permanne, B., Hussain, I. and Beher, D. (2013) Substrate determinants in the C99 juxtamembrane domains differentially affect gamma-secretase cleavage specificity and modulator pharmacology. *J Neurochem,* **125,** 610-619.

Page, R. M., Baumann, K., Tomioka, M. et al. (2008) Generation of Abeta38 and Abeta42 is independently and differentially affected by familial Alzheimer disease-associated presenilin mutations and gamma-secretase modulation. *J Biol Chem,* **283,** 677-683.

Palop, J. J. and Mucke, L. (2010) Amyloid-beta-induced neuronal dysfunction in Alzheimer's disease: from synapses toward neural networks. *Nature neuroscience,* **13,** 812-818.

Paquet, D., Kwart, D., Chen, A. et al. (2016) Efficient introduction of specific homozygous and heterozygous mutations using CRISPR/Cas9. *Nature,* **533,** 125-129.

Parks, A. L. and Curtis, D. (2007) Presenilin diversifies its portfolio. *Trends in genetics : TIG,* **23,** 140-150.

Patel, N. S., Paris, D., Mathura, V., Quadros, A. N., Crawford, F. C. and Mullan, M. J. (2005) Inflammatory cytokine levels correlate with amyloid load in transgenic mouse models of Alzheimer's disease. *Journal of neuroinflammation,* **2,** 9.

Peacock, M. L., Warren, J. T., Jr., Roses, A. D. and Fink, J. K. (1993) Novel polymorphism in the A4 region of the amyloid precursor protein gene in a patient without Alzheimer's disease. *Neurology,* **43,** 1254-1256.

Perez-Revuelta, B. I., Fukumori, A., Lammich, S., Yamasaki, A., Haass, C. and Steiner, H. (2010) Requirement for small side chain residues within the GxGD-motif of presenilin for gamma-secretase substrate cleavage. *J Neurochem,* **112,** 940-950.

Philipson, O., Lord, A., Gumucio, A., O'Callaghan, P., Lannfelt, L. and Nilsson, L. N. (2010) Animal models of amyloid-beta-related pathologies in Alzheimer's disease. *The FEBS journal,* **277,** 1389-1409.

Pollard, S. M., Benchoua, A. and Lowell, S. (2006a) Neural stem cells, neurons, and glia. *Methods in enzymology,* **418,** 151-169.

Pollard, S. M. and Conti, L. (2007) Investigating radial glia in vitro. *Progress in neurobiology,* **83,** 53-67.

Pollard, S. M., Conti, L., Sun, Y., Goffredo, D. and Smith, A. (2006b) Adherent neural stem (NS) cells from fetal and adult forebrain. *Cereb Cortex,* **16 Suppl 1,** i112-120.

Ponte, P., Gonzalez-DeWhitt, P., Schilling, J. et al. (1988) A new A4 amyloid mRNA contains a domain homologous to serine proteinase inhibitors. *Nature,* **331,** 525-527.

Potter, R., Patterson, B. W., Elbert, D. L. et al. (2013) Increased in vivo amyloid-beta42 production, exchange, and loss in presenilin mutation carriers. *Science translational medicine,* **5,** 189ra177.

Price, J. L., McKeel, D. W., Jr., Buckles, V. D. et al. (2009) Neuropathology of nondemented aging: presumptive evidence for preclinical Alzheimer disease. *Neurobiology of aging,* **30,** 1026-1036.

Prokop, S., Shirotani, K., Edbauer, D., Haass, C. and Steiner, H. (2004) Requirement of PEN-2 for stabilization of the presenilin N-/C-terminal fragment heterodimer within the gamma-secretase complex. *J Biol Chem,* **279,** 23255-23261.

Qi-Takahara, Y., Morishima-Kawashima, M., Tanimura, Y. et al. (2005) Longer forms of amyloid beta protein: implications for the mechanism of intramembrane cleavage by gamma-secretase. *J Neurosci,* **25,** 436-445.

Qi, Y., Morishima-Kawashima, M., Sato, T., Mitsumori, R. and Ihara, Y. (2003) Distinct mechanisms by mutant presenilin 1 and 2 leading to increased intracellular levels of amyloid beta-protein 42 in Chinese hamster ovary cells. *Biochemistry,* **42,** 1042-1052.

Qin, J. Y., Zhang, L., Clift, K. L., Hulur, I., Xiang, A. P., Ren, B. Z. and Lahn, B. T. (2010) Systematic comparison of constitutive promoters and the doxycycline-inducible promoter. *PloS one,* **5,** e10611.

Quintero-Monzon, O., Martin, M. M., Fernandez, M. A., Cappello, C. A., Krzysiak, A. J., Osenkowski, P. and Wolfe, M. S. (2011) Dissociation between the processivity and total activity of gamma-secretase: implications for the mechanism of Alzheimer's disease-causing presenilin mutations. *Biochemistry,* **50,** 9023-9035.

Ran, F. A., Hsu, P. D., Wright, J., Agarwala, V., Scott, D. A. and Zhang, F. (2013) Genome engineering using the CRISPR-Cas9 system. *Nature protocols,* **8,** 2281-2308.

Rapoport, M., Dawson, H. N., Binder, L. I., Vitek, M. P. and Ferreira, A. (2002) Tau is essential to beta -amyloid-induced neurotoxicity. *Proc Natl Acad Sci U S A,* **99,** 6364-6369.

Ratovitski, T., Slunt, H. H., Thinakaran, G., Price, D. L., Sisodia, S. S. and Borchelt, D. R. (1997) Endoproteolytic processing and stabilization of wild-type and mutant presenilin. *J Biol Chem,* **272,** 24536-24541.

Reinhard, C., Hebert, S. S. and De Strooper, B. (2005) The amyloid-beta precursor protein: integrating structure with biological function. *EMBO J,* **24,** 3996-4006.

Reitz, C. (2012) Alzheimer's disease and the amyloid cascade hypothesis: a critical review. *International journal of Alzheimer's disease,* **2012,** 369808.

Renzi, F., Zhang, X., Rice, W. J. et al. (2011) Structure of gamma-secretase and its trimeric pre-activation intermediate by single-particle electron microscopy. *J Biol Chem,* **286,** 21440-21449.

Repetto, E., Yoon, I. S., Zheng, H. and Kang, D. E. (2007) Presenilin 1 regulates epidermal growth factor receptor turnover and signaling in the endosomal-lysosomal pathway. *J Biol Chem,* **282,** 31504-31516.

Roberson, E. D., Scearce-Levie, K., Palop, J. J., Yan, F., Cheng, I. H., Wu, T., Gerstein, H., Yu, G. Q. and Mucke, L. (2007) Reducing endogenous tau ameliorates amyloid beta-induced deficits in an Alzheimer's disease mouse model. *Science,* **316,** 750-754.

Rogaev, E. I., Sherrington, R., Rogaeva, E. A. et al. (1995) Familial Alzheimer's disease in kindreds with missense mutations in a gene on chromosome 1 related to the Alzheimer's disease type 3 gene. *Nature,* **376,** 775-778.

Roses, A. D. (1996) Apolipoprotein E alleles as risk factors in Alzheimer's disease. *Annual review of medicine,* **47,** 387-400.

Rossor, M. N., Fox, N. C., Freeborough, P. A. and Harvey, R. J. (1996) Clinical features of sporadic and familial Alzheimer's disease. *Neurodegeneration : a journal for neurodegenerative disorders, neuroprotection, and neuroregeneration,* **5,** 393-397.

Rouhani, F., Kumasaka, N., de Brito, M. C., Bradley, A., Vallier, L. and Gaffney, D. (2014) Genetic background drives transcriptional variation in human induced pluripotent stem cells. *PLoS genetics,* **10,** e1004432.

Rubinsztein, D. C. (2006) The roles of intracellular protein-degradation pathways in neurodegeneration. *Nature,* **443,** 780-786.

Saito, T., Suemoto, T., Brouwers, N. et al. (2011) Potent amyloidogenicity and pathogenicity of Abeta43. *Nature neuroscience,* **14,** 1023-1032.

Sander, J. D. and Joung, J. K. (2014) CRISPR-Cas systems for editing, regulating and targeting genomes. *Nat Biotechnol,* **32,** 347-355.

Sannerud, R., Esselens, C., Ejsmont, P. et al. (2016) Restricted Location of PSEN2/gamma-Secretase Determines Substrate Specificity and Generates an Intracellular Abeta Pool. *Cell,* **166,** 193-208.

Sato, C., Morohashi, Y., Tomita, T. and Iwatsubo, T. (2006) Structure of the catalytic pore of gamma-secretase probed by the accessibility of substituted cysteines. *J Neurosci,* **26,** 12081-12088.

Sato, C., Takagi, S., Tomita, T. and Iwatsubo, T. (2008) The C-terminal PAL motif and transmembrane domain 9 of presenilin 1 are involved in the formation of the catalytic pore of the gamma-secretase. *J Neurosci,* **28,** 6264-6271.

Sato, T., Diehl, T. S., Narayanan, S., Funamoto, S., Ihara, Y., De Strooper, B., Steiner, H., Haass, C. and Wolfe, M. S. (2007) Active gamma-secretase complexes contain only one of each component. *J Biol Chem,* **282,** 33985-33993.

Sato, T., Dohmae, N., Qi, Y. et al. (2003) Potential link between amyloid beta-protein 42 and C-terminal fragment gamma 49-99 of beta-amyloid precursor protein. *J Biol Chem,* **278,** 24294-24301.

Saura, C. A., Tomita, T., Soriano, S., Takahashi, M., Leem, J. Y., Honda, T., Koo, E. H., Iwatsubo, T. and Thinakaran, G. (2000) The nonconserved hydrophilic loop domain of presenilin (PS) is not required for PS endoproteolysis or enhanced abeta 42 production mediated by familial early onset Alzheimer's disease-linked PS variants. *J Biol Chem,* **275,** 17136-17142.

Schellenberg, G. D. and Montine, T. J. (2012) The genetics and neuropathology of Alzheimer's disease. *Acta neuropathologica,* **124,** 305-323.

Scheuner, D., Eckman, C., Jensen, M. et al. (1996) Secreted amyloid beta-protein similar to that in the senile plaques of Alzheimer's disease is increased in vivo by the presenilin 1 and 2 and APP mutations linked to familial Alzheimer's disease. *Nat Med,* **2,** 864-870.

Schroeter, E. H., Ilagan, M. X., Brunkan, A. L. et al. (2003) A presenilin dimer at the core of the gamma-secretase enzyme: insights from parallel analysis of Notch 1 and APP proteolysis. *Proc Natl Acad Sci U S A,* **100,** 13075-13080.

Selkoe, D. J. (2001) Alzheimer's disease: genes, proteins, and therapy. *Physiol Rev,* **81,** 741-766.

Selkoe, D. J. and Hardy, J. (2016) The amyloid hypothesis of Alzheimer's disease at 25 years. *EMBO molecular medicine*.

Senechal, Y., Kelly, P. H. and Dev, K. K. (2008) Amyloid precursor protein knockout mice show age-dependent deficits in passive avoidance learning. *Behavioural brain research,* **186,** 126-132.

Sepulveda-Falla, D., Barrera-Ocampo, A., Hagel, C. et al. (2014) Familial Alzheimer's disease-associated presenilin-1 alters cerebellar activity and calcium homeostasis. *The Journal of clinical investigation,* **124,** 1552-1567.

Shah, S., Lee, S. F., Tabuchi, K. et al. (2005) Nicastrin functions as a gamma-secretase-substrate receptor. *Cell,* **122,** 435-447.

Shankar, G. M., Li, S., Mehta, T. H. et al. (2008) Amyloid-beta protein dimers isolated directly from Alzheimer's brains impair synaptic plasticity and memory. *Nat Med,* **14,** 837-842.

Shen, J., Bronson, R. T., Chen, D. F., Xia, W., Selkoe, D. J. and Tonegawa, S. (1997) Skeletal and CNS defects in Presenilin-1-deficient mice. *Cell,* **89,** 629-639.

Shen, J. and Kelleher, R. J., 3rd (2007) The presenilin hypothesis of Alzheimer's disease: evidence for a loss-of-function pathogenic mechanism. *Proc Natl Acad Sci U S A,* **104,** 403-409.

Sherrington, R., Rogaev, E. I., Liang, Y. et al. (1995) Cloning of a gene bearing missense mutations in early-onset familial Alzheimer's disease. *Nature,* **375,** 754-760.

Shimojo, M., Sahara, N., Mizoroki, T. et al. (2008) Enzymatic characteristics of I213T mutant presenilin-1/gamma-secretase in cell models and knock-in mouse brains: familial Alzheimer disease-linked mutation impairs gamma-site cleavage of amyloid precursor protein C-terminal fragment beta. *J Biol Chem,* **283,** 16488-16496.

Shimojo, M., Sahara, N., Murayama, M., Ichinose, H. and Takashima, A. (2007) Decreased Abeta secretion by cells expressing familial Alzheimer's disease-linked mutant presenilin 1. *Neuroscience research,* **57,** 446-453.

Shirotani, K., Edbauer, D., Kostka, M., Steiner, H. and Haass, C. (2004) Immature nicastrin stabilizes APH-1 independent of PEN-2 and presenilin: identification of nicastrin mutants that selectively interact with APH-1. *J Neurochem,* **89,** 1520-1527.

Siman, R., Reaume, A. G., Savage, M. J., Trusko, S., Lin, Y. G., Scott, R. W. and Flood, D. G. (2000) Presenilin-1 P264L knock-in mutation: differential effects on abeta production, amyloid deposition, and neuronal vulnerability. *J Neurosci,* **20,** 8717-8726.

Soba, P., Eggert, S., Wagner, K. et al. (2005) Homo- and heterodimerization of APP family members promotes intercellular adhesion. *EMBO J,* **24,** 3624-3634.

Soldner, F. and Jaenisch, R. (2012) Medicine. iPSC disease modeling. *Science,* **338,** 1155-1156.

Song, W., Nadeau, P., Yuan, M., Yang, X., Shen, J. and Yankner, B. A. (1999) Proteolytic release and nuclear translocation of Notch-1 are induced by presenilin-1 and impaired by pathogenic presenilin-1 mutations. *Proc Natl Acad Sci U S A,* **96,** 6959-6963.

Sproul, A. A., Jacob, S., Pre, D. et al. (2014) Characterization and molecular profiling of PSEN1 familial Alzheimer's disease iPSC-derived neural progenitors. *PloS one,* **9,** e84547.

Stahl, R., Schilling, S., Soba, P., Rupp, C., Hartmann, T., Wagner, K., Merdes, G., Eggert, S. and Kins, S. (2014) Shedding of APP limits its synaptogenic activity and cell adhesion properties. *Frontiers in cellular neuroscience,* **8,** 410.

Steiner, H., Duff, K., Capell, A. et al. (1999) A loss of function mutation of presenilin-2 interferes with amyloid beta-peptide production and notch signaling. *J Biol Chem,* **274,** 28669-28673.

Steiner, H., Kostka, M., Romig, H. et al. (2000) Glycine 384 is required for presenilin-1 function and is conserved in bacterial polytopic aspartyl proteases. *Nat Cell Biol,* **2,** 848-851.

Steiner, H., Revesz, T., Neumann, M. et al. (2001) A pathogenic presenilin-1 deletion causes abberrant Abeta 42 production in the absence of congophilic amyloid plaques. *J Biol Chem,* **276,** 7233-7239.

Steiner, H., Winkler, E. and Haass, C. (2008) Chemical cross-linking provides a model of the gamma-secretase complex subunit architecture and evidence for close proximity of the C-terminal fragment of presenilin with APH-1. *J Biol Chem,* **283,** 34677-34686.

Stewart, C. R., Stuart, L. M., Wilkinson, K. et al. (2010) CD36 ligands promote sterile inflammation through assembly of a Toll-like receptor 4 and 6 heterodimer. *Nature immunology,* **11,** 155-161.

Stomrud, E., Hansson, O., Zetterberg, H., Blennow, K., Minthon, L. and Londos, E. (2010) Correlation of longitudinal cerebrospinal fluid biomarkers with cognitive decline in healthy older adults. *Archives of neurology,* **67,** 217-223.

Strittmatter, W. J., Saunders, A. M., Schmechel, D., Pericak-Vance, M., Enghild, J., Salvesen, G. S. and Roses, A. D. (1993) Apolipoprotein E: high-avidity binding to beta-amyloid and increased frequency of type 4 allele in late-onset familial Alzheimer disease. *Proc Natl Acad Sci U S A,* **90,** 1977-1981.

Strozyk, D., Blennow, K., White, L. R. and Launer, L. J. (2003) CSF Abeta 42 levels correlate with amyloid-neuropathology in a population-based autopsy study. *Neurology,* **60,** 652-656.

Suguna, K., Padlan, E. A., Smith, C. W., Carlson, W. D. and Davies, D. R. (1987) Binding of a reduced peptide inhibitor to the aspartic proteinase from Rhizopus chinensis: implications for a mechanism of action. *Proc Natl Acad Sci U S A,* **84,** 7009-7013.

Sun, L., Zhao, L., Yang, G. et al. (2015) Structural basis of human gamma-secretase assembly. *Proc Natl Acad Sci U S A,* **112,** 6003-6008.

Suzuki, N., Cheung, T. T., Cai, X. D., Odaka, A., Otvos, L., Jr., Eckman, C., Golde, T. E. and Younkin, S. G. (1994a) An increased percentage of long amyloid beta protein secreted by familial amyloid beta protein precursor (beta APP717) mutants. *Science,* **264,** 1336-1340.

Suzuki, T., Oishi, M., Marshak, D. R., Czernik, A. J., Nairn, A. C. and Greengard, P. (1994b) Cell cycle-dependent regulation of the phosphorylation and metabolism of the Alzheimer amyloid precursor protein. *EMBO J,* **13,** 1114-1122.

Szaruga, M., Veugelen, S., Benurwar, M. et al. (2015) Qualitative changes in human gamma-secretase underlie familial Alzheimer's disease. *The Journal of experimental medicine,* **212,** 2003-2013.

Tabira, T., Chui, D. H., Nakayama, H., Kuroda, S. and Shibuya, M. (2002) Alzheimer's disease with spastic paresis and cotton wool type plaques. *Journal of neuroscience research,* **70,** 367-372.

Takahashi, K., Tanabe, K., Ohnuki, M., Narita, M., Ichisaka, T., Tomoda, K. and Yamanaka, S. (2007) Induction of pluripotent stem cells from adult human fibroblasts by defined factors. *Cell,* **131,** 861-872.

Takahashi, Y., Hayashi, I., Tominari, Y. et al. (2003) Sulindac sulfide is a noncompetitive gamma-secretase inhibitor that preferentially reduces Abeta 42 generation. *J Biol Chem,* **278,** 18664-18670.

Takami, M., Nagashima, Y., Sano, Y., Ishihara, S., Morishima-Kawashima, M., Funamoto, S. and Ihara, Y. (2009) gamma-Secretase: successive tripeptide and tetrapeptide release from the transmembrane domain of beta-carboxyl terminal fragment. *J Neurosci,* **29,** 13042-13052.

Takao, M., Ghetti, B., Hayakawa, I. et al. (2002) A novel mutation (G217D) in the Presenilin 1 gene (PSEN1) in a Japanese family: presenile dementia and parkinsonism are associated with cotton wool plaques in the cortex and striatum. *Acta neuropathologica,* **104,** 155-170.

Takasugi, N., Tomita, T., Hayashi, I., Tsuruoka, M., Niimura, M., Takahashi, Y., Thinakaran, G. and Iwatsubo, T. (2003) The role of presenilin cofactors in the gamma-secretase complex. *Nature,* **422,** 438-441.

Tamaoka, A., Odaka, A., Ishibashi, Y. et al. (1994) APP717 missense mutation affects the ratio of amyloid beta protein species (A beta 1-42/43 and a beta 1-40) in familial Alzheimer's disease brain. *J Biol Chem,* **269,** 32721-32724.

Tanzi, R. E. (2012) The genetics of Alzheimer disease. *Cold Spring Harbor perspectives in medicine,* **2**.

Tapiola, T., Alafuzoff, I., Herukka, S. K., Parkkinen, L., Hartikainen, P., Soininen, H. and Pirttila, T. (2009) Cerebrospinal fluid {beta}-amyloid 42 and tau proteins as biomarkers of Alzheimer-type pathologic changes in the brain. *Archives of neurology,* **66,** 382-389.

Thinakaran, G., Borchelt, D. R., Lee, M. K. et al. (1996) Endoproteolysis of presenilin 1 and accumulation of processed derivatives in vivo. *Neuron,* **17,** 181-190.

Thinakaran, G., Harris, C. L., Ratovitski, T., Davenport, F., Slunt, H. H., Price, D. L., Borchelt, D. R. and Sisodia, S. S. (1997) Evidence that levels of presenilins (PS1 and PS2) are coordinately regulated by competition for limiting cellular factors. *J Biol Chem,* **272,** 28415-28422.

Tolia, A., Chavez-Gutierrez, L. and De Strooper, B. (2006) Contribution of presenilin transmembrane domains 6 and 7 to a water-containing cavity in the gamma-secretase complex. *J Biol Chem,* **281,** 27633-27642.

Tolia, A., Horre, K. and De Strooper, B. (2008) Transmembrane domain 9 of presenilin determines the dynamic conformation of the catalytic site of gamma-secretase. *J Biol Chem,* **283,** 19793-19803.

Tominaga, A., Cai, T., Takagi-Niidome, S., Iwatsubo, T. and Tomita, T. (2016) Conformational Changes in Transmembrane Domain 4 of Presenilin 1 Are Associated with Altered Amyloid-beta 42 Production. *J Neurosci,* **36,** 1362-1372.

Tremml, P., Lipp, H. P., Muller, U. and Wolfer, D. P. (2002) Enriched early experiences of mice underexpressing the beta-amyloid precursor protein restore spatial learning capabilities but not normal openfield behavior of adult animals. *Genes, brain, and behavior,* **1,** 230-241.

Tu, H., Nelson, O., Bezprozvanny, A. et al. (2006) Presenilins form ER Ca2+ leak channels, a function disrupted by familial Alzheimer's disease-linked mutations. *Cell,* **126,** 981-993.

Turner, P. R., O'Connor, K., Tate, W. P. and Abraham, W. C. (2003) Roles of amyloid precursor protein and its fragments in regulating neural activity, plasticity and memory. *Progress in neurobiology,* **70,** 1-32.

Uemura, K., Kitagawa, N., Kohno, R., Kuzuya, A., Kageyama, T., Chonabayashi, K., Shibasaki, H. and Shimohama, S. (2003) Presenilin 1 is involved in maturation and trafficking of N-cadherin to the plasma membrane. *Journal of neuroscience research,* **74,** 184-191.

Urnov, F. D., Rebar, E. J., Holmes, M. C., Zhang, H. S. and Gregory, P. D. (2010) Genome editing with engineered zinc finger nucleases. *Nat Rev Genet,* **11,** 636-646.

Van Dam, D. and De Deyn, P. P. (2011) Animal models in the drug discovery pipeline for Alzheimer's disease. *British journal of pharmacology,* **164,** 1285-1300.

Vassar, R., Bennett, B. D., Babu-Khan, S. et al. (1999) Beta-secretase cleavage of Alzheimer's amyloid precursor protein by the transmembrane aspartic protease BACE. *Science,* **286,** 735-741.

Veeraraghavalu, K., Choi, S. H., Zhang, X. and Sisodia, S. S. (2010) Presenilin 1 mutants impair the self-renewal and differentiation of adult murine subventricular zone-neuronal progenitors via cell-autonomous mechanisms involving notch signaling. *J Neurosci,* **30,** 6903-6915.

Veeraraghavalu, K., Choi, S. H., Zhang, X. and Sisodia, S. S. (2013) Endogenous expression of FAD-linked PS1 impairs proliferation, neuronal differentiation and survival of adult hippocampal progenitors. *Molecular neurodegeneration,* **8,** 41.

Veitia, R. A. (2007) Exploring the molecular etiology of dominant-negative mutations. *The Plant cell,* **19,** 3843-3851.

Verkhratsky, A., Olabarria, M., Noristani, H. N., Yeh, C. Y. and Rodriguez, J. J. (2010) Astrocytes in Alzheimer's disease. *Neurotherapeutics : the journal of the American Society for Experimental NeuroTherapeutics,* **7,** 399-412.

Veugelen, S., Saito, T., Saido, T. C., Chavez-Gutierrez, L. and De Strooper, B. (2016) Familial Alzheimer's Disease Mutations in Presenilin Generate Amyloidogenic Abeta Peptide Seeds. *Neuron,* **90,** 410-416.

Vidal, R., Sammeta, N., Garringer, H. J., Sambamurti, K., Miravalle, L., Lamb, B. T. and Ghetti, B. (2012) The Psen1-L166P-knock-in mutation leads to amyloid deposition in human wild-type amyloid precursor protein YAC transgenic mice. *FASEB journal : official publication of the Federation of American Societies for Experimental Biology,* **26,** 2899-2910.

Villemagne, V. L., Burnham, S., Bourgeat, P. et al. (2013) Amyloid beta deposition, neurodegeneration, and cognitive decline in sporadic Alzheimer's disease: a prospective cohort study. *Lancet neurology,* **12,** 357-367.

Villemagne, V. L., Pike, K. E., Chetelat, G. et al. (2011) Longitudinal assessment of Abeta and cognition in aging and Alzheimer disease. *Ann Neurol,* **69,** 181-192.

Vodovotz, Y., Lucia, M. S., Flanders, K. C. et al. (1996) Inducible nitric oxide synthase in tangle-bearing neurons of patients with Alzheimer's disease. *The Journal of experimental medicine,* **184,** 1425-1433.

Walker, E. S., Martinez, M., Brunkan, A. L. and Goate, A. (2005) Presenilin 2 familial Alzheimer's disease mutations result in partial loss of function and dramatic changes in Abeta 42/40 ratios. *J Neurochem,* **92,** 294-301.

Walsh, D. M., Klyubin, I., Fadeeva, J. V., Rowan, M. J. and Selkoe, D. J. (2002) Amyloid-beta oligomers: their production, toxicity and therapeutic inhibition. *Biochemical Society transactions,* **30,** 552-557.

Walter, J., Capell, A., Hung, A. Y., Langen, H., Schnolzer, M., Thinakaran, G., Sisodia, S. S., Selkoe, D. J. and Haass, C. (1997) Ectodomain phosphorylation of beta-amyloid precursor protein at two distinct cellular locations. *J Biol Chem,* **272,** 1896-1903.

Wang, J., Beher, D., Nyborg, A. C., Shearman, M. S., Golde, T. E. and Goate, A. (2006a) C-terminal PAL motif of presenilin and presenilin homologues required for normal active site conformation. *J Neurochem,* **96,** 218-227.

Wang, J., Brunkan, A. L., Hecimovic, S., Walker, E. and Goate, A. (2004) Conserved "PAL" sequence in presenilins is essential for gamma-secretase activity, but not required for formation or stabilization of gamma-secretase complexes. *Neurobiol Dis,* **15,** 654-666.

Wang, R., Wang, B., He, W. and Zheng, H. (2006b) Wild-type presenilin 1 protects against Alzheimer disease mutation-induced amyloid pathology. *J Biol Chem,* **281,** 15330-15336.

Wang, Z., Wang, B., Yang, L., Guo, Q., Aithmitti, N., Songyang, Z. and Zheng, H. (2009) Presynaptic and postsynaptic interaction of the amyloid precursor protein promotes peripheral and central synaptogenesis. *J Neurosci,* **29,** 10788-10801.

Webster, S. J., Bachstetter, A. D., Nelson, P. T., Schmitt, F. A. and Van Eldik, L. J. (2014) Using mice to model Alzheimer's dementia: an overview of the clinical disease and the preclinical behavioral changes in 10 mouse models. *Frontiers in genetics,* **5,** 88.

Weggen, S. and Beher, D. (2012) Molecular consequences of amyloid precursor protein and presenilin mutations causing autosomal-dominant Alzheimer's disease. *Alzheimer's research & therapy,* **4,** 9.

Weggen, S., Eriksen, J. L., Sagi, S. A., Pietrzik, C. U., Ozols, V., Fauq, A., Golde, T. E. and Koo, E. H. (2003) Evidence that nonsteroidal anti-inflammatory drugs decrease amyloid beta 42 production by direct modulation of gamma-secretase activity. *J Biol Chem,* **278,** 31831-31837.

Weidemann, A., Eggert, S., Reinhard, F. B., Vogel, M., Paliga, K., Baier, G., Masters, C. L., Beyreuther, K. and Evin, G. (2002) A novel epsilon-cleavage within the transmembrane domain of the Alzheimer amyloid precursor protein demonstrates homology with Notch processing. *Biochemistry,* **41,** 2825-2835.

Weidemann, A., Konig, G., Bunke, D., Fischer, P., Salbaum, J. M., Masters, C. L. and Beyreuther, K. (1989) Identification, biogenesis, and localization of precursors of Alzheimer's disease A4 amyloid protein. *Cell,* **57,** 115-126.

Weingarten, M. D., Lockwood, A. H., Hwo, S. Y. and Kirschner, M. W. (1975) A protein factor essential for microtubule assembly. *Proc Natl Acad Sci U S A,* **72,** 1858-1862.

Wen, P. H., Hof, P. R., Chen, X. et al. (2004) The presenilin-1 familial Alzheimer disease mutant P117L impairs neurogenesis in the hippocampus of adult mice. *Experimental neurology,* **188,** 224-237.

Wisniewski, K. E., Wisniewski, H. M. and Wen, G. Y. (1985) Occurrence of neuropathological changes and dementia of Alzheimer's disease in Down's syndrome. *Ann Neurol,* **17,** 278-282.

Wolfe, D. M., Lee, J. H., Kumar, A., Lee, S., Orenstein, S. J. and Nixon, R. A. (2013) Autophagy failure in Alzheimer's disease and the role of defective lysosomal acidification. *The European journal of neuroscience,* **37,** 1949-1961.

Wolfe, M. S. (2007) When loss is gain: reduced presenilin proteolytic function leads to increased Abeta42/Abeta40. Talking Point on the role of presenilin mutations in Alzheimer disease. *EMBO Rep,* **8,** 136-140.

Wolfe, M. S. and Guenette, S. Y. (2007) APP at a glance. *J Cell Sci,* **120,** 3157-3161.

Wolfe, M. S., Xia, W., Ostaszewski, B. L., Diehl, T. S., Kimberly, W. T. and Selkoe, D. J. (1999) Two transmembrane aspartates in presenilin-1 required for presenilin endoproteolysis and gamma-secretase activity. *Nature,* **398,** 513-517.

Woodruff, G., Young, J. E., Martinez, F. J. et al. (2013) The Presenilin-1 Delta E9 Mutation Results in Reduced gamma-Secretase Activity, but Not Total Loss of PS1 Function, in Isogenic Human Stem Cells. *Cell reports,* **5,** 974-985.

World Alzheimer Report 2015. *http://www.alz.co.uk/research/world-report-2015*.

Xia, D., Kelleher, R. J., 3rd and Shen, J. (2016) Loss of Abeta43 Production Caused by Presenilin-1 Mutations in the Knockin Mouse Brain. *Neuron,* **90,** 417-422.

Xia, D., Watanabe, H., Wu, B., Lee, S. H., Li, Y., Tsvetkov, E., Bolshakov, V. Y., Shen, J. and Kelleher, R. J., 3rd (2015) Presenilin-1 knockin mice reveal loss-of-function mechanism for familial Alzheimer's disease. *Neuron,* **85,** 967-981.

Xie, T., Yan, C., Zhou, R., Zhao, Y., Sun, L., Yang, G., Lu, P., Ma, D. and Shi, Y. (2014) Crystal structure of the gamma-secretase component nicastrin. *Proc Natl Acad Sci U S A,* **111,** 13349-13354.

Yagi, T., Ito, D., Okada, Y., Akamatsu, W., Nihei, Y., Yoshizaki, T., Yamanaka, S., Okano, H. and Suzuki, N. (2011) Modeling familial Alzheimer's disease with induced pluripotent stem cells. *Human molecular genetics,* **20,** 4530-4539.

Yamamoto, A., Tagawa, Y., Yoshimori, T., Moriyama, Y., Masaki, R. and Tashiro, Y. (1998) Bafilomycin A1 prevents maturation of autophagic vacuoles by inhibiting fusion between autophagosomes and lysosomes in rat hepatoma cell line, H-4-II-E cells. *Cell structure and function,* **23,** 33-42.

Ying, Q. L. and Smith, A. G. (2003) Defined conditions for neural commitment and differentiation. *Methods in enzymology,* **365,** 327-341.

Yuan, H., Zhai, P., Anderson, L. M., Pan, J., Thimmapaya, B., Koo, E. H. and Marquez-Sterling, N. R. (1999) Recombinant adenovirus is an appropriate vector for endocytotic protein trafficking studies in cultured neurons. *Journal of neuroscience methods,* **88,** 45-54.

Zhang, H., Sun, S., Herreman, A., De Strooper, B. and Bezprozvanny, I. (2010) Role of presenilins in neuronal calcium homeostasis. *J Neurosci,* **30,** 8566-8580.

Zhang, X., Garbett, K., Veeraraghavalu, K., Wilburn, B., Gilmore, R., Mirnics, K. and Sisodia, S. S. (2012) A role for presenilins in autophagy revisited: normal acidification of lysosomes in cells lacking PSEN1 and PSEN2. *J Neurosci,* **32,** 8633-8648.

Zhang, Z., Nadeau, P., Song, W., Donoviel, D., Yuan, M., Bernstein, A. and Yankner, B. A. (2000) Presenilins are required for gamma-secretase cleavage of beta-APP and transmembrane cleavage of Notch-1. *Nat Cell Biol,* **2,** 463-465.

Zhao, G., Cui, M. Z., Mao, G., Dong, Y., Tan, J., Sun, L. and Xu, X. (2005) gamma-Cleavage is dependent on zeta-cleavage during the proteolytic processing of amyloid precursor protein within its transmembrane domain. *J Biol Chem,* **280,** 37689-37697.

Zheng, H., Jiang, M., Trumbauer, M. E. et al. (1995) beta-Amyloid precursor protein-deficient mice show reactive gliosis and decreased locomotor activity. *Cell,* **81,** 525-531.

Zheng, H. and Koo, E. H. (2011) Biology and pathophysiology of the amyloid precursor protein. *Molecular neurodegeneration,* **6,** 27.

Zou, K., Hosono, T., Nakamura, T., Shiraishi, H., Maeda, T., Komano, H., Yanagisawa, K. and Michikawa, M. (2008) Novel role of presenilins in maturation and transport of integrin beta 1. *Biochemistry,* **47,** 3370-3378.

8. Acknowledgements

I want to thank my supervisor Prof. Dr. Sascha Weggen for the challenging project, the constant support and his trust in me and my work.

I thank Prof. Dr. Vlada Urlacher for agreeing to be my second supervisor and mentor.

My deep gratitude also goes to Junior Prof. Dr. Katja Nieweg for teaching me the NSC differentiation protocol and to Dr. Maxi Hofrichter, who helped me with the differentiation into neurons, astrocytes and oligodendrocytes. A special thank you goes to Dr. Dirk Beher and Solenne Ousson for the quantitative Aβ measurements, which have been essential for the success of my doctoral thesis.

To my family at the Institute of Neuropathology: Thank you for the outstanding working atmosphere!!! You made me feel welcome and I enjoyed every single day with you.
Thank you for (daily) cakes and sweets - I have gained 2 kg, for rotten fish from Denmark and barbecues, for carnival brunches and Christmas dinners, for after-work cocktails and dinner, for crazy parties, paintball and canoeing. Susanne Walter, Sandra Baches, Isabella Ogorek, Thorsten Jumpertz, Maxi Faust, Julia Seegel, Julia Ness, Tanja Brüning, Parul Goel, Svenja Trossbach, Sandra Vomund, Ingrid Prikulis, Sascha Steltgens, Sravan Yerabham, Andreas Müller-Schiffmann, Verian Bader, Nick Bradshaw and Rita Marreiros – I had a wonderful time with you and I will miss you deeply!

My last gratitude goes to the members of my family, to my mother Manuela Kurth, my uncle Reinhard Kurth, my aunt Manuela Kurth and my cousin Nadine Kurth. I dedicate my doctoral thesis to you and to Nadine's and my beloved grandparents Maria Kurth and Willi Kurth. Your support, encouragement and love has helped me to endure hardships and to achieve my goals. You mean everything to me!